Diss. ETH No. 16634

SINGLE CHAMBER SOLID OXIDE FUEL CELLS

A dissertation submitted to the

SWISS FEDERAL INSTITUTE OF TECHNOLOGY ZURICH

for the degree of

DOCTOR OF SCIENCES

presented by

BRANDON EDWARD BÜRGLER

Dipl. Werkstoff-Ing. ETH
born February 11th, 1975
citizen of Illgau (SZ)

accepted on the recommendation of

Prof. Dr. Ludwig J. Gauckler, examiner
Prof. Dr. Ilan Riess, co-examiner
Prof. Dr. Christos Comninellis, co-examiner

2006

Acknowledgements

I wish to thank Prof. Dr. L. J. Gauckler for the interesting subject and the possibility to realise my own ideas during the course of this project. We had many hours of interesting and challenging discussions that helped to improve my thesis. Furthermore, I was given the opportunity to present my work to an international audience at many symposia and conferences.

I would like to thank Prof. Dr. Ilan Riess from Technion Haifa (Israel), who introduced me to the fascinating world of single chamber solid oxide fuel cells and also helped me understand the basic theory of such fuel cells.

Thanks also to Prof. Dr. Christos Comninellis from EPFL for being the co-referent of this thesis and for making possible all the conducted catalysis measurements. For the practical help with the catalysis measurements I would also like to thank Dr. Elena Baranova and Dr. György Fóti from EPFL.

I would also like to thank Prof. Nicholas Spencer for being the chairman of my PhD-defense, during which he also helped me to demonstrate a SC-SOFC.

Special thanks go to my colleagues at the Nonmetallic Inorganic Materials Group, especially:

Dr. A. Nicholas Grundy, who helped me to model the thermodynamic equilibrium at SC-SOFC anode and who was always a good friend not just during the numerous coffee breaks. The times we had as “The Old Irish Spudheads” were great fun.

Sybille Vuillemin, for the help with the realisation of micro single chamber SOFCs.

Dr. Michael Jörger and Dr. Eva Jud, who always helped where they could especially in practical things in the lab. They also critically analysed my ideas.

Dr. Michel Prestat, with whom I shared the office during the first three years of my PhD-thesis. He was always prepared to answer questions concerning the electrochemistry of Solid Oxide Fuel Cells.

Irène Urbánek for her support in the paper work and Peter Kocher for technical help.

I want to thank my co-workers, Jennifer Rupp, Ulrich Mücke, David Sager, Daniel Beckel, Toni Ivas, Erwin Povoden, Ming Chen, Frank Filser, Martin Heule, Bengt Halstedt, André Studart, Carlo Neto Pagliosa, Barbara Scherrer, Felix Schröder, Joakim Reuteler, Hans Wyss Ming Chen, Martin Heule, Dainius Perednis, Esther Amstad, Urs Gonzenbach, Anna Infortuna, Ilke Akartuna, Anja Bieberle-Hütter, Zhijian Peng, Zhen Yang and Iwan Schenker.

Special thanks also to Lorenz J. Bonderer for taking over the SEM-Administration. He proved to be a worthy SEM-Administrator. Furthermore we had a great, easygoing holiday in Florida.

I would also like to thank Juan Peña-Martínez for the good time we had during the experimental work and for helping me build up a setup for the characterisation of fuel cells. He taught me how to take life a bit easier.

Special thanks go to Lars Massüger for the help with the XRD-analysis with thin quartz glass capillaries.

Very special thanks go to my students Srđan Vasić, Marco Siegrist, Mirjam Ochsner, Milan Felberbaum, Yannick Santschi, Donya Smida and my “Hilfsassistenten” David Steinlin and Manuela Kobas. They contributed a great deal of what you are holding in your hands. The scientific results they obtained are not what I want to acknowledge solely. It was just great to work together with such fine young scientist and engineers and I learned a lot about the significance of team work and guidance.

I wish to thank my parents Franz Josef and Cecilia Bürgler-Jones and my brothers Franz and Owen, my grand-parents, uncles, aunts, cousins and friends that shared a significant amount of their precious time of their lives with me for supporting me throughout the past years.

I would like to thank my beloved girl-friend Gina Furrer, who was there for me during the last 3 years, giving me confidence and support in personal matters. We spent a wonderful time together.

I want to express my thanks to all my flat mates and good friends for being there.

I want to thank Marc Dusseiller, who was always very critical about everything I do and say during our common time at ETH. He tried to show me that life does not necessarily need to be black and white. He failed. He succeeded, however, to give me back my motivation when I had lost it. Thanx!

Special Thanks go to Kurosh Rezwan, who was my colleague from the very beginning of my ETH-career. He helped me reveal the significance of being professional from the very start of our common lab-work (Werkstoffgrundpraktikum 1996!).

I would also like to thank Bruno Nussberger from the glassblowing workshop for fabricating the parts I needed for my experimental setups.

I would also like to thank Niklaus Koch, Markus Müller and Martin Elsener from the D-MATL workshop for their help with this and that and for the manufacturing of gas mixing devices.

Thanks also to Dr. Kaspar Honegger for his advice especially at the beginning of my PhD.

The demonstration of a SC-SOFC at the beginning of my PhD-defense was possible thanks to Michio Horiuchi from Shinko Electric Industries, who kindly provided the cells and light chain. Thank you very much.

Last but not least I would like to thank the Swiss people as a whole including our ancestors who have built up the whole place and our guests from foreign countries. In my eyes the goal must always be to improve the quality of life on this planet, not just for humans but for all beings.

Contents

Summary

Single chamber solid oxide fuel cells (SC-SOFCs) offer the possibility to simplify solid oxide fuel cells because only one gas compartment is necessary. Both, anode and cathode are exposed to the same mixture of fuel and oxidant. In such a system the driving force for the ionic current in the electrolyte is not due to the difference of oxygen partial pressures in the two sealed gas compartments. It is the selectivity of the two different electrodes for either the partial oxidation of a hydrocarbon at the anode or the reduction of oxygen at the cathode that allows for the generation of an electric current. SC-SOFCs have been demonstrated to give reasonably high power output comparable to conventional solid oxide fuel cells. However, the working principle of SC-SOFCs is not yet fully understood.

This project aims at obtaining more insight into this type of fuel cell operating in methane-air mixtures. The thermodynamic equilibrium of the used gas mixtures was calculated for the experimental operating conditions and the kinetics of the oxidation reactions were studied experimentally. The studied SC-SOFCs were based on the oxygen-ion conducting gadolinia doped ceria ($Ce_{0.9}Gd_{0.1}O_{1.95}$) an anode material consisting of a mixture of metallic Nickel and gadolinia doped ceria and a cathode consisting of porous perovskite $Sm_{0.5}Sr_{0.5}CoO_{3-\delta}$. The prepared cells generated 271 mW/cm^2 at 500°C and 468 mW/cm^2 at 600°C in flowing mixtures of methane and air. It was found that the open circuit voltage and the maximum power density greatly depended on the gas flow rate, the gas composition and the operating temperature but also on the thickness of the anode layer. Furthermore, a pronounced overheating of the cell to temperatures higher than the furnace temperature was observed. The reason for this temperature rise was the parasitic oxidation reaction of methane that occurs at both electrodes, however with the highest rates at the anode.

In the second part of this work, different cell designs were evaluated that are not possible with conventional solid oxide fuel cells. A process was developed, by which micro SC-SOFCs with side by side placement of the electrodes were successfully prepared. Nineteen parallel connected cells with feature sizes in the micrometer range generated an open circuit voltage of 0.65-0.75 V in flowing mixtures of methane and air. The performance of the cell array was limited by the high ohmic resistances of the long conduction paths in the thin electrodes. It could be shown for the first time that a μ-SC-SOFC is a feasible device.

Fully porous fuel cells with a flow-through configuration have been proposed in the literature but they have not been proven to function. Their proof of concept is given in this

work. An anode-supported fully porous SC-SOFC was prepared and gave a reasonable open circuit voltage. The power output was very sensitive to the temperature, the CH_4/O_2-ratio and the total gas flow rate through the cell. At 733°C an open circuit voltage of 0.52 V and a maximum power density of 10 mW/cm^2 for 1000 ml/min were measured. Thus, for the first time the fully porous design of SC-SOFCs with flow-through configuration has been demonstrated.

Zusammenfassung

Einkammerfestelektrolytbrennstoffzellen (EK-FEBZ) sind Brennstoffzellen mit nur einem Gasraum in dem sich ein Gasgemisch aus Brennstoff und Sauerstoff befindet. Die Anode und Kathode einer solchen Zelle werden demselben Gemisch aus Brenngas und Luft ausgesetzt. In einer solchen Zelle entsteht die treibende Kraft für einen elektrischen Strom nicht aufgrund unterschiedlicher Sauerstoffpartialdrücke auf beiden Seiten eines Festelektrolyten, sondern aufgrund der Selektivität der Anode für die Oxidation eines Kohlenwasserstoffs und der Selektivität der Kathode für die Reduktion von Luftsauerstoff. Solche Zellen ermöglichen eine drastische Vereinfachung des Designs von Festelektrolytbrennstoffzellen da statt zwei nur noch eine einzige Gaskammer benötigt wird. In der Vergangenheit konnte gezeigt werden, dass EK-FEBZ angemessene elektrische Leistungen liefern können vergleichbar mit jenen von konventionellen Festelektrolytbrennstoffzellen. Das genaue Funktionsprinzip von EK-FEBZ ist aber noch weitgehend unerforscht.

Zielsetzung der vorliegenden Arbeit war es, ein besseres Verständnis für diese Art von Brennstoffzellen zu erarbeiten, die in Methan-Luft Gemischen betrieben werden. Zuerst wurden die Gleichgewichtszusammensetzungen von Methan-Luft Gemischen für den Temperaturbereich von 500 bis 800°C berechnet. Des Weiteren wurde die Kinetik der massgebenden Oxidationsreaktionen, die an den Elektroden auftreten gemessen. Es wurden Zellen untersucht, die auf dem ionenleitenden Elektrolyten, Cer-Gadoliniumoxid ($Ce_{0.9}Gd_{0.1}O_{1.95}$) basieren. Als Anodenmaterial wurde ein Gemisch von Nickel und $Ce_{0.9}Gd_{0.1}O_{1.95}$ eingesetzt und als Kathodenmaterial $Sm_{0.5}Sr_{0.5}CoO_{3-\delta}$, welches in der Perowskit-Struktur vorliegt. Die hergestellten Zellen zeigten eine elektrische Leistung von 271 mW/cm^2 bei 500°C und 480 mW/cm^2 bei 600°C in strömenden Methan-Luft Gemischen. Die Leerlaufspannung wie auch die maximale Leistung hingen stark vom gewählten Gasfluss, der Gaszusammensetzung, und der Zelltemperatur ab, aber auch von der Anodendicke. Des Weiteren wurde festegestellt, dass im ganzen untersuchten Temperaturbereich immer beide Elektroden die Umsetzung des Methan Luft katalysieren, jedoch mit sehr unterschiedlichen Umsetzungsraten. Eine deutliche Überhöhung der Zelltemperatur im Vergleich zur Ofentemperatur kann auf die parasitärer Methanoxidation hauptsächlich an der Anode zurückgeführt werden.

Im zweiten Teil der vorliegenden Arbeit wurden verschiedene, neuartige Zellendesigns erprobt, die mit konventionellen Festelektrolytbrennstoffzellen nicht möglich wären. Es

wurde ein Prozeß entwickelt, mit dem Mikro EK-FEBZ hergestellt werden konnten, bei denen beide Elektroden auf derselben Seite des Elektrolyts liegen und durch einen schmalen Spalt voneinander getrennt sind. Neunzehn parallelgeschaltete Zellen mit Elektroden in der Größenordnung von Mikrometern, zeigten eine Leerlaufspannung von 0.65-0.75°V in strömenden Methan-Luft Gemischen. Die Leistung der Zellenanordnung war durch den hohen elektrischen Widerstand der langen Strompfade in den dünnen Elektroden begrenzt. Gleichwohl konnte zum ersten Mal gezeigt werden, dass µ-EK-FEBZ realisierbare Brennstoffzellen sind.

Ein zweites Design, welches bereits vor einigen Jahren vorgeschlagen wurde, aber bisher noch nie experimentell demonstriert wurde, ist das vollporöse Design. Der Nachweis, dass vollporöse Zellen, bei welchen das Gasgemisch durch die Zelle hindurch geleitet wird funktionieren, wurde hier erbracht. Die Zellen wurden von einem relativ dicken Anodensubstrat gestützt, welches den Zellen die mechanische Stabilität verlieh. Hierauf wurden poröse Schichten des Elektrolytmaterials und der Kathode aufgebracht und durch diese Dreischichtanordnung das Gasgemisch geleitet. Es konnten vernünftige Leerlaufspannungen an den Zellen gemessen werden. Die Leistung hing stark von der Temperatur, dem Verhältnis von Brenngas (CH_4) zu Sauerstoff, und dem totalen Gasfluss durch die Zelle ab. Bei 733°C konnte eine Leerlaufspannung von 0.52 V und eine maximale Leistung von 10 mW/cm^2 gemessen werden bei 1000 ml/min Gasfluss. Dies ist das erste Mal, dass eine vollporöse EK-FEBZ mit Durchflußkonfiguration erfolgreich getestet werden konnte.

1 Introduction

Fuel cells are one of the most attractive energy conversion systems because they offer high efficiency and low pollution. An advantage of fuel cells is the decentralised generation of electricity and the prospective applications in mobile devices. The history of fuel cells reaches back to the middle of the nineteenth century. Even so the commercialisation of fuel cell systems has still not been accomplished.

1.1 Generalities on Fuel Cells

A fuel cell is an electrochemical device that can convert the chemical energy of a fuel and an oxidant into heat and electric power. It is composed of a cathode where the reduction of the oxidant takes place, an anode, where the oxidation of the fuel takes place and an electrolyte, which carries a charged species from one electrode to the other. As compared to batteries that have to be periodically recharged, fuel and oxidants can be continuously supplied to a fuel cell. Hence, power can be continuously produced. During operation no inherent changes in composition or morphology of the electrodes occur, in contrast to the drastic changes in a Li-ion battery electrode. In 1839 Sir William Grove believed that if it is possible to split water into H_2 and O_2 using electricity, then the reverse reaction should also be possible. His first fuel cell, shown in Figure 1.1, consisted of four connected cells.

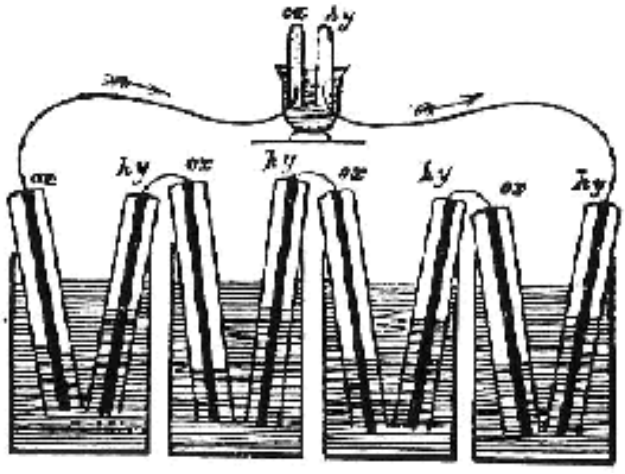

Figure 1.1 The first fuel cell elaborated by Sir William Grove.

Each of these cells was composed of two separate Pt-wires (the anode and the cathode) immerged into dilute sulphuric acid (the electrolyte). The electrodes were surrounded by a gas reservoir, the anode containing H_2 and the cathode O_2. This fuel cell generated electrical power by the electrochemical reaction of H_2 and O_2. The serial interconnection of four cells allowed electrolysing water, in a fifth cell, which is shown at the top Figure 1.1. During the last decades five different types of fuel cells have been developed (Table 1-1): alkaline, polymer membrane, molten carbonate, phosphoric acid and solid oxide fuel cells. The different fuel cell types are usually distinguished by the electrolyte being used. They all have advantages and drawbacks.

Table 1-1 The different types of fuel cells.

Fuel cell type	Mobile ion	Operating Temperature	Applications
Alkaline (AFC)	OH^-	50 – 200 °C	Used in Appolo spacecrafts
Proton exchange membrane (PEM)	H^+	50 – 100 °C	Mobile applications
Phosphoric acid (PAFC)	H^+	~ 220 °C	Systems with 200 kW
Molten carbonate (MCFC)	CO_3^{2-}	~ 650 °C	From kW up to MW
Solid oxide (SOFC)	O^{2-}	500 – 1000 °C	Suitable for all sizes, from several kW up to multi MW

The three first types of cells in Table 1-1 require relatively pure hydrogen to be supplied to the anode. Accordingly, the use of hydrocarbon or alcohol fuels requires an external fuel processing step to be incorporated into the system. This not only increases the complexity and the costs of the system, but also decreases the overall efficiency. In contrast, MCFCs and SOFCs – because they operate at higher temperatures – can utilise directly hydrocarbons or alcohols as the fuel. However, the high operating temperatures can be the cause for rapid degradation of the fuel cell components. In addition, high temperature gas seals in fuel cells pose a technical hurdle that has still not been overcome. In the following we will focus on solid oxide fuel cells.

1.2 Solid Oxide Fuel Cells

The first solid oxide fuel cell (SOFC) was developed in 1937 by Baur and Preis [1]. Since then a lot of progress has been made in terms of materials and processing of SOFCs. An advantage of SOFCs is the possibility of using natural gas as the fuel [2] and the high reaction rates given by the relatively high operating temperature. Thus, expensive catalysts are not

needed. However, the ceramic materials SOFCs are made of, are quite expensive, not easy to handle and difficult to process [3].

The main reason, why SOFCs have not been commercialised are the high costs [4] but also insufficient long-term stability. In the case of SOFCs the reasons for high costs are the materials and technologies required for sealing the cells at high temperatures. Furthermore, the interconnect material is expensive because it has to be highly conducting and must withstand the very reducing (anode) as well as oxidising conditions (cathode) at high temperatures [5]. Only few materials meet these requirements. $LaCrO_3$-based materials have been found to have excellent stability over a wide range of oxygen partial pressures [6] and are still widely used as interconnect. In the past has operating SOFCs at reduced temperatures (550-650°C) has become feasible by the use of novel materials [7] and this has allowed to envisage the use of metallic interconnects, like ferritic stainless steels or chromium based alloys [8].

1.2.1 Principle of Operation

As shown in Figure 1.2, SOFCs consist of three basic elements: electrolyte, anode and cathode. The anode and cathode are both highly porous and located in compartments that are physically separated. In case of SOFCs the electrolyte usually conducts O^{2-}-ions. A standard material for the electrolyte is yttria stabilised zirconia (YSZ). Fuel cells that are based on ceramic proton-conductors have also been demonstrated [9]. The operating temperature of an SOFC is between 500 and 1000°C. The reason for this is that the conduction of oxygen ions in the solid electrolyte is a thermally activated process with quite high activation energy.

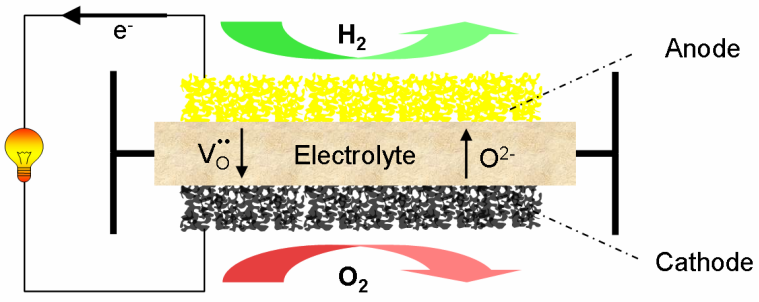

Figure 1.2 Scheme of a solid oxide fuel cell operated on H_2 and O_2. The anode and cathode compartment are physically separated from each other by a gas-tight electrolyte and high temperature sealings.

The most common fuel for SOFCs is hydrogen, which is why the operation principle shall be explained with this fuel here. The electrolyte is commonly referred to an ionic conductor; however, vacant oxygen lattice sites are the veritable charge carriers. Let us, thus, assume oxygen vacancies ($V_O^{\bullet\bullet}$) to be the charge carrying, mobile species. At the interface between the anode and the electrolyte the oxidation of the fuel takes place. H_2 and oxygen ions (O_O^x) are consumed by this reaction and H_2O, oxygen vacancies ($V_O^{\bullet\bullet}$) and electrons (e^-) are formed. Reaction (1.1) describes what is happening at the anode of an SOFC operating on hydrogen:

$$H_2 + O_O^x \rightarrow H_2O + V_O^{\bullet\bullet} + 2e^- \tag{1.1}$$

At the cathode the reduction of oxygen from air occurs (Reaction (1.2)), consuming the electrons that have flown through an electrical circuit and have emerged at the anode by the oxidation of the fuel. Oxygen vacancies are annihilated at the cathode by the insertion of oxygen from the gas phase. For every annihilated vacancy a pair of electrons is consumed. Reaction (1.2) leads to the formation of regular oxygen ions in the crystal lattice at the surface of the electrolyte.

$$\frac{1}{2}O_2 + 2e^- + V_O^{\bullet\bullet} \rightarrow O_O^x \tag{1.2}$$

It can be easily verified that the sum of Reaction (1.1) and (1.2) corresponds to the combustion reaction of hydrogen with water as the product:

$$H_2 + \frac{1}{2}O_2 \rightarrow H_2O \tag{1.3}$$

By the use of an SOFC the Gibb's free energy change ΔG of this reaction can be directly transformed into electric energy:

$$\Delta G = 2F \cdot E \tag{1.4}$$

where F is the Faraday constant (96485 Coulomb) and E the cell voltage. The change of Gibbs free energy for Reaction (1.3) at standard conditions ($\Delta G°$) amounts to 241.8 $kJ \cdot mol^{-1}$ when water is not condensed. The cell voltage E° calculated by Equation (1.4) is 1.185V. This is as high as the voltage of an SOFC can become. If higher voltages are to be generated from fuel cells, a number of cells have to be connected in series in so-called stacks.

The open circuit voltage (OCV) of a cell can also be calculated by the oxygen partial pressure at the cathode $p_C(O_2)$ and at the anode $p_A(O_2)$ using the Nernst equation:

$$OCV = \frac{RT}{nF} \ln \frac{p_C(O_2)}{p_A(O_2)} \tag{1.5}$$

The built up OCV between anode and cathode is due to the different $p(O_2)$ at each side of the fuel cell electrolyte. As shown in Figure 1.2 the electrons of the spatially separated redox reactions are forced to flow through an external circuit that passes through an electric load (any electric power-consuming device). The total current at each point of the electric circuit must be the same. In the electrolyte the current is due to the migration of ions and in the external circuit due to electrons. Thus, the electrodes are sites, where the charge carrying specie is converted from electrons to vacancies or vice versa. More details about fuel cell thermodynamics can be found elsewhere [10].

1.2.2 Losses in Solid Oxide Fuel Cells

In a real fuel cell there are certain losses that limit the efficiency of the conversion from chemical to electrical energy. The performance of fuel cells is commonly evaluated by measuring the cell voltage as a function of cell current. When current is drawn from the cell, the voltage $U(I)$ decreases and reaches the short circuit current at 0 V.

$$U(I) = OCV - (R_E + R_A + R_C)I - \eta_A - \eta_C \tag{1.6}$$

R_E, R_A and R_C are electrolyte, cathode, and anode ohmic resistances, respectively. η_A and η_C are the cathodic and anodic polarizations. An example of a voltage current-characteristic of a single cell is given in Figure 1.3. η_A and η_C represent so-called activation losses that are due to the limited reaction rate of the electrochemical reactions at the anode and cathode. R_E, R_A

and R_C correspond to resistive losses (ohmic) that are due to the material resistance to electron-flow and ion-flow through the electrolyte, the anode and cathode, respectively. According to Ohm's law these losses are proportional to the current density. Mass transport or concentration losses can occur when the cell is operated at high current densities. In this case the mass transport of educts to the electrodes and products away from the electrodes becomes the limiting factor. This loss is also called "Nernstian" loss. The power density of an operating fuel cell can be calculated by multiplying the cell voltage with the current density.

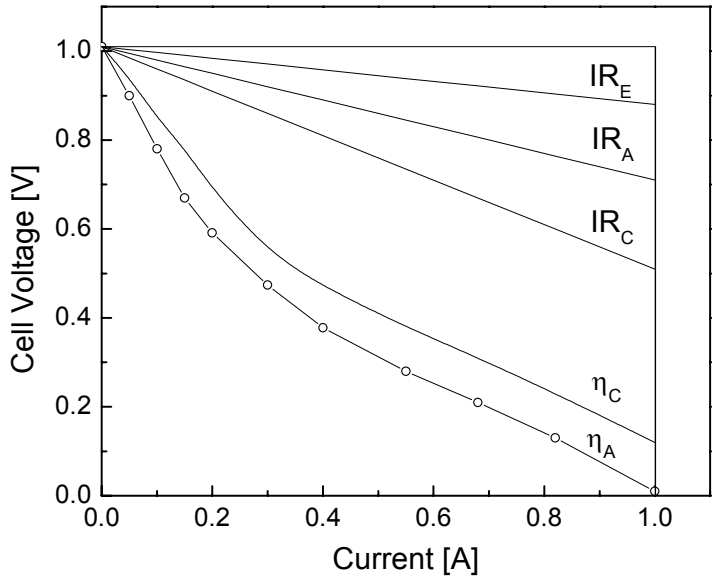

Figure 1.3 Schematic voltage-current characteristic of a solid oxide fuel cell (Graph taken from [11]).

1.2.3 Materials for Solid Oxide Fuel Cells

The nature of the electrolyte not only determines the operating temperature but also the chemistry of the reactions occurring at the anode and the cathode. For conventional fuel cells YSZ is the state of the art material. Apart from the high ionic conductivity at 1000°C (σ_I=0.1 S/cm) YSZ also exhibits extraordinary mechanical properties and chemical resistance to the environment encountered in a fuel cell [12]. The main problem of this material is the high operating temperature necessary to enable the migration of oxygen vacancies through the electrolyte.

The anode of a fuel cell usually is a highly porous Ni-ceramic composite – a so-called cermet [13]. Cermets used in SOFCs need to be ionically and electronically conducting, should have a high porosity for unhindered gas flow to, and away from the reaction sites and

have to match the thermal expansion coefficient of the electrolyte material. The conventional material for anodes is NiO-YSZ. The NiO is reduced to metallic Ni when the fuel enters the anode chamber for the first time putting the cell into operation. When hydrocarbons are to be used as the fuel Cu-CGO cermets can be envisaged as anode material [14].

The cathode materials used in conventional fuel cells are mostly perovskites with high electronic conductivity and a high activity for the oxygen reduction reaction (Reaction (1.2)). For standard fuel cells operating at around 1000°C $La_{0.8}Sr_{0.2}MnO_{3-\delta}$ (LSM) is used, which is a good electronic conductor. If intermediate operating temperatures (around 800°C) are envisaged the use of $La_{0.8}Sr_{0.2}Co_{0.2}Fe_{0.8}O_{3-\delta}$ (LSCF) is advantageous. This material is a mixed ionic electronic conductor (MIEC), which together with the electronic conductivity also exhibits significant oxygen ion conduction. The triple phase boundary, where the cathodic reaction takes place, is enlarged when a MIEC cathode material is used. This lowers the polarisation losses at the cathode (η_C). If an SOFC is to be operated at very low temperatures around 500°C, $Sm_{0.5}Sr_{0.5}CoO_{3-\delta}$ (SSC) was found to be a suitable cathode material [15], however SSC is incompatible with YSZ. For low operating temperatures other electrolyte materials with higher ionic conductivity than YSZ must be used. Doped $LaGaO_3$ based perovskites exhibit high ionic conductivity at intermediate temperatures [16]. The highest conductivity was found for $La_{0.9}Sr_{0.1}Ga_{0.9}Mg_{0.1}O_3$ (LSGM). In recent time, gadolinia-doped ceria (CGO) electrolytes have raised increased interest as electrolytes for SOFCs operating at intermediate temperatures due to their high-ionic conductivity [17]. A summary of the current standard SOFC materials is given in Table 1-2.

Table 1-2 Materials for SOFC components.

Electrolyte	Cathode	Anode
YSZ	LSM	Ni-YSZ
CGO	LSCF	Ni-CGO
LSGM	SSC	Cu-CGO

1.2.4 Designs

The design of a single cell is closely related to the design of an entire stack. Because a single cell only delivers 1 V, a multitude of cells are usually connected in series for obtaining useful voltages. For practical applications this is done by constructing stacks, in which the individual cells are connected in series using interconnects. The OCV, i.e. the voltage of the

cell when no current is flowing, corresponds to the number of individual cells in the stack. SOFCs differ from the other types of fuel cells shown in Table 1-1 (AFC, PAFC, MCFC and PEM) because the operating temperature is much higher (>600°C) and no liquid electrolyte is used. Instead, the electrolyte is a solid, and thus, electrolyte management issues are of no concern for SOFCs. Over the last two decades SOFCs based on YSZ have been developed for an operating temperature range of 900-1000°C. The advantage of the high operating temperature is that internal reforming of hydrocarbons is possible directly on the anode without the need for an external reformer [18,19].

There are two basic designs for SOFC-stacks, the tubular design and the planar design, which are discussed in detail elsewhere [10,12,20,21]. The advantage of the tubular design is that it needs only to be sealed at the beginning of the tubes.

The cell configuration itself depends on the design of the stack. In SOFCs single cells can be classified into two broad categories: self-supporting and external-supporting [22]. In the self-supporting configuration, one of the cell components (mostly the thickest layer) acts as the cell structural support. Thus, self-supporting cells can be designed as electrolyte-supported, anode-supported, or cathode-supported fuel cells. In the external-supporting configuration, the single cells can be either supported by the interconnect or by a porous substrate. One of the most important design criterions for a functioning fuel cell is the separation of anode and cathode by a gas tight electrolyte. Pinholes or cracks in the electrolyte can cause the hydrogen to leak to the cathode compartment where it reacts directly with oxygen. This will decrease the open circuit voltage (OCV) and might even render the fuel cell inoperable. The phenomenon can occur in particular when very thin electrolyte films are used as in the case of anode-supported cells [23].

The development of a suitable stack sealant still presents a challenging task because the requirements for the sealants are stringent due to harsh environments and the high operating temperatures. Sealing of SOFCs can be done by using bonding seals or pressurized seals. For bonding seals materials like high-B_2O_3 glasses [24], earth-alkali silicate glasses such as $BaO{\cdot}Al_2O_3{\cdot}SiO_2$ [25] or glass ceramics are commonly used.

1.2.5 Current Fields of Research

One of the main problems of SOFCs is the high operating temperature leading to a high degradation rate of cell performance and the need for more expensive interconnect and sealing materials. The operating temperature of the cell is mainly determined by the electrolyte resistance. Two ways are possible to decrease the latter, either by using alternative electrolyte

materials with higher ionic conductivity or by decreasing the electrolyte thickness. The feasibility of doped ceria for low temperature fuel cells was demonstrated by Gödickemeier [26]. The cells exhibited low OCVs due to the mixed ionic electronic conductivity but showed high power output when current was flowing. Perednis et al. succeeded to deposit thin, gas tight YSZ electrolyte films by spray pyrolysis on porous anode-supports enabling an operating temperature of YSZ-based fuel cells of below 800°C [23,27].

The specific energy density of hydrogen is the highest of all fuels. However, the volumetric energy density is the lowest. The storage and transportation of H_2 is a problem yet to be tackled for implementing the hydrogen economy [28]. Although hydrogen is considered the ideal fuel for many energy-conversion systems, its widespread use is dependent on technological breakthroughs in its cost and storage. So it is best to assume that in the immediate future, fuel cells will have to use hydrocarbons (such as methane) or alcohols (such as ethanol) as fuel [2]. Ni-based anodes, however, have a too high catalytic activity for the cracking of hydrocarbons. Carbon is formed at Ni anodes at high temperature if not enough steam is added to the fuel leading to the degradation of the anode material. Cu has a lower activity for the cracking reaction and Cu-ceria anodes have been developed in order to solve the coking problem [29]. However, these anodes always performed worse with hydrocarbons than standard anodes running on hydrogen, the reason being the low catalytic activity of Cu. In a very recent work, Hibino operated fuel cells with dry methane at a fuel utilisation of 50% and obtained a maximum power output of 500 mW/cm^2. The cells of this study were based on CGO with anodes that contained less NiO than usually used (only 50 wt%). RuO_2 (3 wt%) had been added to the anode and was the reason for the resistance of the anode to carbon deposition and the good performance [30].

Another interesting field of research that is newsworthy, however in the field of PEM fuel cells is the development of portable, miniaturised fuel cells fabricated on silicon substrates. The miniaturised cells fabricated by Kelley et al. [31] were based on Nafion, and had been fabricated by conventional silicon microfabrication processes. Power densities were in the range of 20 mW/cm^2 with methanol as the fuel.

1.3 Single Chamber Solid Oxide Fuel Cells

One common feature about all fuel cells types (shown in Table 1-1) is the fact that they rely on the strict separation of the oxidant and the fuel in two gas-tightly sealed compartments (see Figure 1.4 a). This makes parasitic direct oxidation of the fuel impossible. Highly active

but unselective electrodes are employed because selective electrodes are not required; only one reaction is possible at each electrode: The reduction of oxygen at the cathode and the oxidation of fuel at the anode. Thus, the electrode materials do not need to be selective for the anodic or cathodic reactions. They only need to have a high activity for the reaction taking place. With electrodes being either selective for the oxidation of fuel (anode) or the reduction reaction of molecular oxygen (cathode) it is possible to expose both electrode to the same mixture of fuel and air (Figure 1.4).

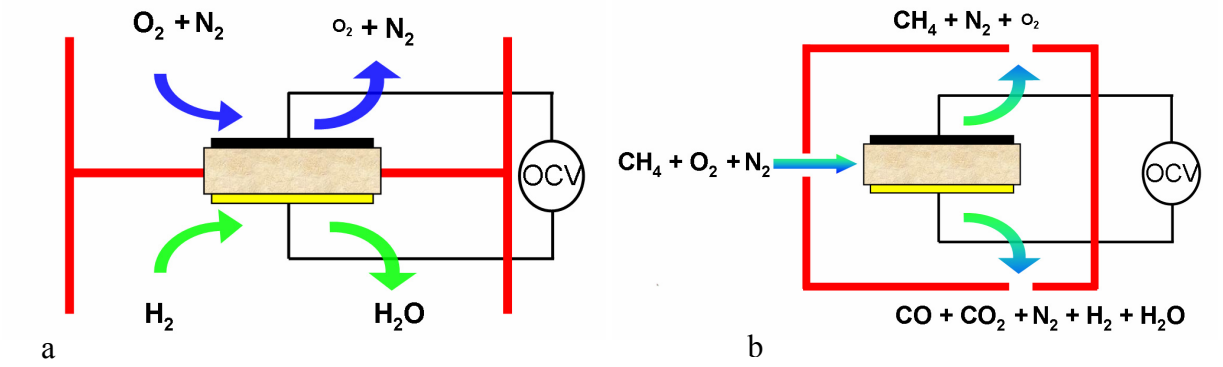

Figure 1.4 Comparison of a) conventional SOFCs and b) SC-SOFCs (see text).

An SOFC that satisfies this criterion does only need one gas compartment and is usually operated in a hydrocarbon-air mixture. Henceforth, such cells shall be referred to as single chamber solid oxide fuel cells (SC-SOFC) because they only have one gas compartment (thus, „single chamber“). Highly active standard materials used in conventional SOFCs like $La_{0.8}Sr_{0.2}MnO_{3-\delta}$ (LSM) $La_{0.8}Sr_{0.2}Co_{0.2}Fe_{0.8}O_{3-\delta}$ (LSCF), Ni-$Zr_{0.8}Y_{0.2}O_{1.9}$ (Ni-YSZ) can be used in SC-SOFCs, but they do not exhibit high enough selectivity at their ideal operating temperature, which leads to a low electrochemical performance. In principle the reactions at the two electrodes are the same for both types of SOFCs. Even so, in the SC-SOFC the selectivity of materials allows the omission of the gas separating membrane.

1.3.1 Potential Advantages Compared to “Double Chamber” SOFCs

No separation of fuel and oxidant is needed in the single chamber design. Complex flow field structures can be omitted and the sealing of the cells from the surroundings is more easily achieved. Apart from the conventional fuel cell designs (planar and tubular) a variety of novel geometries becomes possible. The electrodes can be placed on the same side of the

electrolyte surface being separated by a narrow gap. Fully porous cells can also be envisaged, because the electrolyte needs not to be gas tight. However, the electrolyte must physically separate the anode and cathode for avoiding an internal short circuit. The connection of several cells in parallel and in series on the same electrolyte disc is possible. Practically useful voltages and currents can be reached without the need for a cell stack. In addition the single chamber approach offers great advantages for miniaturisation. As compared to "double chamber" cells, only half the number of gas flow channels is needed and the micro sealing of separate cells is not necessary. Furthermore, the difficulty of having to make two separate gas chambers on the micrometer scale can be circumvented.

1.3.2 Challenges of SC-SOFCs

The operation of the SC-SOFCs relies on the selectivity of the electrodes. Conventional fuel cell materials like LSM, LSCF and Ni-YSZ are unsuitable because they only have a high catalytic activity without the necessary selectivity, especially at high operating temperatures. Selective materials must be found for the future generation SC-SOFCs. Further challenges of the single chamber configuration are that mixtures of fuel and air can be explosive and that it could be difficult to obtain high fuel utilisations, comparable to those reached with conventional SOFCs. In addition parasitic, non-electrochemical reactions will decrease the efficiency and heat the device to higher than the targeted operating temperature.

1.4 References

[1] E. Baur and H. Preis, *Zeitschrift für Elektrochemie*, **1937**, 43, *9*, 727-732.

[2] B. C. H. Steele, *Nature*, **1999**, 400, 619-621.

[3] H. Yokokawa, N. Sakai, T. Horita and K. Yamaji, *Fuel Cells*, **2001**, 1, *2*, 117-131.

[4] G. Cacciola, V. Antonucci and S. Freni, *Journal of Power Sources*, **2001**, 100, *1-2*, 67-79.

[5] F. Tietz, H.-P. Buchkremer and D. Stover, *Solid State Ionics*, **2002**, 152-153, 373-381.

[6] T. Nakamura, G. Petzow and L. J. Gauckler, *Materials Research Bulletin*, **1979**, 14, *5*, 649-659.

[7] M. Sahibzada, B. C. H. Steele, D. Barth, R. A. Rudkin and I. S. Metcalfe, *Fuel*, **1999**, 78, *6*, 639-643.

[8] J. W. Fergus, *Materials Science and Engineering A*, **2005**, 397, *1-2*, 271-283.

[9] W. G. Coors, *Journal of Power Sources*, **2003**, 118, *1-2*, 150-156.

[10] J. Larminie and A. Dicks, "Fuel Cell Systems Explained", 1st ed., Wiley, New York, 2001.

[11] J. Will, A. Mitterdorfer, C. Kleinlogel, D. Perednis and L. J. Gauckler, *Solid State Ionics*, **2000**, 131, *1-2*, 79-96.

[12] N. Q. Minh, *Journal of the American Ceramic Society*, **1993**, 76, *3*, 563-588.

[13] A. Atkinson, S. Barnett, R. J. Gorte, J. T. S. Irvine, A. J. McEvoy, M. Mogensen, S. Singhal and J. M. Vohs, *Nature*, **2004**, 3, 17-27.

[14] M. B. Jörger, "CuO-CGO Anodes for Solid Oxide Fuel Cells", Ph.D. Thesis, Diss. ETH No. 15351, Swiss Federal Institute of Technology, 2004.

[15] C. Xia, W. Rauch, F. Chen and M. Liu, *Solid State Ionics*, **2002**, 149, *1-2*, 11-19.

[16] T. Ishihara, H. Matsuda and Y. Takita, *Journal of the American Chemical Society*, **1994**, 116, *9*, 3801-3803.

[17] H. Inaba and H. Tagawa, *Solid State Ionics*, **1996**, 83, *1-2*, 1-16.

[18] S. H. Clarke, A. L. Dicks, K. Pointon, T. A. Smith and A. Swann, *Catalysis Today*, **1997**, 38, *4*, 411-423.

[19] A. L. Dicks, *Journal of Power Sources*, **1998**, 71, *1-2*, 111-122.

[20] O. Yamamoto, *Electrochimica Acta*, **2000**, 45, *15-16*, 2423-2435.

[21] S. C. Singhal, *Solid State Ionics*, **2002**, 152-153, 405-410.

[22] N. Q. Minh, *Solid State Ionics*, **2004**, 174, *1-4*, 271-277.

[23] D. Perednis, K. Honegger and L. J. Gauckler, in *Fourth European Solid Oxide Fuel Cell Forum, 2000,* A. McEvoy, 819-824.

[24] K. L. Ley, M. Krumpelt, R. Kumar, J. H. Meiser and I. Bloom, *Journal of Materials Research*, **1996**, 11, *6*, 1489-1493.

[25] K. Eichler, G. Solow, P. Otschik and W. Schaffrath, *Journal of the European Ceramic Society*, **1999**, 19, *6-7*, 1101-1104.

[26] M. Gödickemeier, "Mixed Ionic Electronic Conductors for Solid Oxide Fuel Cells", Ph.D. Thesis, Diss. ETH No. 11348, Swiss Federal Institute of Technology, 1996.

[27] D. Perednis, M. B. Joerger, K. Honegger and L. J. Gauckler, in *Solid Oxide Fuel Cells VII (SOFC VII),* H. Yokokawa and S.C. Singhal, 989-993.

[28] S. Dunn, *International Journal of Hydrogen Energy*, **2002**, 27, *3*, 235-264.

[29] S. Park, J. M. Vohs and R. J. Gorte, *Nature*, **2000**, 404, 265-267.

[30] T. Hibino, A. Hashimoto, M. Yano, M. Suzuki and M. Sano, *Electrochimica Acta*, **2003**, 48, *17*, 2531-2537.

[31] S. C. Kelley, G. A. Deluga and W. H. Smyrl, *AIChE Journal*, **2002**, 48, *5*, 1071-1082.

2 Aim of the Thesis

2.1 Background

Solid oxide fuel cells (SOFCs) offer the advantage of efficient and non-polluting electricity generation. In the past 10 years, rapid progress has been made in the materials and the technology of SOFCs. However, because of the high costs, the SOFC-technology is still in a pre-commercial state. Many companies such as Hexis, Siemens-Westinghouse and Roll-Royce are currently developing solid oxide fuel cell systems with the main objective to reduce the costs and to improve the long-term stability. The two main reasons for the high costs of SOFC-system are the rather complicated system designs with the necessity for gas tight separation of the anode and cathode compartments and the use of brittle and expensive ceramic materials.

In spite of extensive technological investigations for improving the existing types of SOFCs (tubular or planar) it is doubtful whether all the possible designs for SOFCs have yet been recognized. In the search of alternative concepts, it became clear that single chamber solid oxide fuel cells (SC-SOFCs) offer the substantial advantage of a drastically simplified design at reasonable power densities comparable to conventional SOFCs. Furthermore, single chamber systems are highly suited for portable applications (up to 20 W), because of much easier thermal management.

2.2 Objectives

The aim of this work is to assess the concept of single chamber solid oxide fuel cells operated in CH_4-air mixtures and to gain a fundamental understanding of this type of fuel cell. In a first step, calculations of the thermodynamic equilibrium concentrations of gas-constituents from methane-air mixtures are addressed. The knowledge of the thermodynamic equilibrium is a valuable tool for finding suitable SC-SOFC operating conditions and helps to understand the relation between the thermodynamic equilibrium and the observed behaviour of the cells in terms of open circuit voltage and power output.

In a second step the kinetics of the different reactions at the anode and the cathode of SC-SOFCs toward the thermodynamic equilibrium is investigated. The measurement of

catalytic activities of single chamber electrodes can provide valuable information for understanding the electrochemical behaviour of SC-SOFCs.

In order to asses the feasibility of SC-SOFCs, the appropriate preparation steps and the electrochemical characterisation are established by trying to reproduce the results known from literature with standard ceramic materials. With these materials and methods the influence of the anode thickness on the electrochemical performance of SC-SOFCs are investigated.

Then a proof of concept for two novel cell designs is done in order to see if the expected advantages can be observed in practice and if these designs are feasible. Micro SC-SOFCs with side by side placement as well as fully porous SC-SOFCs with a flow-through configuration are envisaged. For micro SC-SOFC the expected advantages are the low resistance between the electrodes being only separated by a very narrow gap in the range of a few micrometers. The fully porous design in theory allows for higher fuel utilisations, if the electrodes are close to being perfectly selective.

2.3 Scope

A comprehensive review of the state of the art single chamber fuel cell technology is given in Chapter 3. The thermodynamic considerations of methane-air mixtures will be presented in Chapter 4, followed by the kinetic studies of the reactions at SC-SOFC electrodes in Chapter 5. In Chapter 6 the preparation and characterisation of SC-SOFCs with a classic sandwich design are addressed. The investigation concerning the influence of anode thickness (Chapter 7) is followed by the proofs of concepts for the micro-SC-SOFC (Chapter 8) and the fully porous cell with a flow-through configuration (Chapter 9). All the chapters of this thesis are stand alone pieces of information. For each chapter the necessary experimental and theoretical background as well as the literature is included separately as some chapters are already submitted for publication. Due to this structure repetitions and redundancy cannot be avoided in this thesis.

3 State of the Art: Single Chamber Solid Oxide Fuel Cells

B. E. Buergler and L. J. Gauckler, to be submitted.

ABSTRACT: Fuel cells have been in the focus of interest for many years and the investigations have gone into great detail. Issues of material selection, processing, design, operating conditions, fuels and ageing have been addressed in many scientific papers. However, research in the field of solid oxide fuel cells has concentrated on conventional cells that rely upon the separation of the fuel and the oxidant. An alternative concept is to expose the anode and the cathode of the fuel cell to one and the same gas-mixture composed of fuel and air in a non-equilibrium state. In this chapter the recent achievements and the current understanding of single chamber solid oxide fuel cells are reviewed. In the first part the early stages of this technology and how it evolved are summarised. In the second part, some of the most important, recent results are summarised.

3.1 Definition and Terminology

A single chamber solid oxide fuel cells (SC-SOFCs) is an all solid state electrochemical device that operates at elevated temperatures in uniform mixtures of fuel and oxidant and can directly convert the chemical energy of the gas mixture into heat and electric energy by the use of reaction selective electrodes.

SC-SOFCs can be understood as fuel cells with only one gas compartment (thus, „single chamber“). In conventional fuel cells of any type, the oxidant and the fuel are usually separated by a gas tight electrolyte, thus the cells have a gas compartment for each electrode. The operation of a SC-SOFC relies on the selectivity of the cathode and the anode, which are both exposed to the same gas mixture of fuel and air. The fuel is usually a hydrocarbon and the oxidant mostly air. Hydrogen-air mixtures could in theory also be used but are unfeasible for SOFCs because of their high operating temperature and the resulting danger of explosions. The question of fuels for SC-SOFCs will be addressed in section 3.5.1.

The expression “Single Chamber” was introduced in 1999 by Hibino [1], who made a substantial contribution to the development of this technology. Nowadays single chamber solid oxide fuel cell (SC-SOFC) is the common term most researchers have agreed upon. Many other expressions have been created for what in this work is referred to as a single chamber fuel cell (SCFC). Expressions like “One-chamber Fuel Cell” [2] “Mixed Gas Fuel Cell” (MGFC) [3], “Compact-Mixed-Reactant Fuel Cell” (CMR) [4] or “Fuel Cells with Reaction Selective Electrodes” [5] have also been used in the past. In principle any fuel cell type could work in the single chamber configuration. However, the concept has to date only been proven for direct methanol fuel cells [6] that belong to the class of PEMs and for solid oxide fuel cells.

3.2 Principle of Operation

Any hydrocarbon from methane to butane can be mixed with air and serve as the gas mixtures for SC-SOFCs. Methane was used throughout this work and is used here for elucidating how a SC-SOFC functions. Methane-air mixtures are unambiguously characterised by the ratio of methane to oxygen ratio. In the following the ratio CH_4/O_2 will be denominated x. The operation of a SC-SOFC is based on the different catalytic activities of the anode and cathode for the partial oxidation methane [7-9], shown in Reaction (3.1).

$$CH_4 + \tfrac{1}{2}O_2 \xrightarrow{rr_{CO}} CO + 2H_2 \qquad (3.1)$$

This is a purely chemical reaction occurring on the metallic Ni in the top layers of the SC-SOFC anode, which is usually a Ni-cermet like Ni-CGO. At the anode the reaction rate for Reaction (3.1), rr_{CO}, is high and at the cathode the reaction rate should be ideally zero. Reaction (3.1) creates a very low oxygen partial pressure $p_A(O_2)$ at the interface anode/electrolyte in the range of 10^{-20} atm (see Figure 3.1). Due to the negligible catalytic activity of the cathode for Reaction (3.1), the oxygen partial pressure $p_C(O_2)$ at the interface cathode/electrolyte is roughly the same as in the gas phase (0.15 atm for x=2 and 0.17 atm for x=1). An oxygen concentration cell is formed by the different oxygen partial pressures at the anode/electrolyte and cathode/electrolyte interface and the OCV can be described by the Nernst equation:

$$OCV = -\frac{\Delta G}{nF} = \frac{RT}{nF}\ln\frac{p_C(O_2)}{p_A(O_2)} \qquad (3.2)$$

The OCV of a SC-SOFC therefore depends on two parameters: 1) How fast the partial oxidation (Reaction (3.1)) proceeds at the anode, because this determines $p_A(O_2)$. 2) How tolerant is the cathode to the fuel. This determines how much oxygen actually reaches the cathode/electrolyte interface ($p_C(O_2)$). The OCV is a measure of the driving force for the electric current through the external circuit at zero current. When current is flowing through the cell, the two formed gaseous species CO and H_2 react electrochemically

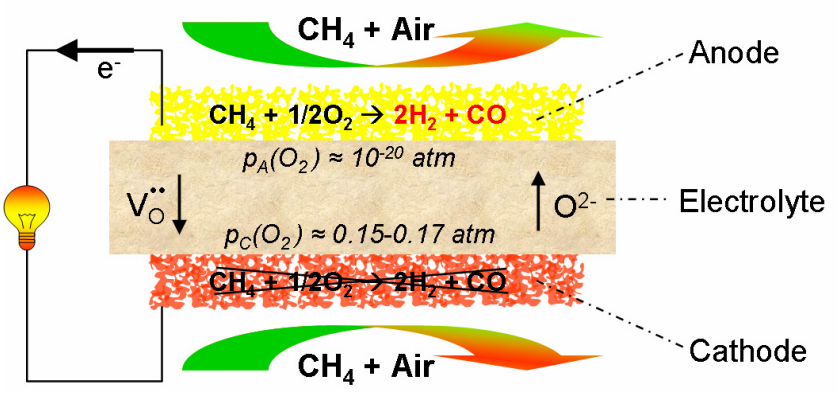

Figure 3.1 Schematic of the operating principle of a SC-SOFC in methane air mixtures.

with oxygen ions O_O^x from the bulk electrolyte at the anode/electrolyte interface according to Reactions (3.3) and (3.4). Using the Kröger-Vink notation it follows:

$$H_2(g) + O_O^x \rightarrow H_2O(g) + V_O^{\bullet\bullet} + 2e^- \tag{3.3}$$

$$CO(g) + O_O^x \rightarrow CO_2(g) + V_O^{\bullet\bullet} + 2e^- \tag{3.4}$$

The oxidation of H_2 and CO is accompanied by the formation of electrons (e^-) and oxygen vacancies ($V_O^{\bullet\bullet}$). At the cathode only the reduction of the oxygen from the methane-air mixture should take place (Reaction (3.5)), consuming the electrons that have flown through the electrical circuit and emerged at the anode by the oxidation of H_2 and CO.

$$\tfrac{1}{2}O_2(g) + V_O^{\bullet\bullet} + 2e^- \rightarrow O_O^x \tag{3.5}$$

Oxygen vacancies ($V_O^{\bullet\bullet}$) are annihilated at the cathode by the reaction with gaseous oxygen. For every annihilated vacancy a pair of electrons is consumed. This reaction leads to the formation of regular oxygen ions O_O^x in the crystal lattice at the surface of the electrolyte.

It was stated that the operation principle of a SC-SOFC is based on the different catalytic activity of the electrode materials for the partial oxidation of methane, Reaction (3.1). If we postulate that H_2 and CO are oxidised electrochemically both at the anode and the cathode at the same rate as the preceding partial oxidation at each electrode, then only the difference of the reaction rates (Δrr_{CO}) of the anode and cathode will lead to an ionic current in the electrolyte (Equation (3.6)). Thus, the higher Δrr_{CO}, the higher the ionic current in the electrolyte will be. For every partially oxidised CH_4, as shown in Reaction (3.1), one CO- and two H_2-molecules are formed. In a subsequent step they are electrochemically oxidised as shown in Reaction (3.7).

$$\Delta rr_{CO} = rr_{CO}^A - rr_{CO}^C \tag{3.6}$$

$$CO + 2H_2 + 3O^{2-} \xrightarrow{\Delta rr_{CO}} CO_2 + 2H_2O + 6e^- \tag{3.7}$$

For every partially oxidised CH_4, $6e^-$ can be released. Now the current J that flows through the external circuit can be calculated by using the following equation:

$$J = 6q \cdot N_A \cdot \Delta rr_{CO} = 6F \cdot \Delta rr_{CO} \tag{3.8}$$

where q is the elementary charge, N_A Avogadro's Number and F Faraday's constant (96'485 Cb). In a CH_4-air mixture there is another, undesired reaction that can occur; the full oxidation of methane:

$$CH_4 + 2O_2 \rightarrow CO_2 + 2H_2O \tag{3.9}$$

The full oxidation of CH_4 can occur at both electrodes or at any surface that is exposed to the gas mixture at high temperatures. Since this is a purely chemical reaction with no contribution to generating electric current it is considered a parasitic reaction. In SC-SOFC anodes a competitive situation of reactions exists, which is influenced by the initial gas composition, the temperature, the activation energies of the reactions and also the dynamic parameters, such as flow rate or current through the cell. Other reactions that are occurring in the anode are the steam reforming Reaction (3.10) and the water gas shift Reaction (3.11). Steam reforming is highly endothermic and is thermodynamically possible at temperatures above 630°C. The advantage of the steam reforming reaction for SC-SOFCs is that it allows the generation of additional hydrogen by the reaction of remanent CH_4 with H_2O that is formed by the electrochemical oxidation of H_2 with oxygen ions. Since steam reforming is highly endothermic, it would seem possible that this reaction can limit the overheating of SC-SOFC anodes, which is caused by the exothermic oxidation reactions shown in Reaction (3.1) and Reaction (3.9).

$$CH_4 + H_2O \rightarrow CO + 3H_2 \tag{3.10}$$

$$CO + H_2O \rightarrow CO_2 + H_2 \tag{3.11}$$

Electrochemical CO-oxidation is much slower as compared to electrochemical H_2-oxidation on Ni-catalysts [10]. Therefore, the water gas shift reaction shown in Reaction (3.11) has a drastic impact on the performance of SC-SOFCs because H_2O can indirectly oxidise the CO, which is formed by the partial oxidation of CH_4. For ceria supported Pt-catalysts the water gas shift reaction can approach the thermodynamic equilibrium at very high reaction rates for temperatures as low as 380°C [11], thereby increasing the amount of available hydrogen fuel. When hydrocarbons are used as the fuel for SOFCs, there is the possibility of carbon deposition, which is also called coking. The high oxygen content of the used hydrocarbon-air mixtures for SC-SOFCs, however, makes carbon deposition unfavourable, which is why we will not consider it here. A concise thermodynamic treatment of all the reactions occurring with methane as the fuel is to be found elsewhere [12].

3.3 A Brief History of Single Chamber Fuel Cells

The beginning of single chamber fuel cells goes back to the early work of nuclear fission where the possibility of radiolytic splitting of water and subsequent recombination of the H_2 and O_2 mixture to generate electricity was discovered [4]. In 1961 Eyraud et al. [13] described an electrochemical device that operated in H_2-O_2 mixtures using the condensed moisture on a porous Al_2O_3-film as the electrolyte. In humid air the Ni-Al_2O_3-Pd cell showed a voltage of -350 mV and in H_2-O_2 mixtures +600 mV. The device was in essence what Dyer described 30 years later [14], but with much lower electrolyte conductivity. The resistance greatly depended on the nature of the electrolyte material, the relative humidity, the temperature and the gas phase. Eyraud et al. found that the adsorbed water was responsible for the ionic conduction of the film and that the addition of NH_3 to the gas mixture reduced the resistance by a factor of 100.

In 1965 Van Gool extended the previous work to the idea of a “surface-migration cell” [15]. His theoretical work states the importance of surface-migration and heterogeneous catalysis for fuel cells operating in gas-mixtures. Let us consider the exothermic, heterogeneous reaction $A + B \rightarrow AB$. All the species in this reaction are gaseous and the reaction is catalysed on a solid surface. A single phase catalyst (Figure 3.2 a) for the reaction of A and B is less efficient than a catalyst with three phases (Figure 3.2 b) because of the distribution of the subsequent reaction steps to different materials. When the materials (M_2 and M_3) are selective the oxidation and reduction reactions are spatially separated. If the support material (M_1) allows the diffusion of adsorbed ions but is electronically insulating and

two electrodes are prepared as shown in Figure 3.2 c, an electromotoric force will build up between the two electrodes which is related to the free energy of the reaction A + B → AB. In this way a "surface-migration cell" is formed.

The choice of electrode materials is intricate: They should allow specific chemisorption of one of the reaction components, should be resistant to the reactants and the reaction products and should not catalyse the direct, non-electrochemical reaction. At least one of the reactants should be able do migrate via the electronically insulating electrolyte surface in an ionic form. If the "surface-migration cell" is compared with an SOFC the absence of mass transport through porous electrodes and the use of the much faster surface-migration as compared to bulk ionic conduction may be an important advantage.

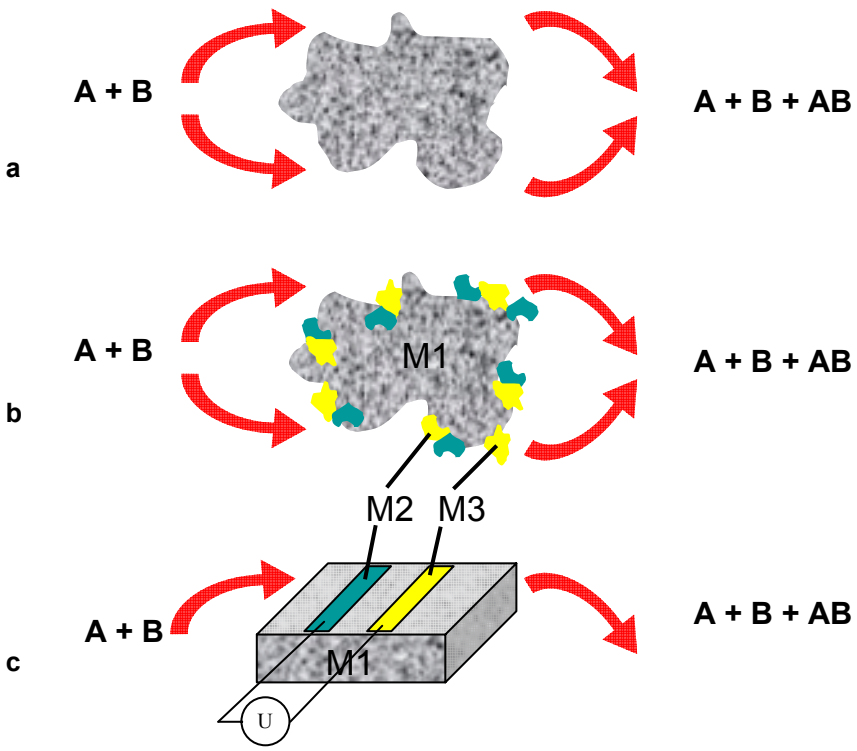

Figure 3.2 Van Gool's idea of the possible use of surface-migration in fuel cells and heterogeneous catalysis. a) Single phase catalyst, b) three phase catalyst with the materials M_2 and M_3 being selective for either A-adsorption or B-adsorption. The electrons flow from M_2 directly to M_3 because the isles of the two materials are short-circuited c) electron flow through an external circuit in a fuel cell with surface-migration [15].

In 1991 Dyer was able to generate electric power from a device with two electrodes made of platinum separated by a thin, ion conducting and porous film [14,16]. The device was supported by a quartz substrate onto which the three functional layers were deposited. Sputtering Aluminium and subsequently transforming the metal to pseudo-boehmite in boiling water yielded the ion conducting electrolyte. These two steps were repeated until the

film had a thickness of about 50 nm. Figure 3.3 shows a scheme of the cell that operated in a mixture of hydrogen and oxygen gas and generated a voltage of up to 1 V at room temperature. The effect was neither thermoelectric nor could it be attributed to a selective gas transport of the membrane. The latter mechanism could be excluded, because when the outer electrode was made of nickel and the inner one of platinum, the polarity of the cell changed. The observed voltages were explained by the electrodes' difference in electrochemical kinetics and the possible difference of local gas ratio depending on the different gettering rates on the different metals.

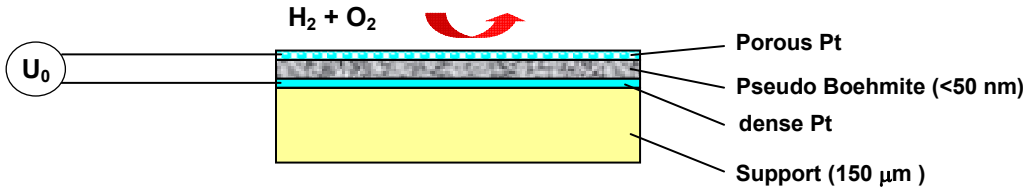

Figure 3.3 The electrochemical device that was described by Dyer [14].

The achieved power density was in the range of 1-5 mW/cm^2 but because the cells were made of very thin films, the *specific* power density with this cell design could easily exceed 100 W/kg.

In Figure 3.4 the number of scientific papers on single chamber fuel cells versus time beginning with the paper by Eyraud in 1961 [13] until today is shown. At total of forty-one scientific papers have been published about SC-SOFCs since then and the rate is increasing.

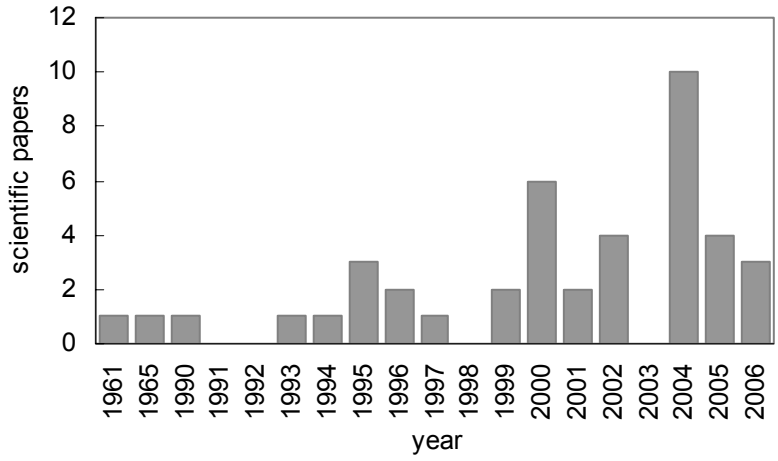

Figure 3.4 Number of scientific papers dealing with single chamber fuel cells since 1961.

For comparison; since the year 2000 the estimated number of scientific papers dealing with SOFCs is more than one thousand per year and the rate is still increasing. Four out of six papers from the year 2000 shown in Figure 3.4 were published by Hibino et al. [2,17-19]. To this day, 2004 was the year with the most publications about SC-SOFCs [6,20-28]. The trend of increasing number of papers over the past few years shows that there is an increased interest in this quite new technology, which is most certainly due to the high power output of SC-SOFCs combined with the substantially simplified cell design.

3.4 The Contribution of Hibino and Co-workers

Hibino had been working on SC-SOFCs for more than ten years [1,2,7,9,17-19,29-33]. The main results from his research are summarised in Figure 3.5 in terms of maximum power density (P_{max}), OCV and operating temperature (T). Three of the papers that are included in Figure 3.5 were published by Asano et al. [8,34,35]. The first cell described in 1993 [7] was based on a YSZ electrolyte with Ni-YSZ anode and Au-cathode.

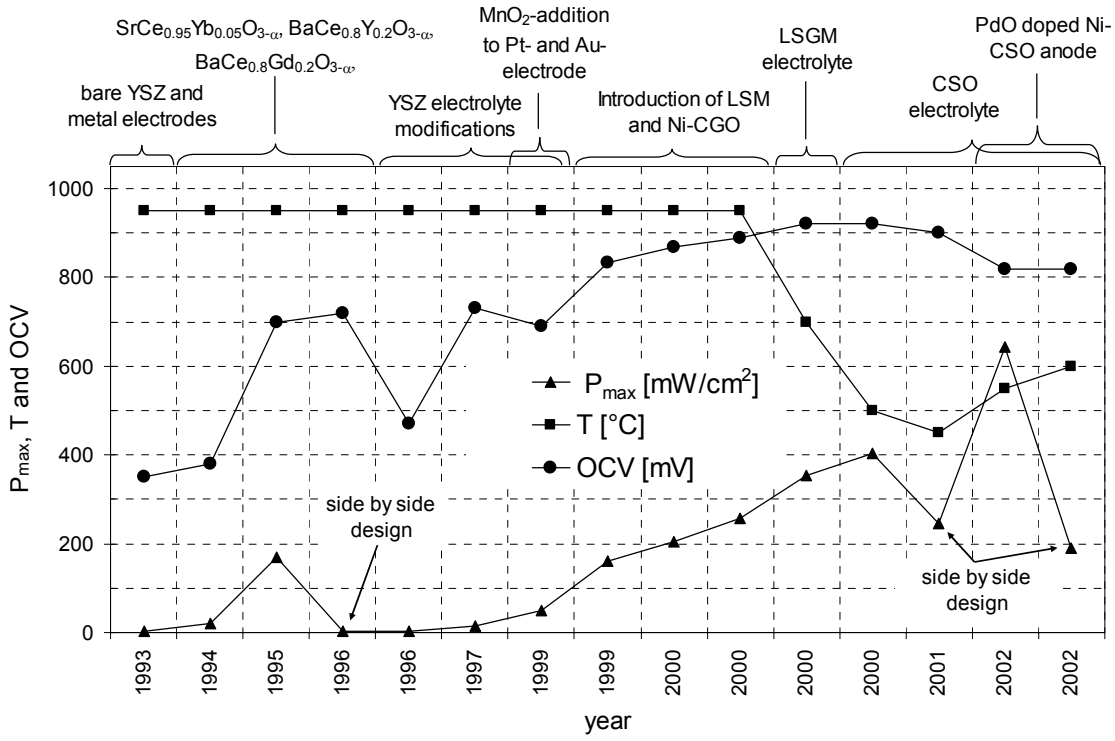

Figure 3.5 The progress and main results of the SC-SOFC research by Hibino et al. over time [1,2,7-9,17-19,29-36]. Methane had been used as the fuel up to the year 2000. The use of higher hydrocarbons became possible in 2000 with the reduction of the operating temperature by the introduction of CSO, a low temperature electrolyte material.

At a flow rate of 210 ml/min methane-air ($CH_4/O_2 = 2$) at an operating temperature of 950°C, the cell gave a stable OCV and similarly low power densities (2.36 mW/cm^2) as the cells described by Dyer [14]. The other cells from the early nineties consisted of Au-cathodes, Pt- or Pd-anodes both prepared by applying and sintering commercial pastes on the two sides of electrolyte discs, 0.5 mm in thickness. The standard electrolyte material for SOFCs, yttria stabilised zirconia (YSZ), was used up to the year 2000. Because of the high ohmic resistance of the electrolyte very high operating temperatures had to be chosen (950°C). Other electrolytes like $SrCe_{0.95}Yb_{0.05}O_{3-\alpha}$, $BaCe_{0.8}Y_{0.2}O_{3-\alpha}$ and $BaCe_{0.8}Gd_{0.2}O_{3-\alpha}$ were employed as well and led to higher OCVs and slightly enhanced performances [8,29,30]. The peak of P_{max} in 1995 (see Figure 3.5) was due to the use of $BaCe_{0.8}Y_{0.2}O_{3-\alpha}$ as electrolyte [8]. The Au-electrode seemed to adhere better on this material, which improved the power output by reducing the overpotential of this electrode.

In 1996 [30] the side by side placement of electrodes (see section 3.6) was applied in SC-SOFCs for the first time. A Pd/$BaCe_{0.8}Gd_{0.2}O_{3-\alpha}$/Au cell was evaluated and it was found that the performance of the cell improved, when the gap between the two electrodes was decreased. The surface roughness also affected the resistance between the two electrodes. A rough surface between the two electrodes caused the resistance to be higher as compared to the case when a highly polished substrate was used. $BaCe_{0.8}Gd_{0.2}O_{3-\alpha}$ was not stable in the used CH_4-air mixture and formed $BaCO_3$ at the surface of the rough electrolyte. Metallic electrodes were used by Hibino up to 1999 and OCVs and maximum power densities could be improved by modifying the YSZ electrolyte by doping with MnO_2 [31], TiO_2 [34], or Pr_6O_{11} [35]. The idea behind these studies was to reduce the overpotential of previous cells' electrodes by doping the electrolyte and thereby making the electrolyte slightly electronically conducting. This may have increased the triple phase boundary length and therefore allowed an improved performance. In addition multivalent cations at the interfaces may lead to altered reaction paths without changing the overall cell reaction, thereby behaving as an electrocatalyst. The metallic electrodes that were modified with MnO_2 showed improved performance (50 mW/cm^2) [31]. It seems that the performance could be improved to some extent, also by the impeded sintering of the metal grains in the electrodes due to the presence of MnO_2, which led to an increase of catalytically active electrode surface area.

In the year 1999 the standard SOFC materials Ni-$Ce_{0.8}Gd_{0.2}O_{1.90}$ (anode) and $La_{0.8}Sr_{0.2}MnO_{3-\delta}$ (LSM, cathode) were introduced and from then on, the power output as well as the OCV were continuously improved. Further work included the use of Ni-cermets with

$Ce_{0.8}Gd_{0.2}O_{1.9}$ (CGO) or $Ce_{0.8}Sm_{0.2}O_{1.9}$ (CSO) as the anode on YSZ-electrolyte. Doping the YSZ-electrolytes and the LSM-cathode with MnO_2 enhanced the catalytic activity and additionally reduced the cathode overpotential as in the case of SC-SOFCs with metallic electrodes. This led to further improvement of the cell performance. Due to the use of YSZ the operation temperature was still at a high level of 950°C.

In the second last publication of 2000, Hibino et al. used a $La_{0.9}Sr_{0.1}Ga_{0.8}Mg_{0.2}O_3$ (LSGM) electrolyte, which is known to be a good ion conductor at intermediate temperatures from 500-800°C [37]. A reasonably high power output of 350 mW/cm^2 could be obtained with the prepared cell at a reduced temperature of 700°C [19]. Due to the lower temperature the OCV had a relatively high value of 920 mV.

In quite recent work, Hibino et al. employed CSO, a low temperature solid electrolyte with mixed ionic electronic conductivity as the electrolyte material for SC-SOFCs [9]. The electrode materials were 30 wt% CSO-containing Nickel anode with 6 wt% PdO (as a catalytic modifier) and $Sm_{0.5}Sr_{0.5}CoO_{3-\delta}$ (SSC) as the cathode. An electrolyte pellet of 150 μm thickness allowed a low operating temperature of only 550°C. Again a methane-air mixture was used with different CH_4/O_2 ratios (x). CH_4-air mixtures had been used in all of the previous work with a flow rate of 300 ml/min. The voltage-current characteristic of this measurement, with the highest area-specific power output measured to this day for electrolyte supported SC-SOFCs, is shown in Figure 3.6.

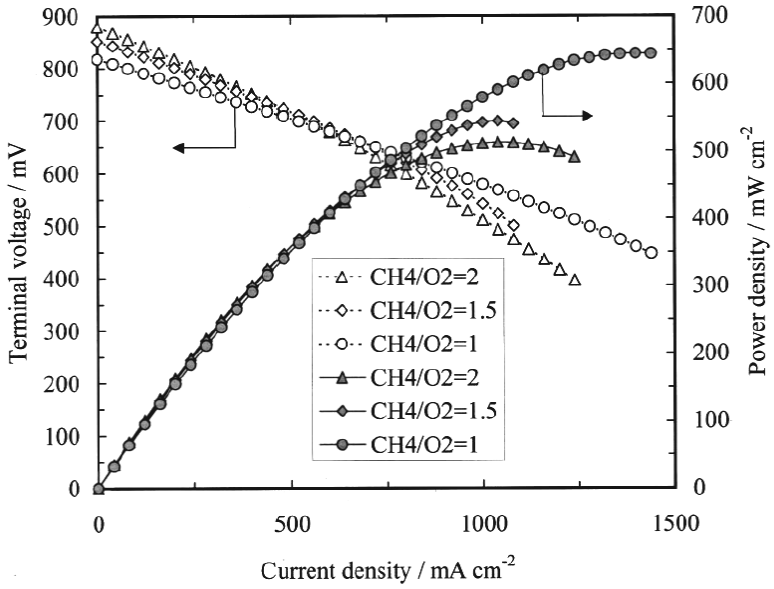

Figure 3.6 Voltage-current characteristic of a Pd-Ni-CSO/CSO/SSC SC-SOFC [9]. The cell had Pt current-collectors for the anode and Au current-collectors at the cathode. The effective temperature of the cell was probably higher due to the pronounced catalytic activity of Pt for the highly exothermic combustion reaction of CH_4 at the anode (see section 3.5.3).

The power density that could be achieved with this fuel cell was 644 mW/cm^2 at 550°C (furnace temperature), which is in the range of the values achieved by conventional two chamber fuel cells at much higher temperatures. The power output of the cells increased in the order x = 2, 1.5 and 1. This might have been due to a higher effective cell temperature with decreasing x-value due to a more pronounced full oxidation of CH_4. Nevertheless, with this work by Hibino et al. it has been demonstrated that SC-SOFCs can generate sufficient power for practical applications. This scientific paper was the last of one Hibino et al. about SC-SOFCs [9] and in the year 2003, there was no publication about the subject (see Figure 3.4).

One of the most important contributions of Hibino et al., was that he could attribute the functioning principle of SC-SOFCs to the difference of partial oxidation of methane of anode and cathode materials [7]. This was possible by mounting the cell in a setup with two separate gas compartments for the anode and the cathode. Both compartments were exposed to the same flow rate of CH_4-air and it was found that the cathode was inactive towards the fuel but the anode led to high concentrations of CO and H_2 in the outlet gas. Up to the year 1999, metallic electrodes were used and this led to poor performance due to the very high overpotential of the electrodes (especially the Au-cathode). Doping the metal electrodes only impeded the strong sintering of the metal-grains as can be seen clearly from the SEM micrographs published in 1999 [31]. In the same year the use of Ni-CGO as anode and LSM as the cathode material for SC-SOFCs was reported, which improved P_{max} by more than a factor of three. This was an important step for improving SC-SOFCs. In the year 2000 Hibino et al. tried to reduce the operating temperature of the cells by using electrolytes that have a higher ionic conductivity. In a first step LSGM was used [19] and reduced the operating temperature to 700°C and in a second step CSO was introduced. This was a mandatory step for increasing the performance of SC-SOFCs. The reduction of the cell temperature allowed for lower parasitic oxidation rates at the cathode and therefore a higher oxygen partial pressure at the cathode. This can increase the driving force for the oxygen ion current through the cell, which in turn allowed for higher power densities.

Hibino et al. also found that the operating temperature of SC-SOFCs can be reduced when using a more reactive hydrocarbon than methane. Fuel-air mixtures with ethane [33], propane [18], butane or with the even more reactive isobutane [19] were evaluated as the mixtures for SC-SOFCs. If those fuels would have been used with cells based on YSZ at 950°C there would have been a severe coking of the fuel cell anodes.

An utmost important finding was that there is a large amount of heat that is generated at the anode due to the exothermic oxidation of the fuel. The actual anode temperature could be more the 200°C higher than the temperature of the furnace [32]. This result indicated that it can be quite difficult to measure the actual operating temperature of a SC-SOFC anode. Actually, one would have to use a pyrometer to accurately measure the temperature of Ni-cermet electrode. There are large thermal gradients and by using a thermocouple very closely placed to the electrode, the measured temperature can be lower than the "real" anode temperature [38].

One problem that becomes important when the operating temperature of SC-SOFCs is to be reduced, is the reduction of NiO to metallic Ni in the anode material. Hibino et al. found that when certain catalytic modifiers are added to the anode, the reduction of the NiO occurs at lower temperatures. As compared to an unmodified NiO-CGO anode, with PdO-doping the operation of the cell became possible at temperatures as low as 550°C. For the cell with unmodified anode the OCV was 0.11 V indicating that the NiO was not reduced to metallic Ni, whereas for the doped anode 0.9 V could be obtained [9]. One important parameter that was not studied by Hibino et al. is the anode-thickness. Since the anode functions both as a chemical reactor for the partial oxidation of the fuel and also electrochemically oxidises the hydrogen-fuel, the anode thickness has a major impact on the performance of SC-SOFC, which needs to be elucidated.

3.5 Progress in SC-SOFCs after the Year 2003

In the year 2004 ten scientific papers were published on the subject of SC-SOFCs. Stefan et al. [26] prepared cells that were similar to those of Hibino [18] and tested them in different gas flow configurations: 1) in a closed end tube 2) in an open tube with the flow of propane-air mixture parallel to the electrolyte disc 3) in a perpendicular configuration to the gas inlet tube, cathode first and 4) anode first. They showed that there is a strong influence of the test chamber configurations on the OCV as well as the power density of the cell, probably because the different configurations led to different gas compositions at the electrodes. It was concluded that the configuration where the anode is exposed to the gas flow first, should be avoided, because it led to the lowest OCV as well as the lowest power output even at higher gas flows. The reason for this is that a lot of oxygen is consumed at the anode and the gas mixture reaching the cathode has a strongly reduced oxygen partial pressure. The fuel

utilisation was calculated to be below 0.3%, which is two orders of magnitude lower than for conventional SOFCs.

In a study by Suzuki et al. [27] on electrolyte supported SC-SOFCs, it was experimentally shown that it is straightforward to connect cells on the same electrolyte in series, The cells were supported on a 0.5 mm thick CSO-electrolyte and were interconnected by a Au-line, which was painted from the anode of the first cell on one side, to the cathode of the second cell on the other side. The OCV of the "SOFC-module" consisting of two individual cells reached a maximum value of 1.6 V at 500°C and decreased to 1.4 V at 575°C. The OCV of a single cell with the same total electrode area as the module showed an OCV of 0.8 V, which in contrast, did not depend on the operating temperature. The difference of OCV-variation with temperature was attributed to different local temperatures but could not be explained in more detail. It is obvious that when the cell arrangements become more complicated, the electrochemical behaviour of the cell cannot be readily explained and is subject to speculations. A theoretical work has been done by Shiratori and Yamazaki [39], in which similar cells like the cells of Suzuki et al. [27] have been numerically modelled. The calculations including ohmic losses in the electrodes revealed that the voltage-current characteristics of segmented series connected cells greatly depend on the dimension of the cell segments.

3.5.1 Fuel-Air mixtures for SC-SOFCs

Basically, any hydrocarbon can be mixed with air to serve as the gas mixure for SC-SOFCs. For every fuel there is a certain operating range where useful power output can be expected from the cell. Usually, fuel-rich hydrocarbon-air mixtures are used for operating SC-SOFCs (fuel-rich). The gas mixture should contain enough oxygen for the cathode to operate reasonably well. Furthermore, there are also some safety limits, which should be considered. At room temperature, the unsafe region for CH_4-air mixtures is between 5 and 15 vol% CH_4 in air, when the temperature is increased this range broadens [40]. Higher hydrocarbons are more reactive than CH_4 and cannot be used at too high operating because they are prone to coking [41].

3.5.2 Anode-Supported SC-SOFCs

As compared to electrolyte supported cells, anode-supported cells offer the advantage that the operating temperature is not as strongly dictated by the electrolyte material, because very thin electrolyte layers can be fabricated since this cell component is no longer the mechanically supporting structure of the cell. The ohmic resistance of anode-supported cells can be drastically lower than for electrolyte supported cells. Therefore, a higher power output can be expected. Hibino et al. already showed that it was possible to improve the performance of electrolyte supported cells by decreasing the electrolyte thickness [32]. For electrolyte-supported cells the minimum thickness that could be utilised in this work was obviously 150 μm. If the performance is to be increased further, one has to go to anode-supported cells where the cell stability is retained by the anode-support. Electrolyte- and anode-supported cells with similar materials were compared in a versatile experimental setup by Napporn et al. [23]. Quite reasonable power densities of 80 mW/cm^2 for the electrolyte supported cell and 360 mW/cm^2 for the anode-supported cell could be achieved in flowing mixtures of CH_4 and air (x = 2) at 800°C. At high current densities the anode-supported cells showed a sudden drop of the cell voltage, characteristic for diffusion polarisation. Therefore, if very thick anodes are used at high current densities the performance of the cell will be limited by the removal of the reaction products, in the case of SC-SOFCs, CO_2 and H_2O.

In a further work by Jacques-Bédard et al. [42] on anode-supported SC-SOFCs, it was found that Ni-YSZ anodes reoxidised causing the OCV to drop to 0.1 V, when exposed to CH_4-air mixtures with an x-value of 0.5. At an x-value of 1 at 800°C a periodic oscillation of the OCV could be observed, with a periodicity of around 20 seconds and an amplitude of 5 mV around the mean value of 0.854 V. The OCV and oscillation frequency depended on the x-value and for x = 0.625 there was a periodicity of 10 hours. The reason for these fluctuation were probably periodic reduction/oxidation cycles of the Ni-catalyst [43]. The most stable conditions in terms of OCV were found to be at x = 2. After 72 hours at OCV and 800°C with a total flow rate of 350 ml/min in CH_4-air (x = 2), a strong ageing of the cell performance had taken place. By analysing the microstructure of the cell it could be found that there was a loss of metallic Ni in the anode-support caused by Ni-volatilisation. This phenomenon had already been discovered on monolith supported Ni-catalyst after partial oxidation tests [44].

Anode-supported SC-SOFCs were also studied by Shao et al. who used propane-air mixtures to operate their cells [24]. Prior to the cathode fabrication the dual-layer cells (anode-support and thin electrolyte) were treated at 600°C in diluted hydrogen in order to

reduce the NiO in the anode. In order not to reoxidise the metallic Ni the cathode had to be calcined in inert gas (N_2 or Ar). The materials were essentially the same as those used by Hibino et al. [9], i.e. Ni-CSO, CSO and SSC. As the current-collecting materials Ag-mesh and paste were used. Catalysis measurements were also carried out, which showed that at too low temperature (furnace temperature below 400°C) the anode only converted a small amount of the provided propane, whereas at too high temperature (above 650°C) the cathode material showed a too high catalytic activity for the parasitic oxidation of propane. It was concluded from these results that there is an optimum operating temperature range for SC-SOFC operation. The obtained power output at a temperature of 525°C was around 180 mW/cm^2 in flowing mixtures of helium, propane and oxygen at flow rates of 120, 10 and 30 ml/min, respectively. This is a relatively low propane flow rate as compared to other studies [9,25]. It was stated that the OCV measurement provides a reasonable screening for suitable operating conditions. However, the maximum OCV and maximum peak power density do not occur under identical conditions.

3.5.3 Effective Cell Temperature

Napporn et al. [22,23] showed that the current-collector mesh can have a significant effect on the effective cell temperature. One cannot simply rely on the so-called furnace temperature. When a Pt-mesh was applied to a blank YSZ pellet in a flowing mixture of CH_4-air there was a pronounced overheating, which at high flow rates of CH_4-air could lead to temperature differences between the cell and the furnace of up to 150°C. The reason for this was the pronounced catalytic activity of Pt in the used gas mixtures for the full oxidation of methane, which is highly exothermic. When gold was used instead of Pt, there was only a negligible temperature difference as compared to the YSZ pellet without any current-collector mesh. Thus, it seems that gold is the current-collector material of choice, when the operating temperature of a SC-SOFC is to be accurately controlled. At temperatures above 900°C Au cannot be used because it forms a eutectic with Ni that melts at around 950°C [22] and this leads to a rapid degradation of the cell performance. It should be noted, that the temperature measurements with Pt current-collectors solely may be somewhat misleading. The temperature is also influenced by the presence of a Ni-cermet anode. Ni-catalysts are very active for the endothermic steam reforming reaction at temperatures above 700°C. When the anode starts to overheat due to the presence of Pt, there will be an onset of the steam reforming reaction that will in turn reduce the anode temperature. This will in a way self-

regulate the anode temperature. Hibino et al. used exclusively Pt current-collectors for the anodes and Au current-collectors for the cathode. According to what has been said, their published cell operating temperatures might be somewhat too low.

3.5.4 Thermally Self Sustaining SC-SOFCs

The parasitic reactions occurring on the fuel cell have been shown to generate a lot of waste heat, which caused the cells to have a higher actual temperature than the surrounding atmosphere [22]. The idea of Shao et al. was to use this heat to sustain the fuel cell temperature in the absence of external heating [45]. The thermally self-sustained SC-SOFC operated on propane-oxygen-helium mixtures and consisted of two series connected anode-supported SC-SOFCs with similar materials and processing as described previously [24,46]. However, the novel cathode material $Ba_{0.5}Sr_{0.5}Co_{0.8}Fe_{0.2}O_{3-\delta}$ (BSCF) was employed and the anode-support was additionally coated with a Ru-CeO_2 catalyst, which made it possible to operate the cell without external heating. The Ru-CeO_2 catalyst was highly active for the full oxidation of the fuel down to 350°C. Obviously it was so active that upon removal of the external heating, the cell anode temperature could not sink to the critical value where the fuel oxidation at the Ni-CSO reaction ceases. At higher temperatures this catalyst had a higher selectivity for the partial oxidation of the fuel, which was an additional advantage. Even with a very thin electrolyte of only 20 μm thickness, the ohmic resistance due to this cell component was responsible for the main part of the losses during operation. However, the cell could be successfully operated in a thermally self-sustaining mode, when the apparatus was isolated by a thermal blanket. The 2-cell stack gave a stable OCV of 1.44 V and showed a maximum power density of approximately 267 mW/cm^2 at 338 mA/cm^2. The efficiency of the cell was still very low (~1%), but the study proved for the first time the feasibility of portable SC-SOFC systems.

3.6 Designs of SC-SOFCs

The concept of single chamber solid oxide fuel cells allows to envisage completely novel cell designs. The three basic designs that are possible with the “single chamber approach” are shown in Figure 3.7. The cells always have three basic components, electrolyte, anode and cathode. For cell-stacks interconnects are needed that connect the anode and cathode of two neighbouring cells. The electrodes must be highly porous for unhindered gas access.

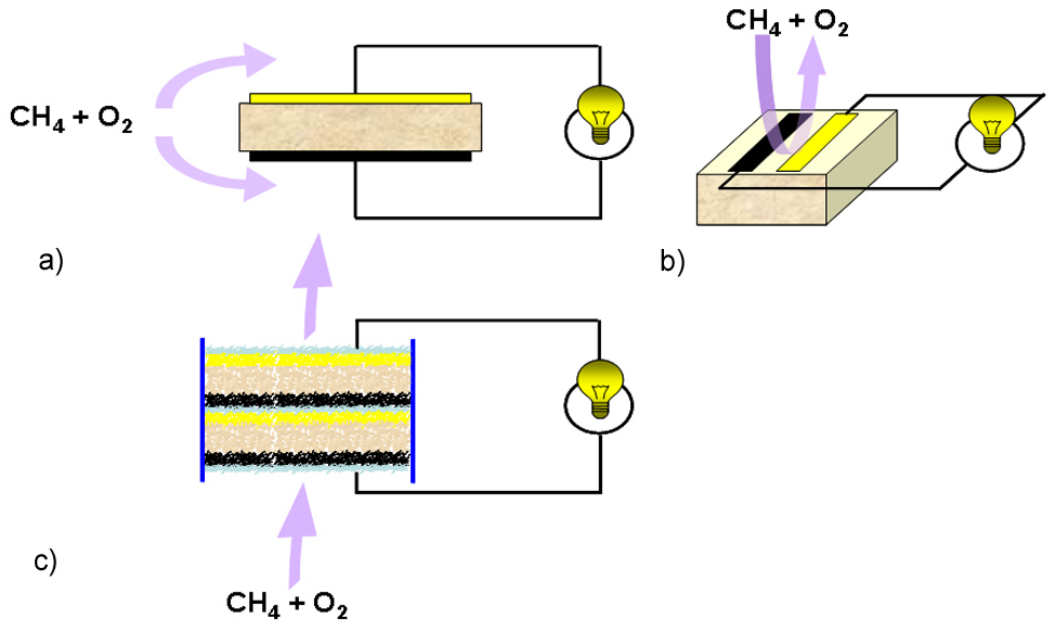

Figure 3.7 The three basic design possibilities for SC-SOFCs. a) Conventional design with electrodes on each side of a dense electrolyte. b) Planar design with side by side placement of electrodes. c) Fully porous design with a flow-through configuration.

At the electrodes the electric current must be collected. This is done with so called current-collectors, which can serve in some cases also as interconnects. The three possible basic cell designs are the sandwich design (Figure 3.7 a) with opposite electrodes on an intermediary electrolyte, the side by side design (Figure 3.7 b), which is not possible with conventional fuel cells and the fully porous cell design (Figure 3.7 c), in which all the cell components are porous. Two interconnected cells are shown in Figure 3.7 c. The layer between the anode and cathode of the two cells represents the interconnect.

3.6.1 Sandwich Design

The design with electrodes placed on opposite sides of an electrolyte is the most common design, which is used exclusively for conventional SOFCs. This basic design can be further split into five further types: anode-supported, electrolyte-supported, cathode-supported, porous substrate-supported and interconnect-supported [47].

3.6.2 Side by Side Design

The side by side design with both electrodes on the same side of an electrolyte substrate was initially proposed by van Gool [15]. In 1996 Hibino et al. showed that side by side cells

can be easily connected in series and in parallel without the use of classic interconnects. They proposed a new cell design with interpenetrating comb-like electrode patterns having feature sizes in the millimetre range [30]. A whole device with housing, gas manifolding and interconnection with the same cell design as described by Hibino had already been patented in 1981 by Louis [48]. The cells of Louis functioned in mixtures of 4% H_2, 4% O_2 and 92% N_2 at room temperature and gave OCVs of around 0.8V but currents in the range of micro amps, which is negligibly low, when compared to the cells of Hibino.

An advantage of the side by side design is that the electrolyte thickness does not play a role as long as it is not too thin, i.e. in the range of some tens of microns. The questions which shapes, geometries, electrochemical properties of the electrodes and which electrolyte thickness are required to obtain an optimal performance was addressed by Fleig et al. in a recent publication [21]. For interpenetrating comb-like structures of anode and cathode, the cells would have to consist of electrodes with characteristic feature sizes in the range of a few micrometers. The losses in such a fuel cell can be minimised by decreasing the gap width between the electrodes. However, there is a minimum gap, which is around 1 μm. If a potential difference of 1 V between the anode and cathode is assumed for a gap width of 1 μm, then the local electric field will have a value of 10^6 V/m, which is very close to the electric field leading to a disruptive discharge ($3 \cdot 10^6$ V/m in air). It is worth mentioning that such a small distance between anode and cathode might cause additional problems. The reaction products of the preceding partial oxidation at the anode, mainly H_2 might easily diffuse via the gas phase to the very nearby cathode, thus modifying the cathode potential or even causing the latter to decompose.

There was one publication, in which the finite element modelling (FEM) of a Micro SC-SOFC (μ-SC-SOFC) with side by side design was described [49]. Cells with ceria electrolyte (not clearly described, probably $Ce_{0.9}Gd_{0.1}O_{1.95}$), NiO-CGO anode and SSC-cathode were modelled. The paper, however, ignored the fact that SC-SOFCs are based on the partial oxidation of a hydrocarbon; hydrogen-air mixtures were assumed and the chemical reaction at the anode was not correctly represented. The results of this work showed that with increasing electrolyte thickness from 10 to 80 μm, the resistance of the cell slightly decreased. With an electrode spacing of 20 μm at a temperature of 500°C, the cell with 20 μm wide and 20 μm high electrodes was calculated to yield a power output in the range of 100 mW/cm^2.

The side by side concept permits the use of thinly fabricated electrolyte layers, however, spin coating [50], spray pyrolysis [51] or pulsed laser deposition can probably not be utilised

because they all produce too thin films (<1 μm). With the side by side design one could also envisage the preparation of active devices similar to transistors but generating power. The concept of μ-SC-SOFCs has to date not been experimentally validated. Regarding the trends towards miniaturisation of SOFCs the single chamber concept also offers an advantage in respect to thermal management. For miniaturised fuel cells the surface to volume ratio becomes higher and heat losses will become more important. Thus, it will be difficult to maintain the cells temperature without external heaters. The operation of SC-SOFCs always leads to a certain amount of parasitic reactions, i.e. non-electrochemical combustion of fuel. This reaction produces heat, which can be used for keeping the cell at the necessary operating temperature.

3.6.3 Fully Porous Design

Van Gool had extended the idea of surface-migration to the use of porous, gas-permeable electrolyte in fuel cells, which can increase the effective surface area [15]. Therefore, the use of a porous electrolyte with suitable porosity could lead to an improved performance of the fuel cell. This could be proven by Suzuki et al., who characterised anode-supported cells with dense and porous electrolyte. The porous electrolyte showed an OCV, which was 0.l V lower than for the cell with the dense electrolyte (OCV = 0.88V) in methane-air mixtures at a cell temperature of 744°C [52]. At the same time the conductivity of the porous, 18 μm thick YSZ electrolyte was higher than was calculated for a fully dense layer, thus proving what van Gool had postulated 40 years ago.

Fully porous cells were also proposed by Priestnall et al. who stated that in principle a compact mixed-reactant (CMR) fuel cell may be based on PEM, AFC, PAFC, MCFC or SOFC [4]. The benefits of such cells could be a higher fuel utilisation as well as much lower costs because expensive sealing and complex manifolding systems would become unnecessary. The most expensive component of a cell, the interconnect, would also become dispensable. The current problem of low fuel utilization in SC-SOFCs (approaching 10% [9]) could be improved by using fully porous cells, in which the contact-times between the gas mixture and the active cell components is much longer. For fully porous single chamber fuel cells, the anode and cathode electrocatalysts must be substantially selective, i.e. the anode should be active for the fuel oxidation and tolerant to oxygen, while the cathode should be active for oxygen reduction and tolerant to the fuel. Instead of generating electricity from a gas mixture as in SC-SOFCs, it would also be interesting to use the fully porous design as a

reactor that is capable of altering the reaction products when an external potential is applied to the electrodes. The partial oxidation of propene over silver catalysts showed that the reaction products are different when the oxygen is supplied by electrochemical pumping through an ion conducting membrane from the products that are formed with oxygen from the gas phase [53]. Interesting effects have been also been found in the reign of non-faradaic electrochemical modification of catalytic activity (NEMCA) [54]. However, this subject is beyond the scope of this PhD-thesis. The fully porous design of electrochemical cells potentially opens a whole new field for this domain.

3.7 Theoretical Work on SC-SOFCs

The first theoretical work in the field of SC-SOFCs by van Gool [15] has already been described in the previous sections. In 1995 Riess et al. described the working principle of SC-SOFCs operating on uniform mixtures of hydrogen and air [55]. Perfectly selective electrodes were assumed: H_2 is oxidised exclusively at the anode, while the cathode is totally inert to H_2. It was stated that a symmetrical cell will not generate an OCV nor deliver electric power. These thermodynamic considerations explain the generation of an OCV in hydrogen-air mixtures. In conventional fuel cells the driving force for the flow of an ionic current is the gradient of chemical potential across the electrolyte. Despite the fact that the concentration of oxygen stays uniform in the gas phase of a SC-SOFC, within the electrolyte it is not. A driving force is generated, yielding the OCV. The value of the latter can be calculated by the Gibbs's free energy change of the chemical reaction that is exploited. In the case here, this is the oxidation of H_2 given in Reaction (3.12)

$$H_2 + 1/2\,O_2 \rightarrow H_2O \tag{3.12}$$

The main finding of this study was that for perfectly selective, reversible electrodes, the OCV generated by a single chamber fuel cell has to be equal to the OCV of a conventional fuel cell, according to the Nernst equation:

$$OCV = -\frac{\Delta G}{z \cdot F} \tag{3.13}$$

ΔG stands for the free enthalpy change of the reaction at the given conditions, F is the Faraday number (96'485 Cb) and z the number of transferred electrons per formula unit. The theoretical value of OCV cannot be achieved in practice because the electrodes are not perfectly selective, i.e. the cathode oxidises some hydrogen and the anode reduces some oxygen. Thus, parasitic reactions lower the OCV.

The described model is well suited for explaining the OCV-generation in the single chamber fuel cell by Eyraud [13], Louis [48] and Dyer [14], because these cells operated in H_2-O_2 mixtures at room temperature. In the case of SC-SOFCs, however, it has been shown that the partial oxidation of methane is the reaction leading to the formation of the OCV [7]. Furthermore, the electrolyte is often a MIEC and not a pure ionic conductor, which leads to the reduction of the observed OCV [19]. For the explanation of the experimental observation of SC-SOFCs the model of Riess et al. can be expanded and refined.

In a more recent work [56], Riess reports about impeded reaction at mixed gas fuel cell (MGFC) electrodes and reasons that none of the electrodes should promote the full oxidation of CH_4, shown in Reaction (3.9). It is stated that the overall electrochemical reaction to be enhanced by the anode is:

$$CH_4 + 4O^{2-} \rightarrow CO_2 + 2H_2O + 8e^- \qquad (3.14)$$

However, as shown above, this cannot be the reaction occurring at SC-SOFC anodes. For cells with Ni-CSO anodes at open circuit conditions, the measurement of the outlet gases showed that there is a substantial amount of H_2 and CO, indicative for the partial oxidation at temperatures of 550-800°C. The concentration of CO_2 in the outlet gas was more than twice as high as the CO-concentration, which indicated that the anode also promoted the full oxidation (Reaction (3.9)) to a great extent. The measurements were done at zero current, therefore the CO_2 cannot stem from the electrochemical oxidation shown in Reaction (3.14). Riess declared that if a SC-SOFC yields a high power output with excess oxygen at the anode ($x < 0.5 \rightarrow$ explosive mixture), then this proves that the full oxidation is negligible. Experimental work showed that the OCV of SC-SOFCs drops to 0.1 V when the x-value approaches 0.5 [42]. No power can be generated from a cell that gives no OCV. It must also be considered that Ni-based anodes must be operated in a reducing atmosphere in order to keep the metallic Ni reduced and not to oxidise it to NiO, which only promotes the full

oxidation [57]. Therefore oxygen rich mixtures are not suitable for the operation of SC-SOFCs if Ni-based anodes are used.

3.8 References

[1] T. Hibino, S. Wang, S. Kakimoto and M. Sano, *Electrochemical and Solid State Letters*, **1999**, 2, *7*, 317-319.

[2] T. Hibino, S. Wang, S. Kakimoto and M. Sano, *Solid State Ionics*, **2000**, 127, 89-98.

[3] S. Raz, M. J. G. Jak, J. Schoonman and I. Riess, *Solid State Ionics*, **2002**, 149, 335-341.

[4] M. A. Priestnall, V. P. Kotzeva, D. J. Fish and E. M. Nilsson, *Journal of Power Sources*, **2002**, 106, *1-2*, 21-30.

[5] M. Goedickemeier, D. Nussbaum, C. Kleinlogel and L. J. Gauckler, in *192nd Meeting of Electrochemical Society, 1997,* Abstract no. 2191.

[6] K. Scott, A. K. Shukla, C. L. Jackson and W. R. A. Meuleman, *Journal of Power Sources*, **2004**, 126, *1-2*, 67-75.

[7] T. Hibino and H. Iwahara, *Chemistry Letters*, **1993**, 7, 1131-1134.

[8] K. Asano, T. Hibino and H. Iwahara, *Journal of the Electrochemical Society*, **1995**, 142, *10*, 3241-3245.

[9] T. Hibino, A. Hashimoto, M. Yano, M. Suzuki, S.-i. Yoshida and S. Mitsuru, *Journal of the Electrochemical Society*, **2002**, 149, *2*, A133-A136.

[10] A. J. Appleby, *Journal of Power Sources*, **1994**, 49, *1-3*, 15-34.

[11] C. Wheeler, A. Jhalani, E. J. Klein, S. Tummala and L. D. Schmidt, *Journal of Catalysis*, **2004**, 223, *1*, 191-199.

[12] M. B. Jörger, "CuO-CGO Anodes for Solid Oxide Fuel Cells", Ph.D. Thesis, Diss. ETH No. 15351, Swiss Federal Institute of Technology, 2004.

[13] C. Eyraud, J. Lenoir, M. Géry and R. Perrin, *Académie de Sciences*, **1961**, 252, 1599.

[14] C. K. Dyer, *Nature*, **1990**, 343, 547-548.

[15] W. van Gool, *Philips Research Reports*, **1965**, 20, 81-93.

[16] C. K. Dyer, Bell Communications Research Inc., *US Patent 244350*, 1989.

[17] T. Hibino, H. Tsunekawa, S. Tanimoto and M. Sano, *Journal of the Electrochemical Society*, **2000**, 147, *4*, 1338-1343.

[18] T. Hibino, A. Hashimoto, T. Inoue, J.-i. Tokuno, S.-i. Yoshida and S. Mitsuru, *Science*, **2000**, 288, 2031-2033.

[19] T. Hibino, A. Hashimoto, T. Inoue, J.-i. Tokuno, S.-i. Yoshida and S. Mitsuru, *Journal of the Electrochemical Society*, **2000**, 147, *8*, 2888-2892.

[20] P. Jasinski, T. Suzuki, F. Dogan and H. U. Anderson, *Solid State Ionics*, **2004**, 175, *1-4*, 35-38.

[21] J. Fleig, H. L. Tuller and J. Maier, *Solid State Ionics*, **2004**, 174, *1-4*, 261-270.

[22] T. W. Napporn, F. Morin and M. Meunier, *Electrochemical and Solid State Letters*, **2004**, 7, *3*, A60-A62.

[23] T. W. Napporn, X. Jacques-Bedard, F. Morin and F. Meunier, *Journal of the Electrochemical Society*, **2004**, 151, *12*, A2088-A2094.

[24] Z. Shao, C. Kwak and S. M. Haile, *Solid State Ionics*, **2004**, 175, *1-4*, 39-46.

[25] T. Suzuki, P. Jasinski, H. U. Anderson and F. Dogan, *Journal of the Electrochemical Society*, **2004**, 151, *10*, A1678-A1682.

[26] I. C. Stefan, C. P. Jacobson, S. J. Visco and L. C. De Jonghe, *Electrochemical and Solid State Letters*, **2004**, 7, *7*, A198-A200.

[27] T. Suzuki, P. Jasinski, H. U. Anderson and F. Dogan, *Electrochemical and Solid State Letters*, **2004**, 7, *11*, A391-A393.

[28] T. Suzuki, P. Jasinski, V. Petrovsky, H. U. Anderson and F. Dogan, *Journal of the Electrochemical Society*, **2004**, 151, *9*, A1473-A1476.

[29] T. Hibino, K. Asano and H. Iwahara, *Chemistry Letters*, **1994**, 485-488.

[30] T. Hibino, K. Ushiki and Y. Kuwahara, *Solid State Ionics*, **1996**, 91, 69-74.

[31] T. Hibino, Y. Kuwahara and S. Wang, *Journal of the Electrochemical Society*, **1999**, 146, *8*, 2821-2826.

[32] T. Hibino, A. Hashimoto, T. Inoue, J.-i. Tokuno, S.-i. Yoshida and M. Sano, *Journal of the Electrochemical Society*, **2001**, 148, *6*, A544-A549.

[33] T. Hibino, A. Hashimoto, S. Masanori, Y. Masaya, Y. Shin-ichiro and S. Mitsuru, *Journal of the Electrochemical Society*, **2002**, 149, *2*, A195-A200.

[34] K. Asano, T. Hibino and H. Iwahara, *Denki Kagaku*, **1996**, 64, *6*, 649-653.

[35] K. Asano and H. Iwahara, *Journal of the Electrochemical Society*, **1997**, 144, *9*, 3125.

[36] T. Hibino, K. Ushiki, T. Sato and Y. Kuwahara, *Solid State Ionics*, **1995**, 81, *1-2*, 1-3.

[37] T. Ishihara, M. Honda, T. Shibayama, H. Minami, H. Nishiguchi and Y. Takita, *Journal of the Electrochemical Society*, **1998**, 145, *9*, 3177-3183.

[38] D. Dissanayake, M. P. Rosynek, K. C. C. Kharas and J. H. Lunsford, *Journal of Catalysis*, **1991**, 132, *1*, 117-127.

[39] Y. Shiratori and Y. Yamazaki, *Electrochemistry*, **2001**, 69, *2*, 92-97.

[40] L. Bernard and G. von Elbe, "Combustion, Flames and Explosions of Gases", Academic Press, New York, 1961.

[41] J. P. Huijsmans, *Current Opinion in Solid State and Materials Science*, **2001**, 5, 317-323.

[42] X. Jacques-Bedard, T. W. Napporn, R. Roberge and M. Meunier, *Journal of Power Sources*, **2006**, 153, *1*, 108-113.

[43] Y. P. Tulenin, M. Y. Sinev, V. V. Savkin and V. N. Korchak, *Catalysis Today*, **2004**, 91-92, 155-159.

[44] P. M. Torniainen, X. Chu and L. D. Schmidt, *Journal of Catalysis*, **1994**, 146, *1*, 1-10.

[45] Z. Shao, S. M. Haile, H. Ahn, P. D. Ronney, Z. Zhan and S. A. Barnett, *Nature*, **2005**, 435, 795-798.

[46] Z. Shao and S. M. Haile, *Nature*, **2004**, 431, *7005*, 170-173.

[47] N. Q. Minh, *Solid State Ionics*, **2004**, 174, *1-4*, 271-277.

[48] G. A. Louis, J. M. Lee, D. L. Maricle and J. C. Trocciola, United Technologies Corp., *US Patent 107191*, 1981.

[49] C.-Y. Chung and Y.-C. Chung, *Journal of Power Sources*, **2006**, 154, *1*, 35-41.

[50] K. Mehta, R. Xu and A. V. Virkar, *Journal of Sol-Gel Science and Technology*, **1998**, 11, *2*, 203-207.

[51] D. Perednis, O. Wilhelm, S. E. Pratsinis and L. J. Gauckler, *Thin Solid Films*, **2005**, 474, *1-2*, 84-95.

[52] T. Suzuki, P. Jasinski, V. Petrovsky, H. U. Anderson and F. Dogan, *Journal of the Electrochemical Society*, **2005**, 152, *3*, A527-A531.

[53] K. Hellgardt, I. W. Cumming and A. Al-Musa, *Solid State Ionics*, **2005**, 176, *7-8*, 831-835.

[54] C. G. Vayenas, S. Bebelis, C. Pliangos, S. Brosda and D. Tsiplakides, "Electrochemical Activation of Catalysis Promotion, Electrochemical Promotion, and Metal-Support Interactions", Kluwer Academic/Plenum Publishers, New York, 2001.

[55] I. Riess, P. J. van der Put and J. Schoonman, *Solid State Ionics*, **1995**, 82, 1-4.

[56] I. Riess, *Solid State Ionics*, **2005**, 176, *19-22***,** 1667-1674.

[57] K. P. Peters, M. Rudolf and H. Voetter, *Brennstoff-Chemie*, **1955**, 36, *17/18***,** 257-288.

4 Thermodynamic Equilibrium of SC-SOFC Relevant Methane-Air Mixtures

B. E. Buergler, N. A. Grundy and L. J. Gauckler, *Journal of the Electrochemical Society*, **2006**, 153, *7*, A1378-A1385.

ABSTRACT: Single chamber SOFCs rely on the selectivity of the anode and cathode materials for either the partial oxidation reaction of a hydrocarbon with oxygen from air (anode) or the oxygen reduction reaction (cathode). The observed open circuit voltages of up to 0.9 V measured in SC-SOFCs suggest a very low oxygen partial pressure to be present at the anode side of the electrolyte whilst at the cathode it is more than 15 orders of magnitude higher but lower than in the gas phase.

As lower boundary of the oxygen partial pressure in the anode the partial pressure of oxygen that is given by the equilibrium state of the gas mixture can be assumed. The initial non-equilibrium gas mixture of a fuel and air will react towards the equilibrium composition, which in turn is only a function of temperature and the initial gas composition. We present here the calculation of thermodynamic equilibrium for methane-air mixtures relevant in SC-SOFCs. Furthermore, we show that the calculation can describe qualitatively the observed OCVs and give guidelines to suitable gas-mixtures for enabling high electric loads in SC-SOFCs.

4.1 Introduction

Single chamber solid oxide fuel cells (SC-SOFCs) have attracted a great deal of attention within the last decade. As compared to conventional SOFCs, single chamber fuel cells operate in a mixture of fuel and air, having both the anode and the cathode exposed to the same gas mixture. This feature enables the fabrication of SC-SOFC modules with novel designs having less critical sealing, improved thermal shock behaviour and the possibility for easier interconnection of cells.

The open circuit voltages as well as the obtainable power outputs of the investigated cells have been continuously improved since the first paper in 1993 [1]. This paper dealt with an SOFC based on yttria stabilised zirconia (YSZ) operating at 950°C on methane-air mixtures fed to both the Ni-YSZ anode and the Au cathode. The open circuit voltage (OCV) of 0.35 V and power output of 2.36 mW/cm^2 were attributed to the different catalytic activity of the anode and cathode for the partial oxidation of methane. This could be shown by measuring the exhaust gases from the anode and the cathode in a double chamber setup fed with mixtures of fuel and air. For the anode the exhaust gas consisted mainly of H_2 and CO with a ratio of 2:1 and some unreacted CH_4. Most of the oxygen and half of the provided methane had reacted in the anode chamber whereas in the cathode chamber only at high temperatures up to 20% of the oxygen was consumed by parasitic oxidation of the fuel. Higher OCV and power densities can be obtained when the cells are operated at lower temperature. The main reason for this is the increasing difference of catalytic activity between the anode and the cathode for the partial oxidation with decreasing temperature. However, highly conductive electrolyte materials like doped ceria are needed at very low operating temperatures. In previous work we have shown, that high power densities comparable to the ones of conventional SOFCs can be obtained with electrolyte supported SC-SOFCs based on Gd-doped ceria [2].

CH_4 is a viable fuel for SC-SOFCs and the lightest of all hydrocarbons, which is why CH_4-air mixtures were evaluated in this work. Mixtures of any other hydrocarbon with air could also serve as the gas mixture for SC-SOFCs. The advantage of propane or butane as compared to methane and ethane is that they can readily be liquefied, thereby allowing storage and transportation at much higher volumetric energy densities.

The theoretical OCV in conventional SOFCs but also in SC-SOFCs is due to the difference of oxygen partial pressure across an anode/electrolyte/cathode trilayer assembly. It can be

calculated from the free energy change, ΔG, of the electrochemical reaction or from the partial pressure of the oxygen at the cathode $p_C(O_2)$ and at the anode $p_A(O_2)$ [3].

$$OCV = -\frac{\Delta G}{nF} = \frac{RT}{nF} \ln \frac{p_C(O_2)}{p_A(O_2)} \tag{4.1}$$

In Equation (4.1), R is the gas constant, T the absolute temperature, F the Faraday constant, and n the electron equivalent of oxygen ($n = 4$). In the case of conventional solid oxide fuel cells, it is evident that there is a difference of oxygen partial pressure at both electrodes because these are located in two separated gas compartments. At the anode side, where the fuel is present, there is a very low concentration of oxygen in the range of 10^{-30}-10^{-15} atm depending on temperature and gas mixture. At the cathode side usually air is present corresponding to an oxygen partial pressure of 0.21 atm. The OCV of a classic SOFC can easily be calculated by the use of Equation (4.1). For SC-SOFCs the situation is more complicated because the oxygen partial pressure in the gas mixture does not correspond to the one present at the anode-electrolyte and cathode-electrolyte interface. If this were the case, the observed OCV would have to be close to 0 V. Knowing $p_A(O_2)$, is the prerequisite for the prediction of the OCV generated by a SC-SOFC. If the anode exhibits an infinite reaction rate, then at the anode-electrolyte interface the equilibrium gas mixture will be present and this equilibrium $p_A(O_2)$ can easily calculated by the use of a thermodynamic database. The thermodynamic equilibrium represents the lower limit of oxygen partial pressure in SC-SOFC anodes because the real catalytic activity will never reach infinity. A similar approach for the calculation of the theoretical OCVs of conventional SOFCs operated with all possible fuel mixtures has been demonstrated in a previous study by Sasaki and Teraoka [4]. However, in SC-SOFCs, $p_C(O_2)$ is not equal to 0.21 atm, it changes when the methane-air mixtures are varied. Furthermore, the nitrogen content coming from air was not included in the previous study.

At the anode the provided fuel (methane) reacts with the oxygen from the initial gas mixture resulting in a low $p_A(O_2)$. The reaction that is responsible for this decrease has been found to be the partial oxidation (Reaction (4.2)) [1] or the full oxidation (Reaction (4.3)).

$$CH_4 + 1/2\,O_2 \leftrightarrow CO + 2H_2 \tag{4.2}$$

$$CH_4 + 2O_2 \leftrightarrow CO_2 + 2H_2O \tag{4.3}$$

The partial oxidation of methane can be carried out at very high temperatures of up to 1300°C (non-catalytic) or at temperatures of only 700°C by using a catalyst, mostly Nickel. Ni-catalysts are very active for the partial oxidation of methane to CO and H_2 in CH_4-O_2 mixtures [5], closely attaining the thermodynamic equilibrium [6] at conditions very similar to those encountered in a SC-SOFC. Three kinds of pathways for the methane partial oxidation over Ni-catalysts have been suggested. One of them is the full oxidation of methane with subsequent CO_2- and H_2O reforming of unreacted CH_4 [7], the other a pyrolysis pathway, in which CH_4 is pyrolysed on the catalyst followed by the oxidation of the formed carbon-containing species to CO without the pre-formation of CO_2 [8]. The third mechanism constitutes the dehydrogenation of CH_4 on the Ni-surface forming CH-radicals and their subsequent reaction of the CH-radicals with O_2 and OH-radicals and recombination of 2 H-atoms on the surface yielding CO and H_2 as reaction products was proposed fifty years ago by Peters [9]. Only the dehydrogenation of CH_4 occurs at the catalyst, all other reaction steps can happen also homogeneously in the gas phase via the very reactive radicals. The proposed mechanism can explain the extremely fast kinetics of the reaction and the very high temperatures in the catalyst. The role of the radicals in the oxidation of methane using nickel as catalyst was further investigated recently [10,11]. The important reactions occurring in the partial oxidation were reviewed by Tsang [12].

For equilibrium considerations, the exact reaction mechanism is not important, as the thermodynamic equilibrium is independent of the reactions leading to it. At the cathode side, where $p(O_2)$ should be as high as possible, the reaction of methane and air ideally should proceed at a negligible reaction rate. The cathode should therefore only allow the oxygen reduction reaction and be inert to the fuel. However, at high temperatures the perovskites that are usually employed in SOFCs become quite active for the partial oxidation of hydrocarbons [13]. Thus, the operating temperature of SC-SOFCs should be kept low in order to keep the parasitic reactions at the cathode within a tolerable limit.

Besides allowing to understand the influence of temperature and gas mixtures on OCV, thermodynamic modelling can also provide guidelines under which conditions a cell can be ideally operated in. In closed circuit conditions a constant flow of oxygen-ions from the cathode to the anode occurs. The ions must be able to react electrochemically at the anode side with carbon monoxide or hydrogen, the products of the preceding partial oxidation. The direct oxidation of a hydrocarbon has been shown to lead to coking if the conditions are not suitable, e.g. the lack of water vapour in the fuel stream [14]. If not enough H_2 and CO are present at the anode, the oxygen partial pressure will increase and at the same time the power

output of the operating cell will drop. Thermodynamic modelling allows predicting the maximum concentrations of H_2 and CO in the SC-SOFC anode at different temperatures for different initial gas mixtures. Sasaki and Teraoka proved the concept of thermodynamic modelling for various fuel cell fuels in a broad temperature regime [15]. They calculated the equilibrium gas mixtures for reformed methane, propane, methanol and ethanol with different steam to carbon ratios. The major constituents of the equilibrium were found to be CH_4, CO, CO_2, H_2 and H_2O as well as solid carbon. Higher hydrocarbons and other species were in the range of ppm. Guidelines for avoiding the formation of carbon, when using all sorts of fuels being partially oxidised at the anode, were also given.

Note should be taken that the calculations put forth herewith do not include the influence of the ionic current when the cell is operating. They represent the conditions that would be found after infinite time at the SC-SOFC anode through which no current is flowing.

We present here the calculated equilibrium gas mixtures relevant for SC-SOFCs as a function of temperature for methane-air mixtures. The influence of 3% moisture in the methane-air mixtures is also elucidated.

4.2 Thermodynamic Modelling

4.2.1 Equilibrium Concentrations of Gas Constituents

The equilibrium calculations were carried out using the Thermocalc database system [16]. The database used was the substance database SSUB published by SGTE [17]. The components of the system are H, C, O and N. The ratio H:C was fixed at 4:1 and the ratio N:O to 3.77327. This corresponds to an oxygen content of 20.95% in dry air [18]. Ar and CO_2, which make up for 0.934 and 0.035 vol% of air were attributed to the inert nitrogen. We therefore considered air to be a mix of nitrogen and oxygen. CH_4 and H_2, which are also present in the earth's atmosphere (1.7 and 0.5 ppm), were neglected. The oxygen content was varied, thereby allowing equilibrium calculations for mixtures of CH_4 and air. Calculations were conducted for temperatures of 100-1100°C and the total pressure was kept fixed at 1 bar. Depending on composition and temperature the stable phase assemblage in this system is either a two-phase mixture of solid carbon (graphite) and the gas phase or single gas phase. The gas phase consists of a mixture of more than 70 species (or molecules). If the constituents of the non-equilibrium gas (in our case CH_4 and O_2) are allowed to react completely with each other, for example in the presence of a perfect catalyst, then the concentration of the species in the gas phase will change until the Gibbs energy is minimized, thus reaching the thermodynamic equilibrium. The only relevant species are CH_4, CO_2, CO, H_2O, H_2, N_2 and O_2 (the latter for the calculation of the theoretical OCV). The concentration of all other species is very low. These species were included in all the performed calculations; however, they are not discussed further. Here, we calculate and discuss the equilibrium concentrations of these species in the gas phase in function of temperature for fixed CH_4/O_2 ratios and in function of composition at fixed temperatures.

4.2.2 Carbon Deposition

As mentioned above, under certain conditions a two-phase mixture of solid carbon and gas is stable. Under these conditions carbon deposition is expected. If the system is considered to be a closed system, then carbon deposition will change the composition of the gas phase, depleting it of carbon. In a real fuel cell the composition of the gas stays constant because it is constantly replenished. The carbon deposition is a slow process and does not influence the gas composition strongly. Furthermore, it was found that carbon deposition did not influence

significantly the activity and selectivity of Ni-rare earth oxide catalysts [5]. Therefore, in our calculations of the equilibrium concentrations of species in the gas phase, we fix the gas composition and do not allow the formation solid carbon. Only when calculating the carbon deposition do we fix the overall composition and calculate the amount of carbon formed.

4.2.3 Calculation of Open Circuit Voltages

For the calculation of the theoretical OCV of SC-SOFCs a purely ionic conductor was assumed as well as perfectly selective electrodes. A perfect anode will give the equilibrium gas at the anode electrolyte interface and the equilibrium oxygen partial pressure will determine the OCV of the fuel cell. A perfect cathode being inert to the fuel will not catalyse any reaction involving CH_4. Therefore, the non-equilibrium oxygen partial pressure is present at a perfect cathode. The OCV of SC-SOFCs was calculated by using the Nernst Equation (4.1). It was assumed that the equilibrium oxygen partial pressure would be present at the anode side of the SC-SOFC whereas at the cathode, $p(O_2)$ would correspond to the non-equilibrium oxygen partial pressure, i.e. the initial O_2-content of the CH_4-air mixture. In reality the OCV of SC-SOFCs could also depend on the electrode thickness and microstructure as well as on the flow rate [2] and geometry of gas flows [19].

4.3 Results and Discussion

4.3.1 Overview of Methane-Air Mixtures for SC-SOFCs

Different non-equilibrium gas mixtures are unambiguously characterised by the ratio of CH_4 and O_2 denoted in the following as x. Some of the following plots are shown as a function of temperature others as function of CH_4/O_2 (x). Most relevant for the SC-SOFC, are x-values of 2, 1.5 and 1. These mixtures are not explosive and contain enough fuel for enabling electric current through the cell. A good deal of experimental work has been carried out using such gas mixtures. Figure 4.1 shows the situation for methane-air mixtures. The maximum concentration of oxygen $x(O_2)$ in the mixture is 20.95% since air contains this amount of oxygen. If we set $x(CH_4) = y$, then $x(O_2) = (1-y)\cdot 0.2095$, which gives the straight, solid line in Figure 4.1. Hence, $x = y / \{(1-y)\cdot 0.2095\}$, which is represented by the dashed line. At high temperatures, mixtures containing 5 to 15 vol% methane in air are explosive (hatched region 1) [20]. Thus, it is not recommended to utilise mixtures with $0.25 < x < 0.85$ for the operation of SC-SOFCs. A CH_4/O_2 ratio of 0.5 will result in complete combustion yielding only CO_2 and H_2O as products.

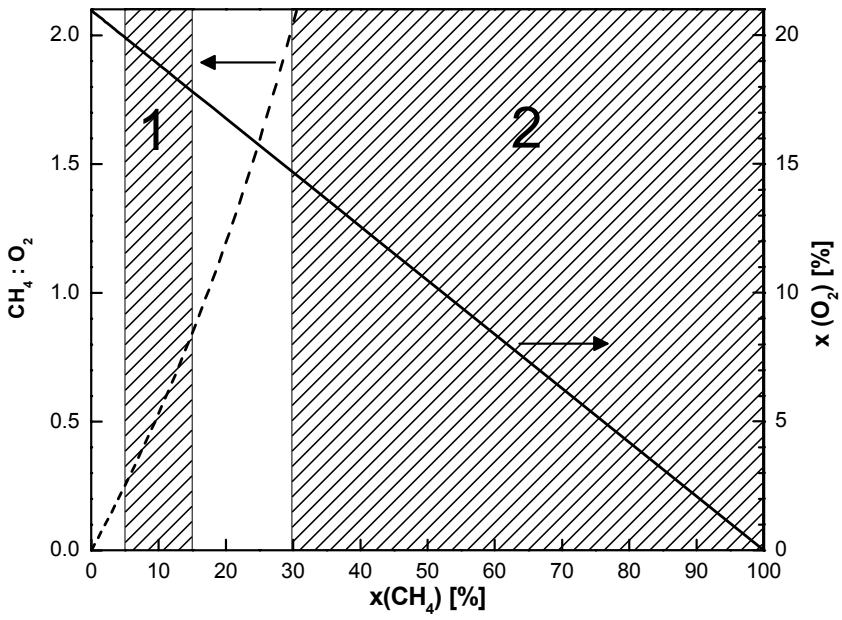

Figure 4.1 Viewgraph for CH_4-air mixtures. $x(O_2)$ and $x(CH_4)$ are the concentrations of oxygen and methane in the gas mixtures. The mixtures within the hatched area (1) are explosive and should not be used for operating of SC-SOFCs. The region with $x(CH_4) > 30\%$ (region 2) will result in carbon deposition.

Mixtures with a methane concentration lower than 5% are not explosive but they will result in a very low power output because of the absence of CO and H_2 in the resulting equilibrium gas mixture as will be seen in the following. 29.5 vol% CH_4 in air correspond to x = 2 and 17.5 vol% CH_4 to x = 1. Depending on operating temperature carbon deposition can take place at high methane concentration in the mixture. At 800°C, as will be seen later, this happens at an x-value larger than 2, corresponding to around 30 vol% CH_4 (hatched region 2). Thus, there is a window of possible CH_4-air mixtures for operating SC-SOFCs between x = 0.85 and x = 2.

4.3.2 Oxygen Partial Pressure for Different Methane-Air Mixtures as a Function of Temperature

In Figure 4.2 the equilibrium oxygen partial pressure as a function of temperature is shown for dry and moist methane-air mixtures. It can be clearly seen that the oxygen partial pressure increases with increasing temperature over many orders of magnitude. Below 500°C, $p(O_2)$ for x = 2, 1.5 and 1 are within one order of magnitude. The $p_A(O_2)$-curve for x = 2 (dry) shows a less pronounced increase at higher temperatures than the curves for x = 1.5 and x = 1. At x = 2 for 600°C and 800°C the oxygen partial pressure is $3.5 \cdot 10^{-26}$ and $1.3 \cdot 10^{-22}$ atm, respectively. For x = 1 at the same temperatures $p_A(O_2)$ is $2.6 \cdot 10^{-25}$ and $1.0 \cdot 10^{-19}$ atm.

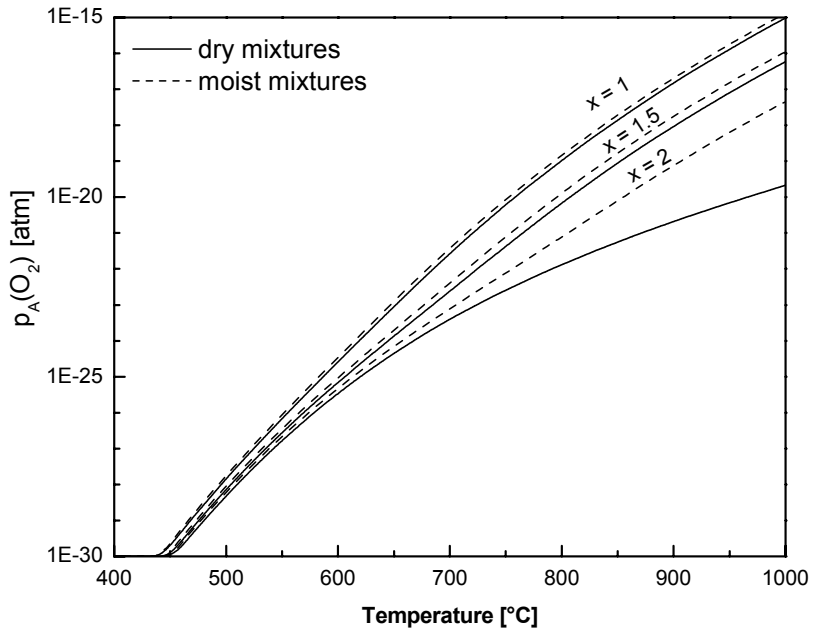

Figure 4.2 Equilibrium $p_A(O_2)$ for different CH_4/O_2 ratios as a function of temperature for dry and moist mixtures.

The dashed lines show the equilibrium oxygen partial pressure for moistened mixtures initially containing 3% of moisture. For moistened mixtures $p_A(O_2)$ is slightly increased as compared to dry mixtures. The effect is most pronounced at $x = 2$ at temperatures above 700°C.

4.3.3 Equilibrium Gas Mixtures

It is interesting to take a look at the equilibrium gas compositions at $x = 2$ for methane-air mixtures at different temperatures. The corresponding plot is shown in Figure 4.3. In the temperature regime where SC-SOFCs can be operated the most drastic changes of equilibrium gas compositions occur. At low temperatures, there are large amounts of H_2O, CO_2 and CH_4 that decrease with increasing temperature in favour of the more useful carbon monoxide and hydrogen. Water and methane are present in negligible quantities at temperatures above 800°C, where the ratio of H_2/CO is constantly 2 according to Reaction (4.2). The concentration of CO, H_2O and CO_2 are all around 6% at 550°C. From 500 to 800°C the H_2-concentration increases by a factor of 2.6 whereas the concentration of CO shows a sixfold increase and the concentration of CO_2 decreases by a factor of 20. For obtaining a high power output in SC-SOFCs it would seem to be more feasible to operate the cell at temperatures above 800°C. However, the reactions towards thermodynamic equilibrium of the gas mixture will also be promoted by the cathode at such high temperatures. This will cause severe losses in a SC-SOFC, which is why the temperature should be kept between 500 and 800°C. At too low temperatures, the concentration of CO and H_2 will be too low to operate the cell at high current densities and there will be a large amount of unreacted CH_4, which decreases the achievable fuel utilisation. The oxygen partial pressure at such low temperatures, will however, be much lower (see Figure 4.2), thereby allowing higher OCVs. Thus, the temperature must be adjusted in such a way that a suitable compromise between low $p_A(O_2)$ and high concentrations of H_2 and CO can be achieved in the anode of a SC-SOFC. It should be noted that the calculations represent the thermodynamic equilibrium and that at low temperature the latter may not be reached because of hindered kinetics.

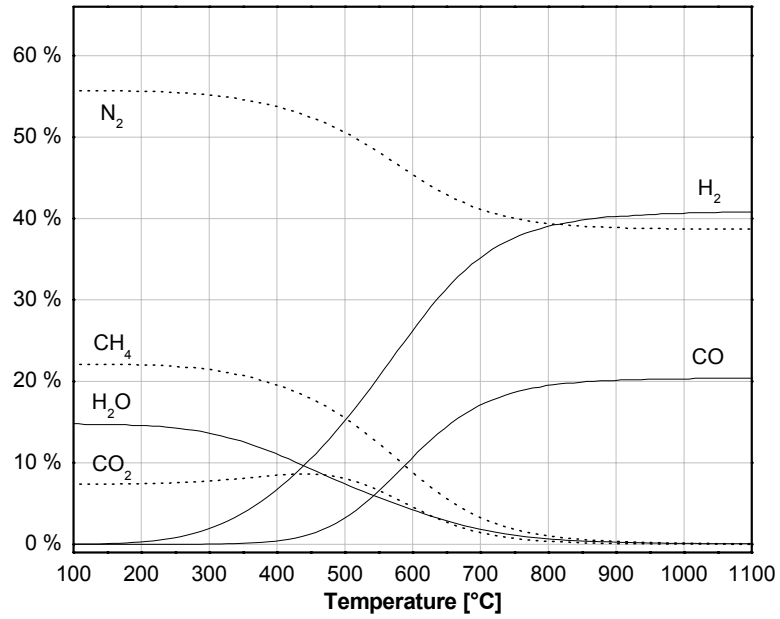

Figure 4.3 Equilibrium gas mixture for and initial CH_4-air mixtures with x = 2 as a function of temperature. The initial concentration is 29.5% CH_4, 14.8% O_2 and 55.7% N_2.

At x = 1.5 (Figure 4.4) the situation changes somewhat; At high temperatures, the concentration of CO_2 and H_2O are much higher than for x = 2. The H_2O concentration is even increasing and the H_2 concentration decreasing when the temperature is increased towards 1100°C as compared to the case for x = 2. The H_2/CO ratio is equal to 2 at 817°C but decreases to 1.8 at 1100°C. At approximately 560°C the concentrations of CO, H_2O, CO_2 and CH_4 are all approximately 6.5%. In Figure 4.5 the equilibrium gas mixture for an initial methane-air mixture with x = 1 is shown. The hydrogen concentration at temperatures above 800°C is clearly lower than at x = 1.5 and the CO_2 as well as the H_2O concentrations are much higher. Thus, the closer the x value to the stoichiometric value of 0.5, the more CO_2 and H_2O will be present in the equilibrium gas mixture. The CO_2 and H_2O that are dealt with here, form by the chemical oxidation of methane with oxygen coming from the initial gas mixture. In a SC-SOFC anode these species should only be formed by the electrochemical oxidation of CO and H_2 with O^{2-}-ions from the electrolyte or as transient species taking part in subsequent reforming reactions. By increasing the oxygen content in the initial gas mixture, the amount of H_2O and CO_2, which are not useful at the anode because they cannot react with O^{2-}-ions, will increase.

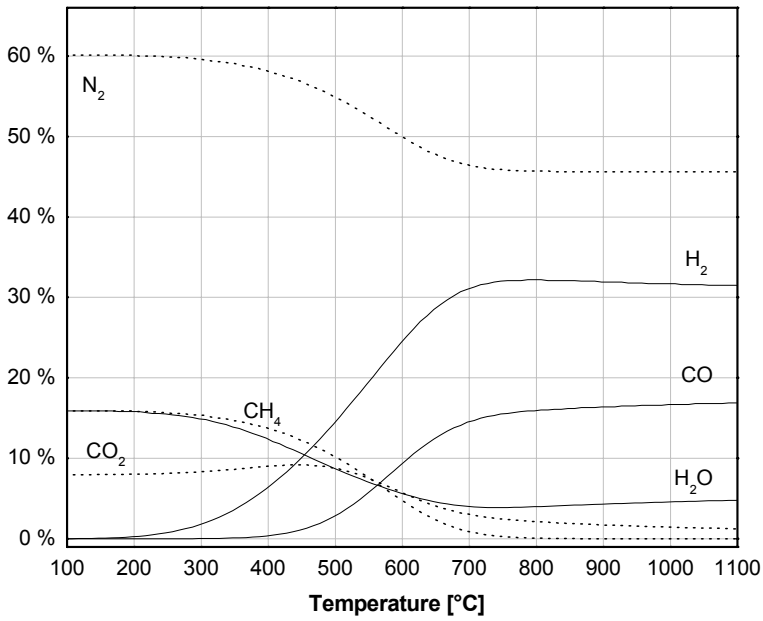

Figure 4.4 Equilibrium gas mixture for and initial CH_4-air mixtures with x = 1.5 as a function of temperature. The initial concentration is 23.9% CH_4, 15.9% O_2 and 60.2% N_2.

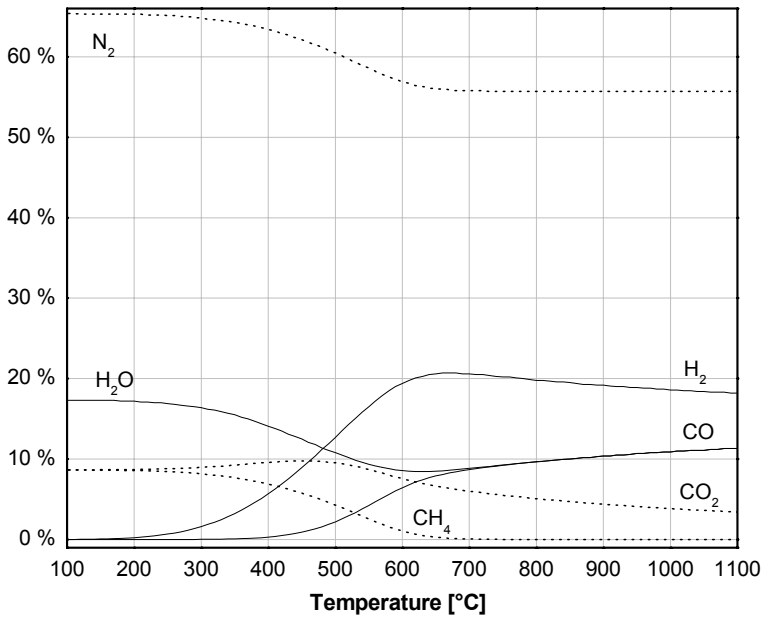

Figure 4.5 Equilibrium gas mixture for and initial CH_4-air mixtures with x = 1 as a function of temperature. The initial concentration is 17.3% CH_4, 17.3% O_2 and 65.4% N_2.

Above 800°C the CO and H_2O concentrations have the same value because the equilibrium is dominated by the water gas shift reaction (Reaction (4.4)) [21].

$$CO_2 + H_2 \leftrightarrow CO + H_2O \qquad (4.4)$$

The H_2/CO ratio is 2 at 815°C but decreases to 1.62 at 1100°C. From a thermodynamic point of view, low x-ratios will lead to more parasitic reactions at the SC-SOFC anode. Assuming perfect electrodes, the x-value of 0.5 would be ideal in terms of efficiency. All the methane-molecules could be fully oxidised by the provided oxygen according to Reaction (4.3). The oxygen molecules are incorporated into the electrolyte at the cathode. At the anode the methane molecules could then be fully, electrochemically oxidised. For every electrochemically oxidised CH_4-molecule, 8 electrons flow through the external circuit. However, this is not feasible in practice because of three reasons. 1) Mixtures with x = 0.5 are highly explosive. An explosion in a SC-SOFC system can cause the failure of the whole system. 2) The whole gas-mixture must be passed over both electrodes. 3) The operation of the SC-SOFC is based on the partial oxidation of methane. At the anode side the provided methane will in any case react with the available oxygen. In Figure 4.6 the equilibrium gases as a function of x are shown for 500, 600, 700 and 800°C. It can clearly be seen that there is a maximum of H_2O and CO_2 at x = 0.5 which corresponds to the stoichiometric gas mixture where the full oxidation can proceed. At x < 0.5 practically no H_2 and CO are present and the gas mixture contains only unusable gases for SC-SOFC anodes such as O_2, CO_2 and H_2O. Such gas mixtures can be expected to give power outputs close to zero, when used for operating SC-SOFCs. The equilibrium gas composition for x < 0.5 is practically the same for all four temperatures. For x > 0.5 a steep increase of the hydrogen and carbon monoxide concentration was calculated. The equilibrium gases will always contain a remanent amount of CH_4. At 500, 600, 700 and 800°C for x = 2 the concentrations of CH_4 are 15.5, 8.8, 3.3 and 1.0%. Thus, by going to high temperatures the amount of unreacted CH_4 can be reduced. If the concentration of unreacted CH_4 is to be low also at low temperatures, it can be done by using lower x-values. When electric current is flowing through the cell, the oxygen partial pressure can be assumed to increase because of the O^{2-}-ions reaching the anode side. Thus, in the plots of Figure 4.6, the equilibrium gas mixture will shift from the initial x-value to lower values.

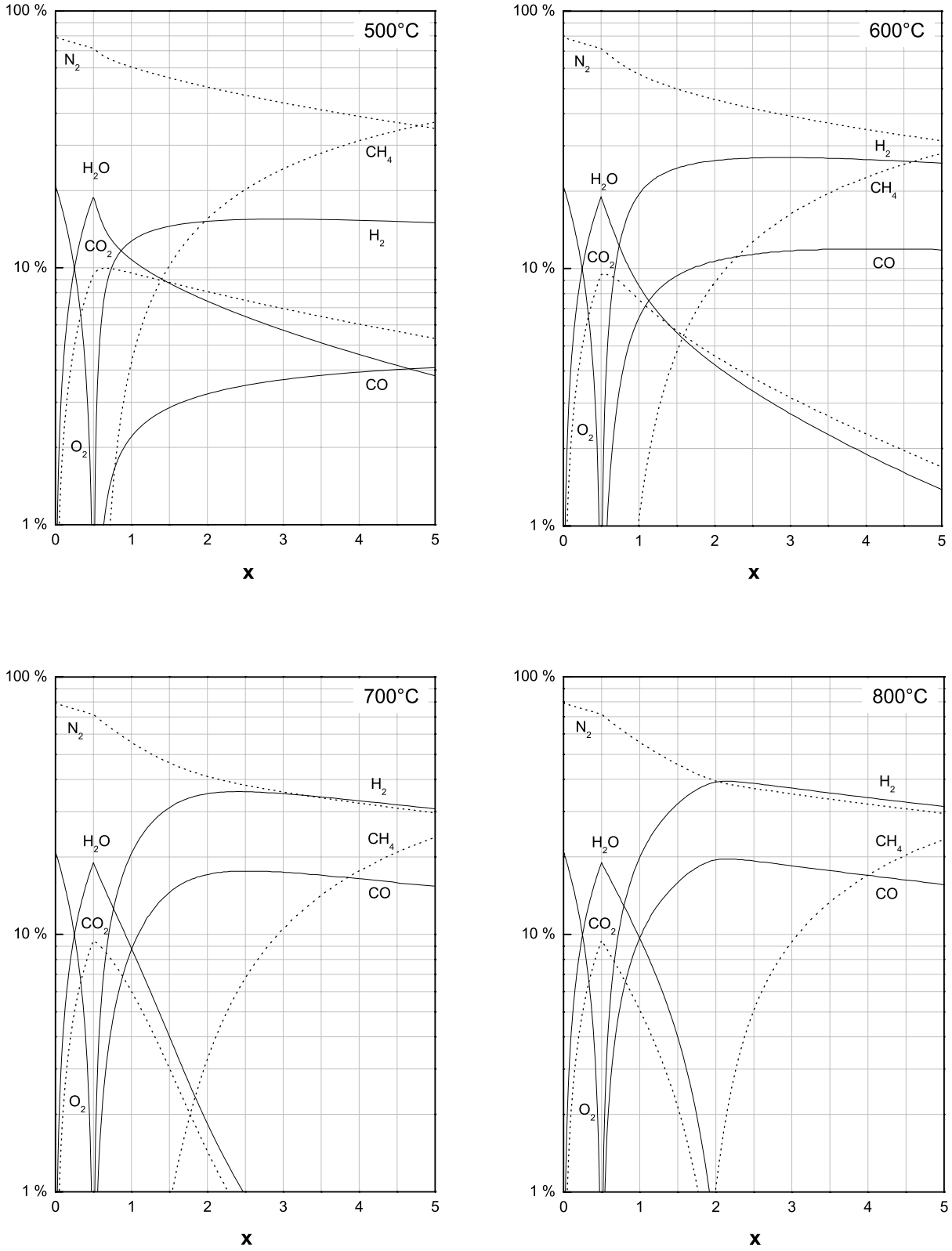

Figure 4.6 Thermodynamic equilibrium at 500°C, 600°C, 700°C and 800°C for methane-air mixtures as a function of CH_4/O_2. At x = 0.5, where the peak values of CO_2 and H_2O occur, the CH_4-air mixture is stoichiometric. This leads to the full oxidation of the fuel yielding only CO_2 and H_2O as the products.

The extent of the x-shift depends on the value of the current through the cell and other parameters such as gas flow rate and anode thickness. It is difficult to assess these parameters and the numerical values. However, the higher the current through the cell the more pronounced the x-shift will be. In theory the current should be adjusted in such a way, that the x-value shifted by the electric current through the cell reaches 0.5, thereby allowing the full oxidation of the provided CH_4 and improved efficiency. If too much current is flowing, as can be seen in Figure 4.6 at $x < 0.5$, the oxygen partial pressure will drastically increase and the unwanted reoxidation of the metallic Nickel in the anode becomes possible. The calculations revealed small amounts of NH_3 to be present in the equilibrium gases, especially at low temperatures (Table 4-1). The NH_3-concentrations as a function of temperature shows a maximum of 0.017% at approximately 435°C for x = 2. The temperature where the maximum is located is only slightly influenced by the x-value. At x = 2 and T = 600°C the equilibrium gas is comprised of 8.8% CH_4, 10.7% CO, 4.6% CO_2, 26.3% H_2, 4.2% H_2O and 45.4% N_2.

Table 4-1 Calculated equilibrium gas mixtures for x = 2, 1.5 and 1 at different temperatures in vol%.

	x	CH_4	CO	CO_2	H_2	H_2O	N_2	NH_3
500	2	15.5	3.2	8.1	15.2	7.4	50.6	0.017
	1.5	10.2	2.9	8.8	14.5	8.7	54.9	0.016
	1	4.3	2.2	9.5	12.7	10.8	60.5	0.014
600	2	8.8	10.7	4.6	26.3	4.2	45.4	0.014
	1.5	4.8	9.4	5.7	24.6	5.6	49.9	0.013
	1	1.1	6.4	7.6	19.4	8.6	56.9	0.010
700	2	3.3	17.1	1.4	35.2	1.8	41.1	0.009
	1.5	0.9	14.5	3.0	31.1	4.0	46.4	0.008
	1	0.1	8.7	6.0	20.6	8.8	55.8	0.005
800	2	1.0	19.5	0.4	39.0	0.7	39.4	0.006
	1.5	0.1	15.9	2.1	32.2	4.0	45.7	0.005
	1	0.0	9.7	5.1	19.8	9.7	55.7	0.002

4.3.4 Carbon Deposition

Solid carbon can form by the Boudouard Equilibrium (Reaction (4.5)) or the decomposition of CH_4 (Reaction (4.6)).

$$2CO \leftrightarrow C + CO_2 \tag{4.5}$$

$$CH_4 \leftrightarrow C + 2H_2 \tag{4.6}$$

The formation of solid carbon via Boudouard is expected to occur at temperatures below 700°C. Decomposition of methane is thermodynamically possible at temperatures above

500°C and with increasing temperature, Reaction (4.6) is entropically driven because for every cracked CH_4 two hydrogen molecules form.

In Figure 4.7 the molar fraction of carbon is plotted as function of the methane to oxygen ratio. At 500°C and x = 1 the formation of carbon is thermodynamically favourable. At this low temperature an explosive mixture would have to be used in order to avoid carbon deposition. When the temperature is increased, the boundary for the carbon formation shifts to higher x. At 800°C carbon will be formed when x = 2 is chosen. At higher temperatures, the amount of formed carbon is higher than at lower temperature. Generally speaking, the formation of solid carbon can be avoided by going higher than 800°C when using x = 2 and by using x-ratios smaller than 1 if the operation temperature is to be low. These results are in good agreement with previous studies [4].

In the work of Hibino et al. [22], the formation of solid carbon was confirmed at a Ni-$Ce_{0.8}Sm_{0.2}O_{1.90}$ SC-SOFC anode when x was higher than 1. When moistened mixtures were used, the formation of carbon could not be observed.

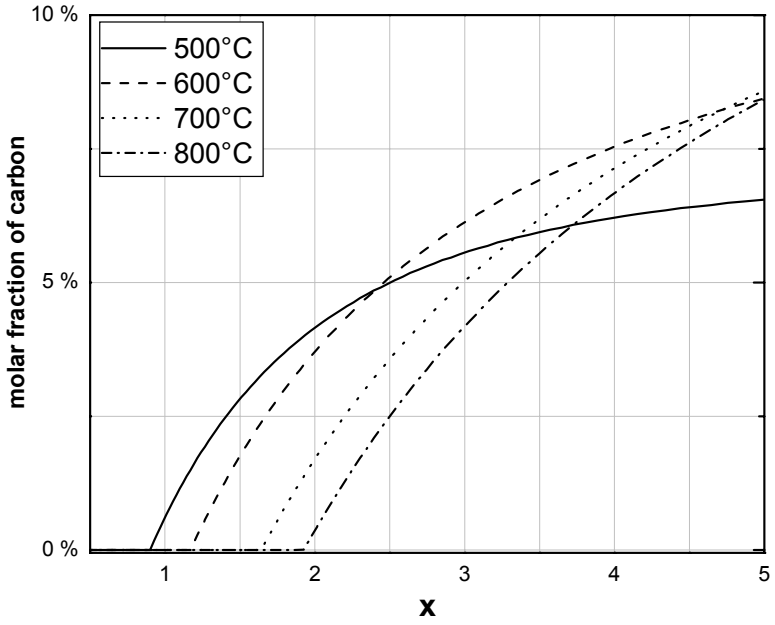

Figure 4.7 Carbon formation as a function of x at different temperatures for dry CH_4-air mixtures.

4.3.5 Carbon Deposition with Moistened CH_4-Air Mixtures

When the gas mixture is passed through a water bubbler containing water of approximately 24°C, the gas mixture will contain around 3% of moisture. In previous work [2], we used

moistened mixtures (x = 1.6) and no carbon deposition was observed at the anodes of the studied SC-SOFCs. The reason for this is that the formation of carbon is thermodynamically not favourable or kinetically hindered. The conditions at which carbon forms when using moistened CH_4-air mixtures are plotted in Figure 4.8. At x = 1.6 carbon can only form at temperatures below 700°C.

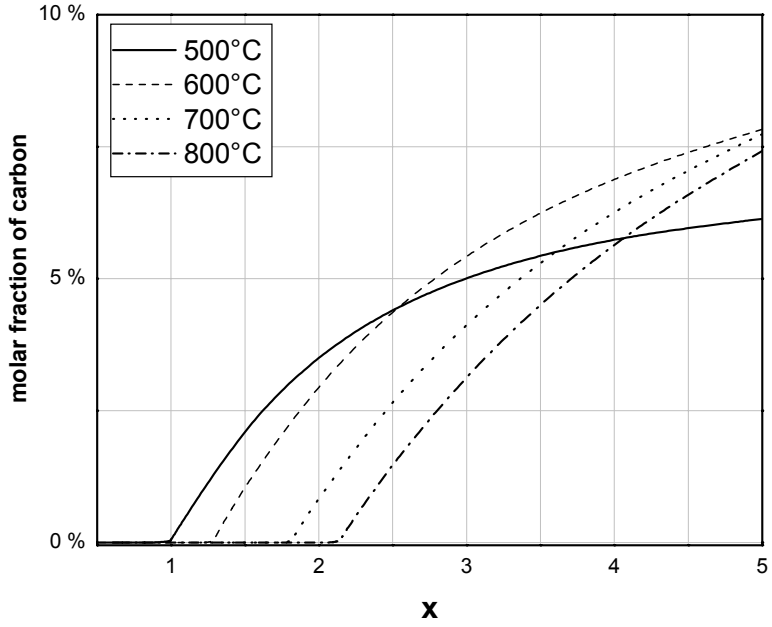

Figure 4.8 Carbon formation as a function of x for 3% water containing CH_4-air mixtures.

It can clearly be seen that the addition of moisture shifts the carbon deposition boundary to higher x-values when comparing Figure 4.7 and Figure 4.8. At 500°C SC-SOFCs can be operated on mixtures with x = 0.9 without the threat of carbon deposition. At 800°C and x = 2 no carbon forms when using moistened mixtures. The H_2O in the gas mixture also reduces the amount of formed carbon.

4.3.6 Open Circuit Voltage Calculation

The calculated OCV is shown in Figure 4.9 a for x ranging from 0.5 to 2. At low temperatures the OCV is not strongly dependent on x, whereas at high temperature, a decrease of the OCV when the x-value is changed from 2 to 0.5 was found. In the range $0.5 < x < 1.5$ the OCV decreased with increasing temperature, mainly because of the increasing oxygen partial pressure at the anode side as shown in Figure 4.2. For x decreasing towards 0.5 a

drastic drop of OCV that is independent of temperature was calculated. For x > 1.6 the OCVs at high temperatures were calculated to be higher than the OCVs at low temperatures as compared to x < 1.6 where the contrary was the case. These results are in agreement with recent experimental results by Jacques-Bédard on anode-supported cells with YSZ-electrolyte [23], which are shown in Figure 4.9 b. The measured OCVs, however, are 0.05-0.10 V lower than the calculated values, and the difference seems to become larger with increasing temperature. This indicates that the oxygen partial pressure at the cathode is lower than the non-equilibrium pressure. It has been shown that a real cathode is not totally inert to CH_4-air mixtures [24]. The real oxygen partial pressure at the cathode can be smaller for x = 1 than for x = 2, even though the non-equilibrium oxygen partial pressure is higher for x = 1. Obviously, the reaction rate of parasitic reactions at the cathode can increase when the oxygen availability is higher, especially at temperatures above 650°C.

In our previous work [2] on cells based on $Ce_{0.9}Gd_{0.1}O_{1.95}$ (CGO) electrolyte for x = 1.6 at 500°C, an OCV of 0.80 V was measured whereas 1.07 V was calculated. The lower OCV can be mainly attributed to an electronic leakage current that occurs in the electrolyte due to the partial reduction of the electrolyte material. At high temperature, the reduction of the OCV becomes more pronounced [25] and adds up to the OCV-reduction caused by the lowered cathode oxygen partial pressure.

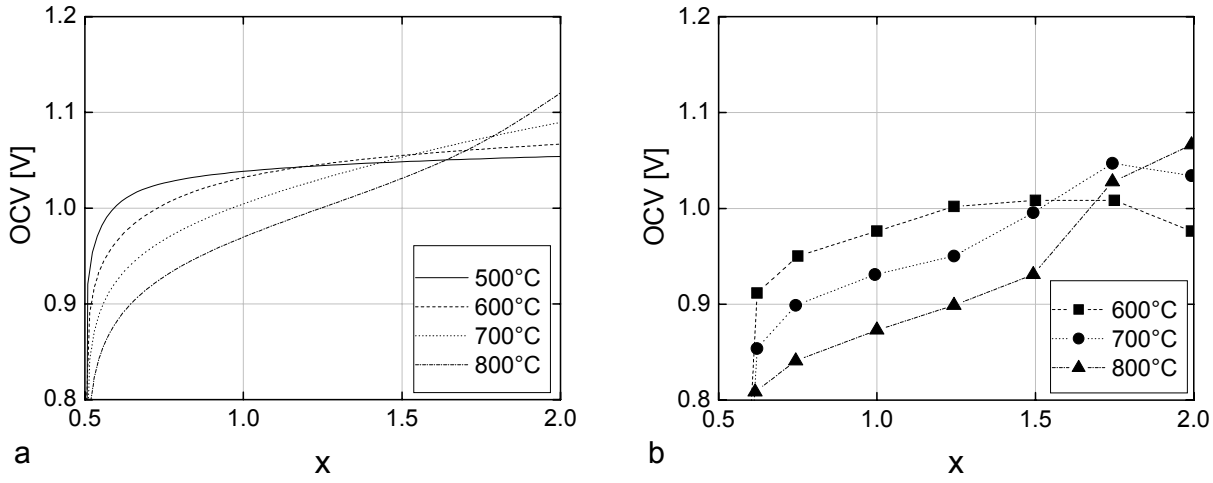

Figure 4.9 a) Calculated OCV for SC-SOFCs operating on CH_4-air mixtures with different x-ratio, assuming perfect electrodes and purely ionic conducting electrolyte. b) Experimentally measured OCVs of anode-supported SC-SOFCs with YSZ-electrolyte [23].

Another reason why the calculated OCVs can differ from the measured ones is the strong heat generation at the SC-SOFC anode. The temperature in this hot spot is difficult to measure by a thermocouple because the thickness of the hot zone is very small and because of the large thermal gradients [26]. Therefore, the real anode temperatures can deviate significantly from those reported, giving higher $p_A(O_2)$ and thus lower OCVs than expected.

For cells based on YSZ (electrolyte-supported) the operation temperature has to be chosen so high that the cathode causes severe losses due to parasitic reactions of CH_4 and O_2. Another problem when using YSZ is the incompatibility with low temperature cathode materials such as $Sm_{0.5}Sr_{0.5}CoO_{3-\delta}$. The reason for this is the formation of $SrZrO_3$ at thecathode-electrolyte interface when the cathode sintering is done at temperatures higher than 900°C [27]. Single chamber SOFCs with CGO electrolyte material can be operated at lower temperature because of the higher electrolyte conductivity. In addition, the catalytic activity of the cathode for parasitical reactions is very low at low temperatures and the OCV-losses due to this electrode become small. However, when using CGO as the electrolyte, there will always be a loss of approximately 20% of the theoretical OCV due to the electronic leakage current at open circuit conditions.

4.4 Conclusions

Equilibrium thermodynamic calculations were conducted for CH_4-air mixtures that have been proven to be suitable for the operation of SC-SOFCs. This was done by using the Thermocalc-software for mixtures of different CH_4/O_2 ratio as a function of temperature. The calculations are in good agreement with the calculations from the nineteen-fifties [21,28,29] and also with more recent results [12] and can also be considered for resolving fuel processing issues. It has been shown that the most drastic changes in the equilibrium concentrations of gas constituents occur in the temperature range where SC-SOFCs are operated. Depending on the initial CH_4/O_2 ratio, the equilibrium phase assemblage is two-phase gas plus solid graphite or a single gas phase. The equilibrium constituents of the gas phase are mainly N_2, CH_4, CO, CO_2, H_2, and H_2O. It was shown that temperatures above 800°C are more suitable due to higher concentration of H_2 and CO and smaller amounts of H_2O and CO_2 in the equilibrium. However, the cathode will oxidise more of the provided methane parasitically if the temperatures are too high. At low temperatures, there is a large amount of remanent CH_4. The cell performance could be improved if it were possible to operate the anode at 200°C higher temperature than the cathode. Thermodynamically, the formation of NH_3 is also possible (see Table 4-1) but in practice this is not expected because breaking the N≡N triple bond requires a high activation energy. Furthermore, the maximum NH_3-concentration was calculated to be lower than 0.02% in the whole temperature regime.

It could be shown that carbon deposition occurs if the temperature is chosen too low and the x-value too high. Adding 3% H_2O to the gas mixtures widens the carbon-free operation range but increases the equilibrium oxygen partial pressure at the anode, thereby decreasing slightly the achievable OCV. In practice moistening hydrocarbon-air mixtures can be easily done by passing the gas through a water-bubbler at room temperature.

Hibino et al. measured 7.7% CH_4, 0.2% O_2, 4.4% H_2 3.8% CO and 10.5% CO_2 in the outlet gas of the anode compartment of a SC-SOFC fed with a methane-air mixtures of x = 1.6 at open circuit conditions at 700°C [30]. The calculated equilibrium concentrations are 1.2% CH_4, 10^{-19} % O_2, 32.4% H_2, 15.3% CO and 2.6% CO_2. Thus, the equilibrium is not reached in the experimental work and the concentrations of H_2 and CO are lower than the calculated ones, whereas the concentrations of CH_4 and CO_2 stemming from the full oxidation are much higher. The H_2/CO ratio is also lower than the equilibrium ratio, which can be explained by the very short residence time of the gases at the anode and the relatively small amount of catalytic material present in the form of a thin layer. Another reason for the

difference between theory and experiment is that due to the flow configuration in the experiments, a certain amount of the gas never gets into contact with the catalyst. Therefore the measured gas composition is a mixture of the unreacted gas with the reacted gas.

The calculation of the theoretical voltage of SC-SOFCs showed that the OCV depends stronger on x at high temperatures than it does at low temperatures. With increasing temperature and decreasing x-value the OCV decreases. However, the used model might be somewhat too simple. Mixed ionic electronic conduction as well as the lowered oxygen partial pressure at the cathode due to the parasitic reactions should be included in order to predict the experimentally measured OCV.

4.5 Outlook

Independent of the exact conditions (temperature, ratio of CH_4/O_2), the knowledge of thermodynamic equilibrium of methane-air mixtures is always the basis for being able to understand the theoretical limits of SC-SOFCs. In recent years SC-SOFCs fuelled with ethane- [31], propane- [13] or butane-air [32] mixtures have been evaluated and it would be desirable to know the thermodynamic equilibrium of the utilised gas mixtures. The calculation of equilibrium concentrations of gas constituents is also the basis to understand the operation of normal SOFCs using the partial oxidation of CH_4 in the anode compartment. This concept has already been proven [33].

As a goal for future experimental work, the development of highly active catalysts with long-term stability in the severe conditions encountered in the SC-SOFC anode is required. The kinetic factors as well as the reaction mechanisms of the partial oxidation are still not fully understood to this day [34]. When carrying out this reaction at a fuel cell anode, the situation becomes even more complicated because of the ionic current and the influence of the electric potential on the catalytic activity. It is of great importance to learn more about this in order to further improve the performance of SC-SOFCs. Moreover, it might be helpful to include the effect of mixed ionic electronic conduction in the electrolyte and non ideal electrodes for the prediction of the experimentally measured OCV.

From a theoretical standpoint, an initial CH_4/O_2 ratio of 0.5 would be ideal, because it would allow the full oxidation of methane according to Reaction (4.3). However, the gas mixture would have to be passed over both electrodes (first the cathode then the anode) being perfectly selective for either oxygen or methane adsorption. In practice $x = 0.5$ is not possible because of the threat of an explosion. However, it might be possible to operate a SC-SOFC at e.g. $x = 1$ and to move the gas equilibrium to $x = 0.5$ by the electric current through the cell, thereby obtaining the desired fuel utilisation.

There will always be some remanent CH_4 at low temperatures. With the trend of decreasing SC-SOFC operating temperatures the amount of unreacted CH_4 will also increase. Thus, when SC-SOFCs are operated at a very low temperature, it will not be possible to obtain a high fuel utilisation because a certain amount of remanent CH_4 being present in the thermodynamic equilibrium. The situation might be better for the heavier hydrocarbons like ethane, propane or butane.

4.6 References

[1] T. Hibino and H. Iwahara, *Chemistry Letters*, **1993**, 7, 1131-1134.

[2] B. E. Buergler, M. E. Siegrist and L. J. Gauckler, *Solid State Ionics*, **2005**, 176, *19-22***,** 1717-1722.

[3] O. Yamamoto, *Electrochimica Acta*, **2000**, 45, *15-16***,** 2423-2435.

[4] K. Sasaki and Y. Teraoka, *Journal of the Electrochemical Society*, **2003**, 150, *7***,** A885-A888.

[5] V. R. Choudhary, V. H. Rane and A. M. Rajput, *Catalysis Letters*, **1993**, 22, 289-297.

[6] P. D. Vernon, M. L. Green, A. K. Cheetham and A. T. Ashcroft, *Catalysis Letters*, **1990**, 6, 181-186.

[7] M. Prettre, C. Eichner and M. Perrin, *Transaction of the Faraday Society*, **1946**, 43, 335-339.

[8] Y. H. Hu and E. Ruckenstein, *Journal of Catalysis*, **1996**, 158, *1***,** 260-266.

[9] K. P. Peters, M. Rudolf and H. Voetter, *Brennstoff-Chemie*, **1955**, 36, *17/18***,** 257-288.

[10] E. B. H. Quah, J. F. Mathews and C.-Z. Li, *Journal of Catalysis*, **2001**, 197, *2***,** 315-323.

[11] E. B. H. Quah and C.-Z. Li, *Applied Catalysis A: General*, **2004**, 258, *1***,** 63-71.

[12] S. C. Tsang, J. B. Claridge and M. L. H. Green, *Catalysis Today*, **1995**, 23, *1***,** 3-15.

[13] Z. Shao, C. Kwak and S. M. Haile, *Solid State Ionics*, **2004**, 175, *1-4***,** 39-46.

[14] S. H. Clarke, A. L. Dicks, K. Pointon, T. A. Smith and A. Swann, *Catalysis Today*, **1997**, 38, *4***,** 411-423.

[15] K. Sasaki and Y. Teraoka, *Journal of the Electrochemical Society*, **2003**, 150, *7***,** A878-A884.

[16] B. Sundman, B. Jansson and J.-O. Andersson, *Calphad*, **1985**, 9, *2***,** 153-190.

[17] *The SGTE substance database, version 1997, SGTE (Scientific Group Thermodata Europe), Grenoble, France*, **1997**,

[18] Römpp, "Chemie", 10th ed., Thieme, Stuttgart, New York, 1997.

[19] I. C. Stefan, C. P. Jacobson, S. J. Visco and L. C. De Jonghe, *Electrochemical and Solid State Letters*, **2004**, 7, *7***,** A198-A200.

[20] L. Bernard and G. von Elbe, "Combustion, Flames and Explosions of Gases", Academic Press, New York, 1961.

[21] K. P. Peters, E. Sattler-Dornbacher and M. Rudolf, *Gas/Wasser/Wärme*, **1955**, 9, *3***,** 47-56.

[22] T. Hibino, H. Tsunekawa, S. Tanimoto and M. Sano, *Journal of the Electrochemical Society*, **2000**, 147, *4***,** 1338-1343.

[23] X. Jacques-Bedard, T. W. Napporn, R. Roberge and M. Meunier, *Journal of Power Sources*, **2006**, 153, *1***,** 108-113.

[24] A. K. Demin and F. Y. Gulbis, *Solid State Ionics*, **2000**, 135, 451-456.

[25] T. Matsui, T. Kosaka, M. Inaba, A. Mineshige and Z. Ogumi, *Solid State Ionics*, **2005**, 176, *7-8***,** 663-668.

[26] D. Dissanayake, M. P. Rosynek and J. H. Lunsford, *Journal of Physical Chemistry*, **1993**, 97, *15***,** 3644 - 3646.

[27] H. Y. Tu, Y. Takeda, N. Imanishi and O. Yamamoto, *Solid State Ionics*, **1997**, 100, *3-4***,** 283-288.

[28] M. von Stein and H. Voetter, *Zeitschrift für Elektrochemie*, **1953**, 57, *2***,** 119-124.

[29] K. P. Peters, E. Kappelmacher and H. Voetter, *Gas/Wasser/Wärme*, **1952**, 6, *9***,** 189-195.

[30] T. Hibino, A. Hashimoto, T. Inoue, J.-i. Tokuno, S.-i. Yoshida and S. Mitsuru, *Journal of the Electrochemical Society*, **2000**, 147, *8***,** 2888-2892.

[31] T. Hibino, A. Hashimoto, T. Inoue, J.-i. Tokuno, S.-i. Yoshida and S. Mitsuru, *Science*, **2000**, 288, 2031-2033.

[32] T. Hibino, A. Hashimoto, T. Inoue, J.-i. Tokuno, S.-i. Yoshida and M. Sano, *Journal of the Electrochemical Society*, **2001**, 148, *6***,** A544-A549.

[33] Y. Hiei, T. Ishihara and Y. Takita, *Solid State Ionics*, **1996**, 86-88, *Part 2***,** 1267-1272.

[34] Y. H. Hu and E. Ruckenstein, *Advances in Catalysis*, **2004**, 297-345.

5 The Catalytic Activity of SC-SOFC Electrode Materials in Methane-Air Mixtures

B. E. Buergler and L. J. Gauckler, partly to be submitted to *Journal of the Electrochemical Society.*

ABSTRACT: The reduction temperature of NiO to metallic Ni in NiO-$Ce_{0.8}Gd_{0.2}Ce_{1.90}$ powder when heat treated in different methane-air mixtures was investigated by the use of thermogravimetry. It was found that the reduction temperature was decreased when the gas mixtures were richer in methane. Catalytically active additives such as Pd, PdO and Pt to the powder induced the reduction of NiO at lower temperatures as compared to the powder without additives.

The catalytic activities of anode and cathode layers with and without Pt current-collectors were characterised in methane-air mixtures by monitoring the concentrations of formed CO as well as CO_2 between 500 and 800°C. It was found that a substantial amount of methane was fully oxidised at both the anode as well as the cathode material. The presence of a Pt current-collector mesh in the NiO-$Ce_{0.8}Gd_{0.2}Ce_{1.90}$ anode drastically altered the catalytic activity as compared to the electrode layer without Pt. Only with Pt current-collector, the difference of the reaction rates for the partial oxidation of methane between the two electrodes was high enough for enabling useful currents to be drawn from SC-SOFCs. The measurement of the reaction rates of an entire cell showed that the reaction rate for CO-formation became lower when current was drawn from the cell. The reason for this was that CO was consumed electrochemically by oxygen ions when current was driven through the cell.

5.1 Introduction

All conventional solid oxide fuel cells (SOFCs) rely on the strict separation of fuel and oxidant by an ion conducting membrane [1]. In contrast to conventional SOFCs, single chamber fuel cells operate in a mixture of fuel and air, and therefore the cell design can be significantly simplified [2,3]. In addition, various hydrocarbon fuels with much higher energy density than hydrogen can be utilised [4]. Mixtures of hydrogen and air are not feasible at the high operating temperatures of SOFCs because of the danger of explosions [5]. When methane-air mixtures are used, the observed open circuit voltage (OCV) is due to the different catalytic activities of the two electrodes for the partial oxidation of methane [3]. The cathode should be as inactive as possible towards any reaction involving the fuel and should only promote the oxygen reduction reaction. In practice, this requirement is difficult to meet because at high temperatures the cathode will also promote the oxidation of the fuel [4,6]. Unlike the cathode, the anode should have a very high activity for the partial oxidation of methane, being the source of the "real" SC-SOFC fuel, i.e. carbon monoxide and hydrogen. Ni-$Ce_{0.8}Gd_{0.2}O_{1.9}$ cermets (Ni-CGO) are well suited as SC-SOFC anodes because of their high activity and low overpotentials [7]. The processing of cermet anodes is usually done starting with powder mixtures of NiO and electrolyte material. These mixtures are often applied via screen printing [8] onto the electrolyte and then sintered at relatively high temperatures of up to 1300°C. Before the cell can be put into operation, the NiO in the anode needs to be reduced to metallic Nickel, which can be done by feeding a reducing gas stream to the anode (e.g. hydrogen). It has been shown that Ni-cermet anodes are very sensitive to the reducing conditions, and that low temperature reduction can lead to improved performance when using CH_4 as the fuel [9]. A challenge with SC-SOFCs is that most perovskites are not stable at low oxygen partial pressures ($p(O_2)$) and can decompose [10]. In recent work [11,12], the perovskite $Sm_{0.5}Sr_{0.5}CoO_{3-\delta}$ (SSC) has been used as the SC-SOFC cathode, because it exhibits a high catalytic activity for the oxygen reduction reaction but low activity for CH_4-oxidation. The low stability at low $p(O_2)$ is the reason, why the reduction of NiO in the SC-SOFC cannot be performed with hydrogen-rich gas as it is usually done for reducing the anodes of conventional SOFCs. Instead, the reduction is carried out directly in the fuel-air mixture after:

$$NiO - CGO \xrightarrow[T_{red}]{CH_4 - Air} Ni - CGO \qquad (5.1)$$

The temperature of reduction (T_{red}) for SC-SOFC anodes is therefore determined by the intended gas mixture and can take place at significantly higher temperatures than the desired operating temperature. As will be seen later the anode of a SC-SOFC with Pt current-collector was reduced at around 740°C in a CH_4-air mixture with x = 2. T_{red} can be reduced by increasing the CH_4/O_2 ratio (x). However, this procedure is difficult to control and once NiO is fully reduced, carbon deposition can occur at the metallic Ni, as has been found by thermodynamic calculations [13] and observed experimentally [14]. Solid carbon can be formed by the Boudouard Equilibrium shown in Reaction (5.2) or the decomposition of CH_4 shown in Reaction (5.3).

$$2CO \leftrightarrow C + CO_2 \tag{5.2}$$

$$CH_4 \leftrightarrow C + 2H_2 \tag{5.3}$$

The formation of solid carbon via Boudouard is expected to occur at temperatures below 700°C. Decomposition of CH_4 is thermodynamically possible at temperatures above 500°C and with increasing temperature, the reaction is entropically driven because for every cracked CH_4, two hydrogen molecules are formed. The formation of carbon at a SC-SOFC anode is detrimental to the cell and leads to irreversible degradation.

In order to reduce a NiO-$Ce_{0.8}Gd_{0.2}O_{1.9}$ anode in CH_4-air (x = 2), Hibino et al. added 1 wt% of PdO that acted as catalyst decreasing the reduction temperature of NiO to less than 550°C [15]. At these conditions the cell with PdO-modified anode gave an OCV of 0.91 V whereas the cell without PdO only exhibited 0.11 V, which indicated that the latter anode was not reduced. The relatively low reactivity of methane as compared to the higher hydrocarbons is the reason for the relatively high reduction temperature of NiO-ceria anodes in CH_4-air mixtures. Using a higher hydrocarbon allows for the NiO-reduction at lower temperatures. In C_2H_6-air mixtures, for example, a NiO-$Ce_{0.8}Sm_{0.2}O_{1.90}$ mixture was reduced already between 600 and 700° [16], which is considerably lower than for CH_4-air ($T_{red} \approx 740$°C).

At the anode of a SC-SOFC the H_2 and CO-providing partial oxidation Reaction (5.4) competes with the full oxidation of CH_4, Reaction (5.5). The latter reaction is not beneficial for the power generation because the reaction products CO_2 and H_2O cannot be further oxidised.

$$CH_4 + 1/2\,O_2 \xrightarrow{rr_{CO}} CO + 2H_2 \tag{5.4}$$

$$CH_4 + 2O_2 \xrightarrow{rr_{CO_2}} CO_2 + 2H_2O \qquad (5.5)$$

Therefore, it would be beneficial to have a catalyst with a high selectivity for the partial oxidation (Reaction (5.4)) and only a very slow reaction rate for the CO_2 formation (Reaction (5.5)). The CO-selectivity, S(CO), of the methane oxidation can be assessed using the following equation, where rr_{CO} and rr_{CO_2} are the reaction rates for the methane partial and full oxidation, respectively:

$$S(CO) = \frac{rr_{CO}}{rr_{CO} + rr_{CO_2}} \qquad (5.6)$$

Without catalyst, the partial oxidation of methane [17,18] can be carried out at very high temperatures of up to 1300°C. When using a suitable catalyst the reaction proceeds at temperatures as low as 700°C. Ni-catalysts are very active for the partial oxidation of methane to CO and H_2 in CH_4-O_2 mixtures [19], closely attaining the thermodynamic equilibrium [20] at conditions very similar to those encountered in a SC-SOFC.

To date the catalytic activity of the Ni-CGO anode and the SSC-cathode and their selectivity are not yet fully understood. In order to gain deeper insight into the catalysis of SC-SOFC electrodes with and without Pt current-collectors, the reaction rates of Reaction (5.4) and (5.5) were assessed. Pt is a common current-collector material for the anode of SC-SOFCs and in previous work [12] it was also used as the current-collector for the cathode. The present work also addresses the question, whether the measured current densities of SC-SOFCs can be explained by the difference of CO-formation rate (Δrr_{CO}) of the anode and cathode.

Another point of interest was the reduction of NiO-CGO powder in CH_4-air mixtures with different additives, such as Pd, PdO or Pt. It has been shown that T_{red} of NiO in the anode can be drastically reduced by the presence of PdO but also other oxides. Thus, the influence of different additives to the NiO-CGO cermet on the course of the NiO-reduction was investigated.

5.2 Experimental

5.2.1 Materials

Two perovskite cathode materials were evaluated. On the one hand the standard material for SC-SOFC cathodes, $Sm_{0.5}Sr_{0.5}CoO_{3-\delta}$ (SSC, Nextech Materials, USA, Lot# 91-82) was studied, on the other hand $Ba_{0.5}Sr_{0.5}Co_{0.8}Fe_{0.2}O_{3-\delta}$ (BSCF, Praxair, USA, Lot# 03-P4363DM), which is a promising candidate for low temperature SOFCs and also for SC-SOFCs [21]. The conventional NiO-CGO anode with 60 wt% NiO was used for all the experiments. The powder had been purchased from Praxair (Lot# 03-P4832DM).

Pieces of Pt-mesh (52 mesh woven from 0.1 mm wire, Alfa Aesar, Germany) were used for as current-collectors for the SC-SOFC electrodes. Amorphous Pt-powder finer than 10 µm (Alfa Aesar, Germany, Lot# H12G19), Pd-powder (60 mesh, Johnson & Matthey, Switzerland) and $PdO{\cdot}H_2O$ (Alfa Aesar, Germany, B25H03) were used as catalytic modifiers for the reduction of NiO-CGO powders.

5.2.2 Reduction of NiO-CGO Powders in Methane-Air Mixtures Measured by Thermogravimetry

The aim of these experiments was to investigate the reduction of the NiO-CGO powder in CH_4-air mixtures and if the presence of additives reduces the reduction temperature (T_{red}). Thermogravimetry is well suited because the reduction of NiO to Ni is accompanied by a weight loss that can be accurately measured. When the 60 wt% NiO-containing NiO-CGO powder is reduced a weight loss of 12.85 wt% is expected. Unmodified NiO-CGO powders were analysed in different CH_4-air mixtures in a first set of experiments. In a second set the CH_4/O_2 ratio (x) was always kept constant at 2 and the NiO-CGO samples were modified with Pd, $PdO{\cdot}H_2O$ and Pt in two different forms (powder or mesh as it was used for the SC-SOFC current collectors). Of course the Pt-powder had a much higher dispersion (surface area/volume) than the Pt-mesh. 5 wt% of these catalytic modifiers were added to a constant amount of 2 g of NiO-CGO powder and their influence on the reduction behaviour was studied. The thermogravimetry values (TG [%]) were always in respect to the amount of NiO-CGO powder without additives.

The thermogravimetry experiments (TG) were carried out in a Netzsch-instrument (STA 449C Jupiter, Germany) in flowing mixtures of CH_4, O_2 and Ar. The total flow rate with

different ratios of CH_4/O_2 was always 100 ml/min with $Ar/O_2 = 3.77$, which is equal to N_2/O_2 in air. All the metallic heat shields in the instrument had been replaced by alumina heat shields. The same alumina TG-crucible was used for all the experiments. It was filled with of 2.00 g of NiO-CGO powder and then heated at 10 K/min to 800°C for one hour. Cooling down to room temperature was done at the same rate. The outlet gases of the instrument were analysed with a mass spectrometer (Balzers GSD 300, Liechtenstein) during the course of the whole measurement.

5.2.3 Preparation of SC-SOFC Electrode Layers for the Measurement of Catalytic Activities

The experiments were carried out with screen printed electrode layers on $Ce_{0.9}Gd_{0.1}O_{1.95}$ (CGO) electrolyte. Electrodes with and without Pt current-collectors were characterised. The surface area of the active layer was always 1 cm^2 and the mask thickness for screen printing 50 μm. A blank CGO-pellet was also measured in order to see to what extent the setup and the blank pellet themselves would promote the reaction between CH_4 and O_2. Measurements were also done with a Pd-modified anode (addition of Pd-CeO_2) and a BSCF cathode. The Pd-CeO_2 catalyst, fabricated by flame spray pyrolysis in a similar way as described in ref. [22], but with Ce- instead of Al-salts, was also characterized itself by painting an organic slurry of this catalyst on one side of a blank CGO pellet. A complete cell, consisting of Ni-CGO/CGO/SSC with Pt current-collectors on each side was also characterized, to see what influence a current through the cell would have on the measured reaction rates of Reactions (5.4) and (5.5).

Electrolyte Pellets

Electrolyte discs were fabricated by uniaxially pressing 7 g of $Ce_{0.9}Gd_{0.1}O_{1.95}$ (CGO, Lot# 9804401, Rhodia, Catalysis & Electronics, France) powder in a 30 mm diameter dye at 40 MPa. The discs were then isostatically pressed at 300 MPa and sintered at 1400°C in air for two hours. A heating rate of 1 K/min and a cooling rate of 5 K/min were applied. In order to obtain flat surfaces the sintered discs were lapped on a Stähli FLM 500 lapping machine equipped with a hybrid steel-copper disc. B_4C-suspension (BC-800, Stähli, Switzerland) was used at 60 rpm and about 1 drop of B_4C-suspension every second. The density of the discs was measured after lapping and exceeded 97% of the theoretical density ($\rho_{th} = 7.29$ g/cm^3).

Organic Pastes for Screen Printing

The organic pastes were essentially the same as used by Gödickemeier for the fabrication of anode layers via screen printing [23] and were prepared as follows: First the ceramic powder was mixed with the two organic powders, Furan-2-Carboxylic Acid (F2C) and Ethyl-Cellulose (Ethocel). Then the solvent Diethylene Glycol Monobutyl Ether Acetate (DGMEA) was added. The formed mixture was subsequently milled in a zirconia container with a zirconia ball using a vibratory mill (Retsch M20, Germany) at 20 Hz for 20 minutes. The consistency of the pastes was similar to that of honey. By using a small amount of Sorbitan monooleate (Span 80), which acts as surfactant and binder at the same time, the solid loading of the organic paste could be increased to 36.5 vol%. The fabricated pastes proved to be suitable for the screen printing process. In Table 5-1 the compositions of the used pastes are summarized.

Table 5-1 Compositions of screen printing pastes.

Paste	m(Powder) [g]	m(F2C) [g]	m(Ethocel) [g]	m(Span80) [g]	m(DGMEA) [g]	Solid Loading [vol%]
NiO-CGO	8.0118	-	-	0.054	2.010	36.5
Pd-NiO-CGO	0.8460 (Pd-CeO_2 0.0827)	-	-	0.0057	0.7312	~16
SSC	4.944	0.0526	0.3032	-	1.508	30
BSCF	4.95	0.0733	0.3361	-	2.25	33

For obtaining Pd-doped NiO-CGO paste similar to the one used in previous work [12], the right amount of Pd-CeO_2 catalyst (10 wt% Pd) was added to the NiO-CGO paste. This was done by dispersing 0.0827g of 10 wt% Pd-CeO_2 nano-catalyst in DGMEA and subsequent desagglomeration by ultrasonification. Some acetone had to be added to the suspension because it was not enough for the desagglomeration procedure. After desagglomeration, the acetone was evaporated at 80°C for a few minutes. Then the Pd-CeO_2-DGMEA paste was mixed with 1.064 g of NiO-CGO paste. The resulting paste had similar consistency like the undoped paste at a reduced solid loading of about 16 vol%. The reason for this was the very fine particles size of the added Pd-CeO_2 catalyst. The paste had a Pd-content of 1 wt% in respect to the NiO-CGO powder.

Screen Printing and Sintering of Specimens

All the measured samples are summarised in Table 5-2. The dimensions of the pellets as well as the sintering temperatures for all the specimens are given. A blank sample (CGO), i.e. without a catalytic layer, was measured, in order to see if the CGO pellet and the setup themselves already catalyse the methane-oxygen reaction. The used pellet was slightly thicker than the samples with a screen printed electrodes but had the same surface finish from B_4C-lapping. Screen printing was done with a mask of 50 μm thickness and 1×1 cm^2 in size. For the specimens with current-collectors, these were placed on the freshly printed layer and covered with some additional paste by using a paint brush. All the specimens were dried at 80°C for at least two hours. The sintering was done at a heating rate of 1 K/min to 500°C and holding there for 1 hour. Then the specimens were heated at 3 K/min to the peak temperature, which was 1100°C for the cathode and 1300°C for the anode materials. The samples were held at the peak temperature for two hours and subsequently cooled down to room temperature at 5 K/min. The specimen NiCGO had a screen printed layer of the standard anode material and no current-collector. NiCGO_Pd, contained 1 wt% Pd and NiCGO_CC was the standard anode material with integrated current-collector. SSC was characterized

Table 5-2 Overview of different specimens for the measurements of catalytic activity.

Specimen	Diameter [mm]	Thickness [mm]	Sintering temperature [°C]
CGO	21.07	1.9	-
NiCGO	20.9	0.45	1300
NiCGO_Pd	21.0	1.45	1300
NiCGO_CC	21.1	0.45	1300
SSC	21.1	1.26	1100
BSCF	21.0	0.44	1100
SSC_CC	21.1	0.45	1100
Pd-CeO_2	23.0	0.25	unsintered

without (SSC) and with current-collector (SSC_CC), BSCF only without current-collector (BSCF). In addition the catalytic activity of the Pd-CeO_2 catalyst was also studied itself, i.e. without mixing it with NiO-CGO powder (Pd-CeO_2). This specimen was prepared by painting the Pd-CeO_2-DGMEA paste directly onto one side of an electrolyte pellet.

5.2.4 Catalytic Activity of an Entire Single Chamber Cell

In order to study the influence of ionic current through the cell on the reaction rates for the CO and CO_2 formation, an entire cell was also characterised. In a first step the anode was screen printed with a mask thickness of 20 μm. The used NiO-CGO paste was based on the formula shown in Table 5-1. The sintering was done with the standard program for anodes with a holding temperature of 1300°C.

After sintering at 1300°C a new layer of NiO-CGO, 20 μm thick was screen printed and the current-collector placed on top. The latter was covered by a thin layer of NiO-CGO paste. The second sintering of the anode was done at 1200°C. The SSC-cathode was prepared by screen printing through a 50 μm thick mask and subsequently placing a Pt current-collector on the freshly printed layer. Sintering was done in the same way as the cathode specimens described in 5.2.3. The cell with an electrolyte thickness of 1.87 mm was connected to the Au-wires from the setup, by winding the Au-wires around the Pt-wires of the cell. Before doing so the wires of the cell were mechanically fixed to the electrolyte with some refractory adhesive. The anode was facing upwards and the cathode down.

5.2.5 Experimental Setup

The experiments were performed in an atmospheric pressure reactor with a volume of 30 cm^3 that was made out of quartz (Figure 5.1). The reactor temperature was controlled by a surrounding furnace. For measuring the catalytic activity of each sample, it was placed at the bottom of the reactor facing upwards. The gas flow had a similar configuration as in the previously used single chamber measurement setup [12]. A K-type thermocouple that was directly placed on the electrode layer was used to monitor the temperature. Measurements were carried out at an interval of 50°C in the temperature range from 500-800°C.

Inlet flow rates were controlled by using mass flow controllers (Bronkhorst, Switzerland). The concentrations of CH_4, CO and CO_2 in the outlet gas were measured by non-dispersive infrared (NDIR) detection (Siemens Ultramat 5E-2R for CO_2 and a Siemens Ultramat 6 for CO and CH_4).

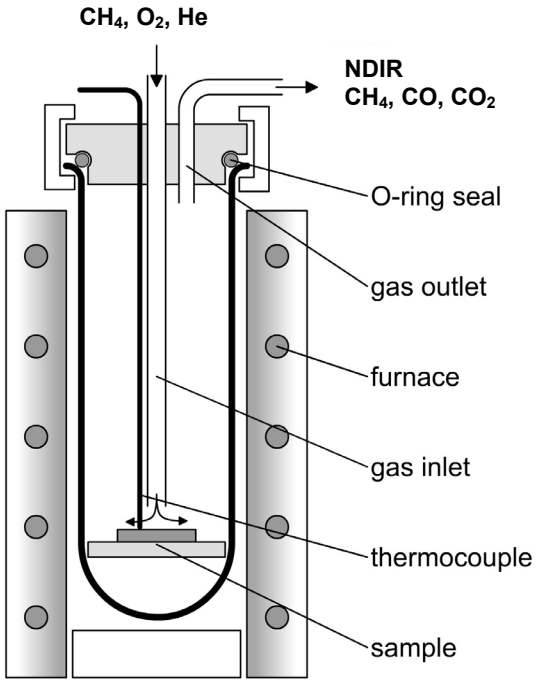

Figure 5.1 Quartz glass atmospheric pressure reactor for the catalysis experiments.

5.2.6 Gas Mixtures

The used gas mixtures are summarised in Table 5-3. All the used gas mixtures were prepared by mixing Carbagas certified standards (Carbagas, Switzerland) of pure He (99.996%), pure CH_4 (99.95%), and 20% O_2-containing He (20% O_2-He, 99.95%).

Table 5-3 Gas flow rates and resulting concentrations for x = 2, x = 1.5 and x = 1.

	CH_4/O_2 = 2		CH_4/O_2 = 1.5		CH_4/O_2 = 1	
	flow rate [ml/min]	flow rate [%]	flow rate [ml/min]	flow rate [%]	flow rate [ml/min]	flow rate [%]
Helium 99.99%	200	66.67	200	66.66	200	66.66
Methane 99.95%	28.6	9.52	23.1	7.70	16.7	5.56
O_2 from 20% O_2-He	14.3	4.76	15.4	5.13	16.7	5.56
He from 20% O_2-He	57.2	19.05	61.5	20.51	66.7	22.22
Total	300	100	300	100	300	100

The used NDIR detector had been calibrated for gases with a CH_4-concentration of less than 10% for a total flow rate of 300 ml/min. In order to obtain gas mixtures with less than 10% of CH_4 at 300 ml/min, the amount of reactive gas, which is the mixture between CH_4 and the 20% O_2-He mixture, was fixed at 100 ml/min. 200 ml/min of pure He was added to all the

mixtures with varying the CH_4/O_2 ratio (x). In order to decrease x, the flow rate of 20% O_2-He was increased and the flow rate of CH_4 decreased.

For x = 2 the concentration of CH_4 amounted to 9.52% and for x = 1 to 5.56%. The gas mixtures are quite similar to gas mixtures that are obtained when diluting mixtures of CH_4 and air. Air contains 20.95% of oxygen [24], whereas the O_2-He mixture was only a 20% mixture.

5.2.7 Calculation of the Reaction Rates

The reaction rates for the CO and CO_2 formation was calculated by multiplying the total flow rate of gas into the reactor in μmol/s with the measured concentrations of CO and CO_2. The total molar flow rate of gases *N* was calculated by using the ideal gas equation:

$$N = \frac{pf_{tot}}{RT} = \frac{10^5 \frac{N}{m^2} \cdot 0.0003 \frac{m^3}{\min}}{8.314 \frac{J}{molK} \cdot 300K} = 0.01203 \frac{mol}{\min} = 200.46 \frac{\mu mol}{s} \qquad (5.7)$$

where p is the total pressure (10^5 Pa) f_{tot} the total flow rate into the reactor at standard conditions ($3 \cdot 10^{-4}$ m^3/min), R the gas constant (8.314 J/mol·K) and T, the absolute temperature (300K).

5.3 Results and Discussion

5.3.1 Reduction of Anode Powders in CH_4-Air Mixtures

In Figure 5.2 the phase diagram of Ni-NiO by Kowalski and Spencer [25] is shown together with the equilibrium oxygen partial pressure of different CH_4-air mixtures [13]. In equilibrium, the NiO-CGO should be in the reduced state in the whole temperature range from 450-1200°C. However, the CH_4-air mixtures cannot react towards the equilibrium composition as there is no metallic Nickel around. Then, the oxygen partial pressure is too high for the NiO to become reduced. At a certain temperature, however, the NiO-CGO powder itself or the added catalytic modifiers will catalyse the reaction between CH_4 and O_2, yielding a low enough $p(O_2)$ for the reduction to commence.

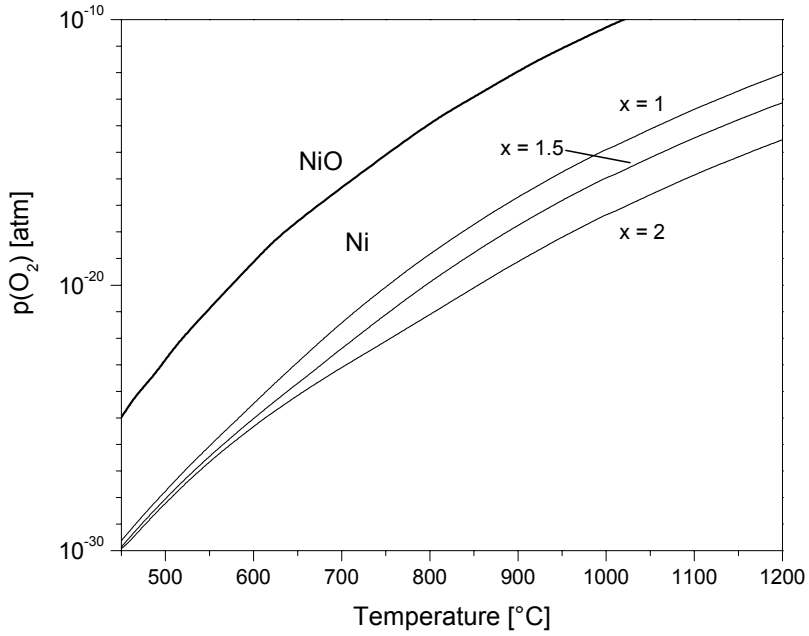

Figure 5.2 Phase Diagram of Ni-NiO as function of oxygen partial pressure [25] and temperature, and equilibrium oxygen partial pressures of CH_4-air mixtures as function of temperature for x = 2, 1.5 and 1 [13].

It can be deduced that at all CH_4/O_2 ratios (x = 1 to 2) the oxygen partial pressure $p(O_2)$ is low enough that metallic Ni is favoured. However, the NiO-reduction during heating in CH_4-air mixtures is kinetically hindered and will only occur at a certain temperature, T_{red} according to Reaction (5.1). T_{red} depends on the x-value of the CH_4-air mixture but also on the heating rate.

An example of a thermogravimetry measurement for unmodified NiO-CGO powder at x = 2 is shown in Figure 5.3. The coloured curves are the measured ion currents of CH_4, CO, CO_2, H_2, H_2O and Ar. The beginning of the full CH_4-oxidation (Reaction (5.5)) was evidenced by increasing CO_2 and H_2O signals starting at around 280°C. At 360° the rate of CH_4-oxidation became higher, as could be deduced from the decrease of the O_2-signal. This was also the temperature where the H_2-signal began to increase, indicating the onset of slight partial oxidation (Reaction (5.4)). The NiO-reduction reaction started at 622°C and was accompanied by a drastic drop of the O_2-signal over three orders of magnitude. The oxygen that was released from the NiO during reduction was apparently removed by reacting with CO and H_2 forming CO_2 and H_2O. These two signals had a maximum during the time of the reduction. In fact, the H_2-signal showed an inverse peak at 660°C, which indicated the hydrogen consumption of the NiO/Ni transformation. After the completion of this transformation during the dwell at 800°C, the H_2- and CO- were the highest signals, and this indicated that the

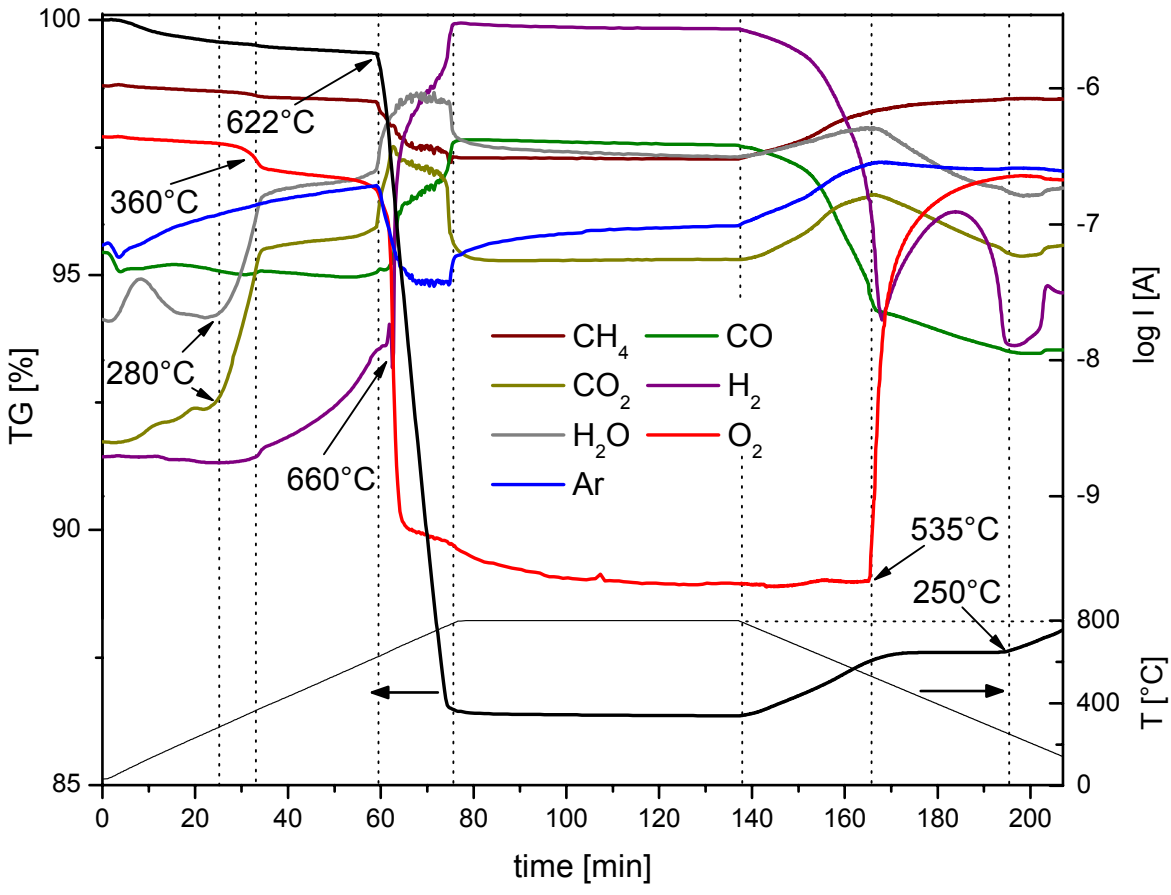

Figure 5.3 Thermogravimetry of NiO-CGO powder in CH_4-O_2-Ar (x = 2) during heating, dwell and cooling.

partial oxidation was the dominant reaction. The amount of H_2 and CO immediately decreased upon cooling at the cost of increasing CO_2, H_2O and CH_4 concentrations. This is in agreement with the thermodynamic equilibrium calculations of CH_4-air mixtures [13]. In the range from 800 down to 463°C the weight of the sample increased by 1.25 wt% (in respect to the initial mass), which was due to carbon deposition that has been shown to occur if at x = 2 the temperature is lower than 800°C [13]. Below 463°C the carbon deposition stopped and was followed by the beginning of superficial reoxidation of Ni-particles at 250°C.

At x = 1 a weight gain of only 0.13% was observed during the cooling, which was caused also by coking, but less severe than compared to the case for x = 2. When the same experiment at x = 2 was repeated at 3 K/min instead of 10 K/min heating and cooling rate the reduction temperature was decreased to 606°C. At the same time the weight gain between 800 and 500°C during cooling was tripled, which corroborates the idea of carbon deposition.

In Figure 5.4 the thermogravimetry measurements are shown for the NiO-CGO powder at x = 1, 1.5, 2 and 7 and for powder, to which the different catalytic modifiers had been added.

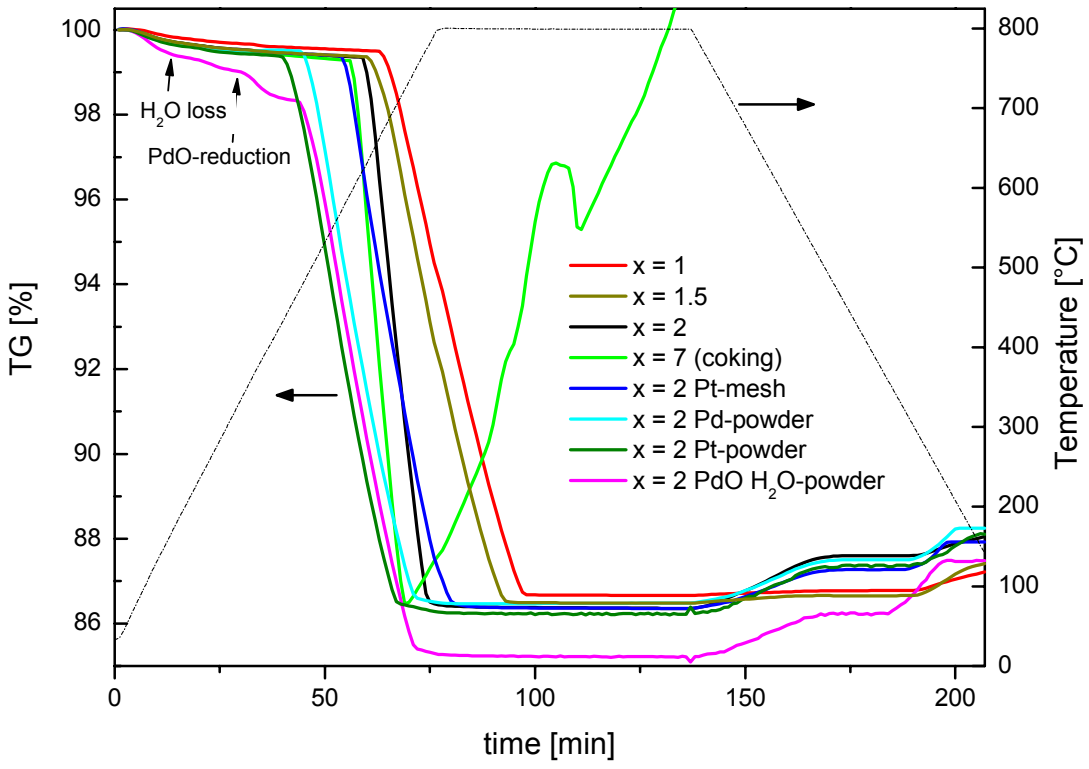

Figure 5.4 Thermogravimetry of NiO-CGO powder in CH_4-O_2-Ar mixtures with varying x and with different catalytic modifiers for x = 2 during heating, dwell and cooling.

It can be seen that each sample had a characteristic temperature at which the NiO reduced to metallic Nickel under otherwise unchanged conditions upon heating. The slopes, i.e. the rate of the reduction reaction also changed in these experiments.

Upon cooling the curve for x = 7 showed a steep weight gain starting from 720°C just after the reduction of the NiO had been completed due to carbon deposition according to thermodynamics. The weight loss at about 110 minutes was due to the carbon-NiO-CGO mixture falling off the TG-crucible. After the measurement the deposited carbon surmounted the rim of the crucible by centimetres. The average weight loss for the measurements with pure powder and varying x-value was 12.88 ± 0.08 wt%. The powder, therefore, showed quite accurately the nominal amount of NiO.

The sample with PdO showed a 1.18 wt% lower TG-signal than the measurement with metallic Pd during the dwell time. The reason for is that in a first stage at temperatures between 100 and 300°C the $PdO \cdot H_2O$ compound dehydrates becoming PdO. In a second stage at a temperature of about 350°C, PdO becomes reduced to metallic Pd, and this induces the reduction of NiO at 471°C. The difference of TG-signals between the Pd- and PdO-modified NiO-CGO is in good agreement with the calculated difference of 1.16 wt% for the dehydration plus the reduction weight loss.

In Table 5-4 the measured the reduction temperature (T_{red}) of all the measured samples are summarised. For the unmodified NiO-CGO powder the reduction temperature decreased with increasing x according to Figure 5.2 and reaches 594°C for x = 7. If a SC-SOFC is supposed to be operated at 600°C with x = 1, it might be feasible to reduce the anode with x =7 for a short time. With x = 1 the anode will not reduce at temperatures below 665°C. However, care must be taken in order not to deposit carbon, which can happen at x = 7 as shown in Table 5-4.

Table 5-4 Reduction temperature of NiO-CGO powder at different x and at x = 2 with Pt-mesh, Pd-powder, PdO-powder and Pt-powder.

	T_{red} [°C]
x = 1	665
x = 1.5	635
x = 2	622
x = 7	594
x = 2 Pt-Mesh	570
x = 2 Pt-Powder	432
x = 2 Pd-Powder	478
x = 2 PdO-Powder	471

The addition of Pt-mesh, as it is normally used for the current-collectors of SC-SOFCs reduced T_{red} by 52°C as compared to the pure NiO-CGO at x = 2. The addition of very fine Pt-powder led to an increased CO_2 and H_2O signal already at 250°C, which was due to the onset of full oxidation after Reaction (5.5) caused by the added Pt-particles. For the undoped NiO-CGO powder this onset was observed at 360°C (see Figure 5.3). As can be seen in Table 5-4, the most drastic reduction of T_{red} was found for the sample containing the amorphous Pt-powder showing the onset of the NiO-transformation already at 432°C. The effect of Pd and PdO addition were quite similar (T_{red} at around 475°C), which can be explained by the fact that PdO is reduced to metallic Pd at around 370°C. The influence of the Pd and Pt additions can be explained by the much higher catalytic activity to the oxidation of methane of these catalysts already at very low temperature as compared to NiO [26]. The highly active modifiers locally induce a low $p(O_2)$ that allow the NiO-reduction to start at lower temperatures.

5.3.2 Reduction of a Sintered NiO-CGO Anode Layer with Integrated Pt Current-Collector

In order to compare the reduction temperature of the NiO-CGO powder with the reduction temperature of a whole SC-SOFC anode, an additional thermogravimetric measurement was done. The specimen consisted of an electrolyte with an anode on one side of the electrolyte that had been prepared as described in 5.2.3. The screen printing was done with a mask thickness of 20 µm and the sintering was done at 1300°C together with the Pt current-collector. In Figure 5.5 the thermogravimetry measurement of an anode layer is shown under the same conditions as the NiO-CGO powder from Figure 5.3. At 536°C an onset for the full oxidation occurred, 176°C higher than for the NiO-CGO powder. The reduction of the NiO in the sintered anode took place at 757°C, which is 135°C higher than for the powdery state. During the reduction a mass loss of 0.48% of the whole specimen (0.505 g) was measured.
From this an anode weight without current-collector of about 20 mg was calculated. There was a weight gain upon cooling, which could be attributed to carbon deposition via the Boudouard reaction (Reaction (5.2)) because during this phase the CO-signal decreased and at the same time the CO_2 showed a peak. Starting from 718°C, the oxygen-current increased over three orders of magnitude and the H_2-signal showed a peak that can be attributed to carbon deposition via CH_4-cracking (Reaction (5.3)), which is thermodynamically favoured at

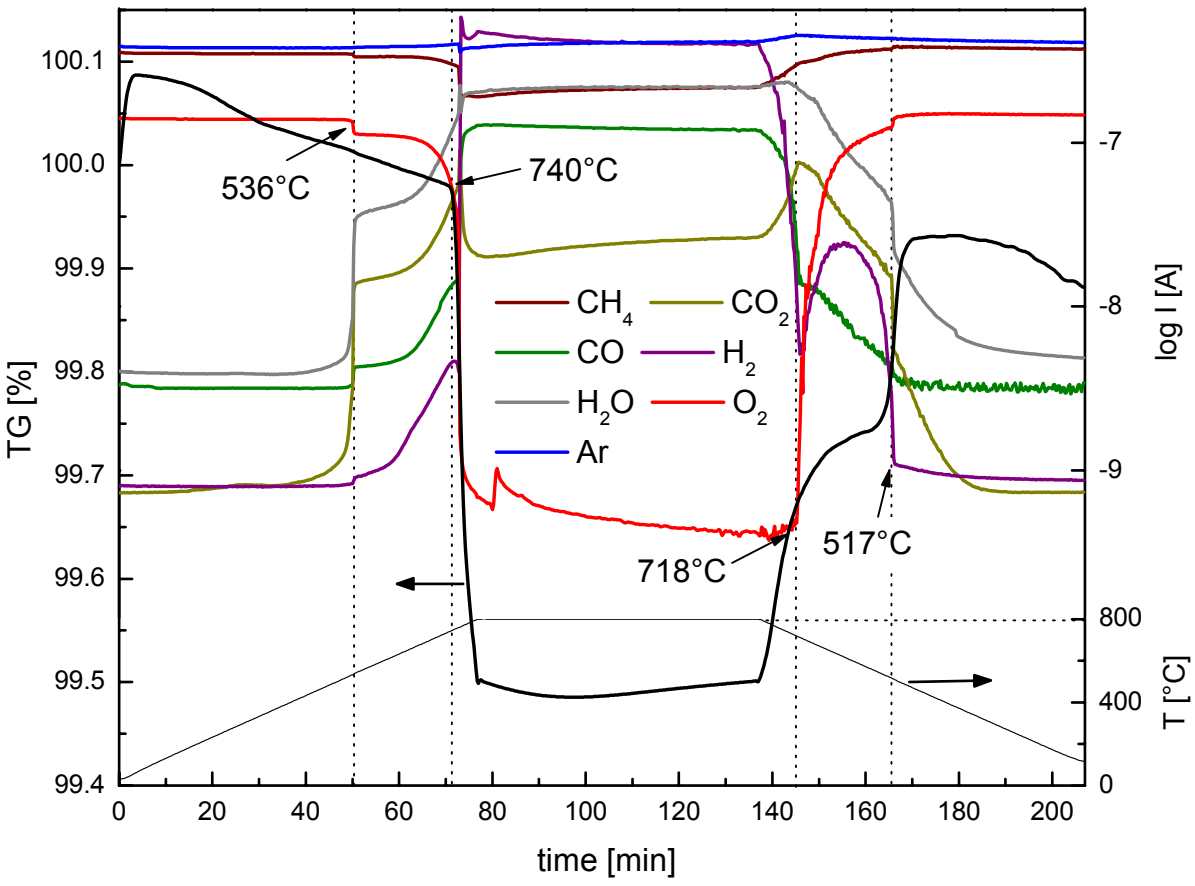

Figure 5.5 Thermogravimetry of a NiO-CGO anode with Pt current-collector mesh in CH_4-O_2-Ar (x = 2) during heating, dwell and cooling.

temperatures above 500°C. At temperatures below 517°C the full oxidation ceased and a situation similar to the one at the beginning was re-established.

From the conducted thermogravimetry experiments of the unsintered NiO-CGO powder (Figure 5.3) and of the anode layer made from this material with Pt current-collector (Figure 5.5) it can be concluded that the state of the material has a strong effect on T_{red}. For the sintered material T_{red} was more than 130°C higher than for the powder. Furthermore the powder showed an onset for the full oxidation at 150°C lower temperatures as compared to the anode layer, which is due to the higher catalytic activity caused by the smaller particle size. As compared to the sintered layer the NiO-CGO powder stayed active for methane oxidation down to 535°C during cooling, whereas the anode layer showed a loss of catalytic activity already at 718°C.

5.3.3 Anode and Cathode Layers without Current-Collectors

In order to evaluate the catalytic activity of the anode and cathode of a SC-SOFC the sintered layers were first studied without current-collectors. In Figure 5.6 the reaction rates for the partial oxidation and the full oxidation for both anode (NiO-CGO) and cathode (SSC) material are plotted as a function of temperature. The reaction rate for both reactions increased with increasing temperature, as could be expected. For both materials the formation rate of CO_2 was almost always higher than the formation rate of CO, which means that a substantial amount of parasitic reactions is occurring at both electrodes. However, for both partial and full oxidation the anode had a much higher activity than the cathode as can be seen by comparing Figure 5.6 a and b (please not the different scale). At 700°C the formation rate for CO_2 at the anode is seven times higher than at the cathode. The formation rate of CO at the anode is more then 5 times higher than at the cathode at the same temperature. A steep increase for the partial oxidation at temperatures above 650°C was found for the SSC-layer, and at 800°C the formation rate of CO was higher than the CO_2 formation rate, which means the cathode becomes selective for partial oxidation. At 800°C the CO reaction rates of both materials were similar: 0.170 µmol/s and 0.140 µmol/s were measured for the anode and cathode layers, respectively.

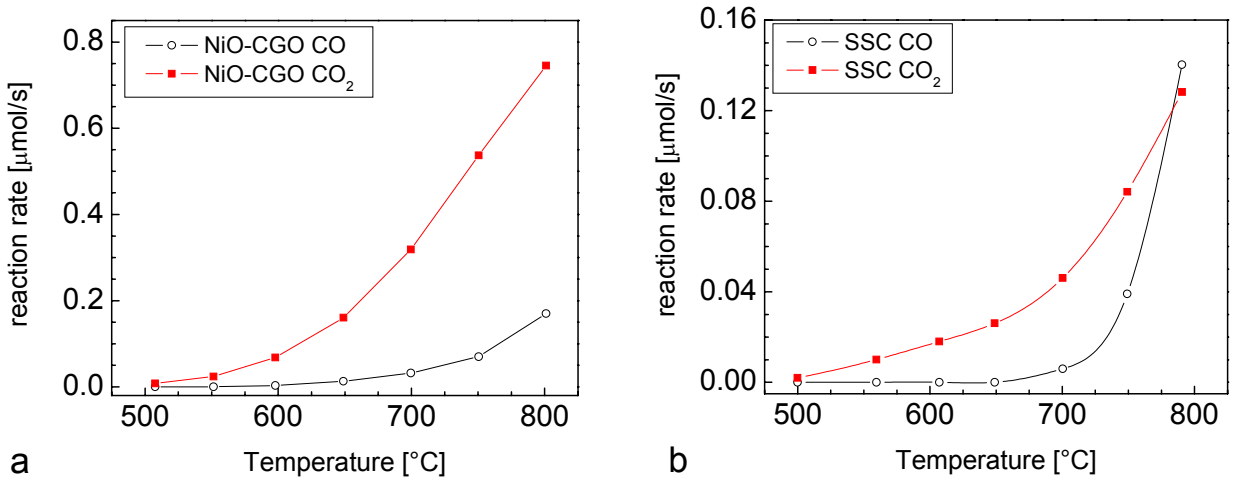

Figure 5.6 Reaction rates for the CO- and CO_2-formation as a function of temperature for a) a NiO-CGO layer and b) a SSC-layer, both without current-collectors at x = 2.

On the one hand the influence of Pd-CeO_2 catalyst being added to the anode was investigated, on the other the catalytic activity of the sole catalyst on a CGO-electrolyte was

studied. The results are summarised in Figure 5.7 a. The CO_2-formation rate of the uncalcined Pd-CeO_2 nano-catalyst on CGO was relatively high but lower than the rate of NiO-CGO. Pd-CeO_2 generated a relatively low amount of CO, as can be seen in Figure 5.7 a. It has been shown that Pd-based catalysts are very active for the full oxidation of CH_4 [27,28]. The reason why the NiO-CGO was more active was due to the higher catalytically active surface area. The Pd-modified NiO-CGO layer, also shown in Figure 5.7 a generated practically no CO_2 and much more CO at temperatures above 750°C. The reason why the Pd-CeO_2 catalyst itself practically only generates CO_2 while it increases the CO-selectivity when added to Ni-CGO material may be due to the internal reforming [29] of the unreacted CH_4 with H_2O that is formed by the full oxidation, which is promoted by Pd-CeO_2.

In Figure 5.7 b the reaction rates for the partial and full oxidation are plotted for the blank CGO pellet, the BSCF sample and, for comparison, the SSC from Figure 5.6 b. The CGO pellet only showed very small activity for the CH_4-oxidiation at temperatures below 750°C. At T > 750°C, however, the blank CGO-pellet started to promote the reaction between CH_4 and O_2 as can be clearly seen. The blank pellet's reaction rate both for CO and CO_2 was always much lower than the reaction rates of the investigated electrodes. BSCF exhibited nearly the same CO_2 formation rate as SSC, save at temperatures above 750°C, where it promoted the full oxidation slightly stronger. The measurement proved the suitability of the BSCF material for SC-SOFCs because the formation rate of CO was clearly lower in the whole temperature range than for SSC.

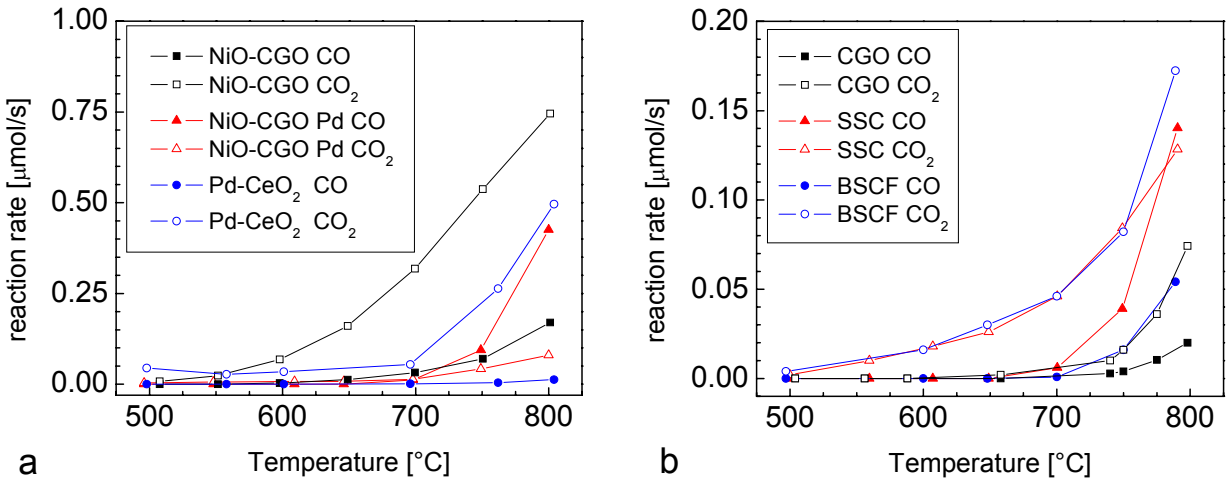

Figure 5.7 a) Formation rates of CO and CO_2 at x = 2 for the modified anodes; NiO-CGO_Pd and the pure catalyst Pd-CeO_2. The NiO-CGO is plotted for comparison. b) Formation rates of CO and CO_2 for the blank pellet (CGO) and the new cathode material BSCF. SSC is plotted for the purpose of comparability.

At high temperatures, however, this material will promote the parasitic full oxidation stronger than SSC, thereby decreasing the possible efficiency of a SC-SOFC having this electrode material.

It was stated that the operation principle of a SC-SOFC is based on the different catalytic activity of the electrode materials for the partial oxidation of methane, Reaction (5.4). In Figure 5.8 a the reaction rates of NiO-CGO and SSC for the partial oxidation are plotted as a function of temperature. CO and H_2 are the products formed by the partial oxidation. If we postulate that CO and H_2 are oxidised electrochemically both at the anode and the cathode at the same rate as the preceding partial oxidation at each electrode, then only the difference of the reaction rates (Δrr_{CO}) of the anode and cathode will lead to an ionic current in the electrolyte (Equation (5.8)). Thus, the higher Δrr_{CO}, the higher the ionic current in the electrolyte will be.

$$\Delta rr_{CO} = rr_{CO}^{A} - rr_{CO}^{C} \tag{5.8}$$

The difference between the reaction rates at both materials Δrr_{CO} is plotted in Figure 5.8 b. It reaches a maximum of 0.011 µmol/s at about 740°C and at temperatures above 800°C the difference becomes negative, i.e. SSC had a higher CO-formation rate than NiO-CGO. For every partially oxidised CH_4, as shown in Reaction (5.4), one CO- and two H_2-molecules are formed. In a subsequent step they are electrochemically oxidised according to Reaction (5.9).

$$CO + 2H_2 + 3O^{2-} \xrightarrow{\Delta rr_{CO}} CO_2 + 2H_2O + 6e^- \tag{5.9}$$

For every partially oxidised CH_4, $6e^-$ are released. Then, the current J that flows through the external circuit can be calculated by using the following equation:

$$J = 6q \cdot N_A \cdot \Delta rr_{CO} = 6F \cdot \Delta rr_{CO} \tag{5.10}$$

where q is the elementary charge, N_A Avogadro's Number and F Faraday's constant (96485 Cb). If methane could be directly electrochemically oxidised at the SC-SOFC anode as shown in Reaction (5.11), a 33% higher current could be obtained because for every oxidised CH_4-molecule, $8e^-$ are released as compared to $6e^-$ for the partial oxidation.

$$CH_4 + 4O^{2-} \rightarrow CO_2 + 2H_2O + 8e^- \qquad (5.11)$$

The current that was calculated with Δrr_{CO} = 0.011 µmol/s using Equation (5.10) amounts to 6.4 mA. This value is much lower than what was measured in our previous work on SC-SOFCs with integrated current-collectors, where short circuit currents of up to 2.2 A were obtained at comparable temperatures. Thus, the difference of catalytic activity for the partial oxidation of methane (Reaction (5.4)) between the NiO-CGO anode and the SSC cathode without current-collectors is too low for allowing a high current through the cell.

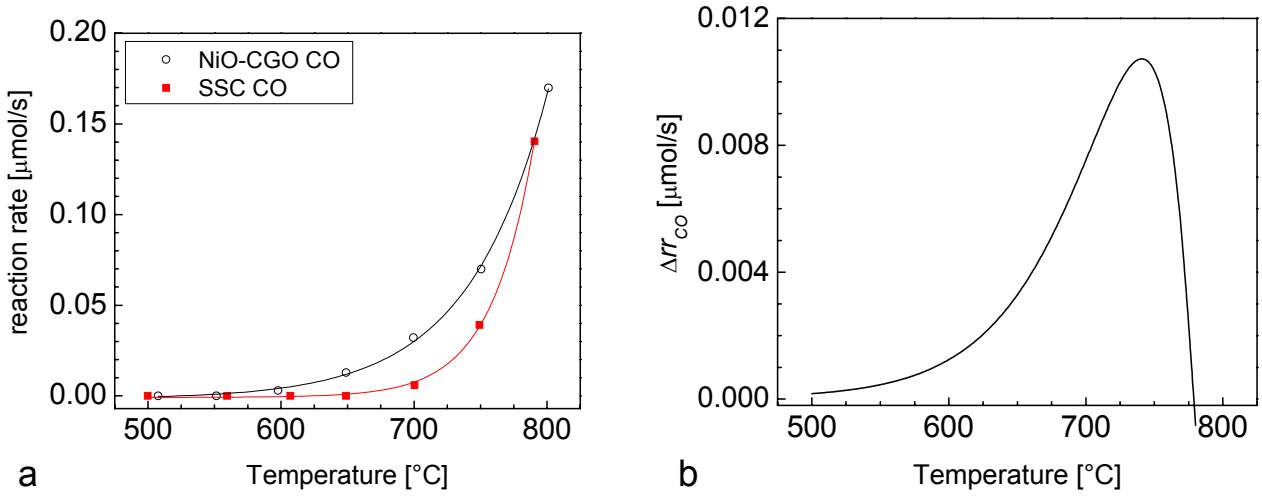

Figure 5.8 a) Reaction rate for the partial oxidation of methane of NiO-CGO and SSC layers as a function of temperature. b) Difference of the reaction rates for the partial oxidation of the NiO-CGO anode and SSC cathode.

5.3.4 Anode and Cathode Layers with Current-Collectors

A fuel cell cannot function if the generated current is not collected in an efficient way from the porous electrodes. As the current-collectors might influence the reaction rates for Reactions (5.4) and (5.5), experiments on electrodes with embedded current-collectors (CC) were performed. For the SSC-electrode with Pt-mesh current-collector (Figure 5.9 b) the measured reaction rates were similar to the situation without current-collector. The CO formation rate was not strongly affected by the presence of the Pt-mesh, but the CO_2 formation rate was about 4 times higher than without Pt for all the measured temperatures. The presence of Pt in the cathode layer therefore increased the amount of parasitic reaction. For the anode the situation looked quite different than without current-collector. The black

curves in Figure 5.9 a correspond to the catalytic activity of the sample during heating; the red curves were measured during cooling.

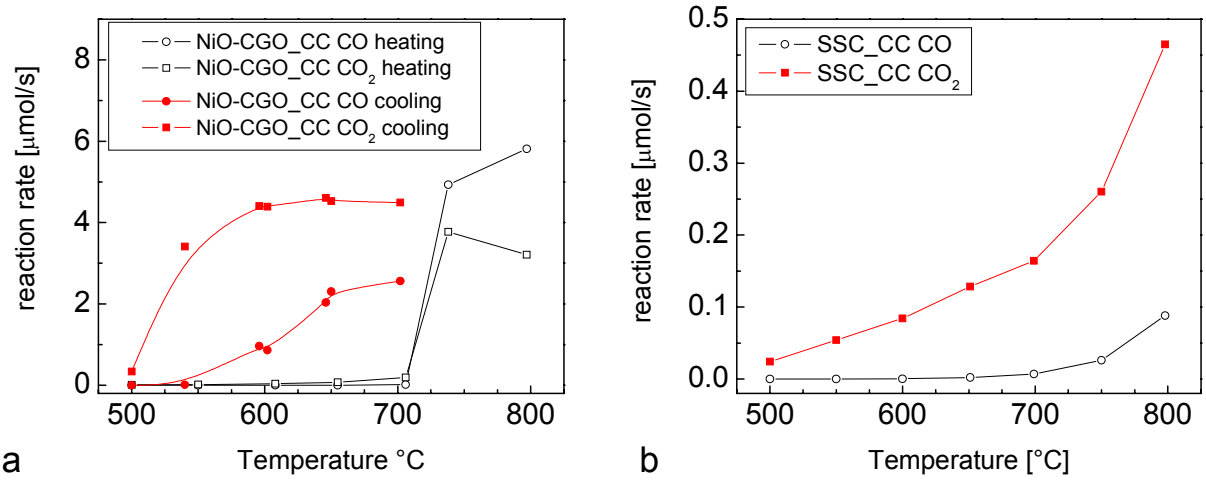

Figure 5.9 Reaction rates for the CO- and CO_2-formation as a function of temperature for a) the anode and b) the cathode layers both with Pt current-collectors at x = 2.

While heating from 700 to 750°C there was a drastic change of catalytic activity for both the partial and the full oxidation, which can be attributed to the reduction of NiO to metallic Ni. This observation is in agreement with the TG-measurement of an anode with current-collector (Figure 5.5). The fast heating rate of 10 K/min caused the anode reduction to be shifted to higher temperature as compared to the lower heating rates used here. Above 738°C, the reaction rate for CO is even higher than for CO_2, which was only observed for this specimen and the Pd-modified anode (NiO-CGO_Pd). During cooling the electrode with Pt-mesh remained in the metallic state at lower temperatures than during heating the reduction had taken place. The catalytic activity showed a hysteresis as it was already observed in ref. [11] in terms of open circuit voltage of the cell during heating and cooling. The reduced Ni-CGO anode (during cooling) showed a 24 times higher activity for the full oxidation and 180 times higher activity for the partial oxidation at 700°C as compared to the unreduced specimen (during heating). The fact that the reaction rate of the partial oxidation increased at the cost of the full oxidation when going from 738 to 800°C indicated that the catalyst under these conditions allows the gas mixture to react towards the thermodynamic equilibrium.

The influence of the gas composition on the reaction rates for the partial and full oxidation at anode and cathode layers with current-collectors is shown in Figure 5.10. The measurements of the anode with current-collector (Figure 5.10 a) showed that rr_{CO_2} increased

when going from x = 2 to x = 1.5. At x = 1 and temperatures below 700°C, the reaction rate could not be measured because the anode showed decreasing reaction rates for both full and partial oxidation, indicating that the Ni began to reoxidise. This had to be avoided, so the plotted values in Figure 5.10 a for x = 1 were obtained during heating as compared to the case for x = 2 and x = 1.5.

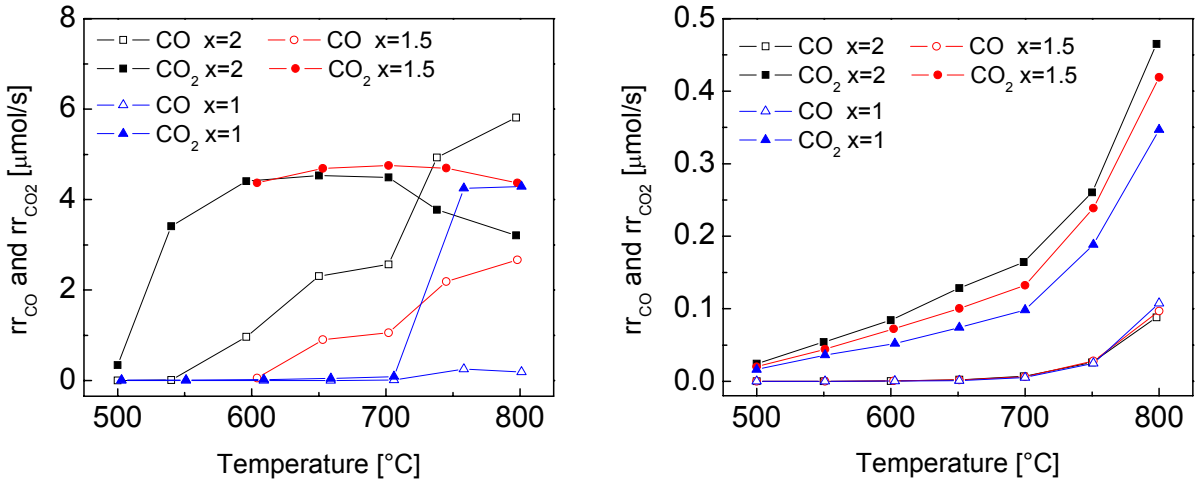

Figure 5.10 Reaction rates for the CO and CO_2-formation at x = 2, 1.5 and 1, for a) NiO-CGO and b) SSC both with current-collectors.

Obviously, when more oxygen was available at the anode, a higher reaction rate for the parasitic full oxidation was obtained. The reaction rate for the partial oxidation rose with increasing x-value. Figure 5.10 b shows the reaction rate for the partial and full oxidation of SSC for different x-values. The reaction rate for the partial oxidation is very low for all gas compositions, while the reaction rate for the full oxidation is clearly higher in CH_4-rich gas.

In Figure 5.11 a the reaction rate of the partial oxidation for the reduced anode and the cathode with current-collectors are plotted on a logarithmic scale versus temperature. When the anode was in the reduced state it had more than 190 times higher catalytic activity at around 740°C than the cathode. The difference of catalytic activity of both electrodes with current-collectors is shown in Figure 5.11 b. The difference increased monotonically with increasing temperature in the whole temperature range. At 740°C, where without current-collector there was a maximum of catalytic activity difference, the difference now was 4.2 µmol/s. This value would in theory allow a short circuit current in the single chamber fuel cell of 2.43 A, as calculated by Equation (5.10). This is in good agreement with the experimentally measured currents from previous work [12].

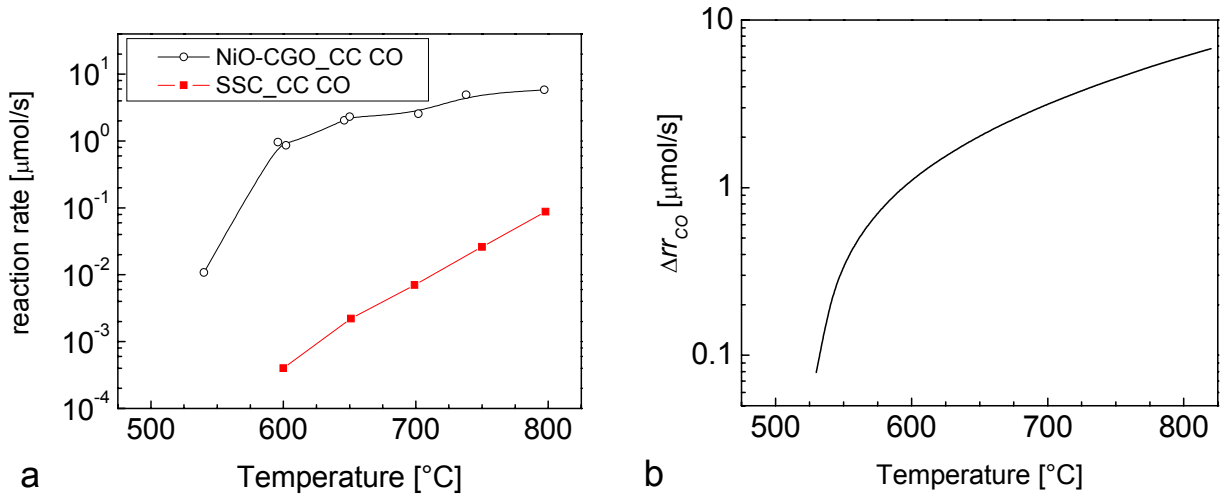

Figure 5.11 a) Reaction rate for the partial oxidation of methane of NiO-CGO and SSC with Pt-mesh. b) Difference of the reaction rates for the partial oxidation of both electrode layers with Pt-mesh.

Of course the very simple model put forth herewith does not include the ohmic resistance of the electrolyte or the electrode overpotentials, which limit the achievable short circuit currents. Nevertheless, the results show that the different catalytic activities of the electrodes for the partial oxidation can explain the high electric currents measured in SC-SOFCs.

5.3.5 The Selectivity of SC-SOFC Materials

A suitable anode material should have a high S(CO) as defined by Equation (5.6). In contrast to the anode, the cathode material should have a very small or zero S(CO). In Figure 5.12 the selectivities for the different gas compositions (x = 2, 1.5 and 1) of all the measured specimens are summarised. The anode layer that was modified with Pd-CeO_2 catalyst (NiO-CGO_Pd) showed the highest selectivity at all x-values. This could explain the high power outputs that were obtained by Hibino et. al [15] in addition to the lowered reduction temperature of the anode. In contrast the ceria pellet having only the Pd-CeO_2 catalyst on top showed the lowest selectivity at nearly all condition. The reason for this is that Pd-catalysts show a very high activity for the full oxidation [26]. A high S(CO) was also found for the NiO-CGO_CC at high temperatures and x = 2, which decreased with decreasing x. The reason for the lower CO-selectivity was the increasing reaction rate for CO_2 and decreasing reaction rate for CO formation with decreasing x. At x = 1 the NiO-CGO_CC had negligible S(CO).

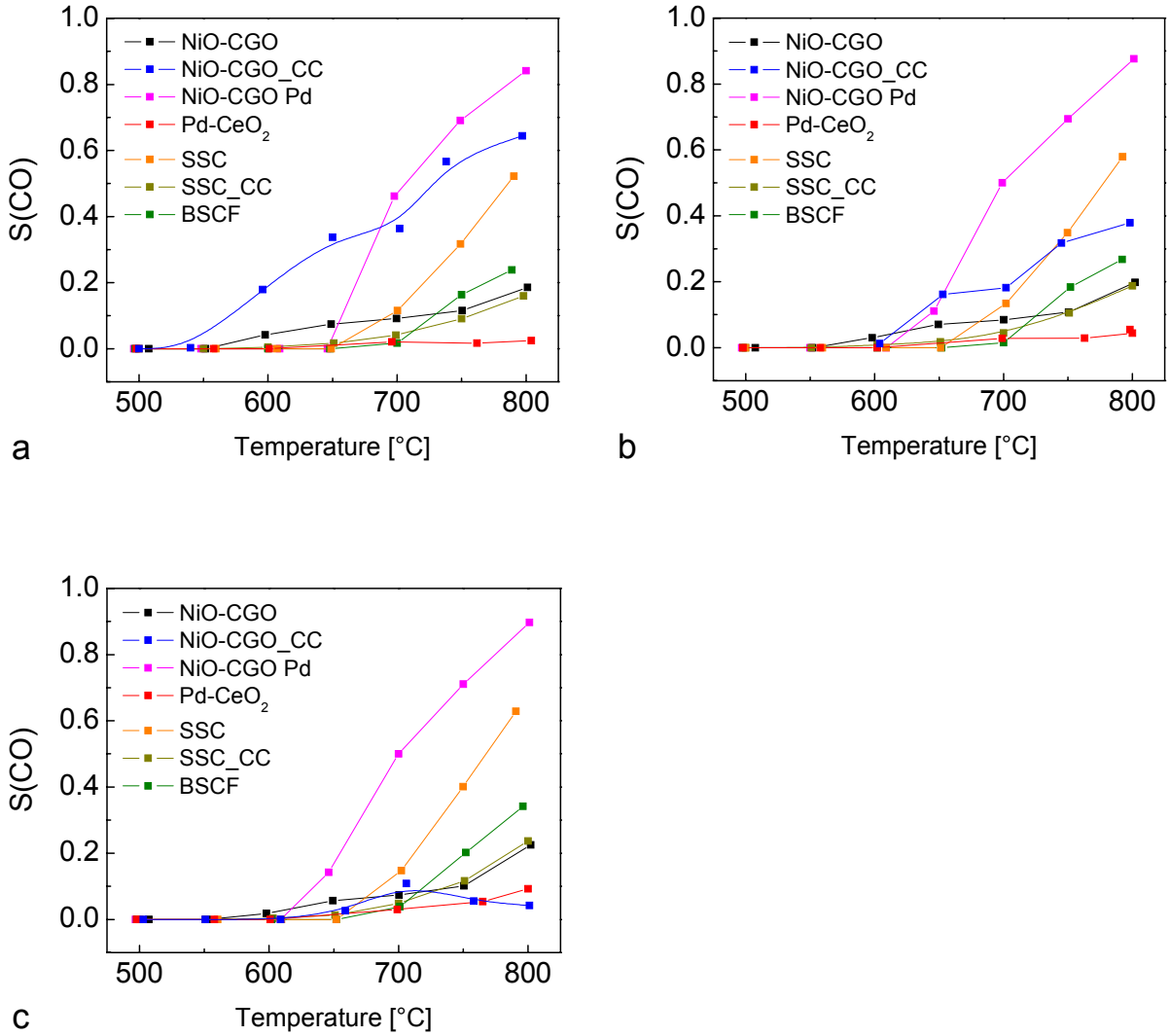

Figure 5.12 Selectivity S(CO) for the partial oxidation of CH_4 of all the characterised specimens at a) x = 2, b) x = 1.5 and c) x = 1.

Both cathode materials SSC and BSCF showed a very low S(CO) at low temperatures and an increased S(CO) at elevated temperatures. For BSCF the onset of S(CO) was found at T > 700°C for SSC already at T > 650°C. The current-collector in SSC_CC decreased the selectivity of this electrode as compared to SSC without current-collector because of the increased CO_2 formation rates caused by the Pt-mesh.

5.3.6 Catalytic Activity of an Entire SC-SOFC

In order to study the influence of current through the cell on the reaction rates for the CO and CO_2 formation, an entire cell was characterised in the same setup with the same gas mixtures as was used for the other experiments. When testing an entire cell a decrease of rr_{CO} and an increase of rr_{CO_2} can be expected when current is drawn from the cell. The reasons for this are the consumption of CO by oxygen ions and the release of CO_2 according to Reaction (5.9).

Upon introduction of the gas mixture with x = 2 (same gas mixtures as for catalysis measurements) at 550°C, the cell voltage rose from 6 mV to 80 mV, which is in the range of the usual OCV for unreduced NiO-CGO anodes. The outlet gas at this condition contained not even traces of CO. The anode of the cell could not be reduced at these conditions so the total flow rate was increased to 400 ml/min (x = 1.8) without He-dilution. After turning off this gas mixture and turning on the initial gas mixture again (x = 2), the OCV suddenly rose to 0.9 V. The reason for the reduction taking place after turning off the gas was that the gas in the reactor became more reducing with time. When it was left in the reactor for a few minutes, the gas mixture reacted towards the thermodynamic equilibrium, which caused a very low $p(O_2)$ that reduced the NiO. After the anode of the cell had been reduced the cell gave an OCV of 0.90 V and a current-density of 45 mA/cm^2 at U_{Cell} = 0.45V, which corresponded to a power output of 20 mW/cm^2. The influence of the cell current on the reaction rates for CO and CO_2 were studied at 600°C for x = 2 and x = 1.5 and the results are shown in Figure 5.13. No measurements were done at x = 1 because the anode had reoxidised, which could be

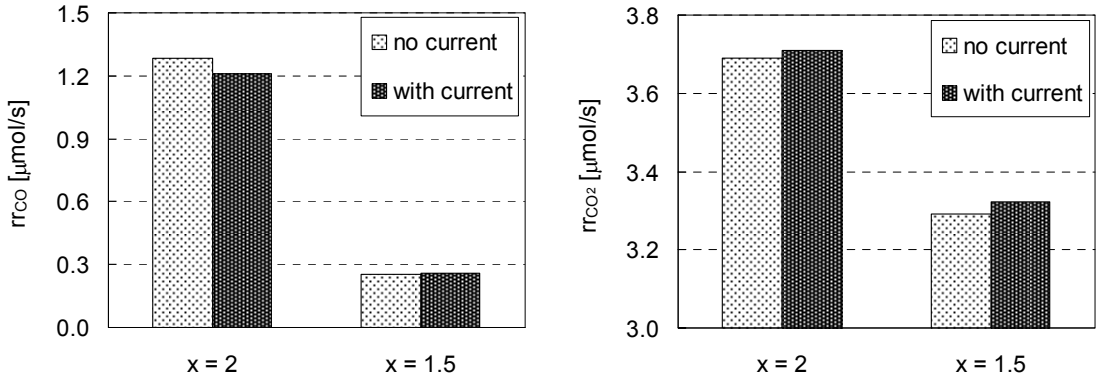

Figure 5.13 Influence of the cell current on a) rr_{CO} and b) rr_{CO_2} at 600°C for a SC-SOFC with 1.87 mm thick electrolyte. The cell current at x = 2 was 40 mA/cm^2 and 50 mA/cm^2 at x = 1.5.

concluded from the low OCV of 0.095 V and the very low CO-concentrations in the outlet gas. These observations were in agreement with the catalytic activity measurements of the NiO-CGO_CC specimen at x = 1.At x = 2, the current through the cell was 40 mA/cm^2 (at 0.38 V), whereas at x = 1.5 it was 50 mA/cm^2 (at 0.41 V). For x = 2 the reaction rate for CO_2 increased with current through the cell, whereas for CO it decreased. The reason for this is that CO stemming from the partial oxidation is electrochemically oxidized to CO_2. By the electric current through the cell, the apparent rr_{CO} is decreased because O^{2-} reacts with CO but also with H_2, which are the products of the partial oxidation. The difference between rr_{CO} without and with current was $7.42 \cdot 10^{-2}$ µmol/s (at x = 2). When using Equation (5.10) with J = 40 mA, a difference of $6.9 \cdot 10^{-2}$ µmol/s is obtained. This agrees reasonably well with the measured difference of $7.42 \cdot 10^{-2}$ µmol/s. At x = 1.5 no change of rr_{CO} could be observed when current was driven through the cell.

5.4 Summary

The reduction temperature of as purchased NiO-CGO powder was studied by thermogravimetry in mixtures of CH_4, O_2 and Ar. It was shown that the reduction temperature (T_{red}) of NiO-CGO depends on the ratio of CH_4/O_2 (x) and that gas mixtures with high CH_4-concentration (high x-value), led to a lower reduction temperature. In gas mixtures having $x = 2$, the NiO reduction began at 622°C, whereas at $x = 1$ an onset of reduction was measured at 665°C.

The addition of Pt-mesh, as it has been used in anodes for SC-SOFCs drastically reduced the reduction temperature down to 570°C. If Pt powder with a higher dispersion as compared to Pt-mesh is used, T_{red} is further reduced down to 432°C. The influence of PdO and Pd were quite similar but the PdO was reduced in a first stage to Pd at temperatures of 350°C. Irrespective of the compound in which the Pd was added (as oxide or metal), T_{red} of NiO was lowered to about 475°C.

The thermo-gravimetric measurement of an anode with Pt current-collector mesh showed that the reduction temperature lies much higher when the NiO-CGO material is in the sintered state ($T_{red} = 740$°C), which was in good agreement with the catalytic activity studies, where an onset of reduction was measured at 738°C. The reduction of NiO to metallic Ni in the NiO-CGO layer only occurred when there was a Pt current-collector mesh embedded within the electrode.

The catalytic activity experiments showed that the difference of catalytic activity for the partial oxidation of CH_4 between the NiO-CGO and SSC layers was too low without Pt current-collectors (unreduced anode). Only for the anode with Pt current-collector at $T \geq 738$°C and $x > 1$, the difference was high enough to enable short circuit current densities in the range of 1 to 3 A/cm^2. For most of the specimens the selectivity for the partial oxidation S(CO) was lower than 0.5. Exceptions were NiO-CGO_CC at $x = 2$ when cooled from high temperature and Pd-CeO_2 modified NiO-CGO in the whole temperature range. At high temperatures SSC showed a high activity for the partial oxidation (high S(CO)), which means that in SC-SOFCs using this material as the cathode, there will be a considerable amount of fuel waste if operated at too high temperatures. The selectivity does not necessarily explain that it is possible to draw useful current from SC-SOFCs. It is the absolute difference between the reaction rates for the partial oxidation of methane that can explain the relatively high power outputs.

The measurement of an entire SC-SOFC with externally applied electrical potential indicated that the apparent reaction rate for the CO formation decreased with current through the cell, whereas the reaction rate for the CO_2 formation increased.

5.5 Outlook

The study of catalytic activity of electrode materials is of great importance for gaining a more thorough understanding of SC-SOFCs operating in hydrocarbon-air mixtures. In order to further improve the performance of SC-SOFCs, cathode materials that are more tolerant to the used fuels are needed. Furthermore, an anode material that is highly active for the partial oxidation of the hydrocarbon fuel is required. As the cathode becomes active for parasitic reactions at higher temperatures and the anode becomes oxidised in the used fuel-air mixtures at low temperatures, there is only a limited temperature range, in which SC-SOFCs can be operated. The results with the catalytic modifiers suggested that it is possible to broaden the possible temperature range to lower temperatures by the use of certain additives that keep the metallic Ni in the anode in the reduced state.

The reason for the drastically higher reduction temperature of the sintered anode as compared to unsintered powder cannot be understood with the carried out experiments. The reason for the observations cannot solely be due to the increased grain size after sintering. The grain size did not change so drastically during sintering because NiO and CGO are homogeneously distributed and the grains cannot grow like in a single-phase material. The experiments should be repeated with powders having different grain size of NiO, which can be produced by calcination at different temperatures. Then the activation energy of the NiO-reduction could be evaluated in an Arrhenius plot, by plotting the logarithm of grain size versus the inverse reduction temperature.

5.6 Acknowledgements

The authors would like to thank Dr. Elena Baranova, Dr. György Fóti and Prof. Dr. Christos Comninellis for making the measurements in their laboratory at EPFL possible and for their assistance with all the conducted catalysis measurements. Furthermore the authors would like to thank Dr. Karsten Wegner and Dr. Reto Strobel (PLT, Federal Institute of Technology, Zurich) for providing the Pd-CeO_2 catalyst.

5.7 References

[1] N. Q. Minh, *Solid State Ionics*, **2004**, 174, *1-4***,** 271-277.

[2] T. Hibino and H. Iwahara, *Chemistry Letters*, **1993**, 7, 1131-1134.

[3] K. Asano, T. Hibino and H. Iwahara, *Journal of the Electrochemical Society*, **1995**, 142, *10***,** 3241-3245.

[4] T. Hibino, A. Hashimoto, T. Inoue, J.-i. Tokuno, S.-i. Yoshida and S. Mitsuru, *Journal of the Electrochemical Society*, **2000**, 147, *8***,** 2888-2892.

[5] B. Lewis and G. von Elbe, "The Reaction between Hydrogen and Oxygen", 1961. p. 23-57.

[6] A. K. Demin and F. Y. Gulbis, *Solid State Ionics*, **2000**, 135, 451-456.

[7] T. Hibino, S. Wang, S. Kakimoto and M. Sano, *Electrochemical and Solid State Letters*, **1999**, 2, *7***,** 317-319.

[8] J. Will, A. Mitterdorfer, C. Kleinlogel, D. Perednis and L. J. Gauckler, *Solid State Ionics*, **2000**, 131, *1-2***,** 79-96.

[9] C. Mallon and K. Kendall, *Journal of Power Sources*, **2005**, 145, *2***,** 154-160.

[10] T. Nakamura, G. Petzow and L. J. Gauckler, *Materials Research Bulletin*, **1979**, 14, *5***,** 649-659.

[11] B. E. Buergler, M. Siegrist and L. J. Gauckler, in *Sixth European Solid Oxide Fuel Cell Forum, 2004,* M. Mogensen, 1405-1413.

[12] B. E. Buergler, M. E. Siegrist and L. J. Gauckler, *Solid State Ionics*, **2005**, 176, *19-22***,** 1717-1722.

[13] B. E. Buergler, N. A. Grundy and L. J. Gauckler, *Journal of the Electrochemical Society*, **2006**, 153, *7***,** A1378-A1385.

[14] T. Hibino, H. Tsunekawa, S. Tanimoto and M. Sano, *Journal of the Electrochemical Society*, **2000**, 147, *4***,** 1338-1343.

[15] T. Hibino, A. Hashimoto, M. Yano, M. Suzuki, S.-i. Yoshida and S. Mitsuru, *Journal of the Electrochemical Society*, **2002**, 149, *2***,** A133-A136.

[16] T. Hibino, A. Hashimoto, S. Masanori, Y. Masaya, Y. Shin-ichiro and S. Mitsuru, *Journal of the Electrochemical Society*, **2002**, 149, *2***,** A195-A200.

[17] S. C. Tsang, J. B. Claridge and M. L. H. Green, *Catalysis Today*, **1995**, 23, *1***,** 3-15.

[18] E. Ruckenstein and Y. Hang Hu, *Applied Catalysis A: General*, **1999**, 183, *1***,** 85-92.

[19] V. R. Choudhary, V. H. Rane and A. M. Rajput, *Catalysis Letters*, **1993**, 22, 289-297.

[20] P. D. Vernon, M. L. Green, A. K. Cheetham and A. T. Ashcroft, *Catalysis Letters*, **1990**, 6, 181-186.

[21] Z. Shao, S. M. Haile, H. Ahn, P. D. Ronney, Z. Zhan and S. A. Barnett, *Nature*, **2005**, 435, 795-798.

[22] R. Strobel, F. Krumeich, W. J. Stark, S. E. Pratsinis and A. Baiker, *Journal of Catalysis*, **2004**, 222, *2***,** 307-314.

[23] M. Gödickemeier, "Mixed Ionic Electronic Conductors for Solid Oxide Fuel Cells", Ph.D. Thesis, Diss. ETH No. 11348, Swiss Federal Institute of Technology, 1996.

[24] Römpp, "Chemie", 10 ed., Thieme, Stuttgart, New York, 1997.

[25] M. Kowalski and P. J. Spencer, *Calphad*, **1995**, 19, *3***,** 229-243.

[26] R. B. Anderson, K. C. Stein, J. J. Feenan and L. J. E. Hofer, *Industrial and Engineering Chemistry*, **1961**, 53, *10***,** 809.

[27] A. D. Frantzis, S. Bebelis and C. G. Vayenas, *Solid State Ionics*, **2000**, 136-137, 863-872.

[28] Z. Li and G. B. Hoflund, *Journal of Natural Gas Chemistry*, **2003**, 12, 153-160.

[29] S. H. Clarke, A. L. Dicks, K. Pointon, T. A. Smith and A. Swann, *Catalysis Today*, **1997**, 38, ***4*****,** 411-423.

6 Single Chamber Solid Oxide Fuel Cells with Integrated Current-Collectors

B. E. Buergler, M. E. Siegrist, L. J. Gauckler, *Solid State Ionics*, **2005**, *176* (19-22), 1717-1722.

ABSTRACT: Single chamber solid oxide fuel cells (SC-SOFCs) based on the system $Sm_{0.5}Sr_{0.5}CoO_{3-\delta}$ / $Ce_{0.9}Gd_{0.1}O_{1.95}$ / Ni-$Ce_{0.8}Gd_{0.2}O_{1.90}$ were investigated. Pt-meshes that were embedded in both electrodes were used as current-collectors in order to achieve low overpotentials. The cells generated 271 mW/cm^2 at 500°C and 468 mW/cm^2 at 600°C on a gas mixture of methane and air (CH_4/O_2 =1.6) with a total flow rate of 1500 ml/min. The air flow rate was varied (260, 780, 1120 and 1340 ml/min) while the flow rate of methane was kept at 380 ml/min. It was found that the open circuit voltage (OCV) and the maximum power density (P_{max}) were strongly dependent on the airflow and the operating temperature. The influences of Palladium-addition to the anode as well as Co-doping of the electrolyte on the OCV and P_{max} have been studied and compared to an unmodified cell. Pd-containing anodes allow for higher power outputs at low airflow. The presence of Co in the electrolyte raises the OCV but decreases the maximum power density.

6.1 Introduction

Conventional fuel cells rely on the strict separation of the oxidant and the fuel in order to prevent parasitic side reactions. Highly active but non-selective electrodes are used. However, with reaction selective anode and cathode materials it is possible to operate a fuel cell in a mixture of fuel and air. In the past, high costs have hampered the commercialisation of fuel cell systems. For SOFCs the costs are partly due to processes and technologies required for sealing the cells at high temperatures. Single chamber solid oxide fuel cells (SC-SOFCs) with reaction selective electrodes offer the possibility to simplify SOFC designs because only one gas compartment is necessary. Both anode and cathode are exposed to the same mixture of fuel and oxidant. In such a system the driving force for the ionic current in the electrolyte is not due to the difference of oxygen partial pressures in the two sealed gas compartments. It is the selectivity of the two different electrodes for either the partial oxidation of methane (anode) or the reduction of oxygen (cathode) that gives rise to the observed OCV.

This approach was proposed by van Gool [1] and is in principle applicable to all fuel cell types. So far, however, this concept has only been tested for SOFCs and direct methanol fuel cells [2]. The first functioning "Single Chamber" device based on boehmite-electrolyte was fabricated by Dyer in 1990 [3]. It operated at room temperature on a mixture of hydrogen and oxygen gas and generated a voltage of up to 1 V and a maximum power density of 5 mW/cm^2. A theoretical explanation for the operating principle of a SC-SOFC was given by Riess et al. [4]. One of the first SC-SOFCs was based on Yttrium Stabilised Zirconia (YSZ) and operated on mixtures of methane and air at 950°C[5]. The anode was made of Ni-YSZ and the cathode of Au. The cell generated an OCV of 0.35V and a maximum electric power of 2.4 mW/cm^2. It could be concluded that the observed OCV was due to the difference of catalytic activity of anode and cathode for the partial oxidation of methane:

$$CH_4 + \tfrac{1}{2}O_2 \rightarrow CO + 2H_2 \qquad (6.1)$$

At the anode the reaction rate is high and the two formed species (CO and H_2) react electrochemically with oxygen ions from the bulk electrolyte according to reactions (6.2) and (6.3). Using the Kroger-Vink notation it follows:

$$H_2(g) + O_O^x \rightarrow H_2O(g) + V_O^{\bullet\bullet} + 2e^- \qquad (6.2)$$

$$CO(g) + O_O^x \rightarrow CO_2(g) + V_O^{\bullet\bullet} + 2e^- \qquad (6.3)$$

At the cathode the formation of CO and H_2 is impeded and only the reduction of molecular oxygen occurs, which is given in Reaction (6.4).

$$\tfrac{1}{2}O_2(g) + V_O^{\bullet\bullet} + 2e^- \rightarrow O_O^x \qquad (6.4)$$

Due to the higher ionic conductivity of ceria as compared to YSZ, SC-SOFCs based on this electrolyte can be operated at temperatures below 600°C. This allows for higher OCVs because high temperatures decrease the difference of catalytic activity for Reaction (6.1) of the two electrodes. At 800-1000°C perovskite cathodes become quite active towards Reaction (6.1) [6]. Recent reports from Hibino on ceria-based SC-SOFCs contain interesting but unconfirmed results [7,8].

This work aims at reproducing and verifying the high OCVs and power densities that have been obtained so far. Furthermore, we want to investigate the influence that Co-doping of the ceria based electrolyte has on the performance of the cells. It has been shown that Co-addition to nano-sized ceria allows for significantly lower sintering temperatures [9]. For a prospective co-sintering step of anode and electrolyte or even the whole cell it is necessary to reduce the sintering temperature of the electrolyte from 1400°C to 1200°C. The effect of Pd-addition to the anode as a catalytic modifier was also investigated.

6.2 Experimental

6.2.1 Electrolyte Discs

Cobalt doped (2 cat-%) and undoped $Ce_{0.9}Gd_{0.1}O_{1.95}$ (CGO) (Rhodia, France) was used as the electrolyte. Doping was carried out by dispersing 50 g of CGO powder in 150 ml ethanol and subsequently adding a solution of 1.68 g $Co(NO_3)_2 \cdot 6H_2O$ in 10 ml of ethanol under stirring. The mixture was then homogenised by sonification for 10 minutes. 4 g of Poly Acryl Acetate were added and served as the binder. The suspension was then dried by evaporating the ethanol at 60°C under constant stirring. The obtained powder was calcined at 400°C for 5 hours.

Electrolyte discs were fabricated by uniaxially pressing 7 g of doped or undoped (as received) powder in a 30 mm diameter dye at 40 MPa. The discs were then isostatically pressed at 300 MPa and sintered at 1200°C (Co-doped) and 1400°C (undoped) in air for two hours. A heating rate of 1 K/min and a cooling rate of 5 K/min were applied. The density of the discs was measured after lapping off 0.1 mm on each side. It always exceeded 97% of the theoretical density for the undoped and 96% for the Co-doped material (ρ_{th} = 7.29 g/cm^3).
The lapping technique was employed for obtaining discs with defined thickness and coplanar surfaces. A Stähli FLM 500 lapping machine equipped with a hybrid copper-steel disc and B_4C-suspension (BC-800, Stähli Switzerland) was used at 60 rpm and about 1 drop of B_4C-suspension per second. The minimal thickness that could be achieved was 190 μm.
After lapping the discs were cleaned in diluted hydrochloric acid in an ultrasonic bath for 2 minutes. For better electrolyte-electrode adhesion the electrolyte surface was roughened with wetted SiC grinding paper (grit 180) and cleaned in ethanol in an ultrasonic bath.

6.2.2 Electrode preparation

Both anodes and cathodes (1 cm^2) were similarly prepared by screen printing with a mask of 50 μm thickness. 60 wt% NiO containing $Ce_{0.8}Gd_{0.2}O_{1.9}$ (SSC, Salt Lake City, USA) was used as the anode and $Sm_{0.5}Sr_{0.5}CoO_{3-\delta}$ perovskite (Nextech Materials, Worthington, USA) as the cathode. Current Collectors were made by point welding flattened Pt-wire diagonally onto a completely flat Pt-mesh 1 × 1 cm^2 in size (52 mesh woven from 0.1 mm wire, Alfa Aesar). The electrodes were fabricated by screen printing a first layer onto the electrolyte, placing the current-collector on the freshly printed layer and then covering the metal mesh by a second screen printed layer. This procedure yielded electrodes with integrated current-collectors for

which a low overpotential can be expected. The anode and cathode were sintered at 1200°C and 1100°C respectively for 1 h in air. The heating rate was 1 K/min from room temperature to 500°C with a dwell time of 1 h at this temperature and 3 K/min from there to the peak temperature. The samples were cooled down to room temperature at 5 K/min.

From an electrochemical viewpoint it would have been desirable to use Au current-collectors due to the inertness of this metal towards CH_4-air mixtures. However, Au current-collectors could not be used, because they would have melted during the sintering of both electrodes. Furthermore, when embedding completely the Pt-meshes in the electrode materials, the use of Pt should not interfere with selectively working SSC and Ni-CGO electrodes.

6.2.3 Anode Modification

In order to improve the catalytic activity of the anode for the partial oxidation of methane, Pd was added to the anode in the form of a fine dispersion. This was done by adding ceria supported Pd-catalyst (Pd-CeO_2) to the NiO-CGO powder prior to screen printing. The ceria supported Pd with a metal content of 5 wt-% had a particle size of 30 nm with Pd-clusters smaller than 5 nm. It was fabricated by flame spray pyrolysis as described for Pd-Al_2O_3 earlier [10], but with Ce- instead of Al-precursors. The Pd-content in the NiO-CGO amounted to only 0.11 wt%.

6.2.4 Electrochemical Characterisation

The fuel cells were heated at a rate of 2 K/min in a quartz glass apparatus that is depicted in Figure 6.1. This apparatus consisted of two parts and could be disassembled in the middle, where the cell was located. The latter was supported on three glass knobs inside a short glass tube with slits through which the gas could exit. The anode and cathode atmospheres were separated by the constant flow of the same gas mixture to both electrodes. The pathway of the gas-mixture is indicated in Figure 6.1. Mixing of methane and air took place just before the gas reached the cell in a small mixing chamber. Moistened air was used in all the experiments. Pt-wires by which the cell could be electrically contacted exit the setup through horizontal glass tubes. Temperature measurement was done with a K-type thermocouple in a thin glass tube about 1 cm away from the cathode.

Gas flow rates were controlled using rotameters for CH_4 and air (Voegtlin V100, Switzerland). At 400°C a gas mixture with CH_4/O_2 =7 and a total flow rate of 640 ml/min was applied and further heating of the fuel cell to 500°C was carried out.

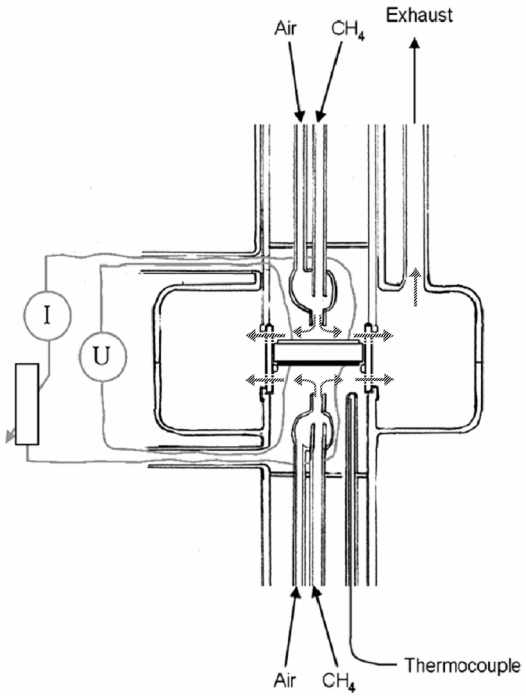

Figure 6.1 SC-SOFC measurement setup with mounted cell. The arrows indicate the pathway of the gas mixture in the setup.

The voltage current characteristics of all the fabricated cells were measured at 500, 600 and 700°C with 4 different gas mixtures. The air flow rate was varied (260, 780, 1120 and 1340 ml/min) while the CH_4 flow rate was kept constant at 380 ml/min for all experiments (corrected flow rates compared to data of our previous report [11]. Heating to the next higher temperature was always done with 2 K/min at 380 ml/min CH_4 flow rate and 260 ml/min air flow. The current voltage characteristics were measured using a Galvanostat (IM600, Zahner GmbH, Germany).

6.2.5 Measurement of the Effective Electrode Temperatures

The temperature of the testing chamber was measured using a K-type thermocouple (1 mm thickness) connected to Kane-May KM300 readout device. The tip of the thermocouple was located in a small glass tube on the cathode side of the cell about 1 cm away from the latter (Figure 6.1). Pronounced thermal gradients can be present in SC-SOFCs and therefore the effective anode and cathode temperatures were measured by placing two additional thermocouples on each of the electrodes. Thereby, the influence of the flow rate on the effective temperature could be studied.

6.3 Results and Discussion

Figure 6.2 shows the cross section of one of the fabricated cells. On the left side the anode can be seen on the right the cathode. The electrodes were approximately 150 µm thick and

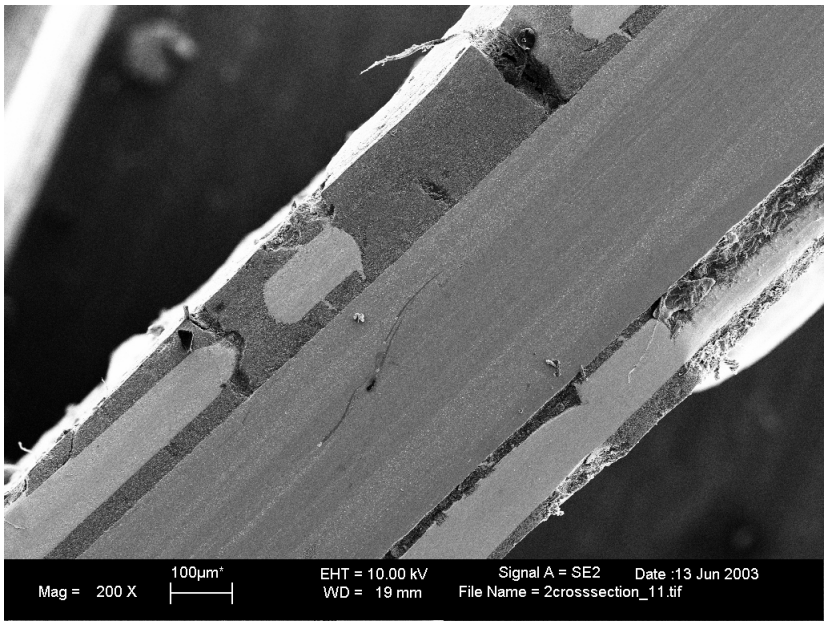

Figure 6.2 Cross section of one of the SC-SOFCs with the anode on the left and the cathode on the right side (both 150 µm thick) and an electrolyte thickness of 0.3 mm. The bright regions correspond to the integrated Pt-current-collectors.

adhered very well to the electrolyte disc. The integrated current-collectors (bright regions) were 80 µm in thickness. Figure 6.3 shows the microstructure of the cell components: a) anode, b) electrolyte and c) cathode.

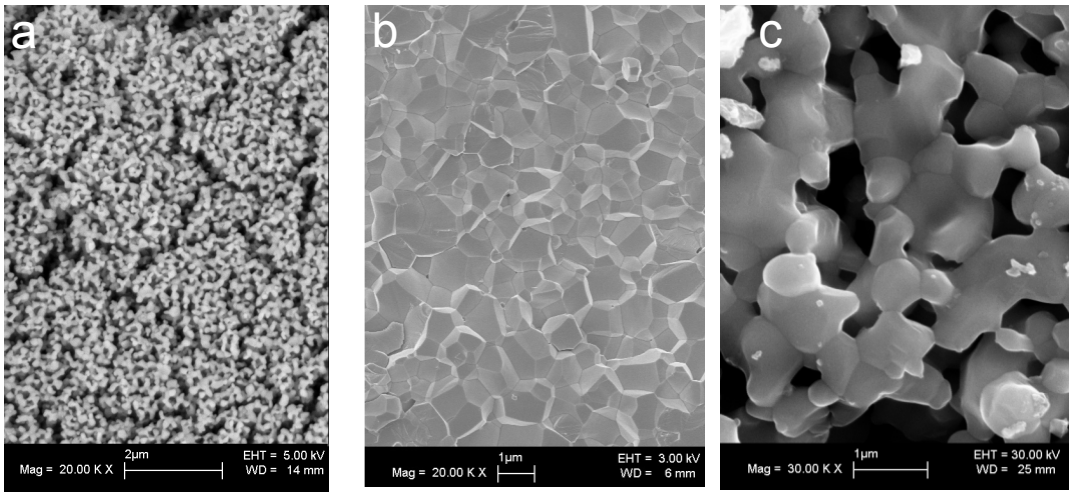

Figure 6.3 Microstructure of cell components: a) backscattered electron image of anode, b), micrograph of dense CGO-electrolyte and c) image of highly porous cathode.

The anode had a very fine microstructure due to a small initial particle size and the relatively low sintering temperature. The surface area was large and the pores below 1 μm in diameter. The undoped CGO had a grain size of approximately 1-2 μm and only exhibited very few pores. A coarse but porous structure was found for the cathode due to the relatively high sintering temperature of 1100°C. The sintering temperature needs to be reduced for subsequent experiments.

A temperature cycle with a ramp of 2 K/min during heating and 5 K/min during cooling of one of the SC-SOFCs with 190 μm thick electrolyte is shown in Figure 6.4.

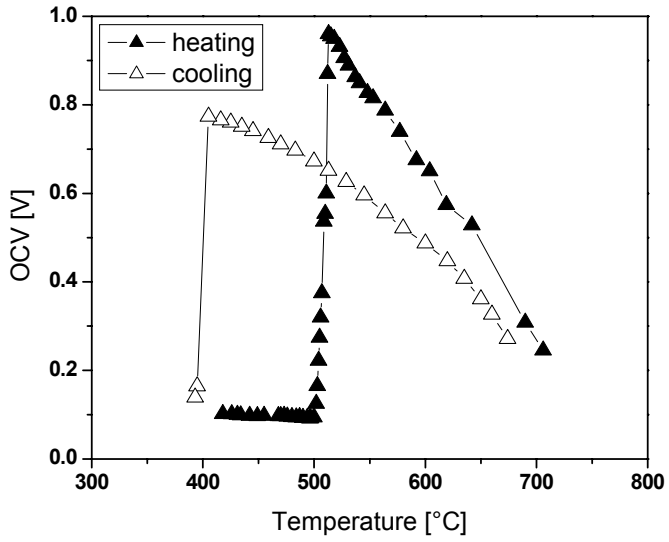

Figure 6.4 OCV of a SC-SOFC with 0.19 mm thick electrolyte as a function of temperature with 380 ml/min methane and 260 ml/min airflow during heating (▲) with 2 K/min and cooling (△) with 5 K/min.

A gas mixture with CH_4/O_2=7 and a total flow rate of 640 ml/min was used for this measurement. Below 500°C the OCV amounts to approximately 0.1 V. Above 500°C, however, the OCV abruptly increased to 0.96 V. This behaviour can be attributed to the reduction of the NiO in the anode to metallic Ni which was accompanied by a pronounced heat generation at the anode. The heat results from the onset of Reaction (6.1) that is exothermic (ΔG (500°C) = -170 kJ/mol). Upon further increase of temperature the OCV decreased monotonically and at 700°C it reaches a value of about 0.3 V. Note that at higher air flows higher OCVs could be obtained. For 1120 ml/min air flow at 700°C an OCV of 0.70 V was measured with this cell. A hysteresis effect was observed during cooling and the OCV was generally lower than during the heating stage. This can be attributed to an irreversible change of the anode material during the temperature cycle. The cell could be

operated at temperatures down to 400°C before the Ni was reoxidised to NiO. The measurements were conducted within 5-6 hours. OCVs have been shown to be stable over more than 50 hours. However, shortly after the reduction of NiO upon heating, the OCV was usually much higher than the OCV after a few hours at the same conditions. This is another reason why OCV versus temperature behaviour showed a hysteresis and OCVs upon heating was higher than during cooling.

Figure 6.5 shows the measured U-I characteristic of a cell at 600°C for different air flows. The thickness of the electrolyte was 290 µm. For 260 ml/min air flow rate an OCV of 0.56 V was measured. The power output under these conditions was only 63 mW/cm^2. The main reason for this was the too low oxygen concentration for the reduction reaction at the cathode which was concluded from the U-I curve. Above 780 ml/min the OCV did not change as a function of air flow rate and reached a constant value of 0.68 V. The maximum power density was, however, greatly influenced by the air flow rate and reached a maximum value of 468 mW/cm^2 at 1120 ml/min. Further increase of air flow rate to 1340 ml/min decreased the performance of the cell. It must be noted that the effective cell temperature changed when the air flow rate to the cell was varied, which will be seen later.

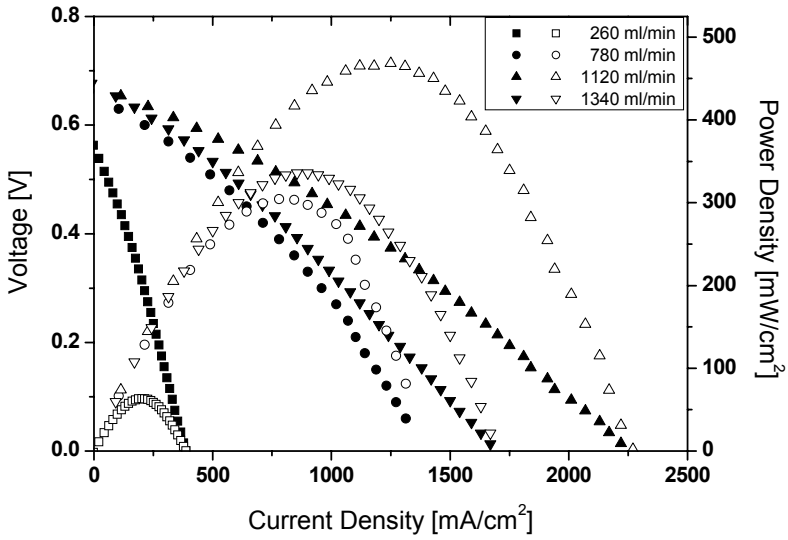

Figure 6.5 Voltage (closed symbols) and power density (open symbols) vs. current density of a SC-SOFC with 0.29 mm thick electrolyte at 600°C for different air flow rates (260, 780, 1120 and 1340 ml/min) and a constant flow rate of 380 ml/min CH_4.

In Figure 6.6 the same cell is shown at different temperatures at 260 ml/min airflow. The OCV decreased when the temperature was raised. It could be observed that the same power

output was obtained at 500 and 600°C, which can be explained by the counteracting of OCV and the cells electric resistance. At 600°C the OCV is lower than at 500°C but when current is drawn, the cell voltage does not decrease as steeply as at 500°C primarily due to the markedly lower electrolyte resistance. At 180 mA/cm^2 the cell gave the same voltage at 500 and 600°C yielding a power output of 63 mW/cm^2. Relatively low OCVs and power outputs could be obtained at this low airflow. There are two reasons for this. The first reason is the low oxygen partial pressure of only 85 mbar at the cathode leading to a low OCV and high cathode overpotentials at high current densities. The second reason concerns the anode and is due to the lack of oxygen in the methane-air mixture leading to low concentrations of CO and H_2 because the partial oxidation can not fully proceed.

In Figure 6.7 the voltage-current characteristics are shown at an air flow rate of 1120 ml/min, which corresponds to a mixture having $CH_4/O_2 = 1.6$. It can clearly be seen that much higher OCV and P_{max} can be obtained at high gas flow. At these conditions the partial oxidation is favoured leading to high CO and H_2 concentrations at the anode but also to a higher oxygen partial pressure of 0.16 at the cathode. The OCV and P_{max} followed the same trend as in the previous case for 260 ml/min airflow, at 600°C, however, markedly higher P_{max} could be obtained than at 500°C.

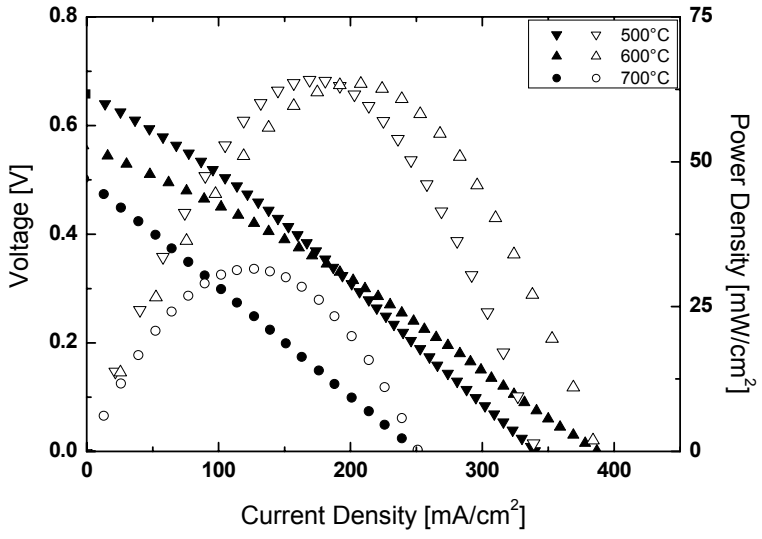

Figure 6.6 Voltage (closed symbols) and power density (open symbols) vs. current density of the same SC-SOFC as in Figure 6.5 at different temperatures for 260 ml/min air flow rate and 380 ml/min CH_4.

The performance of the fabricated SC-SOFCs was greatly dependent on temperature and airflow. At 500°C operating temperature the cells usually had maximum power output for 780 ml/min airflow, at 600°C the maximum was obtained for 1120 ml/min. At 700°C the cells showed some degradation and always exhibited lower OCV and P_{max} than at 600°C. This was partially due to the increasing electronic conductivity of the mixed conducting electrolyte

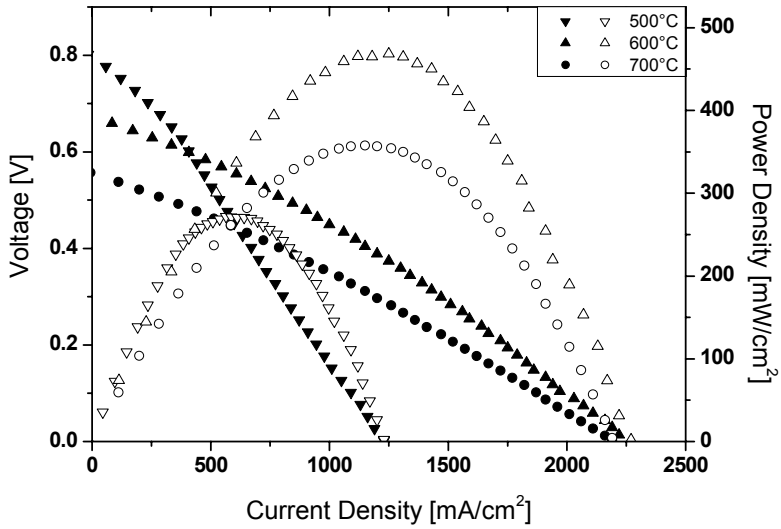

Figure 6.7 Voltage (closed symbols) and power density (open symbols) vs. current density of the same SC-SOFC as in Figure 6.5 at different temperatures for 1120 ml/min air flow rate and 380 ml/min CH_4.

under these conditions. We assume that at low airflows the cathode does not dispose of enough oxygen for the oxygen reduction Reaction (6.4). This yields a low OCV and P_{max}. At too high airflows, however, the anode-electrolyte interface sees too much oxygen, especially when current is flowing. This diminishes the driving force for the oxygen ions and leads to lower power outputs. Another reason for lower OCV and power outputs at high temperatures and airflows is also the pronounced non-electrochemical combustion of the fuel at the electrode surfaces. This led to a higher effective cell temperature than the nominally measured one. The results of the effective temperature measurements are shown in Figure 6.8. The temperature at the anode was higher than the cathode temperature at all conditions. At $T_{nominal}$ = 700°C and 240 ml/min airflow rate the anode reached a temperature of more than 780°C, which indicated a strong heat generation. The difference of anode and cathode temperature decreased with increasing airflow due to cooling phenomena. A pronounced heat generation occurs at the anode because of all the reactions of CH_4 with O_2 being exothermic.

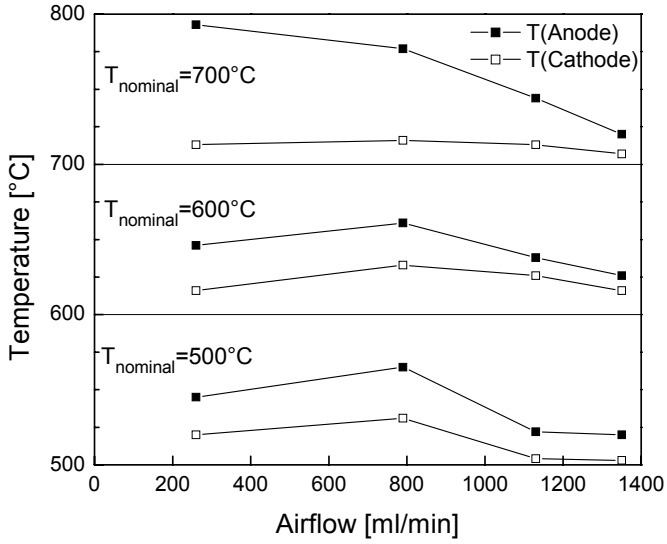

Figure 6.8 Measured electrode temperatures as a function of airflow for different nominal temperatures and 380 ml/min CH_4 for a cell with 390 μm thick electrolyte.

In Figure 6.9 the influence of Pd at a) 260 ml/min and b) 1120 ml/min is compared to a similar cell with neither Pd in the anode nor Co in the electrolyte (same cell as in Figure 6.5). The OCV increased at all tested temperatures for low and high airflows due to the presence of Pd in the anode. At low airflows Pd increased the maximum power density. However, at high airflows the cells with Pd had a lower P_{max}. It can be concluded that the addition of 0.11 wt% Pd to the anode improved the catalytic activity of the Ni-CGO anode.

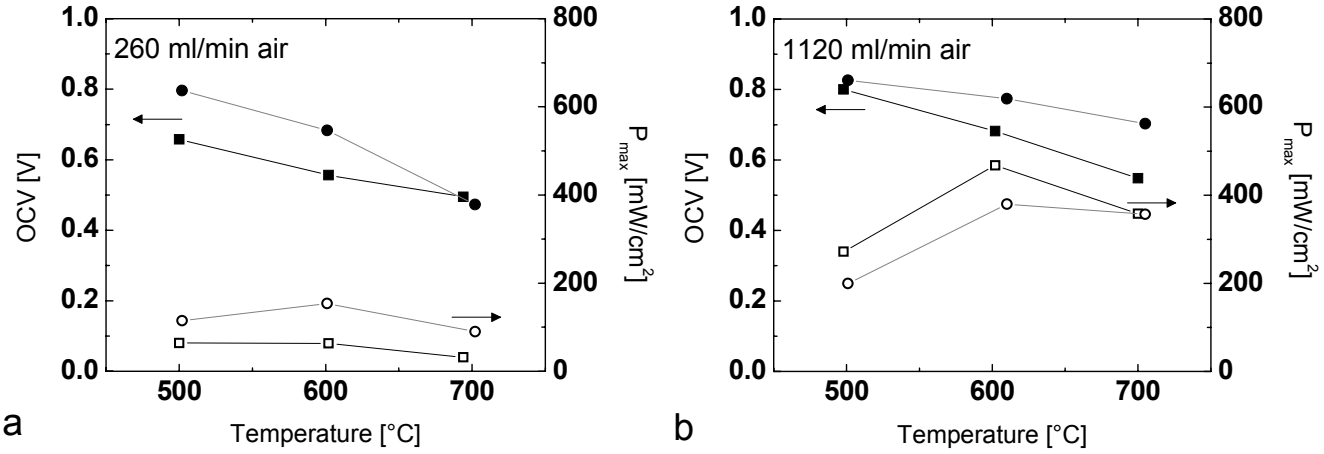

Figure 6.9 Influence of Pd-modified anode on OCV and P_{max} at 380 ml/min CH_4 for a) 260 ml/min and b) 1120 ml/min airflow. Undoped anode (■) OCV; (□) P_{max}. Pd-doped anode (●) OCV; (○) P_{max}.

This was, however, only true for low airflows for which an increase of P_{max} was found. For higher airflows the added amount of Pd seemed not to be sufficient for enhancing the anode performance. Co-doped CGO powder allowed for a sintering temperature that was 200°C lower than for the undoped powder. The influence of Co on the fuel cell performance is shown in Figure 6.10 and is compared to the same cell as was used Figure 6.9. The influence of Co on the performance of the SC-SOFC was similar to the influence of Pd in the anode. Co increased the OCV at nearly all conditions but only increased P_{max} for low airflows. The reason for this behaviour needs to be clarified. It is plausible that the Co-oxide with multivalent cation can change the reaction path without changing the overall cell reaction. The adsorption state of oxygen is altered at the interfaces between the electrodes and the electrolyte and this has an influence on OCV as well as P_{max}. In the case of Pd the interfaces between the electrodes and the electrolyte are the same as for the unmodified cells. Concerning the parasitic non-electrochemical combustion of the fuel, it is reasonable to assume that this effect does not change dramatically as compared to the undoped cells, because only small amounts of Co and Pd were added.

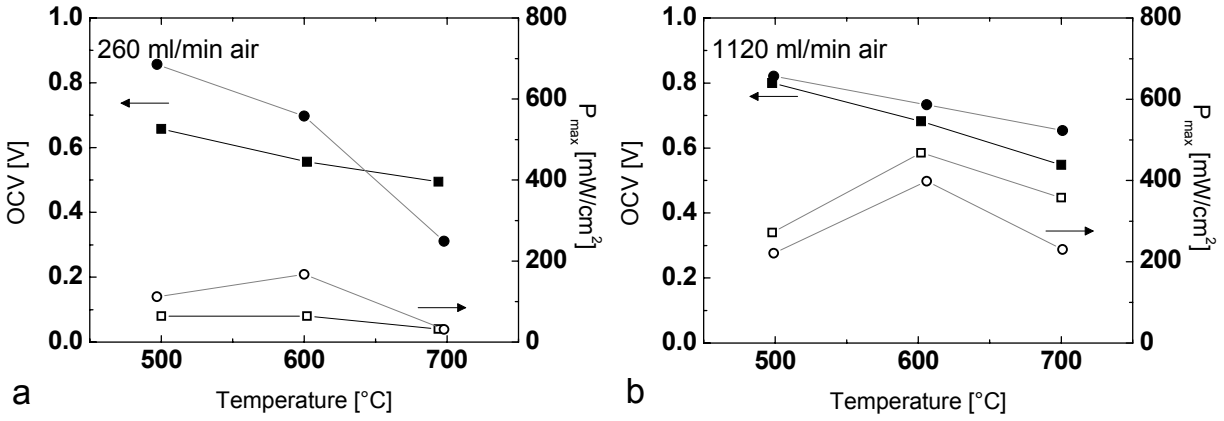

Figure 6.10 Influence of Co-doped electrolyte on OCV and P_{max} at 380 ml/min CH_4 for a) 260 ml/min and b) 1120 ml/min airflow. Undoped anode (■) OCV; (□) P_{max}. Pd-doped anode (●) OCV; (○) P_{max}.

6.4 Summary

Single chamber SOFCs based on $Sm_{0.5}Sr_{0.5}CoO_{3-\delta}/Ce_{0.9}Gd_{0.1}O_{1.95}/Ni\text{-}Ce_{0.8}Gd_{0.2}O_{1.90}$ were fabricated. The cells generated high OCVs and high power outputs. Maximum power densities of 271 mW/cm^2 at 500°C, 468 mW/cm^2 at 600°C and 358 mW/cm^2 at 700°C were obtained with a gas mixture of methane and air (CH_4/O_2 =1.6) with a total flow rate of 1500 ml/min. We thus confirm the results of previous work from Hibino [8]. In this work much higher flow rates were used than in previous work, which is partially caused by the different flow geometry due to another type of setup as well as to the rather thick electrodes. A pronounced heat generation was observed at the anode leading to a temperature difference between the two electrodes of up to 100°C. The use of 2 cat-% Co-doped electrolyte as well as the Palladium-doping of the anode led to higher OCVs at all temperatures and air flows. However, only for low airflows did these measures increase the maximum power output of the cells.

6.5 Acknowledgements

The authors would like to thank Dr. Karsten Wegner and Reto Strobel (PLT, Federal Institute of Technology, Zurich) for providing the Pd-CeO_2 catalyst.

6.6 References

[1] W. van Gool, *Philips Research Reports*, **1965**, 20, 81-93.

[2] K. Scott, A. K. Shukla, C. L. Jackson and W. R. A. Meuleman, *Journal of Power Sources*, **2004**, 126, *1-2***,** 67-75.

[3] C. K. Dyer, *Nature*, **1990**, 343, 547-548.

[4] I. Riess, P. J. van der Put and J. Schoonman, *Solid State Ionics*, **1995**, 82, 1-4.

[5] T. Hibino and H. Iwahara, *Chemistry Letters*, **1993**, 7, 1131-1134.

[6] A. K. Demin and F. Y. Gulbis, *Solid State Ionics*, **2000**, 135, 451-456.

[7] T. Hibino, A. Hashimoto, T. Inoue, J.-i. Tokuno, S.-i. Yoshida and M. Sano, *Journal of the Electrochemical Society*, **2001**, 148, *6***,** A544-A549.

[8] T. Hibino, A. Hashimoto, M. Yano, M. Suzuki, S.-i. Yoshida and S. Mitsuru, *Journal of the Electrochemical Society*, **2002**, 149, *2***,** A133-A136.

[9] C. Kleinlogel and L. J. Gauckler, *Solid State Ionics*, **2000**, 135, *1-4***,** 567-573.

[10] R. Strobel, F. Krumeich, W. J. Stark, S. E. Pratsinis and A. Baiker, *Journal of Catalysis*, **2004**, 222, *2***,** 307-314.

[11] B. E. Buergler, M. Siegrist and L. J. Gauckler, in *Sixth European Solid Oxide Fuel Cell Forum, 2004,* M. Mogensen, 1405-1413.

7 The Influence of Anode Thickness on the Electrochemical Behaviour of SC-SOFCs

B. E. Buergler, Y. Santschi, M. Felberbaum and L. J. Gauckler, *Ceramic Engineering and Science Proceedings*, 2006, 27, 4, in press.

ABSTRACT: The influence of the anode thickness (9-60 μm) on the behaviour of single chamber solid oxide fuel cells (SC-SOFCs) was investigated in a double chamber cell setup in different flows of methane-air mixtures. The open circuit voltage (OCV) decreased with increasing gas flow rate to the anode and at the same time the power density increased. Oscillations of the OCV at high flow rates were observed for cells with thin anodes. These oscillations were caused by periodic reduction/reoxidation cycles of the Ni in the anode cermet material. Cells with thick anodes showed the highest OCV and the highest maximum power densities. These anodes had a higher catalytic activity for the partial oxidation of methane and created a lower oxygen partial pressure at the anode/electrolyte interface. As compared to thin anode layers, thick anodes also formed more hydrogen and carbon monoxide per unit time, which led to higher power outputs.

7.1 Introduction

Single chamber fuel cells only have one gas compartment and operate in a non-equilibrium gas mixture of fuel and oxygen [1-7]. In theory, the concept can be applied to all types of fuel cells, when selective electrodes for either the reduction or oxidation reactions are used. The operation principle of single chamber solid oxide fuel cells (SC-SOFCs) is based on the different catalytic activities of the electrode materials for the partial oxidation of methane [3]. The single chamber configuration of Fuel Cells promises a substantial simplification of SOFC-systems. This has led to an increased interest in this type of fuel cell [8], despite substantial drawbacks such as the relatively low fuel utilisation and parasitic oxidation of the fuel causing an overheating of the cells. The waste heat due to parasitic reactions when premixing fuel and oxidant can be used for keeping the fuel cell at the desired operating temperature. A very recent publication showed that SC-SOFCs can be operated in a self-sustaining (no external heating) conditions by using a novel design of the cell system. By the interconnection of two individual cells [9] Shao et al. obtained approximately 246 mW/cm^2 at 1.0 V from two anode-supported SC-SOFCs operating in propane-oxygen-helium mixtures at 500-600°C. The anode-supports that were used had a thickness of 0.7 mm, which is nearly two orders of magnitude thicker than the usual anode thickness in electrolyte-supported cells. For electrolyte supported cells the reported anode thicknesses were in the range of 1-20 μm [4]. In our recent work the anode thickness was around 150 μm [10]. In some publications dealing with SC-SOFCs the anode thickness is not defined at all [11,12] and there is a complete lack of studies dealing with the influence of the anode thickness on SC-SOFCs. The aim of this study was to elucidate the influence of the anode thickness on the performance of SC-SOFCs and to validate the model that is described in the following Section 7.2.

In single chamber SOFCs both electrodes are exposed to the same flow of fuel and air. If the gas flow or composition is changed both electrodes are affected. In order to solely investigate the influence of the gas flow and gas composition on anodes with different thicknesses, the experiments were carried out with a double chamber setup, with separate cathode and anode compartments. Platinum was used as the current-collector material as it had been done in previous studies about SC-SOFCs in methane-air mixtures [10]. The reason why Pt was used is that it can be co-sintered at 1300°C together with the electrodes, whereas gold or silver would have melted. Nickel could not be used because it would have oxidised during the sintering. The current-collector meshes were always covered with a porous layer of anode material, thus as little Pt as possible was exposed directly to the gas mixtures.

Furthermore, it was found that at 700°C in CH_4-air mixtures a porous Pt-layer did not promote the reaction between CH_4 and O_2 [13]. The catalytic surface of the Ni-cermet is by orders of magnitude higher than the one of the Pt current-collector.

7.2 Theory

The influence of the anode thickness on the OCV of SC-SOFC shall be explained in this section by a novel model. Three half-cells (n = 1,2 and 3) with different anode thicknesses (t_n), different oxygen partial pressures (p_n) at the anode/electrolyte interface and different resulting open circuit voltages (OCV_n) are shown in Figure 7.1. The cathode conditions (not shown in Figure 7.1) for the different half-cells are always the same. Fuel-rich methane-air mixtures are assumed ($CH_4/O_2 > 1$) that are fed to the anode in a vertical flow configuration as it was the case in previous experimental work [10]. On the right hand side of Figure 7.1 the logarithm of the oxygen partial pressure $p(O_2)$ in the porous anode is plotted as a function of the distance from the anode surfaces. In the gas phase above the anode the non-equilibrium oxygen partial pressure $p^{neq}(O_2)$ prevails, which is the oxygen partial pressure of the unreacted gas mixture.

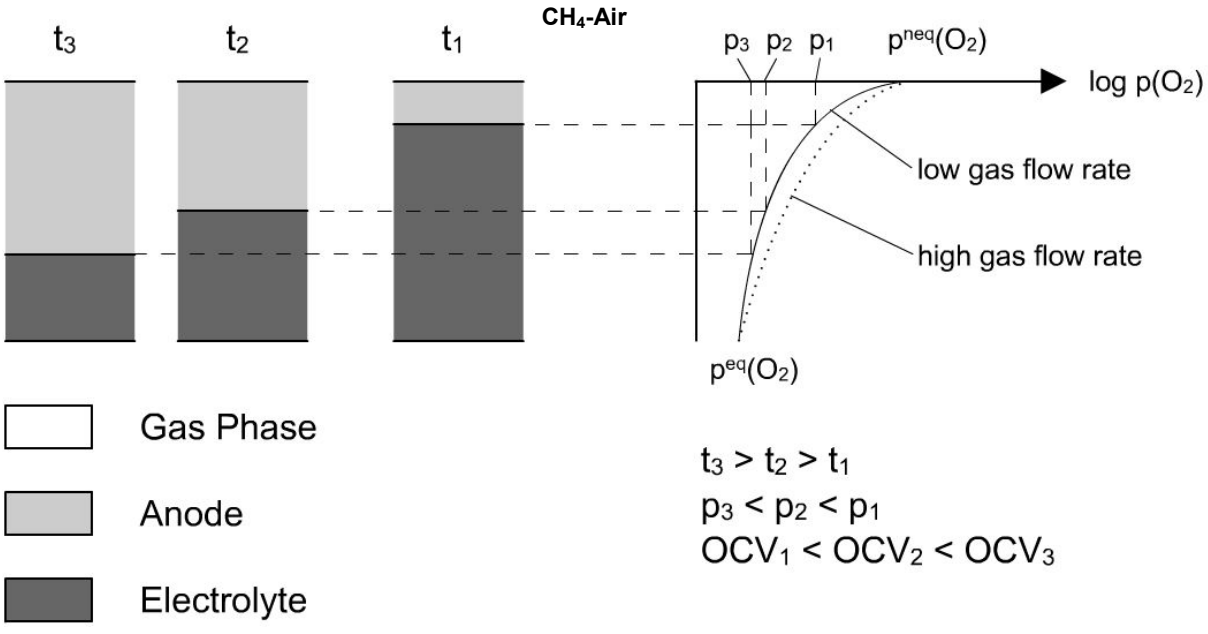

Figure 7.1 Scheme for understanding the influence of anode thickness on the open circuit voltage of SC-SOFCs (see text for detailed description). t, p and OCV stand for the anode thickness, the oxygen partial pressure at the anode/electrolyte interface and the open circuit voltage, respectively.

With increasing distance from the anode surface within the anode, $p(O_2)$ decreases and approaches the equilibrium oxygen partial pressure $p^{eq}(O_2)$. The reason for this decrease are two competing reactions in the porous anode layer: The partial oxidation of CH_4 shown in Reaction (7.1) and the full oxidation of CH_4 according to Reaction (7.2). The latter reaction is strongly exothermic and can be considered to be purely parasitic because the formed products, CO_2 and H_2O cannot be further oxidised.

$$CH_4 + 1/2\,O_2 \rightarrow CO + 2H_2 \qquad (7.1)$$

$$CH_4 + 2O_2 \rightarrow CO_2 + 2H_2O \qquad (7.2)$$

Reaction (7.1) and (7.2) lead to a decrease of oxygen partial pressure $p(O_2)$ in the anode as shown on the right hand side of Figure 7.1. The resulting oxygen partial pressure at the anode/electrolyte interface (p_n) depends on the anode thickness (t_n) as shown in Figure 7.1. For thicker anodes a lower p_n will be present as compared to thin anodes and this will result in a higher OCV of the cell ($t_3 > t_2 > t_1$ ⇨ $OCV_3 > OCV_2 > OCV_1$). When a higher flow rate is applied more unreacted oxygen can penetrate deeper into the anode layer, thereby increasing (p_n) at the anode/electrolyte interface. From the proposed model, the following predictions can be made: 1) SC-SOFCs with thick anodes give a higher OCV than cells with thin anodes. 2) Increasing the flow rate will lead to a decrease of OCV for both thick and thin anodes.

7.3 Experimental

Cells based on the system Air/$Sm_{0.5}Sr_{0.5}CoO_{3-\delta}$/$Ce_{0.9}Gd_{0.1}O_{1.95}$/Ni-$Ce_{0.8}Gd_{0.2}O_{1.90}$/ CH_4-Air were investigated. All the prepared cells were supported by a 1 mm thick electrolyte disc and were produced in a similar manner as described elsewhere [10], with exception of the electrode printing procedure. The electrolyte discs were prepared by uniaxially pressing CGO10 powder ($Ce_{0.9}Gd_{0.1}O_{1.95}$, Lot# 03-P5049BM.1, Praxair, USA) in a 30 mm diameter dye at 40 MPa. Then these discs were isostatically pressed at 300 MPa and sintered at 1500°C in air for four hours. The heating rate was 1 K/min and the cooling rate 5 K/min. The density of the discs always exceeded 98% of the theoretical density of the material (ρ_{th} = 7.29 g/cm^3). Grinding and subsequent lapping with a Staehli FLM 500 machine using B_4C-suspension (BC-800, Staehli, Switzerland) was then carried out until the desired thickness had been reached.

Both anodes and cathodes (1×1 cm^2) were similarly prepared by screen printing. Three different anode thicknesses were prepared by using 20 μm and 100 μm masks. For obtaining even thicker anodes than achievable with a single print through the 100 μm mask, double printing with this mask was carried out. This was done by drying the first layer and then printing a second layer on top. After the screen printing step the current-collector was gently placed on the freshly printed layer and dried at 80°C for a few hours in a hot-air cabinet. 60 wt% NiO-containing $Ce_{0.8}Gd_{0.2}O_{1.9}$ (Lot# 03-P4832DM, Praxair, USA) was used as the anode material. Current-collectors consisted of a Pt-wire that was point-welded onto a completely flat Pt-mesh 0.9×0.9 cm^2 in size (52 mesh woven from 0.1 mm wire, Alfa Aesar, Germany).

The cathode preparation was always the same, using the same paste and the same screen printing mask (50 μm) for all the prepared cells. $Sm_{0.5}Sr_{0.5}CoO_{3-\delta}$ powder (Lot# 91-82, Nextech Materials, USA) was used as the cathode material. The anode was prepared before the cathode and the sintering of both electrodes was done in two steps with 1300°C peak temperature for the anode and 1100° for the cathode. The heating rate was 1 K/min from room temperature to 500°C with a dwell time of 1 hour at this temperature and 3 K/min from there to the peak temperature for 2 hours. The samples were cooled down to room temperature at 5 K/min. The Pt current-collectors were mechanically fixed to the electrolyte disc with a small amount of refractory adhesive (Firag, Germany) at the outside of the

electrodes. Digital photographs of the anode and cathode of one of the prepared cells are shown in Figure 7.2 a and b.

In order to evaluate the printed anode thickness, reference samples were prepared. These specimens were broken in two and the cross section was analysed in a Scanning Electron Microscope (SEM, LEO 1530, Germany).

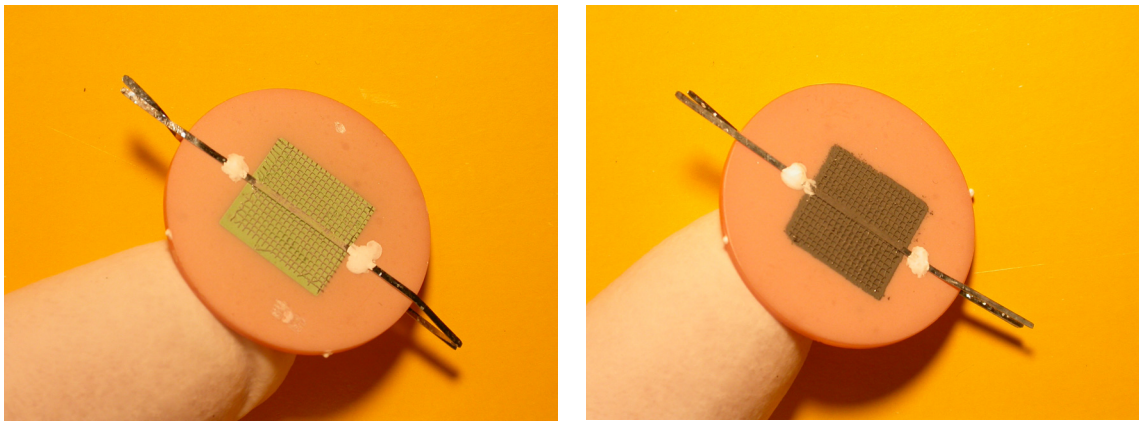

Figure 7.2 a) Anode side and b) cathode side of one of the prepared cells showing the electrodes (1x1 cm^2), the current-collector and the two Pt-wires attached by a small amount of refractory adhesive. The diameter of the electrolyte was 23 mm.

The cells were mounted in the test rig shown in Figure 7.3 with the anode facing down. The four Pt-wires going into of the setup were connected to the electrode terminals of the cells by point-welding. This allowed to carry out four point measurements of the electrochemical performance of the cell. The voltage-current characteristics were measured by scanning from the OCV to 0 V with a slew rate of 5 mV/s using a potentiostat (IM6, Zahner, Germany). The OCV measurements over longer time were also measured with this device.
The test rig consisted of two glass tubes with cylindrical attachments that were placed in a horizontal tubular furnace. Between those attachments the cell was inserted by the use of two alumina rings. Between the alumina rings and the glass tubes some ceramic paper (Insulfrax, 1 mm, not shown) was used for allowing a soft contact and the Pt-wires to exit. The setup was unsealed but gas could only leak out of the system and not into it. The cathode was exposed to a constant flow rate of 500 ml/min of dry air while the anode was fed with a varying total flow rate of moistened CH_4-air mixture with $CH_4/O_2=2$. A thermocouple that had been covered with a thin layer of refractory adhesive (Firag, Germany) was placed very close to the anode and was used to monitor the anode temperature (T_{Anode}). The cells were slowly heated at 3 K/min so that T_{Anode} reached 730°C. Then 500 ml/min airflow to the cathode was turned on.

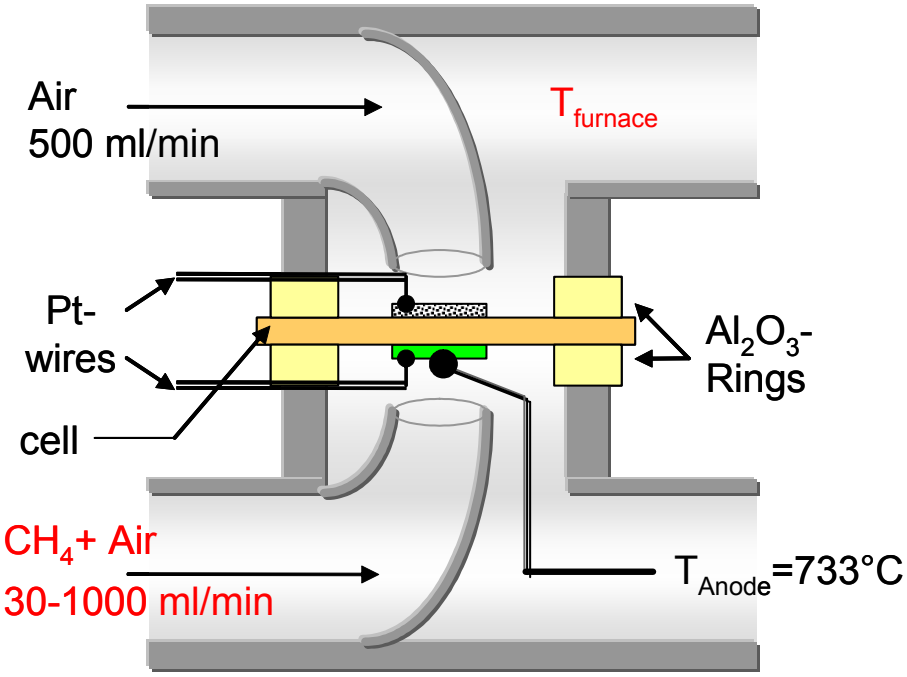

Figure 7.3 Test rig for the characterisation of SC-SOFCs in a double chamber configuration. The cathode (facing upwards) is exposed to a constant flow rate of air (500 ml/min) while the anode was exposed to a varying flow rate of CH_4-air mixture with $CH_4/O_2 = 2$. The furnace temperature ($T_{furance}$) was always readjusted to obtain an anode temperature (T_{Anode}) of 733°C.

Before introducing the CH_4-air mixtures at the anode side, the glass tube was flushed with nitrogen for a few minutes. Then a flow rate of 500 ml/min of CH_4-air mixture was fed to the anode, which led to a slight temperature rise to approximately 750°C. This temperature rise and the presence of the reducing CH_4-air mixture led to the reduction of the NiO to metallic Ni in the NiO-CGO anode material. Thereafter, the furnace temperature ($T_{furnace}$) was readjusted so that T_{Anode} was equal to 733°C. For all the experiments a CH_4-air mixture with a CH_4/O_2 ratio of 2/1 was used. This mixture was moistened by passing it through a water bubbler at 24°C (3% H_2O). The anode flow rate was varied from 30-1000 ml/min.

7.4 Results and Discussion

In Figure 7.4 the cross-sectional views of the reference samples for the evaluation of the anode thickness are shown. The three obtained thicknesses were 9, 21 and 60 µm. The anode layers adhered well to the electrolyte.

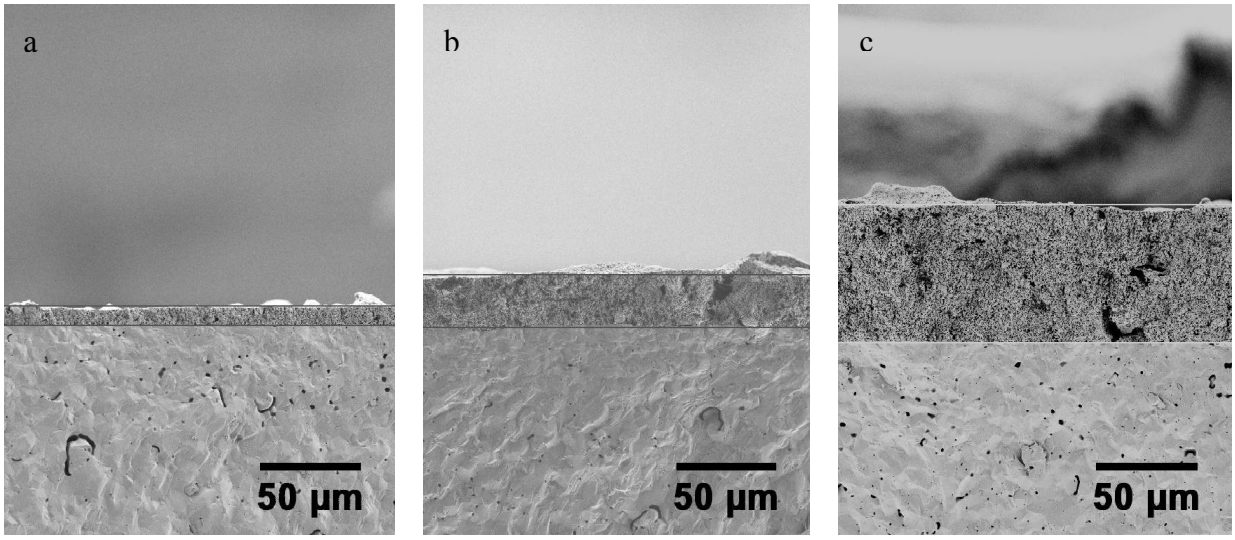

Figure 7.4 SEM micrographs of reference samples for the evaluation of the anode thickness after screen printing and sintering. a) 20 µm mask giving a final thickness of 9 µm b) 100 µm mask giving a final thickness of 21 µm and c) 100 µm mask with two screen printed layers on top of each other giving a final thickness of 60 µm.

A topview of a typical anode layer is shown in Figure 7.5 a. The grain size of the as-prepared anode layers was in the range of 250 nm, both for the NiO and the CGO grains. Upon reduction of the NiO in the material there was a pronounced increase of porosity to about 50 vol%. A SEM-micrograph of an anode cross-section is given in Figure 7.5 b. The CGO-grains remained unchanged after the reduction. The metallic Ni formed struts on which the CGO-grains were supported. The pore size for the reduced anode material was estimated to be in the range of 1 to 3 µm.

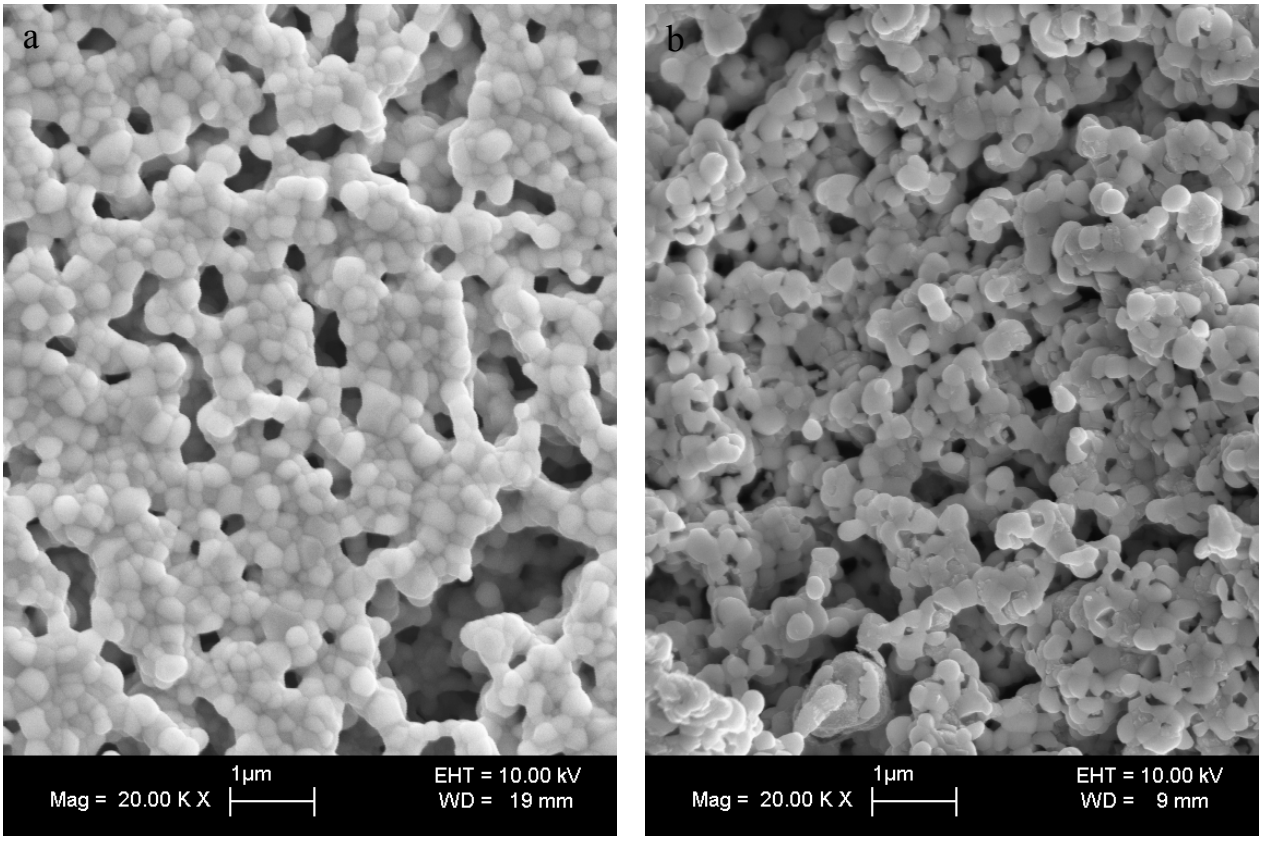

Figure 7.5 a) Topview of an as prepared NiO-CGO anode. b) Cross-sectional view of a Ni-CGO anode after reduction in CH_4-air mixtures.

In Figure 7.6 the OCV of a cell with a very thin anode (9 µm) is plotted as a function of time for three different CH_4-air flows. At 1000 ml/min the OCV fluctuated strongly around a mean value of 0.76V with a period between 20 and 50 seconds. At 500 ml/min the period increased to 60-100 seconds, the fluctuations had a greater magnitude but the mean OCV had increased to 0.81V. From the maximum voltage of a period there was a continuous decrease of the cell voltage and at a certain point it dropped massively but increased immediately again to a maximum. At 250 ml/min flow rate to the anode the cell voltage seemed to be stable at 0.85 V, at least within the time of the measurement, showing only a slight decrease in the range of some millivolts. The reason for the unstable cell behaviour could have been temperature oscillations during the partial oxidation caused by the periodic oxidation/reduction of the catalyst [14]. Such temperature fluctuations in catalyst beds of silica supported Ni-catalyst have already been observed by Hu et al. [15].

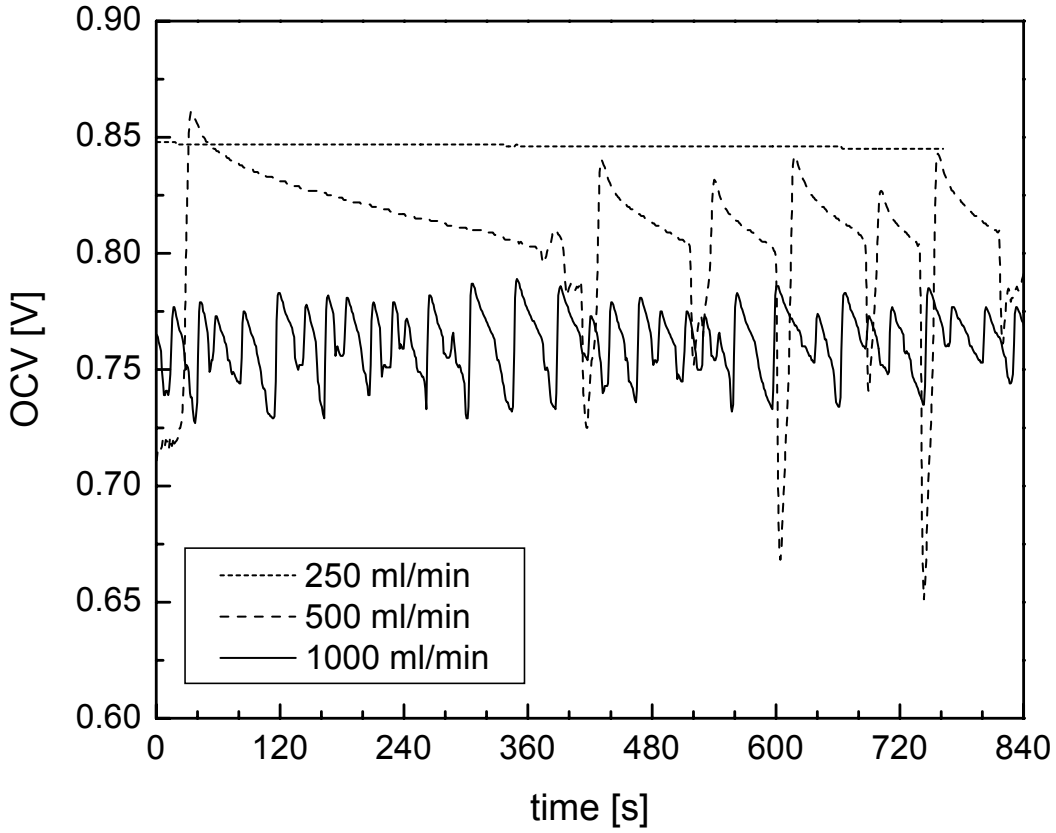

Figure 7.6 OCV of a cell with a 9 μm thick anode as a function of time for three different CH_4-air flow rates.

When the gas phase temperature was increased, the oscillation time decreased and so did the magnitude of the oscillations. The authors stated that the oscillatory behaviour does not occur for every support material, e.g. Ni-Al_2O_3 did not show any oscillations.

In Figure 7.7 to Figure 7.9 the measured voltage-current characteristics of the same cell are shown at 1000, 500 250 ad 70 ml/min. The oscillatory behaviour was also observed during the discharge of the cell. At high flow rates the cell current broke down more frequently during the measurements. At 250 ml/min (Figure 7.9) a regular voltage-current relation was obtained and at 150 ml/min too (not shown).

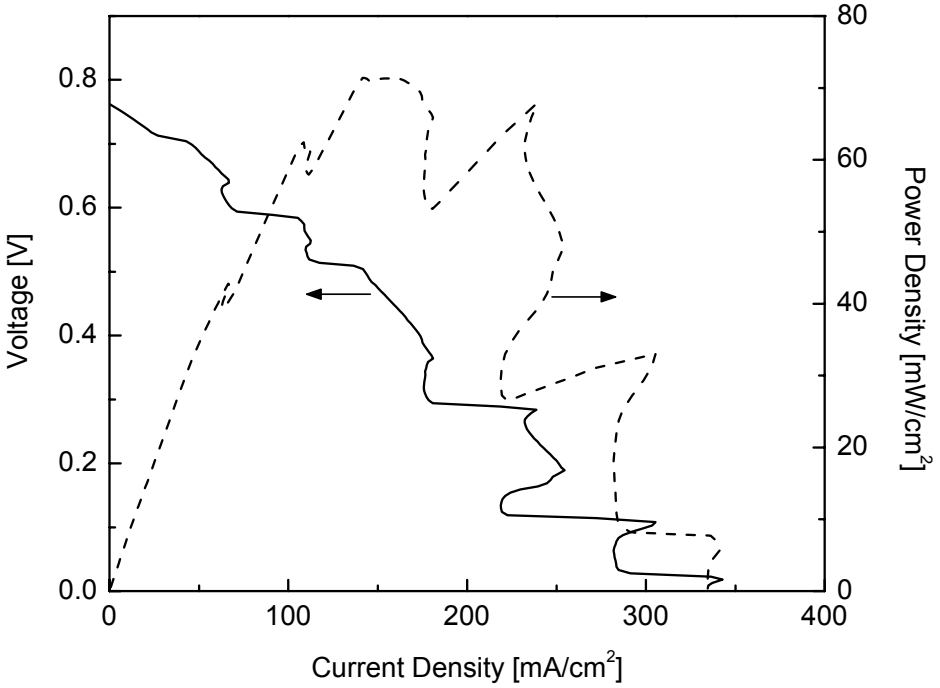

Figure 7.7 Voltage-current characteristic of the same cell as in Figure 7.6 at a flow rate of 1000 ml/min.

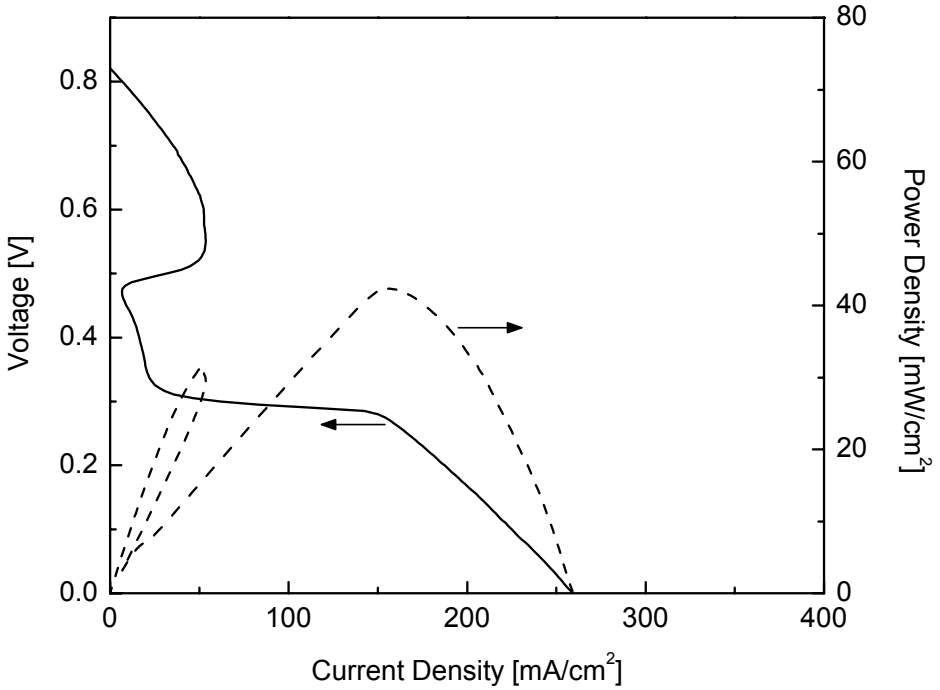

Figure 7.8 Voltage-current characteristic of the same cell as in Figure 7.6 at a flow rate of 500 ml/min.

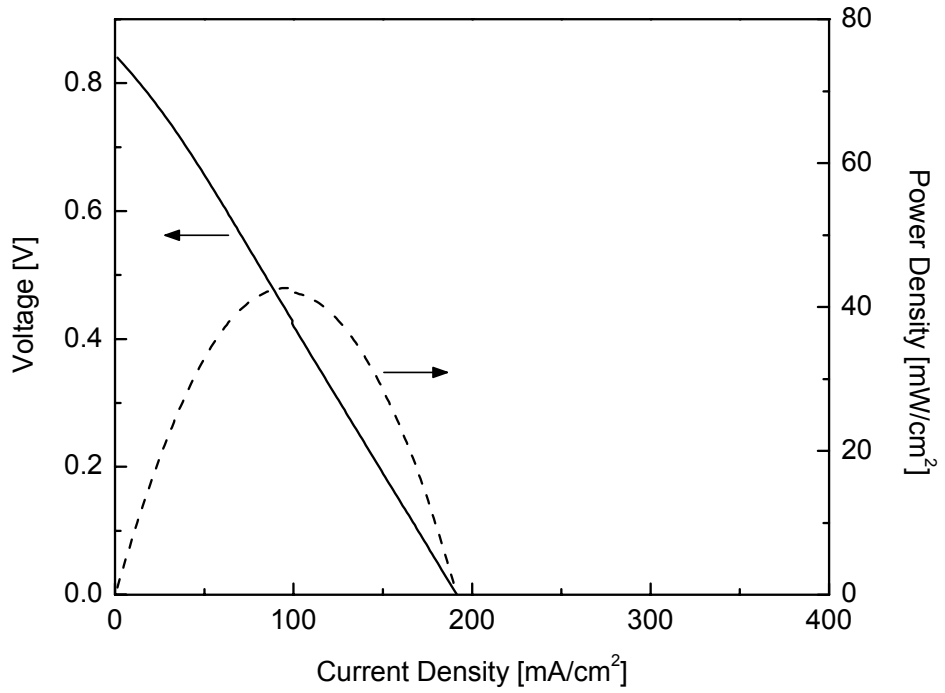

Figure 7.9 Voltage-current characteristic of the same cell as in Figure 7.6 at a flow rate of 250 ml/min.

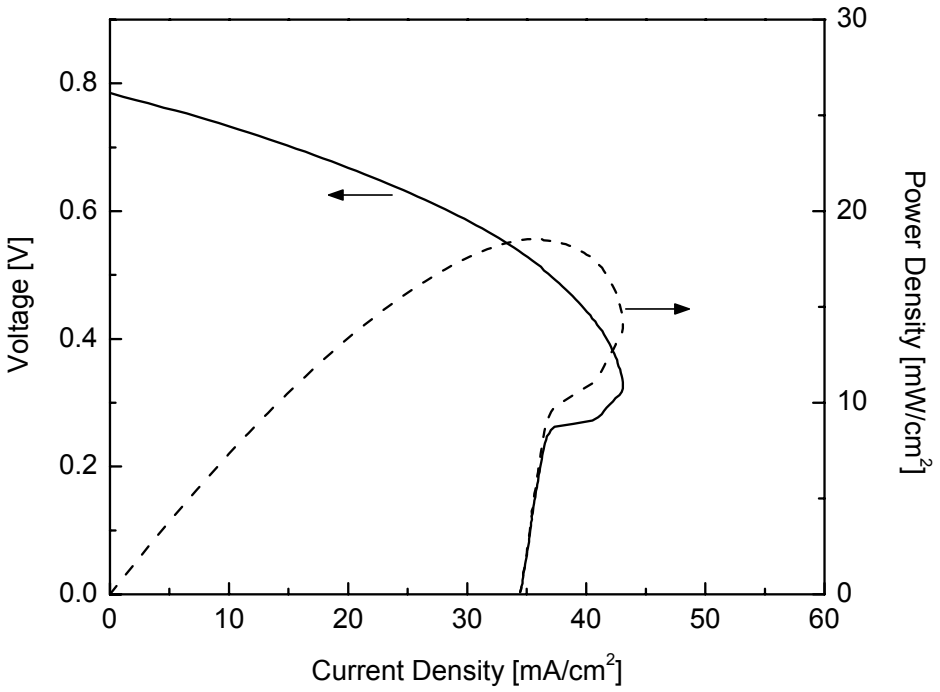

Figure 7.10 Voltage-current characteristic of the same cell as in Figure 7.6 at a flow rate of 70 ml/min. Above 50 mA/cm^2 the voltage drops. Note the different scale as compared to the previous figures.

At lower flow rates the situation changed: The OCV was 0.80 V at 70 ml/min but at high current densities of around 50 mA/cm^2 a severe voltage drop was observed (Figure 7.10). Obviously the used flow rate was too low and led to a too small amount of CO and H_2 being available for the reaction of the O^{2-}-ions at the anode side. The results indicated that the Ni-anode was partially electrochemically reoxidised to NiO.

The dependence of the OCV and maximum power density on the anode flow rate is summarised in Figure 7.11 for a cell with a 60 µm thick anode. The OCV reached a maximum at around 150 ml/min while the power density increased monotonically with increasing gas flow. Below 70 ml/min there was not enough gas to obtain a low oxygen partial pressure at the anode/electrolyte interface. This was the reason why the OCV drops at low flows. At high flow rates more unreacted oxygen reached the anode-electrolyte interface causing the oxygen partial pressure to increase. However, a second effect could also play a role. With increasing flow rate the effective anode temperature increased. It is known that the OCV decreases with increasing cell temperature for similar SC-SOFCs [4]. The increased cell temperature would cause an enhanced catalytic activity as well as lower polarization resistance of the anode.

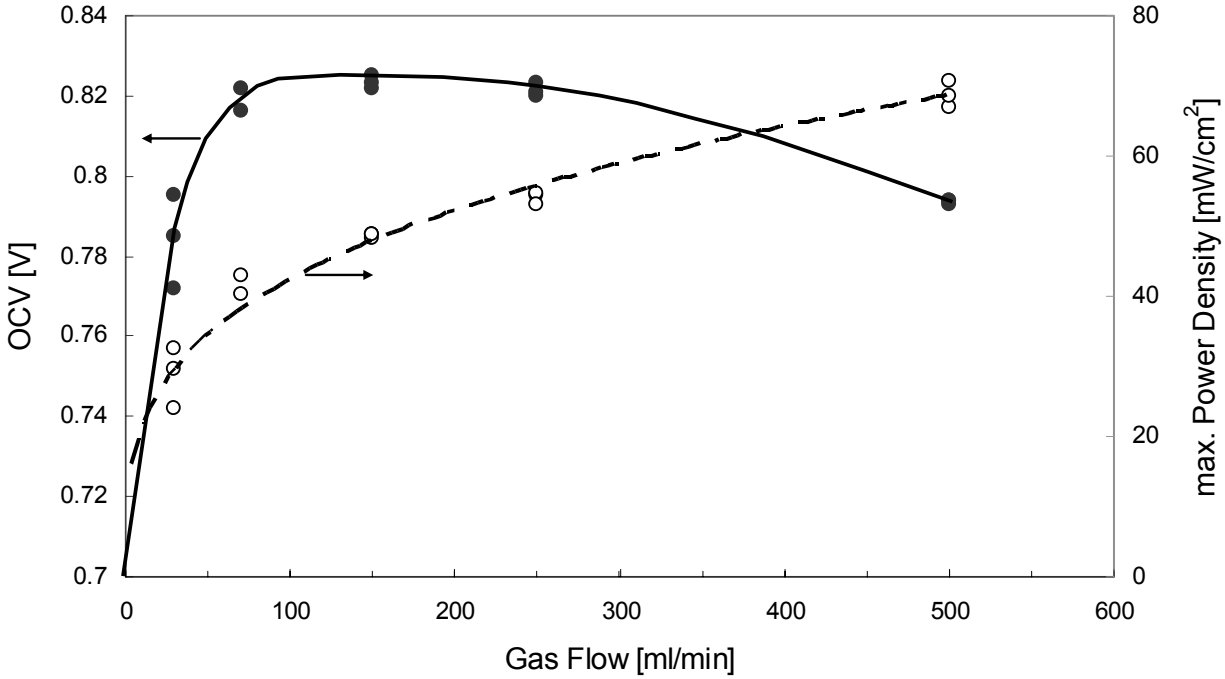

Figure 7.11 Open circuit voltage and maximum power density of a cell with a 60 µm thick anode as a function of the gas flow rate. The lines are for guiding the eye only.

In Figure 7.12 the voltage-current characteristics of three cells are shown at 500 ml/min flow rate to the anode of and an airflow of 500 ml/min to the cathode. The cell with the thickest anode showed the highest OCV and the highest maximum power density, whereas the cell with the 9 μm anode showed the lowest power output and a pronounced voltage drop at around 150 mA/cm^2. This drop can be attributed to the limited catalytic activity of the anode that led to a lack of H_2 and CO fuel and caused the electrochemical reoxidation of Ni.

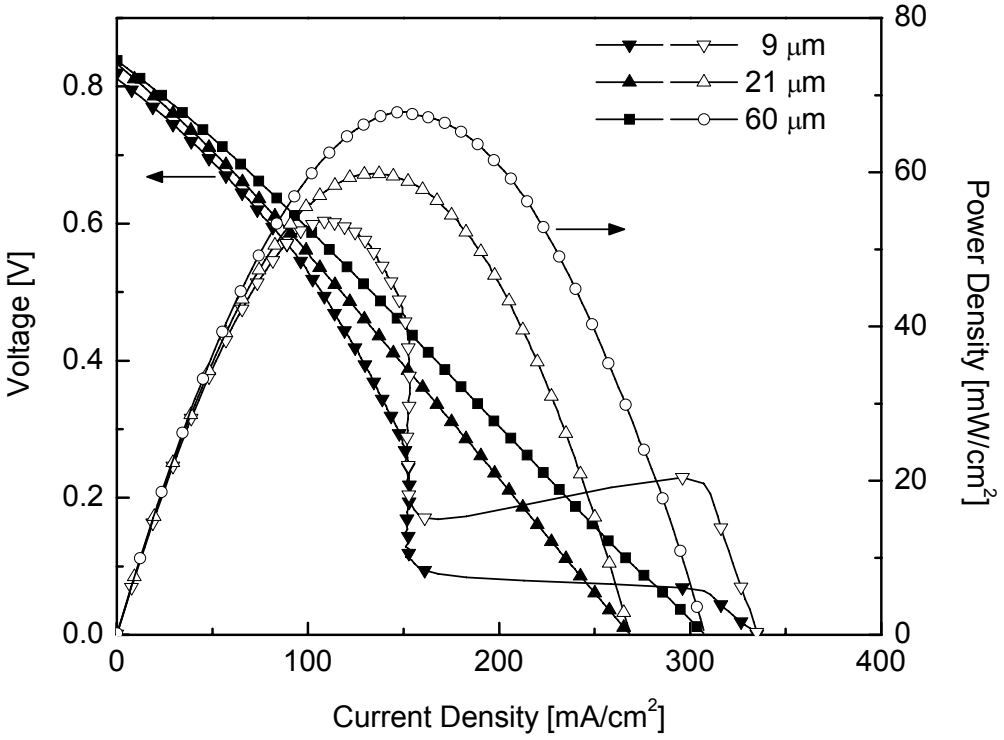

Figure 7.12 Voltage-current characteristic of three individual cells with 9, 21 and 60 μm thick anode at a flow rate of 500 ml/min CH_4-air mixture with CH_4/O_2=2.

The reason for the sudden increase of current after this drop is unclear but may be due to the beginning of another reduction/oxidation cycle. At a flow rate of 500 ml/min to the anode, this cell with 9 μm thick anode had an irregular voltage-current characteristic, as shown before in Figure 7.8.

The influence of the flow rate on the OCV and on the necessary furnace temperature ($T_{furance}$) for maintaining the anode temperature at 733°C is shown in Figure 7.13 for the 9 μm and 60 μm thick anode.

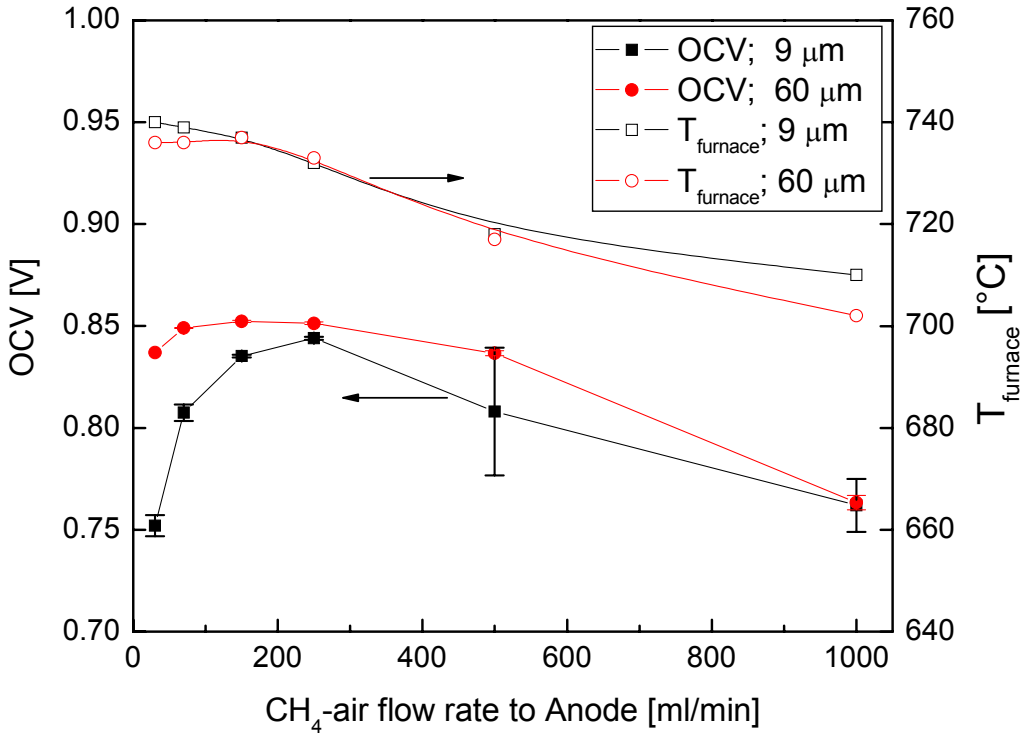

Figure 7.13 Open circuit voltage of three individual cells with 9, 21 and 60 µm thick anode at different flow rates of CH_4-air mixture to the anode and 500 ml/min air to the cathode.

The OCV reached a maximum at around 150-250 ml/min. For the cell with the thick anode, the OCV was not as strongly depending on the total flow rate as for the cell with the thin anode. The cell with the 60 µm thick anode had a higher OCV than the cell with the 9 µm thick anode at all the measured gas flows. The OCV decreased with increasing flow rate to the anode for both anode thicknesses. The observations that thick anodes gave high OCVs and that the measured OCVs decreased with increasing flow rate to the anode are in agreement with the predictions from the model that was presented in section 7.2. The fact that at low flow rates there was a continous decrease of OCV cannot be explained by the proposed model. Obviously there was a minimum flow rate to the anode for which a high OCV could be obtained. As shown in Figure 7.13, $T_{furnace}$ had to be decreased when the flow rate to the anode was increased. The reason for this is that the heat generation mainly due to the parasitic and highly exothermic Reaction (7.2) becomes more pronounced at higher flows rates because of a higher catalytic turnover. With exception of intermediate flow rates from 200 to 500 ml/min the thicker anode always exhibited a clearly stronger heat generation than the thin anode, which is due to the presence of a larger amount of catalytically active surface.

7.5 Summary

Single chamber SOFCs with different anode thickness ranging from 9-60 μm were prepared and measured in a double chamber setup, in which the anode was separated from the cathode compartment. At the cathode side a constant flow rate of 500 ml/min air was present ($p(O_2) = 0.21$ atm). The results for the cell with a 9 μm thick anode showed that under certain conditions there were large oscillations of the measured OCVs as well as voltage-current characteristics. The reasons for this were reduction/oxidation cycles of the Ni/NiO during the partial oxidation of CH_4 causing periodic temperature changes, which manifested themselves as oscillations of the OCV. There seemed to be an ideal flow rate to the anode, where regularly shaped voltage-current characteristics could be obtained. This range was 150-250 ml/min for the 9 μm thick anode, 150-500 ml/min for the 21 μm thick anode and 150-1000 ml/min for the 60 μm thick electrodes. Thus, thick anodes allow more stable operation at higher gas flows. It was found that the OCV decreased with increasing flow rate to the anode and that thick anodes gave a higher OCV and higher maximum power densities than thin anodes, which had been predicted by the proposed model of the influence of anode thickness on SC-SOFCs. It could be shown that the maximum power density increased with increasing flow rate to the anode even for the unstable conditions encountered with a 9 μm thick anode. However, high flow rates are inappropriate because they favour large fluctuations of the power output.

It would be interesting to investigate the influence of the cathode thickness. However, it is expected that the influence of the cathode thickness will have a less drastic effect on the electrochemical behaviour of SC-SOFCs than the anode thickness.

7.6 References

[1] W. van Gool, *Philips Research Reports*, **1965**, 20, 81-93.

[2] C. K. Dyer, *Nature*, **1990**, 343, 547-548.

[3] T. Hibino and H. Iwahara, *Chemistry Letters*, **1993**, 7, 1131-1134.

[4] T. Hibino, A. Hashimoto, M. Yano, M. Suzuki, S.-i. Yoshida and S. Mitsuru, *Journal of the Electrochemical Society*, **2002**, 149, *2*, A133-A136.

[5] P. Jasinski, T. Suzuki, F. Dogan and H. U. Anderson, *Solid State Ionics*, **2004**, 175, *1-4*, 35-38.

[6] I. C. Stefan, C. P. Jacobson, S. J. Visco and L. C. De Jonghe, *Electrochemical and Solid State Letters*, **2004**, 7, *7*, A198-A200.

[7] T. Suzuki, P. Jasinski, H. U. Anderson and F. Dogan, *Electrochemical and Solid State Letters*, **2004**, 7, *11*, A391-A393.

[8] M. A. Priestnall, V. P. Kotzeva, D. J. Fish and E. M. Nilsson, *Journal of Power Sources*, **2002**, 106, *1-2*, 21-30.

[9] Z. Shao, S. M. Haile, H. Ahn, P. D. Ronney, Z. Zhan and S. A. Barnett, *Nature*, **2005**, 435, 795-798.

[10] B. E. Buergler, M. E. Siegrist and L. J. Gauckler, *Solid State Ionics*, **2005**, 176, *19-22*, 1717-1722.

[11] T. Hibino, A. Hashimoto, T. Inoue, J.-i. Tokuno, S.-i. Yoshida and S. Mitsuru, *Science*, **2000**, 288, 2031-2033.

[12] T. Hibino, A. Hashimoto, T. Inoue, J.-i. Tokuno, S.-i. Yoshida and M. Sano, *Journal of the Electrochemical Society*, **2001**, 148, *6*, A544-A549.

[13] T. Hibino, A. Hashimoto, T. Inoue, J.-i. Tokuno, S.-i. Yoshida and S. Mitsuru, *Journal of the Electrochemical Society*, **2000**, 147, *8*, 2888-2892.

[14] Y. P. Tulenin, M. Y. Sinev, V. V. Savkin and V. N. Korchak, *Catalysis Today*, **2004**, 91-92, 155-159.

[15] Y. H. Hu and E. Ruckenstein, *Ind. Eng. Chem. Res.*, **1998**, 37, *6*, 2333-2335.

8 Micro Single Chamber Solid Oxide Fuel Cells

B. E. Buergler, S. Vuillemin, M. Ochsner and L. J. Gauckler, to be submitted to *Journal of Power Sources*.

ABSTRACT: In single chamber solid oxide fuel cells the Nernst voltage is generated by the selectively operating electrodes. These cells are operated in mixtures of fuel and air using only one gas compartment without the need of seals. This concept allows completely new design options. One of these options is the possibility to fabricate cells with both electrodes on the same side of an electrolyte disc. In this study, Micromolding in Capillaries was used for the preparation of both anodes and cathodes on an electrolyte substrate. The electrodes were prepared by filling capillaries between an electrolyte substrate and a PDMS-mold from two sides with two different materials. The process, however, requires a cosintering step of both electrodes, which could be critical.

The prepared cell consisted of an array of 19 individual cells that were connected in parallel. An open circuit voltage of 0.65-0.75 V was measured in flowing mixtures of methane and air. The maximum power density was limited by the ohmic resistance of the long conduction paths along the thin electrodes due to their connection in parallel.

It was shown that the proposed concept and process can be applied for the fabrication of micro single chamber solid oxide fuel cells. The cell resistance may be significantly reduced when connecting the cells in series using interconnections between anode and cathodes of adjacent cells.

8.1 Introduction

In 1965 van Gool proposed a novel fuel cell design using surface-migration of ions on a solid electrolyte in mixtures of fuel and air [1], which was patented by Louis in 1981 [2]. This new type of electrochemical cell in hydrogen air mixtures comprised laterally spaced side-by-side catalyst layers as electrodes with a gap between the catalysts being bridged by a solid electrolyte. In 1990 Dyer was able to generate electric power from a thin film device, which operated at room temperature in hydrogen air mixtures [3]. The concept of single chamber solid oxide fuel cells (SC-SOFCs) operating at temperature of over 500°C was demonstrated in practice for the first time by Hibino [4]. In the single chamber configuration there is only one gas compartment, thus the electrodes can be placed beside each other on the same electrolyte surface whereas in conventional SOFCs the electrodes are placed on opposite sides. It has been shown that the side by side cell design can generate an open circuit voltage (OCV) and that the ohmic resistance of the cell decreased as the gap between the electrodes became smaller [5]. The potential interconnection of cells on the same electrolyte disc was pointed out. Two series connected cells on the same substrate made of yttria stabilised zirconia (YSZ) showed an OCV that was twice as high as the OCV of a single cell. On the other hand two cells connected in parallel exhibited only half of the resistance. Cells with a gap width of 1 mm that were operated at 950°C in methane-air mixtures yielded a power output in the range of 45 mW/cm^2. By keeping the YSZ substrate but using $La_{0.8}Sr_{0.2}MnO_3$ and $Ce_{0.8}Gd_{0.2}O_{1.9}$-containing Nickel cermet as cathode and anode respectively, the performance of the cells with the same geometry could be improved to 120 mW/cm^2 [6] as compared to 45 mW/cm^2 [5] obtained with metallic electrodes. Ceria based electrolytes allowed for a drastic reduction of the operating temperature. Cells with $Ce_{0.8}Gd_{0.2}O_{1.90}$-electrolyte (CGO) showed an OCV of about 800 mV and a maximum power density of 122 mW/cm^2 at 500°C [7]. At this temperature the ceria solid solution is primarily an ionic conductor even at a oxygen partial pressure ($p(O_2)$) of down to 10^{-25} atm [8].

Hibino proposed a new cell design with interpenetrating comb-like electrode patterns on the same surface of an electrolytic material having feature sizes in the millimetre range [9]. However, this design was never experimentally validated. The questions which shapes, geometries, electrochemical properties of the electrodes and which electrolyte thickness are required to obtain an optimal performance was addressed by Fleig et al. in a recent publication [10]. For interpenetrating comb-like structures of anode and cathodes, the cells would have to have electrodes with characteristic feature sizes of a few micrometers.

The aim of this study was to demonstrate the concept of the side by side design with electrode widths and spacings in the micrometer range and to develop a suitable process for the preparation of these micro SC-SOFCs (μ-SC-SOFC). Promising techniques can be found in the domain of Soft Lithography that allows to deposit polymers and ink molecules onto various substrates [11,12]. It has been shown that it is possible to adopt the soft lithography technique to ceramics by using ceramic suspensions [13,14]. By Micromolding in Capillaries (MIMIC), which is one of the soft lithography techniques, Heule et al. were able to fabricate porous SnO_2-microlines [15], which could be used as sensor arrays [16] for miniaturised gas sensors. The electrodes of a μ-SC-SOFC would have to be quite similar to these microlines in terms of dimensions and structure. But in order to fabricate alternating lines of anode and cathode material for μ-SC-SOFCs, a modified MIMIC process had to be developed. By filling closed-end capillaries from opposite sides of a PDMS-mold with suspensions containing the anode and cathode materials both electrodes can be fabricated in one single step. No tedious aligning has to be done for the preparation of anode and cathode microlines being separated by a very narrow gap of a few micrometers. The gas permeability of the polydimethylsiloxan (PDMS) mold [12] allows filling microchannels that are closed at one end. The proposed process inherently produces cells connected in parallel by the electrode material deposited at the entrance of the capillaries. If the cells were to be connected in series, the preparation of interconnection lines between the anodes and the cathodes of neighbouring cells would have to be done and an additional aligning step would be required.

The performance of the μ-SC-SOFC was compared with the performance of cells with electrode dimensions and spacings in the millimetre range. These cells with side by side design were fabricated in a similar way as previously described [17] by screen printing the electrode layers. Four parallel connected cells were also prepared having the same design as the μ-SC-SOFC but with electrodes being 10 times wider and the gap width being more than 35 times larger. The voltage current characteristics of the prepared cells were measured in methane-air mixtures.

8.2 Experimental

8.2.1 Powders

The powders that were used for the preparation of SC-SOFCs are summarised in Table 8-1. The average particle size was estimated from the specific surface area (SSA) that was measured by N_2-adsorption (BET). The densities of the powders were measured by Helium pycnometry.

Table 8-1 Powders used for the preparation of SC-SOFCs.

Powder	Function	Supplier	SSA [m^2/g]	Particle Size [nm]	Density [g/cm^3]	Lot Nr.
NiO-CGO (60-40)	Anode	SSC	13.52	60.1	6.93	03_P1464BM
$Sm_{0.5}Sr_{0.5}CoO_{3-\delta}$ (SSC)	Cathode	Nextech	5.46	336	6.53	91-82
$Ce_{0.9}Gd_{0.1}O_{1.95}$ (CGO10)	Electrolyte	Rhodia	35.84	22.9	7.29	9804401

8.2.2 Electrolyte Pellets

Electrolyte discs were fabricated by uniaxially pressing 7 g of $Ce_{0.9}Gd_{0.1}O_{1.95}$ (CGO, Lot# 9804401, Rhodia, Catalysis & Electronics, France) powder with an average particle size of 22.9 nm (measured by BET) in a 30 mm diameter dye at 40 MPa. The discs were then isostatically pressed at 300 MPa and sintered at 1400°C in air for two hours. A heating rate of 1 K/min and a cooling rate of 5 K/min were applied. In order to obtain flat surfaces the sintered discs were lapped on a Stähli FLM 500 lapping machine equipped with a hybrid copper-steel disc. B_4C-suspension (BC-800, Stähli Switzerland) was used at 60 rpm and about 1 drop of B_4C-suspension every second. The density of the discs was measured after lapping and exceeded 97% of the theoretical density (ρ_{th} = 7.29 g/cm^3).

8.2.3 Cell Designs

All the prepared cells had the side by side placement of electrodes with varying electrode and gap dimensions. On the one hand, cells with electrodes in the millimetre range were prepared; on the other, cells with micrometer sized electrodes. The “Macro”-cell

(M-SC-SOFC) shown in Figure 8.1 a, had an electrode size of 0.5×1.0 cm^2 with a 1.2 mm spacing between the anode and the cathode. The "Milli"-cell (m-SC-SOFC) had eight electrodes, each with a size of 0.1×1.25 cm^2 and an intracellular spacing of about 0.25 mm. The μ-SC-SOFC design (Figure 8.1 c) had a total of 92 electrodes, each with 0.01 × 1.0 cm^2 and a spacing of 10 μm between all electrodes. Pt-mesh and wire was used as the current-collectors for all the cells.

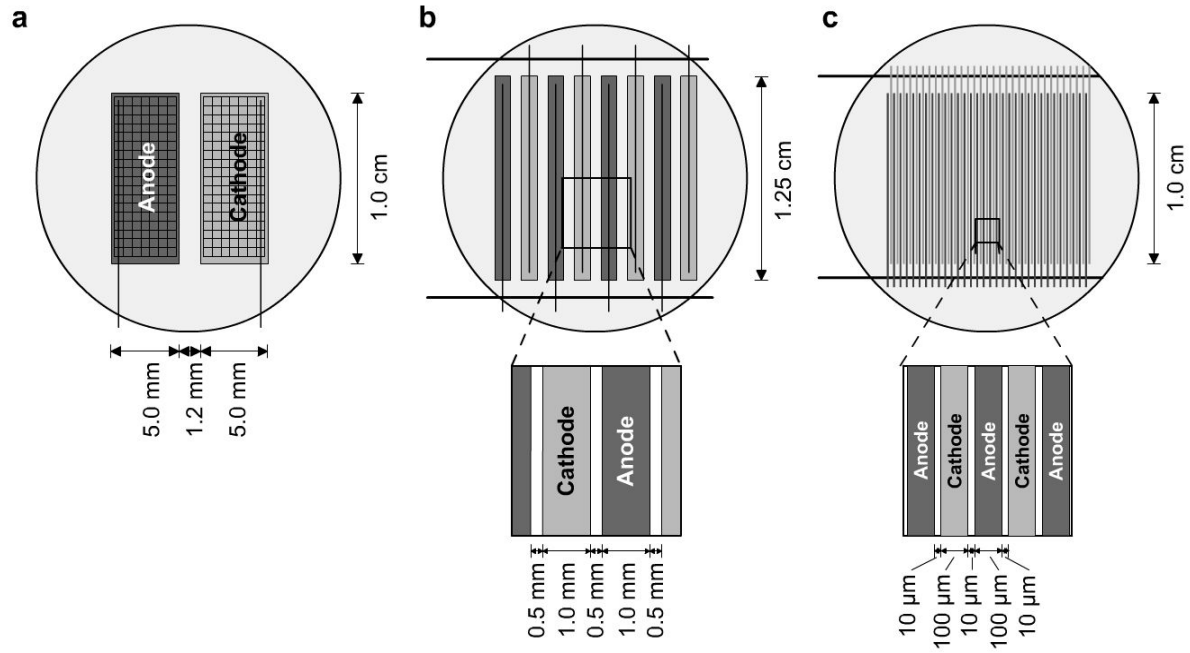

Figure 8.1 Dimensions of the prepared side by side SC-SOFCs. a) M-SC-SOFC with 0.5 cm wide electrodes separated by a gap of 1.2 mm. b) m-SC-SOFC with four parallel connected cells with electrode lengths and widths of 12.5 mm and 1 mm, respectively. c) μ-SC-SOFC with electrode lengths and widths of 1 cm and 100 μm, respectively. The gap between the electrodes is 10 μm wide.

8.2.4 Preparation of M-SC-SOFCs

The preparation steps for the M-SC-SOFCs are depicted in Figure 8.2. Both anode and cathode (0.5 × 1.0 cm^2) were similarly deposited in a side by side configuration by screen printing them onto the electrolyte disc. A mask of 50 μm thickness was used in combination with suitable organic pastes, of which the preparation is described in section 5.2.3. 60 wt% NiO containing $Ce_{0.8}Gd_{0.2}O_{1.9}$ (SSC, Salt Lake City, USA) was used as the anode and $Sm_{0.5}Sr_{0.5}CoO_{3-\delta}$ (Nextech Materials, Worthington, USA) as the cathode. Current collectors were made by point welding Pt-wire onto a completely flat Pt-mesh 0.5 × 1 cm^2 in size (52 mesh woven from 0.1 mm wire, Alfa Aesar). The current-collector was placed on the

freshly printed layer, which was subsequently dried. The anode was printed and sintered first (Figure 8.2 a-c), and then the cathode was prepared in a very similar manner as shown in Figure 8.2 d-e. Both electrodes were sintered at 1200°C for 1 h in air. The heating rate was 1 K/min from room temperature to 500°C with a dwell time of 1 h at this temperature and 3 K/min from there to the peak temperature. The samples were cooled down to room temperature at 5 K/min. Digital photographs of the prepared cell before and after the measurement are shown in Figure 8.8.

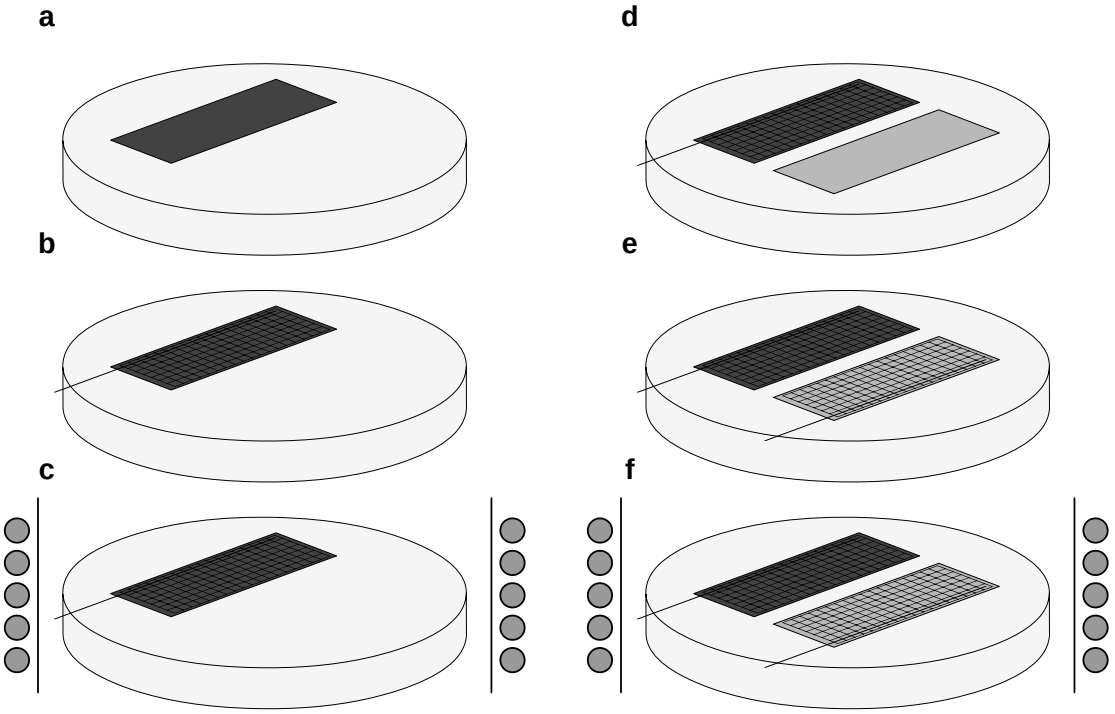

Figure 8.2 Preparation of M-cells. a) Screen print anode onto ion conducting CGO substrate. b) Place current-collector on the anode layer c) sinter anode together with current-collector d) screen print cathode beside anode. e) Place current-collector on cathode layer. f) Sinter cathode layer: M-SC-SOFC with feature sizes in the range of millimetres.

8.2.5 Preparation of m-SC-SOFCs

The preparation steps of m-SC-SOFCs with four parallel connected cells are depicted in Figure 8.3. The cells had eight electrodes that were 12.5 × 1 mm in size. Therefore, the total electrode area was 1 cm^2; the cell area including intercellular as well as intracellular gaps was 1.41 cm^2. In a first step, four anode strips were screen printed through a mask of 50 μm thickness, which were subsequently sintered in the same way as described in section 8.2.4. but with a peak temperature of 1300°C (Figure 8.3 a and b). After that the cathode layers were

printed (Figure 8.3 c) through the same mask forming an average gap between the two electrodes of 0.27 mm and between the electrodes of adjacent cells of 0.37 mm. After the screen printing the edges of the electrodes spread out a little so that the final electrode width for both electrodes was about 1.1 mm. Flat Pt-wires that had been covered with the organic pastes of either the anode or cathode material were placed on the corresponding electrodes, and then sintering with a peak temperature of 1100°C was done (Figure 8.3 d and e). Finally, the four anode and cathode contacts were point-welded each to a piece of Pt-wire (Figure 8.3 f).

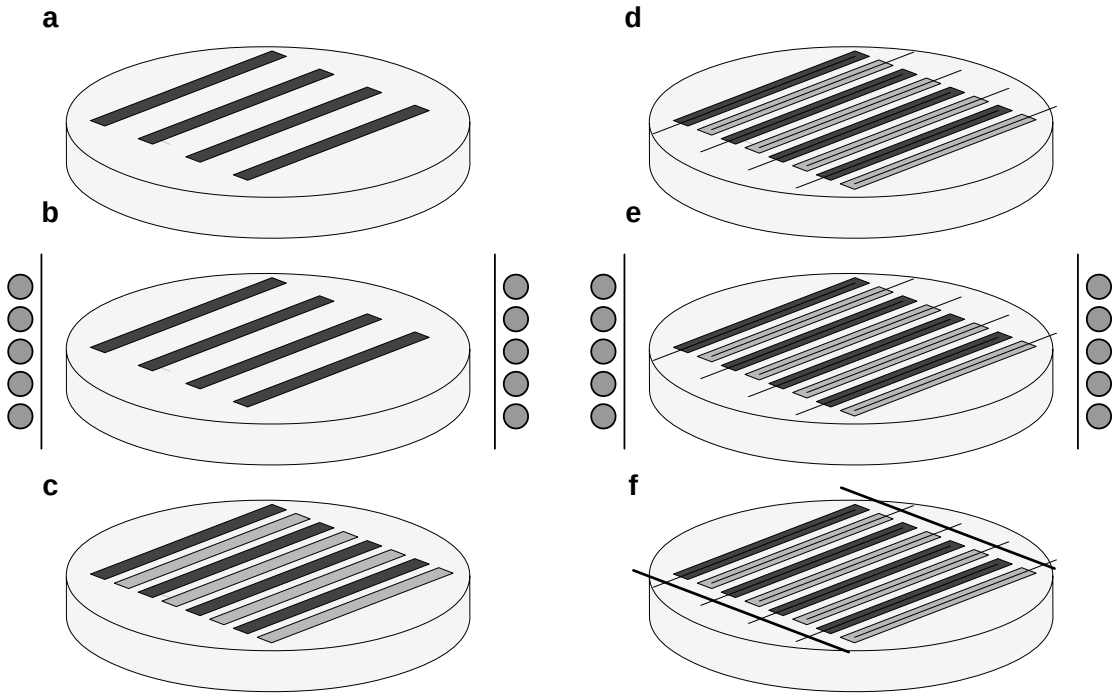

Figure 8.3 Preparation of the m-SC-SOFC consisting of four parallel connected cells. a) Screen print four anode strips in a single step. b) sinter anodes. c) print cathode strips. d) place current-collectors on electrodes. e) sintering of electrodes with current-collectors f) point weld the cathode contacts to the cathode bus and the anode contacts to the cathode bus.

8.2.6 Preparation of µ-SC-SOFCs

Cathode and Anode Powders

The commercial $Sm_{0.5}Sr_{0.5}CoO_{3-\delta}$ powder (Nextech Materials, Worthington, USA), of which a SEM-micrograph is shown in Figure 8.4, had a bimodal particle size distribution. A certain fraction of particles was larger than 2 µm, which is critical for the MIMIC process because the microchannels were only 7 µm in height. This fraction of large particles was

removed by sedimentation of a well desagglomerated and stabilized suspension in a glass tube of 4 m length for ten days. After this time the large particles had sedimented at the bottom of the glass tube leaving behind the supernatant with fine particles, which was removed from the tube and dried. Only this powder fraction was used for preparing μ-SC-SOFCs. A micrograph of the powder after sedimentation (Figure 8.4 b) shows that the large particles had been

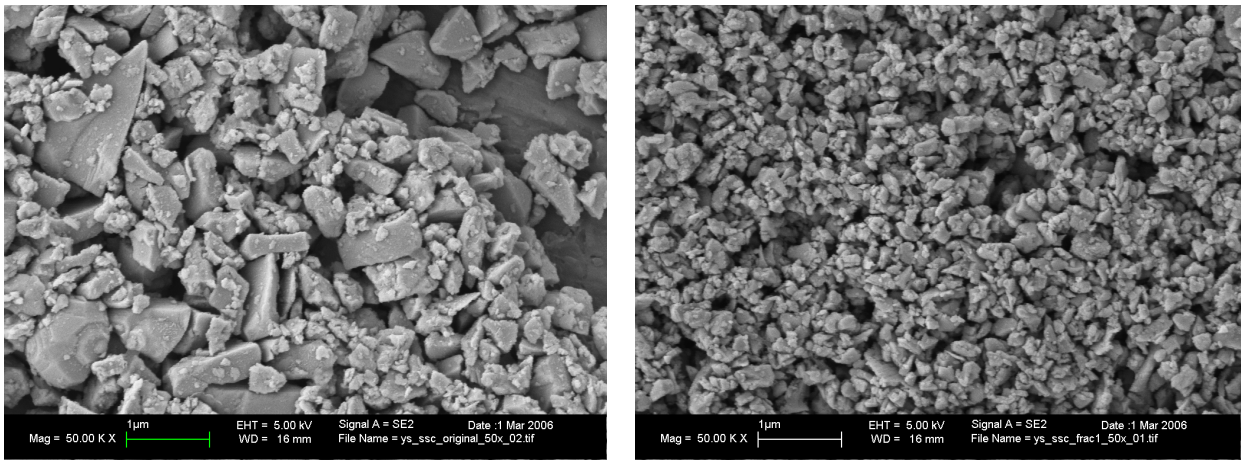

Figure 8.4 $Sm_{0.5}Sr_{0.5}CoO_{3-\delta}$ powder. a) As purchased with large particles in the range of 2 μm and b) after sedimentation. The large particles are not present any more, thus making this powder suitable for MIMIC.

successfully removed by the sedimentation step. The average particle size after sedimentation was 0.30 μm. Commercial powder of 60 wt% NiO containing $Ce_{0.8}Gd_{0.2}O_{1.9}$ (SSC, Salt Lake City, USA) was used as anode material.

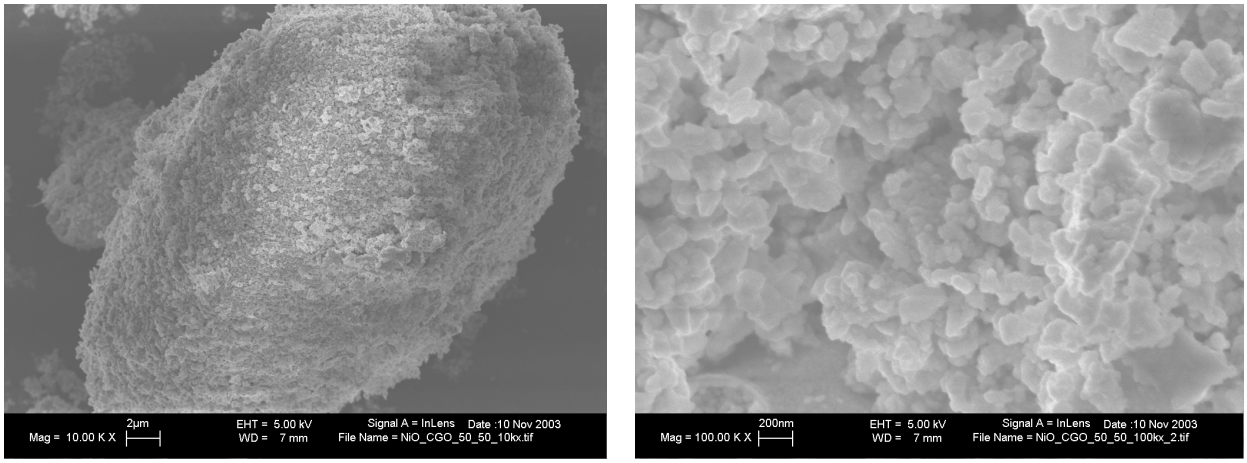

Figure 8.5 60 wt% NiO containing $Ce_{0.8}Gd_{0.2}O_{1.9}$ that was used for the fabrication of the anodes. a) agglomerates with 20-50 μm diameter that must be destroyed prior to the use in the MIMIC process. b) The primary particles forming the agglomerates are in the range of 50-200 nm in size.

As shown in Figure 8.5 a and b, the nano-particles formed agglomerates that had to be destroyed before the material could be used. This was done on a vibratory mill (Retsch MM 200) at a frequency of 20 Hz for 20 minutes. The anode powder had an average grain size of 60 nm, which allowed to sinter it a relatively low temperature of around 1100-1300°C.

Suspensions for MIMIC

The most important parameters for a suitable suspension are the particle size, solid loading, the properties of the solvent and the wettability on the PDMS material and the CGO substrate. The capillaries of the PDMS-mold are only 7 μm high and if there are particles or agglomerates in the suspension being larger than that they will block the entrance of the capillaries and stop the filling process. Thus, powders must be used with a particle size smaller than about 1 μm and the suspensions must be thoroughly desagglomerated. The solid loading of the suspension must be as high as possible to avoid excessive drying shrinkage and to obtain thick and continuous electrodes. But if it is too high, the increased viscosity will impede the filling of the capillaries. The influence of solid loading of the used suspensions on the lines was studied by Heule [18]. The solvent is another very important parameter. With ethanol the MIMIC process can not work at ambient conditions because the drying is too fast. Neither could diethylene glycol monobutyl ether acetate with much slower drying rate be used because it swelled the PDMS-mold and led to detachment of the mold from the substrate. Aqueous suspensions of both powders were used in this study. Water was mixed with Poly acrylic acid sodium salt (PAA; Molecular weight 2000 g/mol, Aldrich) such that the amount of PAA amounted to 1 wt% of the powder. Then the ceramic powder was added and homogenised by ultrasonification under stirring for 10 minutes. The suspensions were brought to pH 9 by adding ammonia (25 % in H_2O) and were stable for several days without stirring. Different solid loadings were evaluated. For too low solid content no material is deposited in the microchannels whilst for too high solid loading the capillaries can not be filled, because the slurry is too viscous. Cathode and anode suspensions with 13 vol% and 23 vol% of solid material respectively, exhibited suitable properties for the filling of microchannels.

Preparation of the Micromold

The master for the PDMS-molds was a photolithographically structured photo resist (AZ 4562, Clariant, Inc., Wiesbaden, Germany) covered silicon test grade wafer. Prebaking of

the resist was performed on a hot plate for 3 minutes at 90°C. The exposure of the 7 µm thick photo resist was done by a mask aligner (Suss MA-6) and the structures were developed in a mixture of Shipley developer 251 and water (1:3).

For the fabrication of the PDMS-molds the structured wafer was placed in a Petri dish and covered with a 10/1 mixture of PDMS prepolymer/catalyst (Dow Corning, Inc., Midland, MI) under flow box conditions. The PDMS was cured for 2 hour at 60°C. Then the mold was carefully peeled off and two reservoirs for the suspensions were cut into the PDMS to open the ends of the capillaries on the two sides. After immersion in n-hexane for 60 minutes for removing non-reacted monomers the PDMS-mold was oxygen-plasma treated for 2 minutes in a Harrick PDC-32G steriliser. This turned out to be very important especially for aqueous suspensions of the electrode materials. In Table 8-2 the contact angles θ of water on PDMS and CGO are summarised before and after the plasma treatment. It is clear that without plasma-treatment the MIMIC process could not have been done due to the micro channels being non wetting. The filling of the capillaries would have been impossible. Because of 48% of the micro channels surface being CGO it was of great importance to carry out the plasma cleaning also with the CGO substrate.

Table 8-2 Contact angle of water on PDMS and CGO-pellets before and after oxygen plasma treatment.

θ with PDMS before plasma cleaning	**θ with PDMS after plasma cleaning**	**θ with CGO before plasma cleaning**	**θ with CGO after plasma cleaning**
95	<7	65 ± 9.3	16 ± 1.7

Micromolding in Capillaries

All the steps for the fabrication of µ-SC-SOFCs are schematically shown in Figure 8.6. First the PDMS-mold was placed on the CGO substrate and 20 µl of each suspension was filled into each reservoir (Figure 8.6 a and b). The filling of closed end capillaries was possible but at a rate that was more than hundred times slower than in the case of open end channels. The reason for this was the increasing pressure of the air trapped in the capillary as the channels were being filled. Therefore, the filling process was limited by the air permeability of the PDMS-mold. The diffusion rate of air through the mold is proportional to the pressure difference across the PDMS and inversely proportional to the surface area of the capillary and the thickness of the mold. The filling velocity of the channels was in the range

of 50 µm/s as measured by microscopy. The adhesion of PDMS on CGO substrates was sufficient to perform the MIMIC process. After filling of the capillaries (Figure 8.6 c), the reservoirs were emptied (Figure 8.6 d) and sealed by adhesive tape in order to avoid too fast drying of the suspensions. Drying the green electrodes was problematic when the material in the reservoir dried before the material in the capillary did. Then, through capillary forces of the powder in the reservoir, a flux of material in the opposite direction towards the channel entrance occurred that partially removed the structured material. To avoid this, the suspension in the reservoir was removed after complete filling of the microchannels. Finally, the PDMS-mold was carefully removed from the CGO substrate as shown in Figure 8.6 e.

The described process was difficult to reproduce and turned out to be suitable only for prototyping of small electrochemical devices. The filling of microchannels is a statistical process so the filling length may vary considerably from channel to channel. Some of the cathode microchannels had been completely filled but most of them had not. This means that not all the electrodes were interdigitating. It was also observed that the anode microlines were always shorter than the cathode microlines, indicating that an increase of solid loading will decrease the average filling length, as already noticed by Heule [17].

Sintering and Electric Contacting

The proposed electrode preparation process requires the co-sintering of the anode and cathode material (Figure 8.6 f). To ensure a good contact between the electrolyte and the anode and for obtaining a stable anode-microstructure a rather high sintering temperature of up to 1300°C is required. The cathode material should, however, not be sintered at temperatures above 1100°C [19] because the microstructure becomes very coarse. Therefore, the cathode determines the maximum cosintering temperature, which was chosen to be at 1100°C. The sintering was done in the same way as described in section 8.2.4 with 2 hours holding time at the peak temperature. The anodes and cathodes were connected as shown in Figure 8.6 g using Pt-Paste (Heraeus C3605S) and flattened Pt-wire (Agar Scientific E404-1, 0.1 mm in diameter) at the beginning of the electrode arrays.

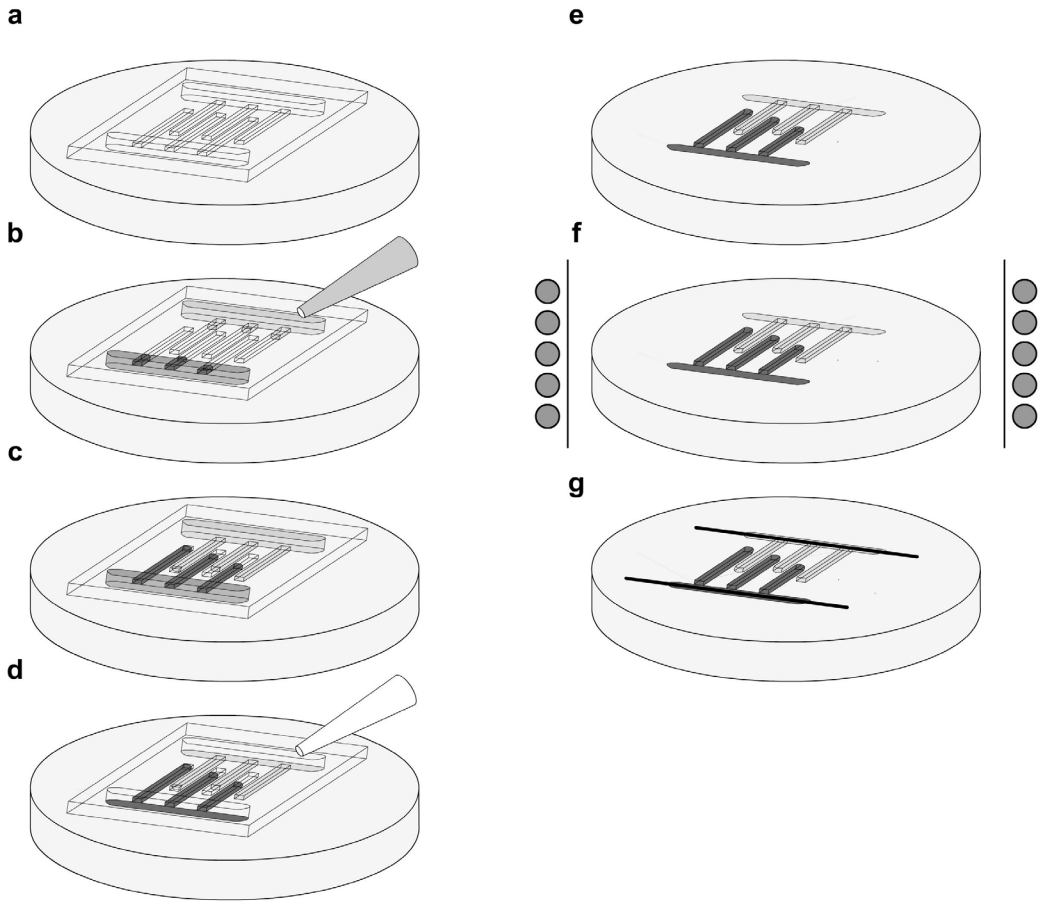

Figure 8.6 Schematic of the Micromolding in Capillaries process for the preparation of μ-SC-SOFCs. a) Place PDMS-mold on ion conducting CGO substrate. b) Apply suspension droplet in the reservoirs at the opening of the microchannels on each side of the mold. c) Capillary forces fill microchannels with anode and cathode suspensions from opposite sides of the PDMS-mold. d) Excess suspension is removed from the reservoirs and the microlines are slowly dried. e) Remove PDMS-mold: interdigitating array of anode and cathode stripes forming a Micro SC-SOFC. f) Co-sinter both electrode arrays. g) Apply Pt-paste and flattened Pt-wire as current-collectors with subsequent heat treatment.

First a layer of Pt-paste was screen printed perpendicular to each electrode array where the reservoir was located during the MIMIC step. Then a Pt-wire was placed on top of each side of the cell. The Pt-paste/wire current-collectors were heat treated at 1100°C for 1 hour according to the instructions of the Pt-paste supplier. The Pt-wires were then fixed to the CGO substrate by refractory adhesive (Firag, Germany).

8.2.7 Connecting the Cells and Electrochemical Characterisation

The fabricated cells were heated to 650°C in the test rig shown in Figure 8.7. In this setup the cell is supported in a round quartz glass holder and the gas flow comes from the top

through a quartz glass tube in a centro-symmetrical configuration. The thermocouple (Type K) was placed very closely at the cells surface and was covered with a thin layer of refractory adhesive (Firag, Germany) in order to prevent erroneous temperature readings. Fuel cell tests were done at temperatures from 500-650°C in methane-air mixture with different CH_4/O_2 ratios (in the following denoted x). The total gas flow rate was varied from 100-300 ml/min. The voltage current characteristics of the cell were obtained by a voltage sweep from the OCV to 0V at a rate of 2-5 mV/sec using a potentiostat (IM600, Zahner GmbH, Germany). This rate was found to be sufficiently low for allowing the cell to equilibrate during the whole measurement.

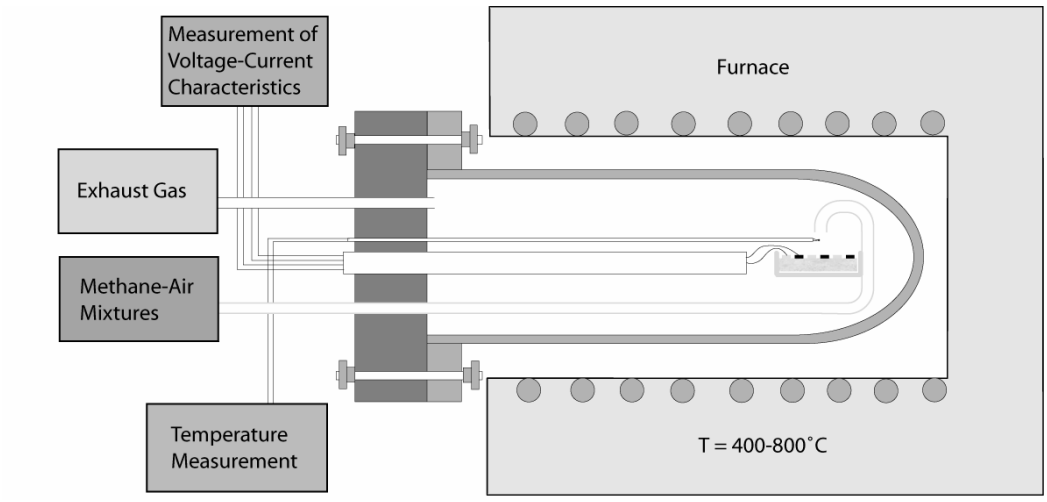

Figure 8.7 SOFC test rig for single chamber cells.

8.3 Results and Discussion

8.3.1 M-SC-SOFCs

The measured cell is shown in Figure 8.8 a before and b after the measurement. The green electrode (right) corresponds to the anode and the black electrode (left) to the cathode in Figure 8.8 a. A gap of 1.2 mm width separates the two electrodes both having a surface area of 0.5 cm^2. The Pt-mesh and wire can clearly be seen on both electrodes. In Figure 8.8 b the cell is shown after the measurement. The anode had turned predominantly black due to the reduction of NiO to metallic Ni in the reducing CH_4-Air mixtures, while the cathode showed no observable changes. Close to the gap the anode material had turned white as a result of pronounced micro structural changes.

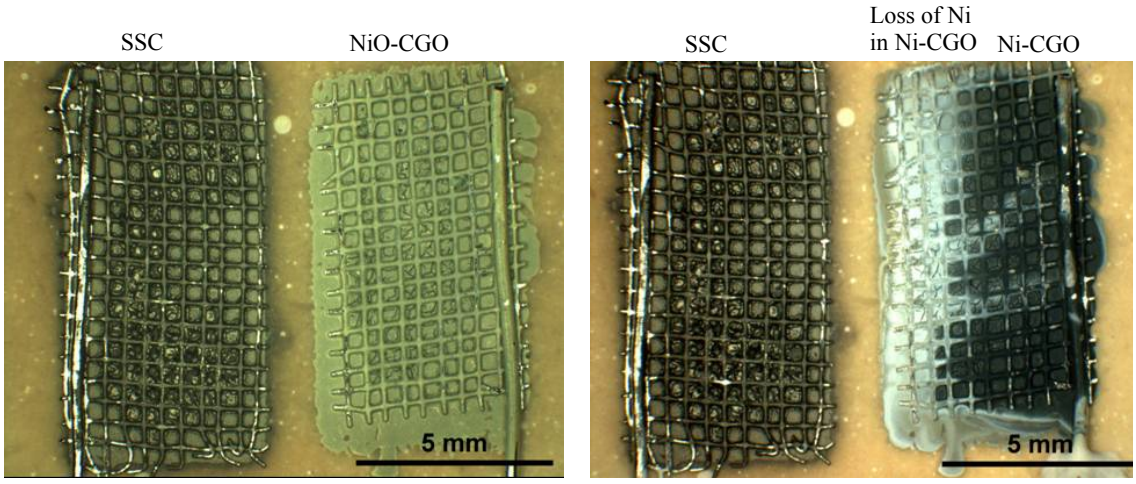

Figure 8.8 M-SC-SOFC a) before and b) after measurement in mixtures of CH_4 and air. The white region of the anode (left side) in b) close to the gap was active while 60% of the electrode surface stays inactive. Pt-mesh and wire current-collectors were used for both electrodes.

SEM-micrographs of the unreduced anode and the black and white regions of the reduced anode are shown in Figure 8.9. The unreduced anode (Figure 8.9 a) had a homogeneous, porous microstructure of NiO and CGO with a grain size of approximately 200 nm. The black area of the reduced anode far away from the gap (Figure 8.9 b) consisted of metallic Nickel and CGO. The metallic phase can clearly be distinguished from the ceramic CGO-grains and is the reason why the material appears black. In the white region of the anode very close to the gap a loss of the metallic Ni was evidenced by SEM and also XRD, leaving behind a ruptured microstructure of CGO-grains (Figure 8.9 c). The CGO-particles still had the same size as in the black region but insufficient interconnectivity. The loss of metallic Nickel was the cause for the change of colour from black to white. In Figure 8.9 d, a region in the white part is

shown where metallic Nickel had segregated to the surface of the anode layer. Volatilisation of Ni during the partial oxidation of methane at temperatures of around 730-830°C is not an unknown phenomenon; Torniainen et al. [20] noticed the slow deactivation of monolith supported Ni-catalyst and could attribute this to the loss of Ni. They did not give an explanation how this loss occurred. The temperature of the fuel cell could have easily reached temperatures above 700°C, where the Ni-volatilisation was possible. Jacques-Bédard et al. reasoned that the loss of Ni in SC-SOFCs operating in CH_4-air mixtures could have been due to the formation of gaseous $Ni(OH)_2$ that was slowly but constantly removed by the incoming gas flow [21].

X-ray diffraction (XRD) measurements of the unreduced anode showed that the material was composed of NiO and CGO. The black region in the reduced anode (in Figure 8.8 b)

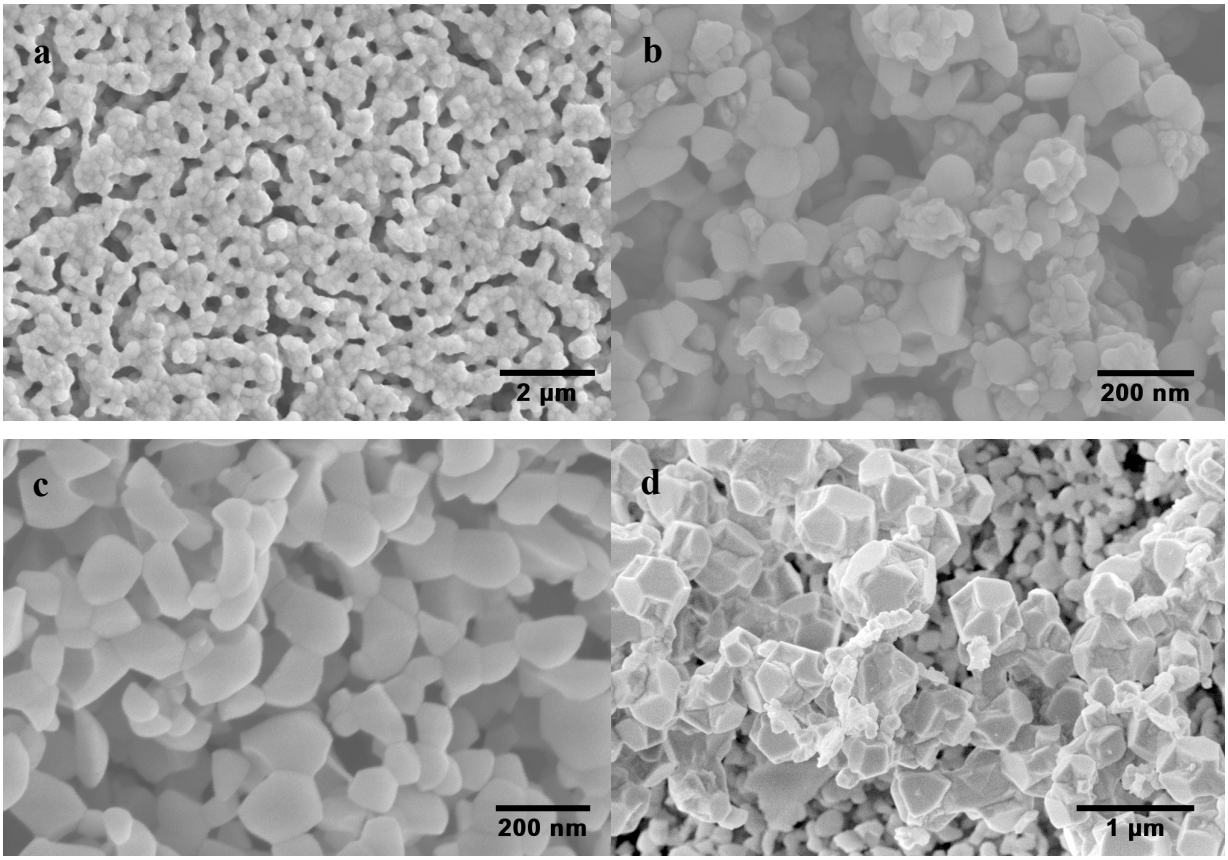

Figure 8.9 SEM-micrographs of the anode before (a) and after the measurement (b, c and d) of the M-SC-SOFC from Figure 8.8. a) The unreduced anode has a homogeneous, porous structure of NiO and CGO. b) The anode structure in the black regions far away from the gap consists of metallic Nickel and CGO-grains c) the anode structure in the white region very close to the gap where the metallic phase was lost. d) Ni-segregations on the surface of the anode material close to the gap.

indicated the presence of metallic Ni as well as some NiO, which was due to the superficial oxidation of the Ni-grains during the cooling of the fuel cell under CH_4-air mixture. The XRD-pattern of the white region showed the presence of CGO and some NiO but the peak for metallic Nickel had become very small as compared to the same peak of the black region. This confirmed the Ni-loss that was already observed by SEM. The observations suggest that only a small part of the anode close to the gap contributes to the fuel cell performance, while 60% of the surface area (black region) does not. The remote regions of both electrodes have long paths for the ionic current, which leads to high ohmic resistances. Therefore, the regions far away from the electrode gap stay inactive and it does not make sense to exceed a certain electrode width. In Figure 8.10 the voltage current characteristics of the M-SC-SOFC is shown at a temperature of 500°C and 600°C. The OCV was close to 0.8 V for both temperatures while the maximum power density reached 0.81 mW at 500°C and 2.1 mW at 600°C. Due to the very large gap size of 1.2 mm the cell had a total resistance of 71 Ω at 600°C.

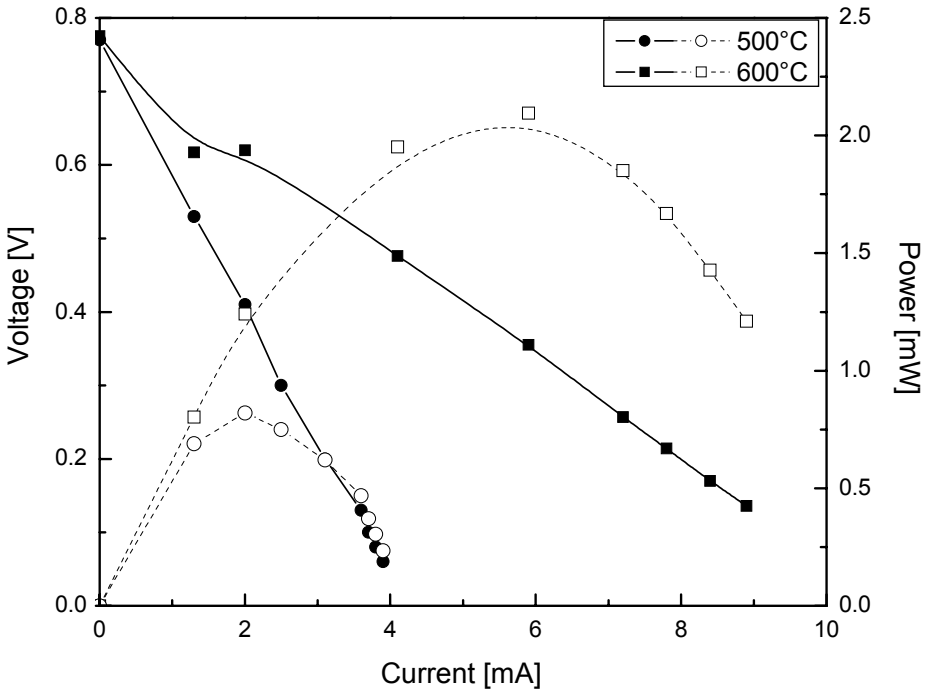

Figure 8.10 Voltage Current Characteristic of the M-SC-SOFC at a furnace temperature of 500 and 600°C and a total flow rate of 125 ml/min CH_4-air mixture ($CH_4/O_2 = 3.2$).

8.3.2 m-SC-SOFC

A digital photograph of the m-SC-SOFC with four parallel connected cells is shown in Figure 8.11. The average distance between the two electrodes of one cell was 0.27 mm, between the electrodes of adjacent cells 0.36mm. The total area of the cell was 1.41 cm^2.

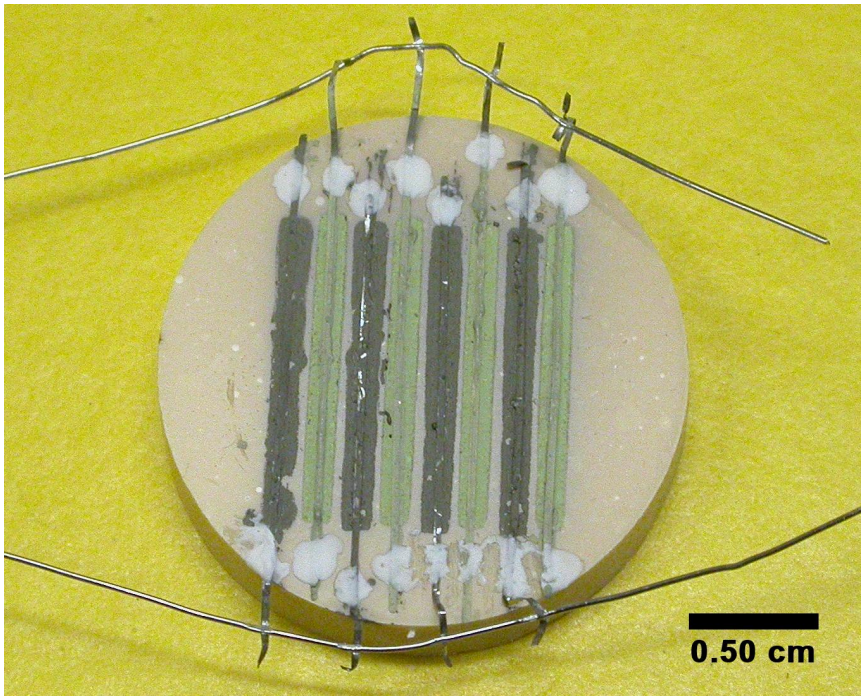

Figure 8.11 m-SC-SOFC: Four parallel connected SC-SOFCs on a CGO substrate. The Pt-wires used as current-collectors were attached to the electrolyte by small dots of refractory adhesive.

In Figure 8.12 the voltage current characteristic of the m-SC-SOFC is shown for different x-values at 650°C and 100 ml/min CH_4-air flow. The OCV reached a value of 0.72 V at x = 1 and 0.70 V at x = 1.5. When x = 2, the OCV was around 0.5 V and the cell behaviour was very unstable giving strongly fluctuating OCV. This is the reason why the voltage-current characteristic was not measured at these conditions. The maximum power output reached 1.18 mW at x = 1.5.

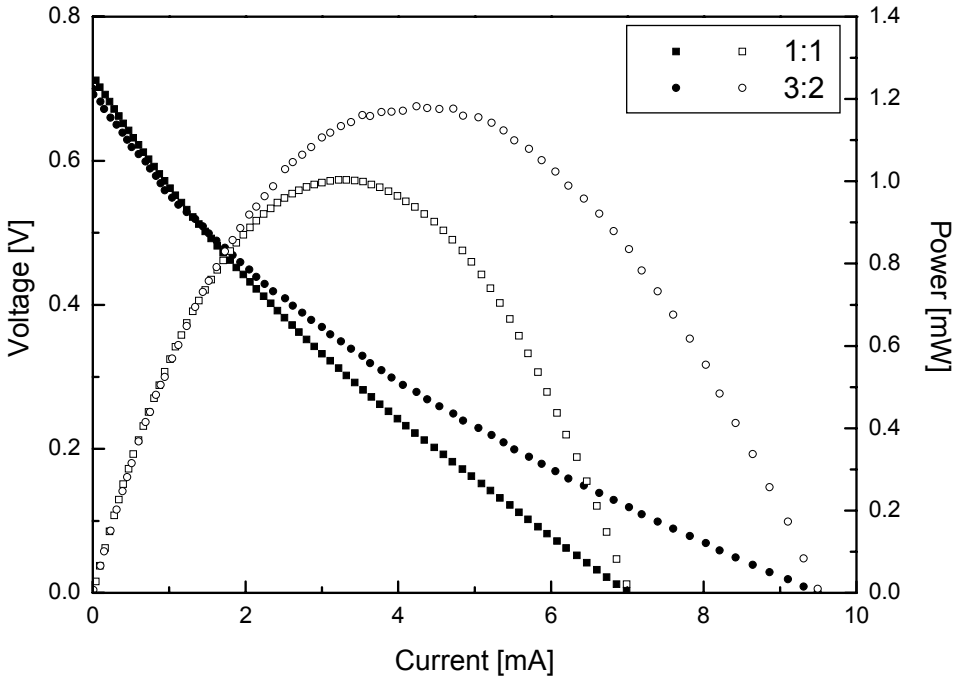

Figure 8.12 Voltage current characteristic of the fabricated m-SC-SOFC at different CH_4/O_2 ratio at 650°C with a total flow rate of 100 ml/min CH_4-air mixture. At x = 2 it was not possible to obtain a stable OCV, which is the reason why the voltage-current characteristic was not measured.

8.3.3 μ-SC-SOFC

In Figure 8.13 a digital photograph of the prepared μ-SC-SOFC is shown. Interdigitating microlines of anode and cathode materials only 100 μm wide were obtained by the modified MIMIC process. There was a statistical distribution of the final microline length, which was the reason why the electrodes were interdigitating only in a small region as shown in Figure 8.13. In total 19 active cells with interdigitating electrodes were present. The active area, including the area of the gaps, amounted to 5.08 mm^2, which was estimated by light microscopic analysis of the cell. Figure 8.13 shows a SEM-micrograph of the region where the electrodes were interdigitating. The MIMIC process allowed the preparation of sub-millimetre electrodes that were separated by a very narrow gap of 14 μm. No cross contamination of anode and cathode material was observed. The anode had a final width of 96.8 μm, while the cathode had a width of 91.4 μm. The initial width of the electrodes was 100 μm, the initial gap width 10 μm. This means that during the sintering step there was a lateral shrinkage of 3.2% for the anode and 8.6% for the cathode.

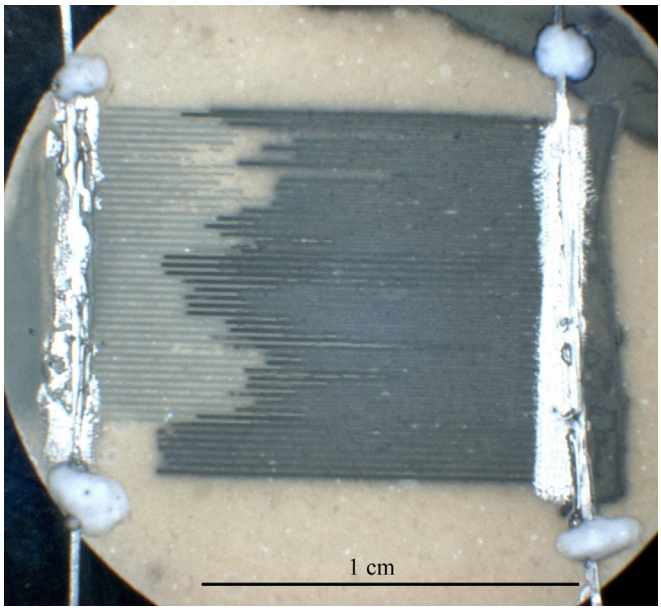

Figure 8.13 Optical micrograph of the finished µ-SC-SOFC prepared by MIMIC showing the cathode array (black), the anode array (grey), the electrolyte substrate, the Pt current-collectors as well as the refractory adhesive for fixing the Pt-wires to the electrolyte substrate.

The high shrinkage of the cathode was accompanied by the formation of small cracks. The main reasons for this are the low solid loading of the MIMIC-suspension and the relatively high sintering temperature of 1100°C. The gap width increased from an initial value of 10 µm to 14 µm. The electrodes were approximately 2-3 µm in height.

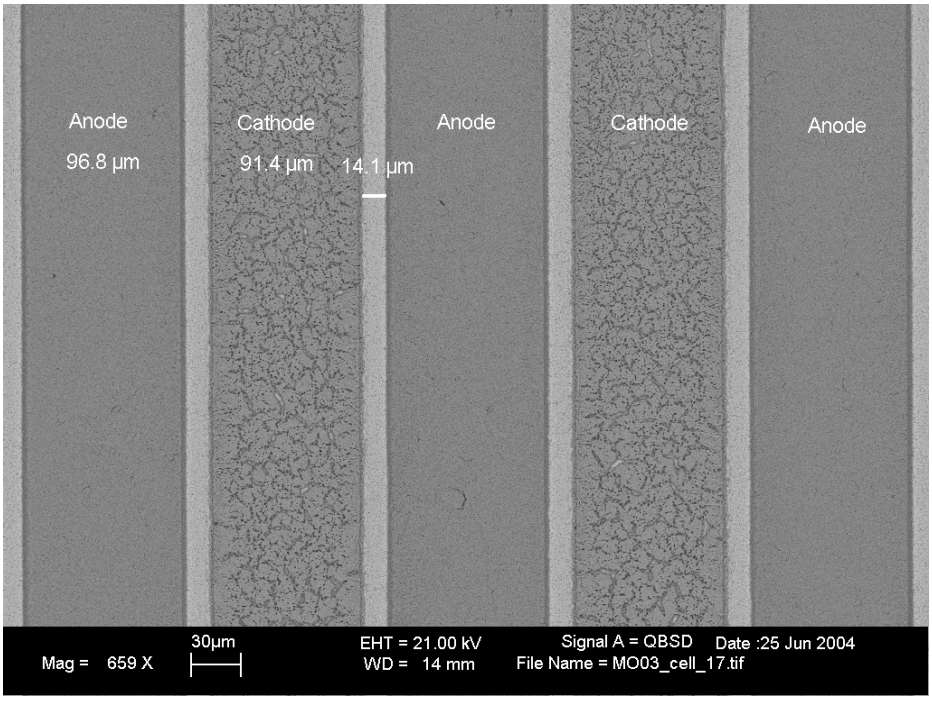

Figure 8.14 Topview of a part of the active area of the µ-SC-SOFC fabricated by MIMIC.

In Figure 8.15 the voltage current characteristic of the fabricated μ-SC-SOFC is shown for a total flow rate of 100 ml/min of CH_4-air mixtures with varying gas composition (x). The maximum power output was slightly higher than 0.86 mW. At 650°C the ohmic resistance of the cell was 164 Ω and the reason for this large resistance was due to the long conduction paths within the 100 μm wide and 3 μm thick electrodes to the active sites of the cell. The resistance of all anode and cathode strips was calculated to be around 23 Ω and 70 Ω, respectively. It was found that the OCV as well as the maximum power output decreased when decreasing the x from 2 to 1, i.e. when using leaner gas mixtures. Thus, the reason for the decrease in OCV is likely to be due to the anode.

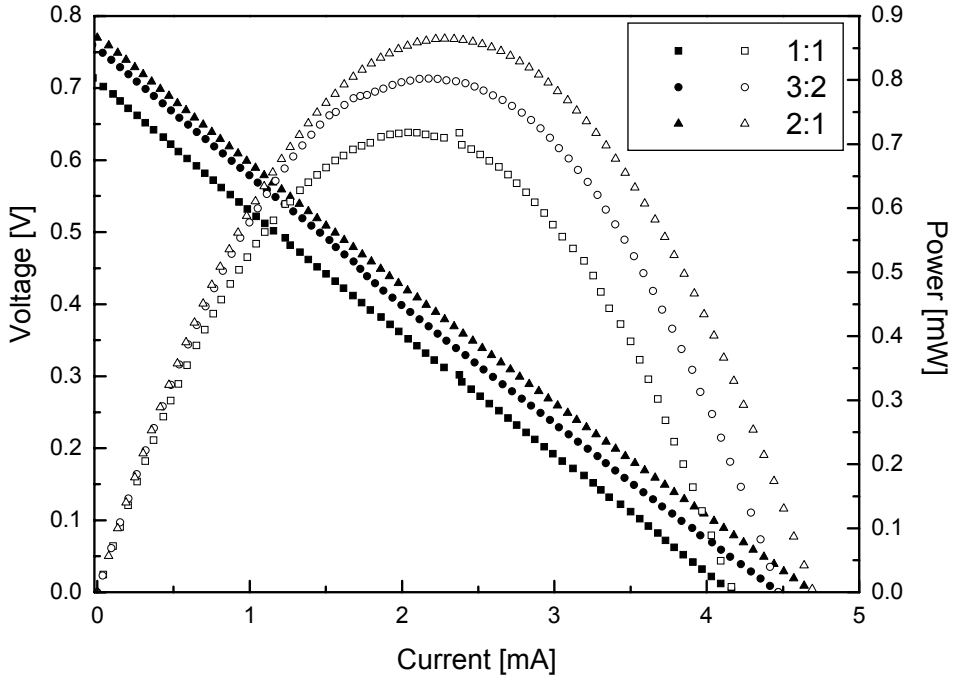

Figure 8.15 Voltage current characteristic of the fabricated μ-SC-SOFC at different CH_4/O_2 ratio at 650°C with a total flow rate of 100 ml/min CH_4-air mixture.

In the ideal case, the cathode should be totally inert to the fuel. Therefore, at the cathode/electrolyte interface an oxygen partial pressure equal to partial pressure in the gas phase should prevail. On the other hand, the anode should catalytically convert all the provided oxygen and produce a low $p(O_2)$ at the anode/electrolyte interface. However, in case of a very thin anode, a low oxygen partial pressure can not be maintained. If more oxygen is fed to the anode surface than can be converted, the remaining oxygen will be present at the

anode/electrolyte interface. This lowers the chemical potential difference and therefore OCV, as observed with x = 1. Consequently, if the flow rate of gas mixture increases, the OCV should decrease. In fact, when the flow rate was increased to 300 ml/min, the OCV was no longer a function of x and the absolute value was 0.65 V, which was lower than the value at 100 ml/min. The maximum power output also decreased to about 0.6 mW.

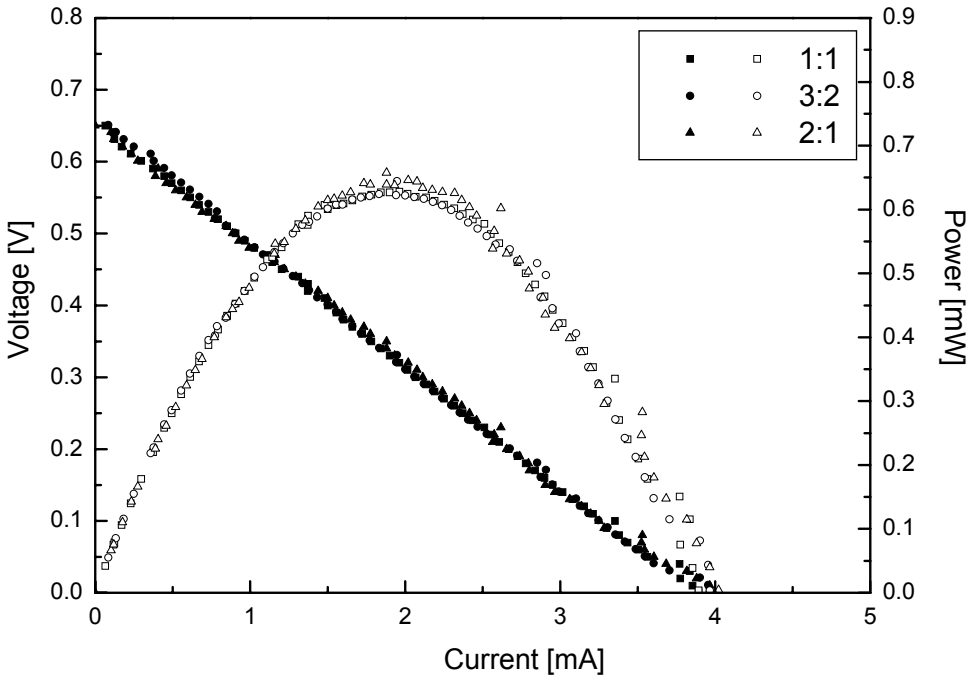

Figure 8.16 Voltage current characteristic of the fabricated µ-SC-SOFC for different CH_4/O_2 ratios at 650°C with a total flow rate of 300 ml/min CH_4-air mixture.

8.3.4 Comparison Millimetre and Micrometer Cell

The characteristics of the different cells, such as total area of the cell, the electrode area, gap area, power density and specific power density are summarised in Table 8-3. The intra- as well as intercellular spacings, the percentage of gap area of the whole cell area and the cell resistances, which were derived from the U-I curves, are also summarised. For obtaining the specific power density, the measured power density was divided by the total cell area. The electrode area of the m-SC-SOFC was larger than 1 cm^2 because the paste spread from the edges after the screen printing step. The nominal number of cells was 46 with a total area of 1.011 cm^2. Because of the limitations of MIMIC by the statistic filling length of microchannels, not all the cells were active, i.e. with interdigitating electrodes. The µ-SC-

SOFC only had 19 active cells with a total area of 0.051 cm^2 of which only 9% were taken by intra - and intercellular gaps. The advantage of the μ-SC-SOFC is that the gap area between the electrodes is very small as compared to normal cells, which leads to a better utilisation of the surface area.

In addition the reduction of the electrolyte's ohmic resistance with decreasing gap width allows for higher specific power densities. The high number of cells for μ-SC-SOFC and the possibility of their easy interconnection make it possible to obtain useful voltages without the need for constructing a fuel cell stack.

Table 8-3 Characteristics of the prepared SC-SOFCs

	M-SC-SOFC	**m-SC-SOFC**	**μ-SC-SOFC**
Number of Cells	1	4	19
area of cell [cm^2]	1.124	1.406	0.051
Electrode area [cm^2]	1.000	1.140	0.043
Gap area [cm^2]	0.124	0.266	0.005
Power density [mW]	2.1	2.05	0.86
Specific power density [mW/cm^2]	1.87	1.46	16.92
intracellular spacing [m]	$1.2 \cdot 10^{-3}$	$3.6 \cdot 10^{-4}$	$1.0 \cdot 10^{-5}$
intercellular spacing [m]	-	$4.5 \cdot 10^{-4}$	$1.0 \cdot 10^{-5}$
gap area [%]	11.0	18.9	9.0
Cell resistance [Ω]	71	51	164

The prepared cells at the conditions yielding the highest power output are compared in Figure 8.17. The cells had an OCV between 0.70 and 0.77 V and a power output in the range of 0.9-2.1 mW. The M- and m-cells nearly had the same power output at the given conditions and the μ-SC-SOFC showed the lowest power output, due to the very small active area of 0.051 cm^2 but also because of the high ohmic resistance of the long and narrow electrode strips. The situation changes somewhat when the power output of the cells was normalized to the area of the cells. In Figure 8.18 the area specific voltage current characteristics are plotted. It can be clearly seen that the μ-cell showed the highest specific power output of 17 mW/cm^2.

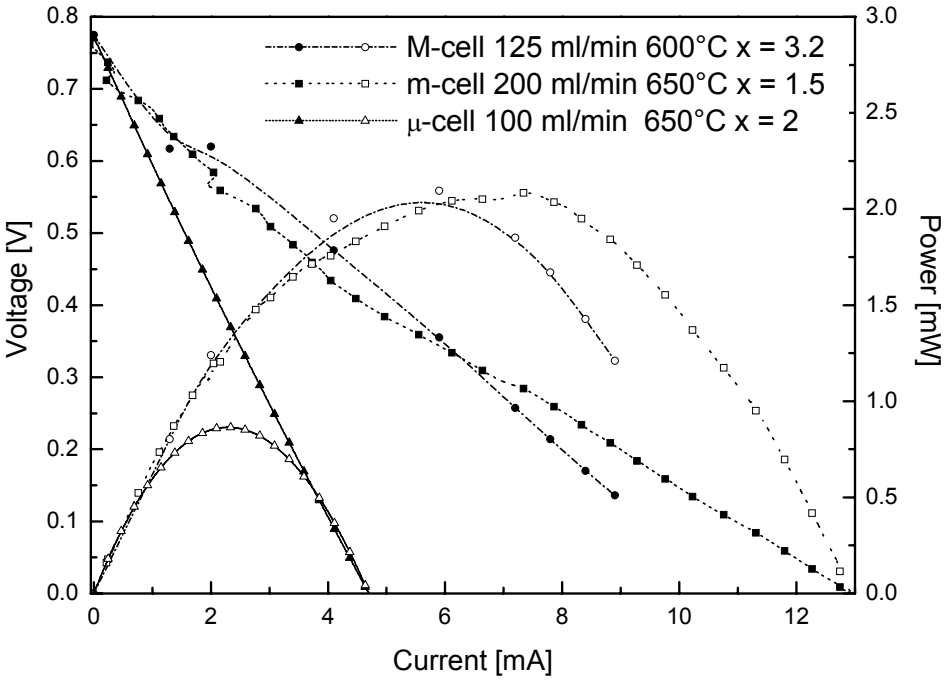

Figure 8.17 Voltage current characteristics of prepared side by side SC-SOFCs.

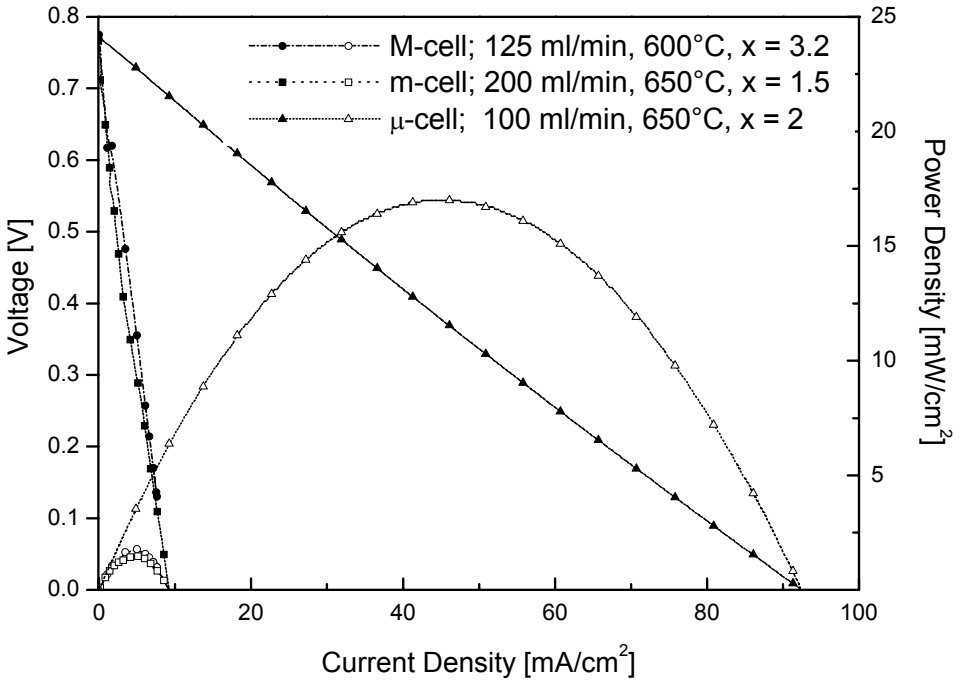

Figure 8.18 Voltage current characteristics of the prepared side by side SC-SOFCs normalised to the cell area.

The cells with electrodes in the millimetre-range both had a quite similar area specific power output. Thus, we have shown that miniaturised SC-SOFCs can allow to have enhanced area specific power output as compared to millimetre-sized cells.

8.4 Summary

Micro single chamber solid oxide fuel cells were successfully fabricated by Micromolding in Capillaries of electrodes on CGO electrolytes. Alternating electrodes of anode and cathode materials were fabricated by using closed end capillaries in PDMS-molds. These were filled by capillary action from opposite sides with suspensions of both electrode materials. Not all the capillaries could be filled and only an incomplete array of cells was formed with electrodes that were interdigitating only in certain regions. A suitable cosintering temperature for the fabricated electrodes was found to be at 1100°C.

The parallel connected array of 19 cells generated a voltage of 0.77V and a power output of approximately 17 mW/cm^2 at 650°C. The power was normalised to the active area of the cell array as observed by light microscopy including the gaps between the electrodes. Active cells were those having interdigitating electrodes that were free of cracks from the active zone to the Pt current-collector located at the end of the electrodes. The excessive ohmic resistance of the cell was due to the long conduction path within the very narrow and flat electrodes to the active sites, i.e. where the electrodes were interdigitating. When comparing to the performance of the M-SC-SOFC and m-SC-SOFC, it becomes clear that micro SC-SOFCs have a great potential in terms of area specific performance.

The described MIMIC-process yielded cells, which were connected in parallel by the deposited material, where the reservoir of the MIMIC step was located. However, series connection of cells will make the array of cells more flaw-tolerant, because cracks perpendicular to the electrodes will not block the whole current coming from beyond this point of the electrode. Furthermore, it will not be necessary to have a current-collector for every electrode because the voltage drop across the width of one electrode will be very small due to the short distance of the conducting path. Thus, for µ-SC-SOFCs we propose the series-connection of cells. The required voltage can be adjusted by the number of cells. The envisaged power output of the cell-system can then be adjusted by choosing the appropriate length of the electrodes.

8.5 Acknowledgements

The authors would like to thank Lars Massüger for the help with the XRD-analysis with thin quartz glass capillaries and Dr. Marc Dusseiller for contributing some of the Figures.

8.6 References

[1] W. van Gool, *Philips Research Reports*, **1965**, 20, 81-93.

[2] G. A. Louis, J. M. Lee, D. L. Maricle and J. C. Trocciola, *Solid Electrolyte Electrochemical Cell*. 1981, United Technologies Corp.: US.

[3] C. K. Dyer, *Nature*, **1990**, 343, 547-548.

[4] T. Hibino and H. Iwahara, *Chemistry Letters*, **1993**, 7, 1131-1134.

[5] T. Hibino, K. Ushiki, T. Sato and Y. Kuwahara, *Solid State Ionics*, **1995**, 81, *1-2***,** 1-3.

[6] T. Hibino, H. Tsunekawa, S. Tanimoto and M. Sano, *Journal of the Electrochemical Society*, **2000**, 147, *4***,** 1338-1343.

[7] T. Hibino, A. Hashimoto, S. Masanori, Y. Masaya, Y. Shin-ichiro and S. Mitsuru, *Journal of the Electrochemical Society*, **2002**, 149, *2***,** A195-A200.

[8] T. Matsui, M. Inaba, A. Mineshige and Z. Ogumi, *Solid State Ionics*, **2005**, 176, *7-8***,** 647-654.

[9] T. Hibino, K. Ushiki and Y. Kuwahara, *Solid State Ionics*, **1996**, 91, 69-74.

[10] J. Fleig, H. L. Tuller and J. Maier, *Solid State Ionics*, **2004**, 174, *1-4***,** 261-270.

[11] Y. Xia and G. M. Whitesides, *Angewandte Chemie International Edition*, **1998**, 37, *5***,** 550-575.

[12] Y. Xia and G. M. Whitesides, *Annual Review of Materials Science*, **1998**, 28, *1***,** 153-184.

[13] U. P. Schönholzer and L. J. Gauckler, *Advanced Materials*, **1999**, 11, *8***,** 630-632.

[14] U. P. Schönholzer, R. Hummel and L. J. Gauckler, *Advanced Materials*, **2000**, 12, *17***,** 1261-1263.

[15] M. Heule and L. J. Gauckler, *Sensors and Actuators B: Chemical*, **2003**, 93, *1-3***,** 100-106.

[16] S. G. Charati and S. A. Stern, *Macromolecules*, **1998**, 31, *16***,** 5529-5535.

[17] M. Heule, J. Schell and L. J. Gauckler, *Journal American Ceramic Society*, **2003**, 86, *3***,** 407-412.

[18] R. Maric, S. Ohara, T. Fukui, T. Inagaki and J.-i. Fujita, *Electrochemical and Solid-State Letters*, **1998**, 1, *5***,** 201-203.

[19] B. E. Buergler, M. E. Siegrist and L. J. Gauckler, *Solid State Ionics*, **2005**, 176, *19-22***,** 1717-1722.

[20] P. M. Torniainen, X. Chu and L. D. Schmidt, *Journal of Catalysis*, **1994**, 146, *1***,** 1-10.

[21] X. Jacques-Bedard, T. W. Napporn, R. Roberge and M. Meunier, *Journal of Power Sources*, **2006**, 153, *1***,** 108-113.

9 Fully Porous Single Chamber Solid Oxide Fuel Cells

B. E. Buergler, D. Smida and L. J. Gauckler, to be submitted to *Solid State Ionics*.

ABSTRACT: The preparation and characterisation of a fully porous single chamber solid oxide fuel cell (FP-SC-SOFC) with flow-through configuration is reported. The cell was made of Ni-$Ce_{0.8}Gd_{0.2}O_{1.90}$ as the anode, $Ce_{0.9}Gd_{0.1}O_{1.95}$ as the electrolyte and $Sm_{0.5}Sr_{0.5}CoO_{3-\delta}$ as the cathode. The cell had an anode-supported structure with a very thin (~30 μm) and highly porous electrolyte and cathode layer. Pt current-collectors were used both at the anode and cathode. The FP-SC-SOFC was assembled into a module, which could be fitted into the measurement setup.

The electrochemical properties of the cell were very sensitive to changes in anode temperature, the CH_4/O_2 ratio and the total flow rate. At 733 °C and a CH_4/O_2 ratio of 1/1, an OCV of 525 mV and a maximum power density of 10 mW/cm^2 for 1000 ml/min were obtained. Thus, for the first time the fully porous design of SC-SOFCs with flow-through configuration has been demonstrated. The cell behaviour suggests that the cathode was the limiting factor in the measured FP-SC-SOFC.

9.1 Introduction

In single chamber SOFCs both electrodes are exposed to a gas mixture of fuel and air and leaks in the electrolyte are of no concern [1]. However, the anode and cathode must be physically separated from each other in order to avoid a short circuit in the cell. If the electrolyte of the cell is permitted to be porous, the fabrication costs could be drastically reduced. The electrolyte layer could be processed by screen printing and sintering at relatively low temperature because full density would not have to be achieved. Suzuki et al. compared the performance of anode-supported SC-SOFCs with dense and with porous electrolytes [2] and found that the porous electrolyte had a smaller resistance to the ionic current than the dense one. The reason for this had been postulated by van Gool [3] 40 years ago and was due to the enhanced ionic conductivity at the surface of the electrolyte. The results of Suzuki et al. [2] showed that the cell with porous electrolyte had an OCV that was 0.1 V lower than for the cell with dense electrolyte, which could be attributed to the fact that some hydrogen reached the cathode through the pores in the electrolyte, thereby reducing the oxygen partial pressure at the cathode. The power output of porous cell at 744°C was 660 mW/cm^2 in flowing mixtures of CH_4-air (900 ml/min). In previous work [4] we have shown that electrolyte supported SC-SOFCs based on Ni-$Ce_{0.8}Gd_{0.2}O_{1.9}$ /$Ce_{0.9}Gd_{0.1}O_{1.95}$/ $Sm_{0.5}Sr_{0.5}CoO_{3-\delta}$ performed well at a furnace temperature of 700°C (350 mW/cm^2. The SC-SOFCs described here are based on the same materials as previously used [5]. They were fully porous anode-supported cells with a thin electrolyte layer (30 μm in thickness) fabricated by screen printing. The main difference to Suzuki's work [2] is that here the cells were operated in a flow-through configuration. It has been shown that the flow configuration during the measurement of SC-SOFCs has a drastic effect on the OCV and the power output. Stefan et al. showed that the configuration where the anode is exposed to the gas mixture first and reaches the cathode afterwards, should be avoided [6]. This is why in the described experiments, the cathode was always the electrode that was exposed to the gas at first. The aim of this work was to make a proof of concept for fully porous SC-SOFCs with flow-through configuration.

9.2 Experimental

9.2.1 Anode Precursor Powder

The anode powder that was used for the fabrication of the anode-supports contained 70wt% of NiO and 30wt% of $Ce_{0.8}Gd_{0.2}O_{1.9}$. The powder had been purchased of Praxair Speciality Ceramics (Lot#, 03-P2854DM) and had a d_{50}-value of 0.53 µm. In order to prepare a highly porous anode pellet, a mixture of NiO-CGO70 and graphite (50vol%) had to be prepared. This powder was then pressed to pellets, and the carbon burned out during sintering. The mixing of carbon and NiO-CGO powder was done as follows:

In a first step two suspensions (compositions given in Table 9-1) were prepared, one containing the NiO-CGO powder and the other containing the graphite (Timcal, Timrex KS10) with a d_{50}-value of 6 µm.

Table 9-1 Composition of the two suspensions used for mixing the anode powder with graphite.

	NiO-CGO suspension [g]	Graphite suspension [g]
NiO-CGO70 (anode material)	97.48	-
Graphite (pore former)	-	97.48
Butylacetate (solvent)	47.684	228
Sorbitan monooleate (Span80, surfactant)	1.289	-
Polyvinylbutyral (binder)	1.475	-

The shape of the graphite particles was highly anisotropic. The thickness of the particles was in the range of 0.1-1 µm. The suspension with NiO-CGO was ball-milled with 200g of ZrO_2-balls for 50 hours. It was this suspension that contained the surfactant (span 80) and the binder. The graphite suspension was only stirred for a few hours before both suspensions were mixed and stirred for about 24 hours. The mixture was dried by heating it in a beaker to 140°C. The completely dried cake was quite hard and had to be homogenised by a mortar and pestle in order to obtain a powder mixture, which was suitable for pressing.

9.2.2 Anode-Supports

The anode-supports were prepared by pressing 3.5 g of the NiO-CGO-Graphite precursor powder in a dye with a diameter of 30 mm at 140 MPa. The so-formed pellets had a good mechanical stability. Then the pellets were cold-isostatically pressed at 300 MPa. The pellets that had a black appearance due to the graphite were sintered at T_s= 1300°C. During the slow heating at 1 K/min the carbon was given enough time to slowly burn out leaving behind a porous structure of the anode material. This was important because when the heating was done at 10 K/min, the oxidation of the carbon generated such a low oxygen partial pressure that the NiO in the material reduced to metallic Ni. The specimens were held at the peak temperature for 4 hours and then cooled to room temperature at 5 K/min. The unsintered and sintered anode-supports are compared in Table 9-2. After uniaxial pressing, the pellets had a diameter of 30 mm. During the cold isostatic pressing the pellets shrunk to 26.5 mm.

Table 9-2 Comparison of unsintered and sintered anode-supports.

	unsintered	sintered
Appearance	black	green
Diameter [mm]	26.54	21.78
Thickness [mm]	2.28	1.89
Weight [g]	3.47	2.52
Density [g/cm^3]	2.75	3.6

Sintering at 1300°C led to the expected mass loss of 27%. The shrinkage in radial and vertical direction was measured to be 18% and 17%, respectively. Due to the NiO in the pellets, they had the characteristic green colour after sintering. The highly porous anode-support material was characterised in terms of porosity and microstructure. The density of the samples ρ_S was determined by weighing the anode-support mass (m), measuring the sample height (h) and the diameter (d) and inserting these values into Equation (9.1). The porosity P was calculated by Equation (9.2), where ρ_{th} is the theoretical density of the NiO-CGO70 material (6.868 g/cm^3).

$$\rho_S = \frac{4m}{\pi \cdot h \cdot d^2} \tag{9.1}$$

$$P = 1 - \frac{\rho_S}{\rho_{th}} \tag{9.2}$$

Mercury Intrusion Porosimetry (MIP, Carlo Erba Instruments, 2000) was applied in order to evaluate the pore size and pore size distribution. The microstructure of the anode-support and the other cell components was evaluated by Scanning Electron Microscopy (SEM, LEO 1530, Germany).

9.2.3 Electrolyte and Cathode Pastes for Screen Printing

In order to prepare thin electrolyte and cathode layers by screen printing, pastes had to be prepared. The composition of the pastes are shown in Table 9-3. $Ce_{0.9}Gd_{0.1}O_{1.95}$ (CGO) powder was provided by Praxair (Lot# 03-P5049BM.1), $Sm_{0.5}Sr_{0.5}CoO_{3-\delta}$ (SSC) by Nextech Materials (Lot# 91-82).

Table 9-3 Electrolyte paste composition

	Electrolyte paste [g]	Cathode paste [g]
$Ce_{0.9}Gd_{0.1}O_{1.95}$	7.0	-
$Sm_{0.5}Sr_{0.5}CoO_{3-\delta}$	-	4.96
Furan-2-carboxylic acid	0.12	0.05
Ethyl Cellulose	0.23	0.30
Diethylene glycol monobutyl ether acetate	3.08	2.06

The paste preparation was done in as follows. First the ceramic powder was mixed with the two organic powders, furan-2-carboxylic acid and ethyl-cellulose. Then the solvent diethylene glycol monobutyl ether acetate was added. This mixture was subsequently milled in a zirconia container with a zirconia ball using a vibratory mill (Retsch M20, Germany) at 20 Hz for 20 minutes.

9.2.4 Preparation of FP-SC-SOFCs

The anode served as porous support for the cells. Both the electrolyte as well as the cathode was prepared by screen printing on the support through circular masks with a mask thickness of 50 μm. The diameter of the circular screen printing masks was 20 mm for the electrolyte and 16 mm for the cathode. After screen printing the layers were always dried for

at least 2 hours at 80°C. The cathode had a smaller diameter than the electrolyte in order to avoid a possible short circuit in the cells. After screen printing the electrolyte had a diameter of about 21.1 mm and the cathode 16.2 mm. The sintering was done in two separate steps first the electrolyte and then the cathode at a heating rate of 1 K/min to 500°C and holding there for 1 hour. The specimens were heated further at 3 K/min to the peak temperature, which was 1300°C for the electrolyte and 1100°C for the anode materials. The samples were held at the peak temperature for two hours and subsequently cooled down to room temperature at 5 K/min. The cathode was printed after the electrolyte had been sintered and was sintered together with the Pt current-collector, which had been covered by some cathode-paste. The electrolyte layer was prepared by printing and sintering twice in order to avoid physical contact between the anode and the cathode through pinholes.

Two flatly pressed, circular Pt-meshes (52 mesh woven from 0.1 mm wire, Alfa Aesar, Germany) 12.75 mm in diameter onto which Pt-wires were point-welded were used as current-collectors for both electrodes. On the anode side, a Cr and Pt sputtering was first performed in order to improve the contact between the Pt and NiO-CGO. A Cr-layer was sputtered at first because Cr leads to a good contact between ceramics and metals. A layer of Pt was then sputtered on the Cr in order to avoid Cr-oxidation. The sputtering was done in a BAL-TEC (SCD 050) sputter coater in the following manner: 1) Cathodic etching of the anode-support for 1 min at 10 mA and 10^{-1} mbar (shutter of sputter target 3/10 closed). 2) Presputtering of Cr-target for 5 min and 100 mA at 5 10^{-2} mbar (shutter closed). 3) Sputtering of Cr for 11 min at 150 mA and 5 $\cdot 10^{-2}$ mbar (shutter opened). 4) Target changed from Cr to Pt. 5) Cathodic etching of Cr-layer for 1 min at 10mA at 10^{-1} mbar (shutter 3/10 closed). 6) Sputtering of Pt for 3min at 60 mA at 5 10^{-2} mbar (shutter opened).

After the sputtering procedure a Pt-layer was screen printed onto the sputtered layer (mask thickness 20 μm). A commercially available Pt-paste was used (Heraeus C3605S). The Pt-mesh was placed on the freshly printed paste and subsequently dried. On the cathode side, the Pt-mesh was placed directly on the freshly screen printed layer of SSC. The Pt was covered with a small amount of SSC-paste. The cathode with current-collector was sintered together with the Pt-paste and Pt-mesh at the anode side using the temperature program described above. A schematic of the fully porous anode-supported SC-SOFC is shown Figure 9.1.

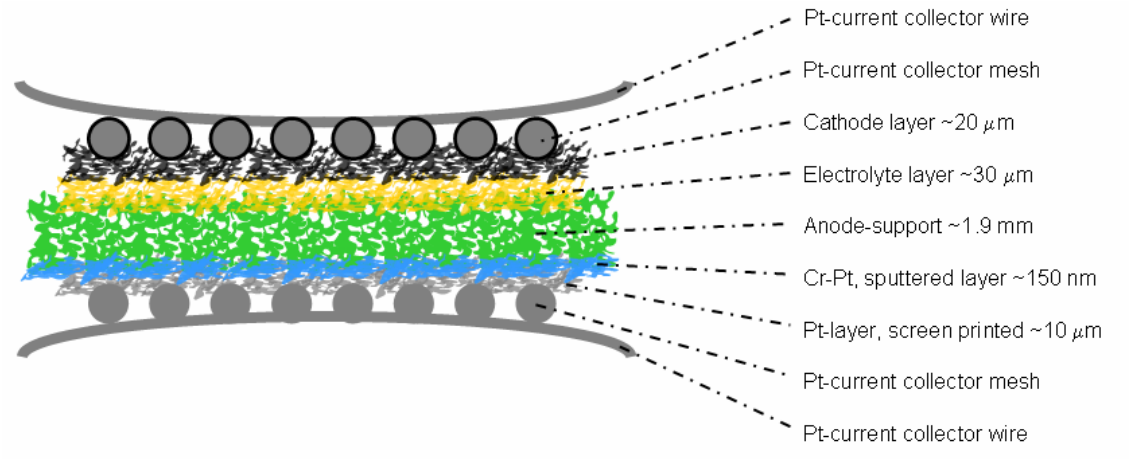

Figure 9.1 Scheme of the anode-supported fully porous SC-SOFC.

In comparison to the anode-support the cell had a very small thickness. The cathode and electrolyte layer were 20-30 µm in thickness. The Cr- and Pt-layer had a nominal thickness of 100 and 50 nm, respectively. The cell was electrically contacted by point welding the Pt-wires of the cell to the Pt-wires of the setup.

9.2.5 Electrochemical Characterisation

In order to characterise the anode-supported cells in the setup that had been previously used, it had to be assembled into a module, which consisted of an outer tube and two rings between which the cell was confined. Both the outer tube and the inner rings were made of Al_2O_3. Between the inner and the outer ring, there was a layer of Insulfrax ceramic felt (Unifrax, Germany), which had a thickness of 1 mm and kept the rings in position by friction. A schematic of the module is shown in Figure 9.2 a and a digital photograph in Figure 9.2 b.

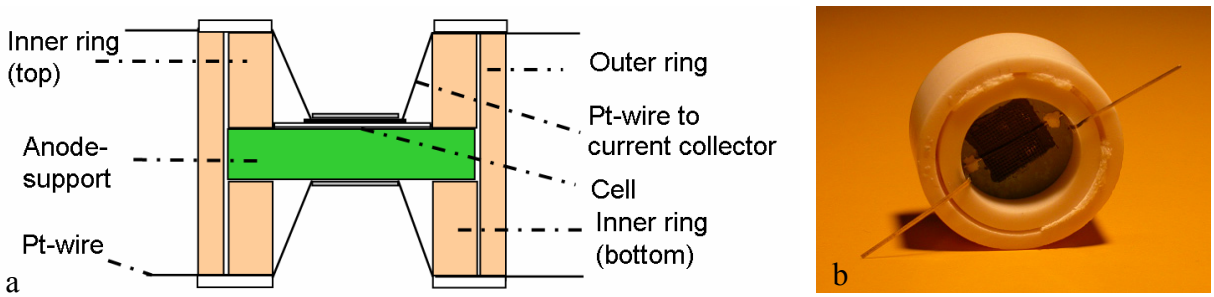

Figure 9.2 a) Scheme of the FP-SC-SOFC module. b) Digital photograph of the finished module that is ready for installation in the measurement setup.

The electrochemical characterisation was done in the setup shown in Figure 9.3 a consisting of two quartz glass tubes between which the module is mounted. The setup had two tubes of which each one had a closed end. This resulted in a flow-through configuration where the gas had to pass through the FP-SC-SOFC. The cell was always mounted upwards so that the cathode would be the first electrode to be in contact with the gas mixture. Temperature monitoring of the anode was done by a K-type thermocouple that was placed at the surface of the anode and had been covered with some refractory adhesive (Firag, Germany). All the temperatures given in the following refer to temperatures that were measured with this thermocouple. The setup was not gas tightly sealed, which means that there was a certain loss of gas flow, which needed to be assessed. This was done by flowing nitrogen through the heated setup (733°C) with different samples and measuring the amount of gas coming out at the exhaust with a gas flow meter (Voegtlin, red-y, GCM). A module without a cell in it (only the outer ring in Figure 9.2 a) and modules with a blank anode-support, a cell with unreduced and reduced anode and a dense pellet were evaluated.

Before characterising a whole FP-SC-SOFC, the NiO of a blank anode-support (without cell) was reduced to metallic Ni first. This was done by making a module with a blank anode-

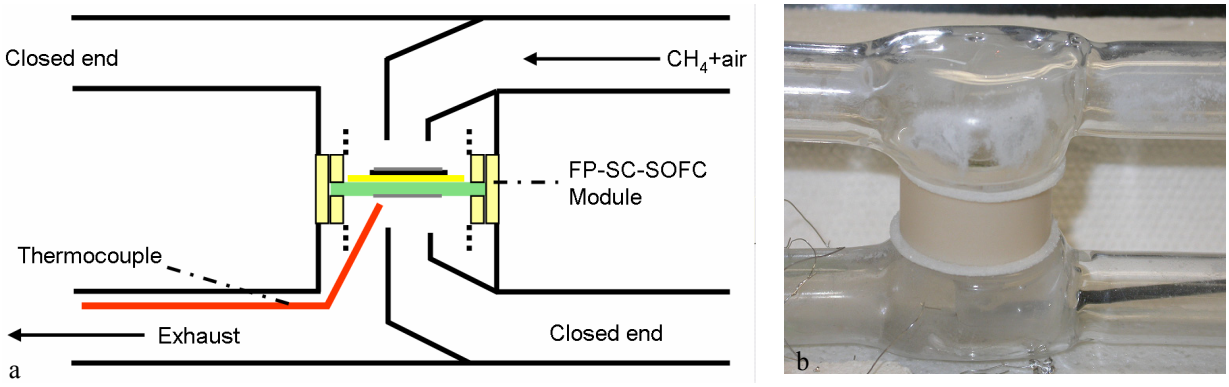

Figure 9.3 a) Schematic of the measurement setup with built-in module for the characterisation of FP-SC-SOFCs. b) Digital photograph of the measurement setup with FP-SC-SOFC module between the two quartz glass tubes.

support and then exposing it to a flowing mixture of CH_4-air with an x-value (CH_4/O_2) of 2. The aim was to see, if the reduction of the anode-support was possible without the formation of cracks. The cells were connected by point-welding the Pt-wires entering the setup to the Pt-wires of the module. Voltage-current characteristics (U-I-curves) were measured a

Potentiostat (Zahner IM6, Germany) with at a slew rate of 5 mV/s. All the measurements including the flow-through experiments were done with gas mixtures that had been passed through a water bubbler at 24°C (~3% H_2O). Methane-air mixtures were used for all the experiments.

9.3 Results and Discussion

9.3.1 Anode-Supports

Cross sectional SEM micrographs of the anode-supports that were sintered at 1100, 1200, 1300 and 1350°C are shown in Figure 9.4. It can be clearly seen that there was a drastic difference in the microstructures depending on the sintering temperatures. The microstructure of the anode-supports shown in Figure 9.4 a and b show a structure in which the NiO-CGO material has only sintered partially in certain regions. The sample sintered at 1200°C (Figure 9.4 b) showed a more pronounced local sintering but also a more pronounced overall interconnectivity of the grains. However, this specimen still had a too low mechanical stability and it became clear that a sintering temperature exceeding 1200°C was necessary in order to obtain anode-support material that that can be easily handled. After sintering the anode-supports at 1300°C, the SEM analysis revealed a highly interconnected, porous structure of NiO-CGO material (Figure 9.4 c). A coarser microstructure was found when the sintering temperature was chosen to be 1350°C (Figure 9.4 d); Both the grains and the pores (as will be seen later) had a larger size as compared to the material sintered at 1300°C. In order to see how homogeneously the NiO and CGO was distributed in the anode material, a back-scattered electron micrograph of the anode-support was taken (Figure 9.5). Back-scattered electrons are particularly suited for distinguishing heavy and light elements and the NiO-CGO composite is an ideal material for this technique. NiO (light element) appears dark and CGO (heavy elements) bright. As could be clearly seen, both phases are very homogeneously distributed, which was due to the powder fabrication process (flame spray pyrolysis).

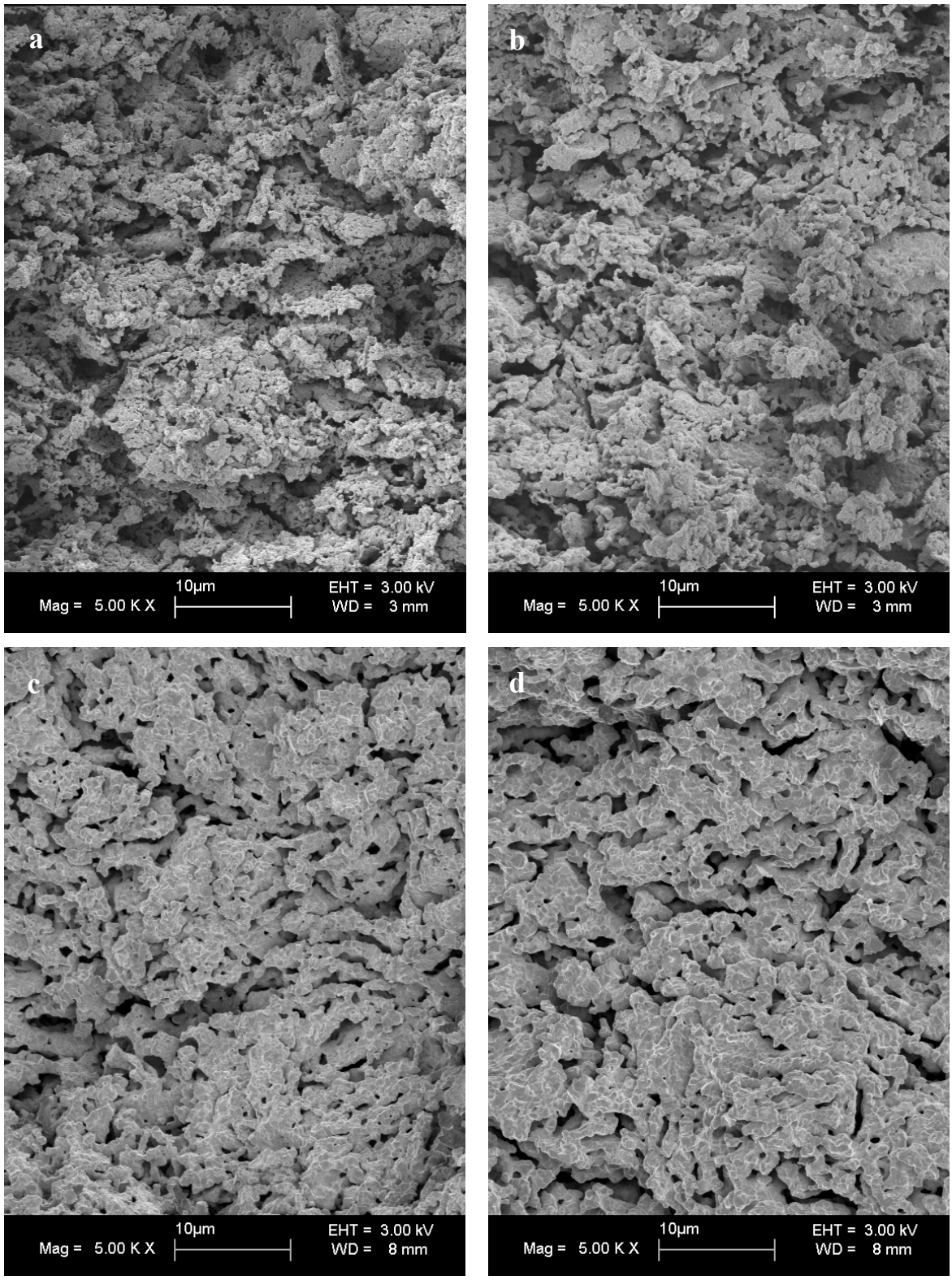

Figure 9.4 SEM micrographs of anode-supports that were sintered at a) 1100, b) 1200, c) 1300 and c) 1350°C.

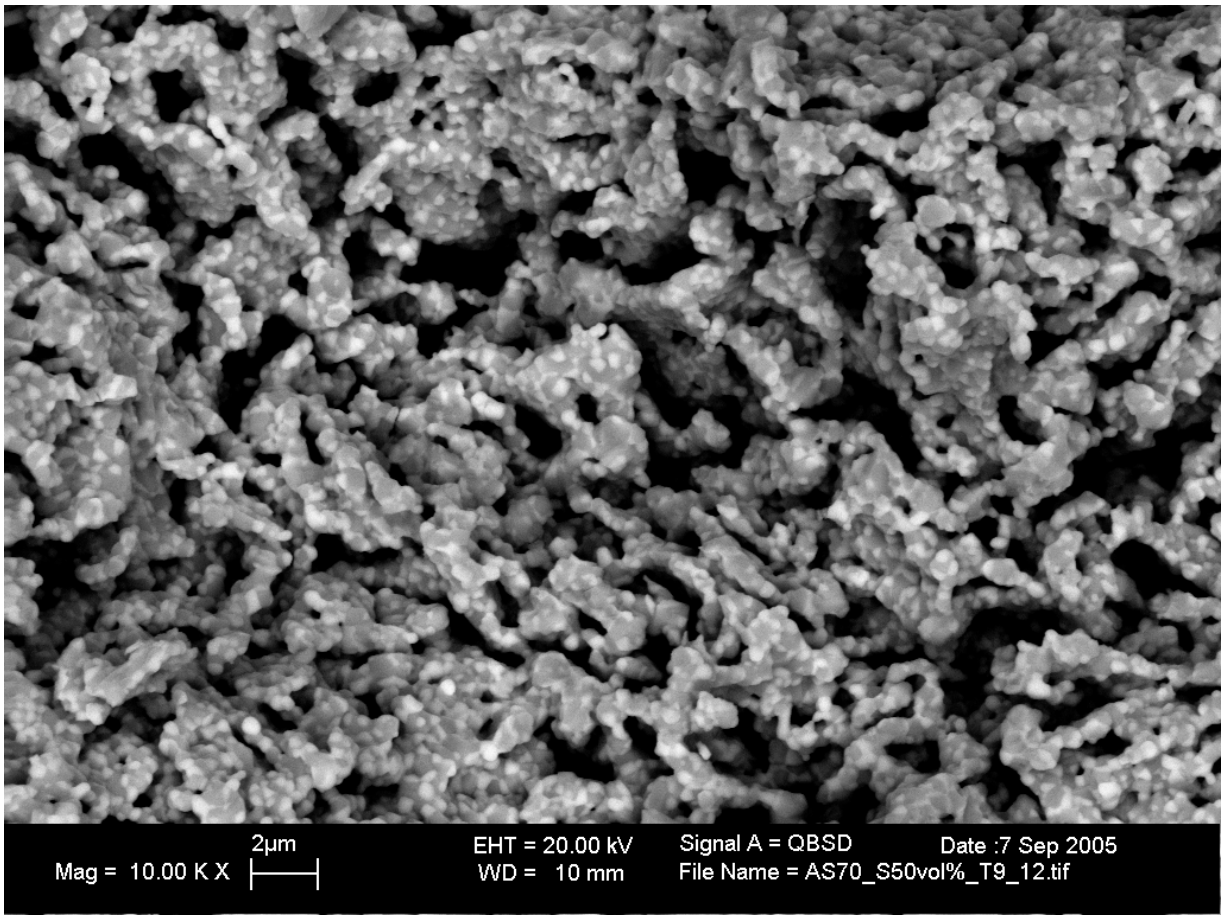

Figure 9.5 SEM-micrograph (cross sectional view) obtained by the use of backscattered electrons. The bright regions correspond to CGO, the dark regions to NiO. Both phases are homogeneously distributed. Elongated pores are formed due to the platelet-morphology of the burnt out graphite.

In Figure 9.5 there are less bright than dark appearing grains, which corresponds to the fact that the material contains less CGO than NiO (30 wt% CGO, 70 wt% NiO). The anode-support sintered at 1300°C showed a very high porosity but still had a good mechanical stability.

In Figure 9.6 the porosity that was derived from the dimensions and weights of the anode-supports determined by the use of Equation (9.1) and Equation (9.2) is plotted as a function of the sintering temperature for the anode-supports. As could be expected, the overall porosity decreased with increasing sintering temperature, because a higher sintering temperature with the same dwell time leads to a more pronounced shrinkage. The specimens that had been sintered at 1100°C and 1200°C had an insufficient mechanical stability. At a sintering temperature of 1300 and 1350°C, the samples were found to be stable enough for handling at a porosity of 47.6 and 41.4%, respectively. In order to obtain the maximum porosity at sufficiently high mechanical stability the sintering temperature for the anode-support was chosen to be 1300°C.

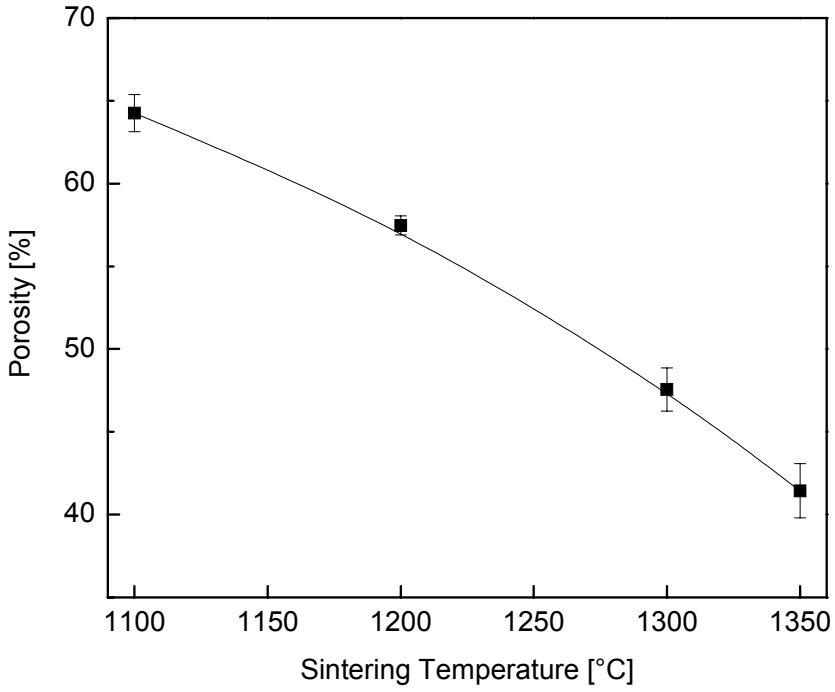

Figure 9.6 Porosity of NiO-CGO anode-supports as a function of the sintering temperature.

In Figure 9.7 the pore size distribution measured by mercury porosimetry are shown for three different sintering temperatures. For all three sintering temperatures the pore size was between 0.1 and 2 μm with the broadest distribution for the specimen that was sintered at 1200°C. One should be aware that in these distributions the smaller pore sizes are amplified due to the well known bottle neck effect. The sample that was sintered at 1200°C also contained a substantial amount of very large pores (0.9-2 μm), which could have been responsible for the bad mechanical stability. Toward small pore sizes a shoulder in the curve indicated the uncompleted sintering of the material, which could be already seen in the SEM-micrograph (Figure 9.4 b). The narrowest pore size distribution was found for a sintering temperature of 1350°C. This sample had a larger average pore size than the sample sintered at 1300°C. This agreed well with the conclusions that could be drawn from the SEM-micrographs shown in Figure 9.4 c and d. Obviously a higher sintering temperature led to a larger average pore size, which was due to a higher shrinkage. However, as can be seen in Figure 9.6, the absolute porosity was substantially lower (41.4%). This means that during

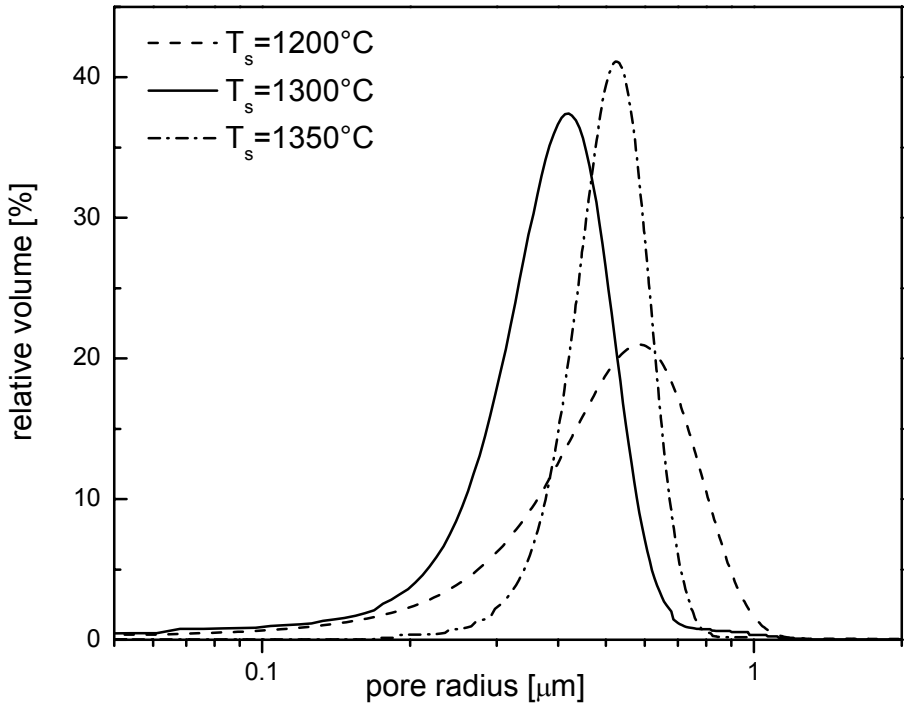

Figure 9.7 Pore size distribution of anode-supports measured by mercury intrusion porosimetry.

sintering, local shrinkage of densely packed areas of NiO-CGO powder occurred while the less dense areas where the graphite pore former had been located were coarsening. This behaviour can be ascribed to local rearrangement NiO and CGO particles during the initial stages of sintering [7]. The reduction test of the blank anode showed that it was possible to reduce the anode-support without crack-formation. When moist N_2 was fed to the reduced anode it slowly reoxidised due to the presence of water in the gas. The reoxidation of the sample in moistened nitrogen led to the formation of cracks near the circumference of the pellet. Therefore, the reoxidation of the anode-supports should be avoided by all means. In Figure 9.8 a SEM-micrograph of a reduced anode-support is shown. A drastic structural change had occurred during the reduction (for comparison see Figure 9.5 of the unreduced anode-support). The reduction of the NiO led to the formation of voids where the NiO-grains had been in the initial structure. The metallic Ni had aggregated and formed struts on which CGO particles were located impeding a further. aggregation of the metallic Ni. The highly porous, reduced anode-support exhibited no cracks.

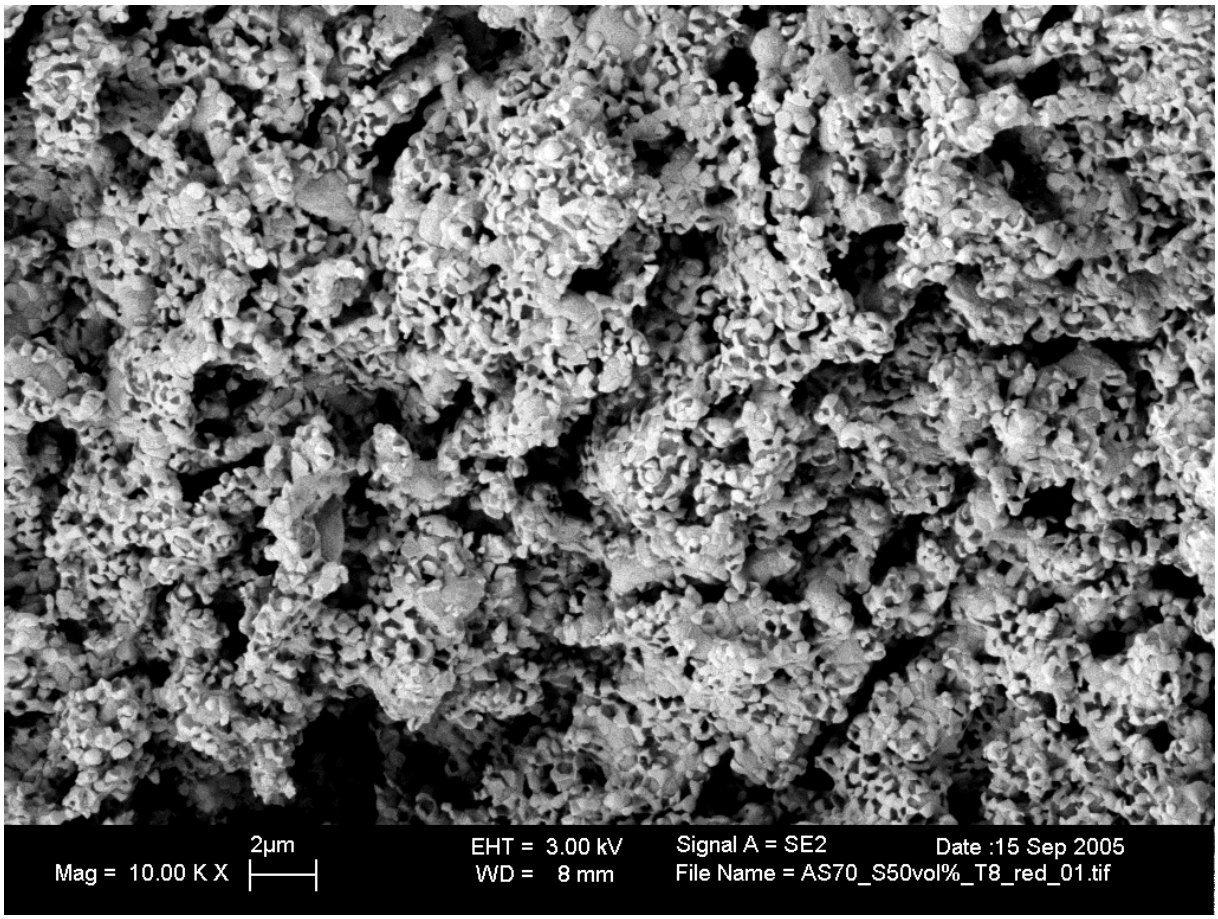

Figure 9.8 SEM-micrograph (cross sectional view) of an anode-support that had been reduced in flowing mixture of CH_4-air. The reduction of the NiO leads to the formation of voids in the microstructure. The metallic Ni aggregates and forms struts. The CGO particles impede a further aggregation of the metallic Ni.

The as sintered anode-support sintered at 1300°C had a different pore size distribution than the reduced specimen. In Figure 9.9 the pore size distribution measured by mercury porosimetry are shown for an unreduced anode-support and a reduced one. Upon reduction of the NiO to metallic Ni, the average pore size in the anode-support increased from 0.42 to 0.49 µm, which corresponds to an increase of nearly 17% in pore size. This should allow for a more unhindered gas flow through the FP-SC-SOFC, as will be seen later. The total porosity of the anode-support increased from 47.7% to approximately 60.2% as was determined by the weight and the dimensions of the pellets.

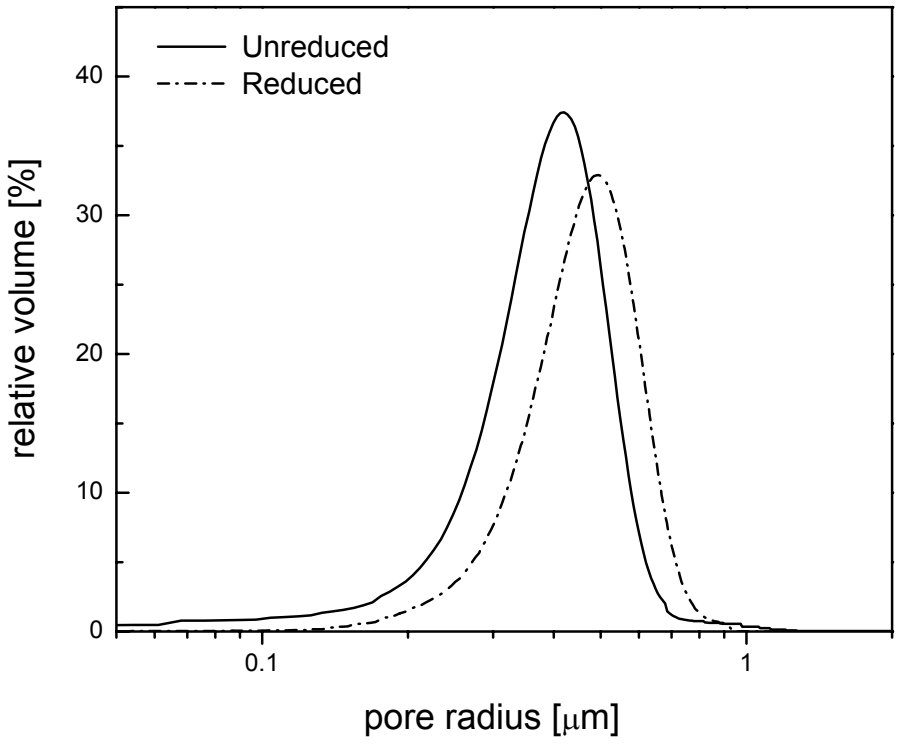

Figure 9.9 Pore size distribution of the anode-support that had been sintered at 1300°C in the unreduced and the reduced state measured by mercury intrusion porosimetry.

9.3.2 Flow-Through Measurements

In order to characterise the gas flow through the porous cells, different modules were mounted in the test-rig and the gas going through the module was measured at different gas flows. In Figure 9.10 the results of the flow-through experiments at 733°C are summarised. At a flow rate of more than 200 ml/min the gas flow passing through the setup reaches the maximum value and becomes independent of the absolute flow. For this reason a flow rate above 200 ml/min was used for all the experiments. When a dense pellet was mounted into the module as shown in Figure 9.2 only about 40% of the nitrogen that flowed into the setup, came out of the exhaust. There was a small gap between pellet and the outer ring, which allowed for a moiety of the flow to pass by the dense pellet. However, more than 60% of the inlet gas leaked out of the setup when a dense pellet was used. The anode-support without a cell on it showed a higher outlet flow than the anode-support with a cell, which can be explained by the fact that the cell additionally hinders the flow through the porous structure.

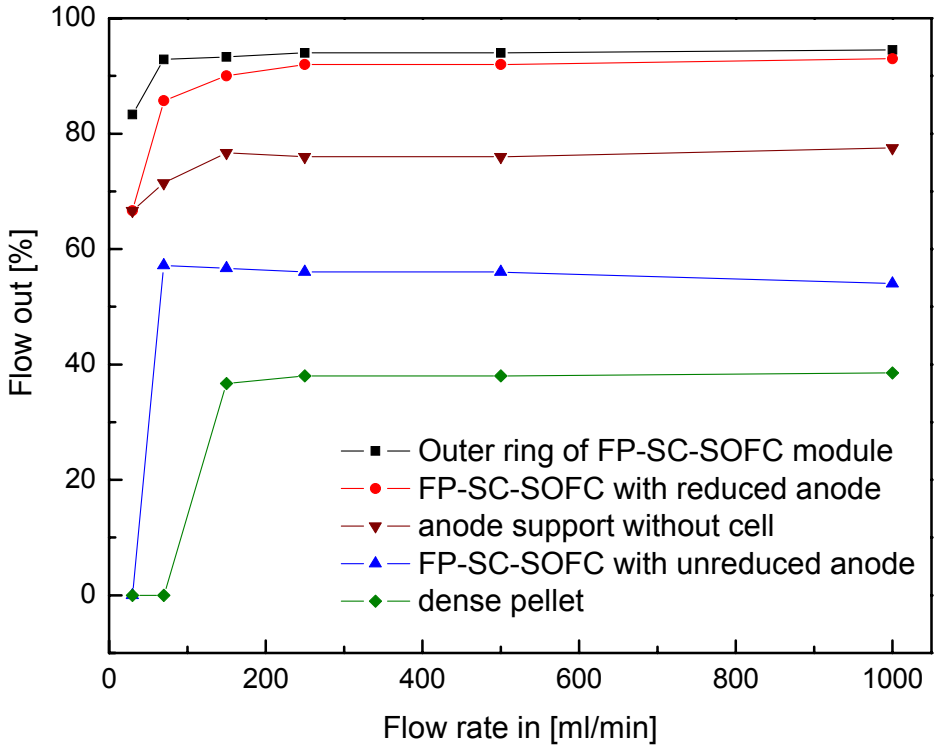

Figure 9.10 Flow-through measurements for the blank outer ring of the FP-SC-SOFC module, the FP-SC-SOFC with reduced and unreduced anode, a blank anode-support and a dense pellet at 733°C.

When only the outer ring of the module was mounted, more than 95% of what flowed in came out of the exhaust of the setup. A pronounced increase of the outlet flow was found after the anode of a FP-SC-SOFC had been reduced, which corresponds to the increased pore size but also to the increased overall porosity of the reduced anode-support.

9.3.3 Electrochemical Characterisation

Prior electrochemical experiments, the FP-SC-SOFC was reduced for about 12 hours in a flowing mixture of CH_4-air (x = 2) at a total flow rate of 250 ml/min at 733°C. The reduction of the anode-support could be evidenced by the temperature rise from 733°C for the unreduced support to 767°C for the reduced support. The OCV at a flow rate of 250 ml/min and x = 2 was around 45 mV and therefore the flow rate was increased to 1000 ml/min. The temperature of the fuel cell increased rapidly to above 800°C after the increase of the total

flow. After that the furnace temperature was readjusted in order to reach an anode temperature of 733°C.

The measurement of the voltage-current characteristics for 250, 500 and 1000 ml/min total flow rate at 733°C is shown in Figure 9.11. The OCV as well as the maximum power increased with increasing gas flow. At 1000 ml/min the cell reached a power density of 10 mW/cm^2. The results suggested that fully porous SC-SOFCs required a rather high flow rates both for achieving a high OCV but also for obtaining a high maximum power density.

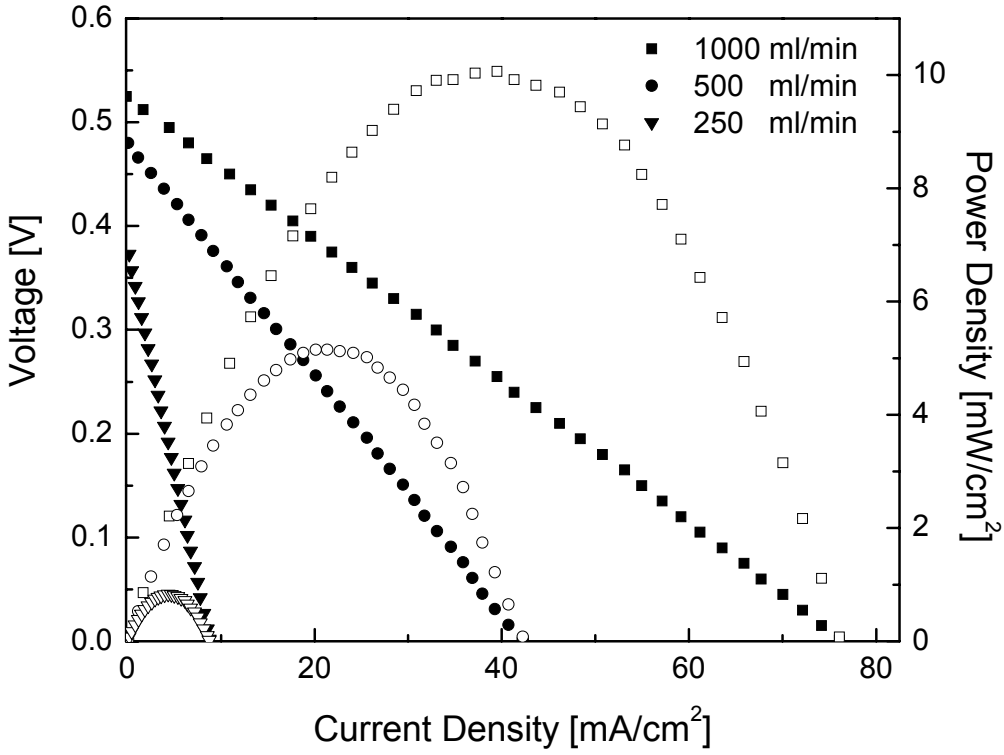

Figure 9.11 Voltage current characteristic of a FP-SC-SOFC with flow-through configuration at different total flow rates of CH_4-air at x = 1 and an anode temperature of 733°C.

In order to see the influence of temperature, we decreased the anode temperature from 733°C to 633°C by lowering the furnace temperature. The corresponding voltage-current characteristics are shown in Figure 9.12. A higher OCV could be obtained when the temperature was decreased from 733 to 633°C. This behaviour is similar to the observation made for SC-SOFCs with dense electrolytes [5]. The reason for the observed temperature dependency of the OCV is twofold: On the one hand with decreasing temperature the oxygen partial pressure at the cathode increased due to a lower catalytic activity for oxygen-

consuming parasitic reactions. On the other the electronic leakage current in the mixed ionic electronic conductivity of CGO increases when the temperature of the cell is increased [8]. Both phenomena lead to a reduced OCV at higher temperature. However, when the temperature was decreased the ohmic resistance of the electrolyte increased and a lower power output was obtained at 633°C as compared to 733°C.

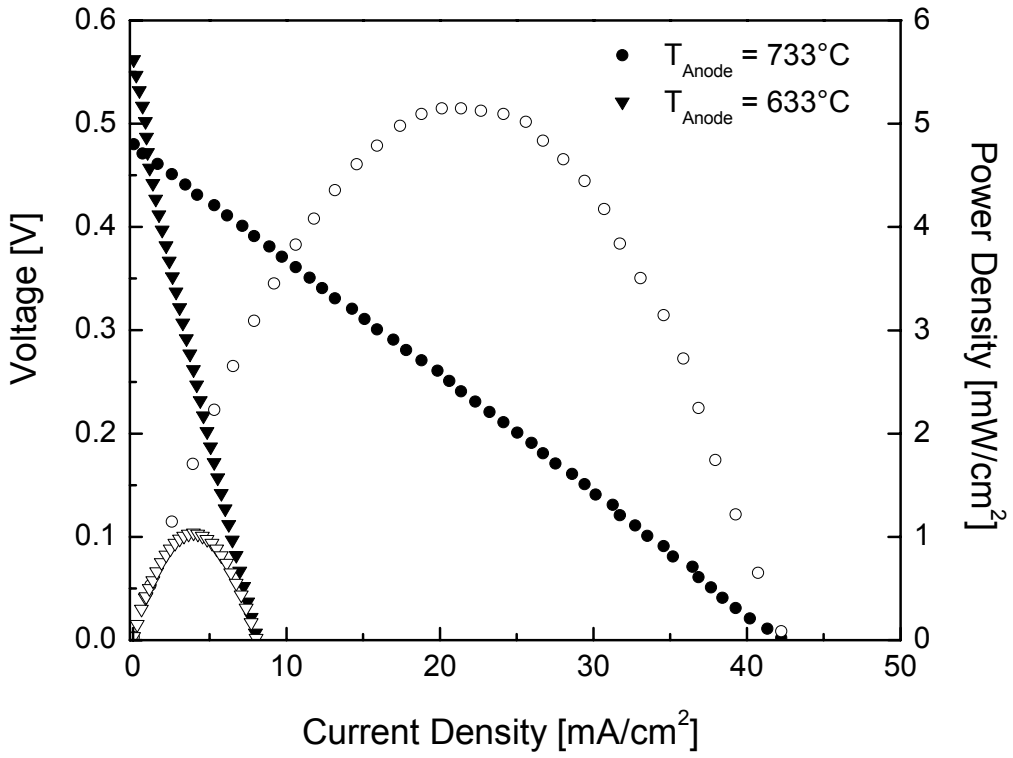

Figure 9.12 Voltage current characteristic of a FP-SC-SOFC with flow-through configuration at 733 and 633°C at a total flow rate of 500 ml/min CH_4-air (x = 1).

The variation of the OCV with flow rate (Figure 9.13 a) and anode temperature (Figure 9.13 b) was studied further in order to find suitable conditions for the operation of fully porous SC-SOFCs. The OCV as a function of the flow rate at T_A = 733°C is shown in Figure 9.13 a. For x = 1 and x = 2 the OCV increased with increasing gas flow. A higher OCV could be obtained for x = 1 than for x = 2. At a flow rate of less than 500 ml/min and x = 2 the availability of oxygen for the cathode was obviously not high enough, which is why the cell gave only a very low OCV. For x = 1 the initial concentration of oxygen is 17.3%, whereas for x = 2 it is only 14.8%. The reason for the low OCV cannot be the anode, because at these conditions the anode is reduced and should be very active for the partial oxidation of methane.

Another reason for low OCV at low flow rate is that the reaction products from the anode can easily reach the cathode side through the porous electrolyte [2].

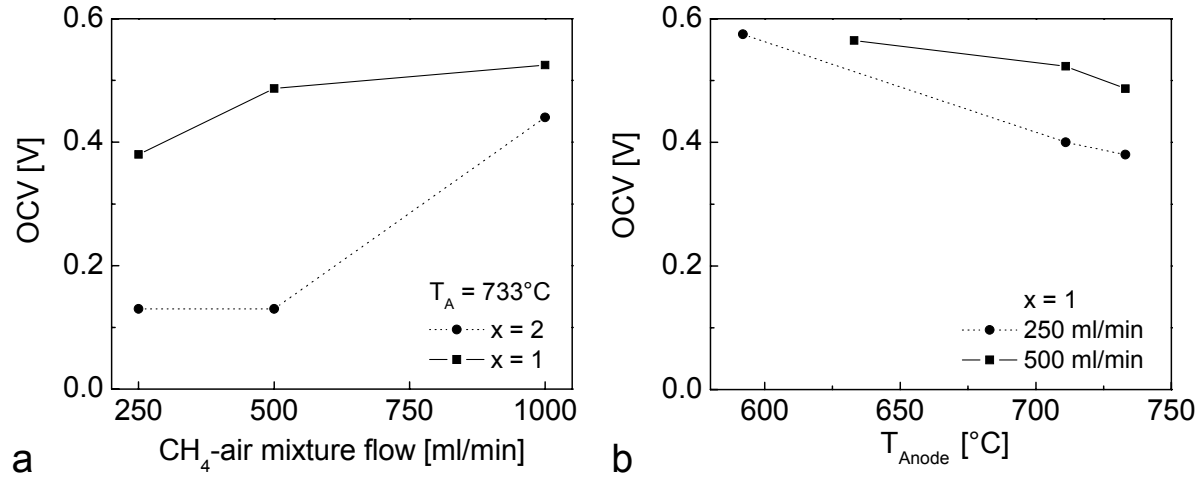

Figure 9.13 Dependency of OCV on a) the CH_4-air mixture flow rate and b) on the anode temperature T_A.

For the flow-through configuration the reaction products can not reach the cathode anymore when the flow rate becomes higher, because they are flushed through the porous cell away from the cathode. This is probably the reason, why there is such a drastic increase of OCV at x = 2 when changing the f_{tot} from 500 to 1000 ml/min.

In Figure 9.13 b the dependency of the OCV on the anode temperature is plotted. The OCV decreased with increasing temperature due to the above stated reasons. At a higher total flow, higher OCVs could be measured, the reason being the higher effective oxygen partial pressure at the cathode side. The cathode has only a limited capacity for the parasitic oxidation of the fuel. If the flow rate to the cathode is increased, the percentage of parasitically consumed oxygen does not increase as strongly as the amount of provided oxygen, which is available for the oxygen reduction reaction. Another reason for the increase of OCV with higher flow rates is the fact that higher flows through the cell keep the reaction products from the anode away from the cathode. The results on porous SC-SOFCs with flow-through configuration showed that the obtained OCVs were smaller than for electrolyte supported SC-SOFCs where 0.68 V were obtained at 700°C [5].

9.3.4 Microstructure of the Cell Components

A cross-sectional SEM-micrograph of the cell that was characterised electrochemically is shown in Figure 9.14. The functional layers had a good contact and were highly porous.

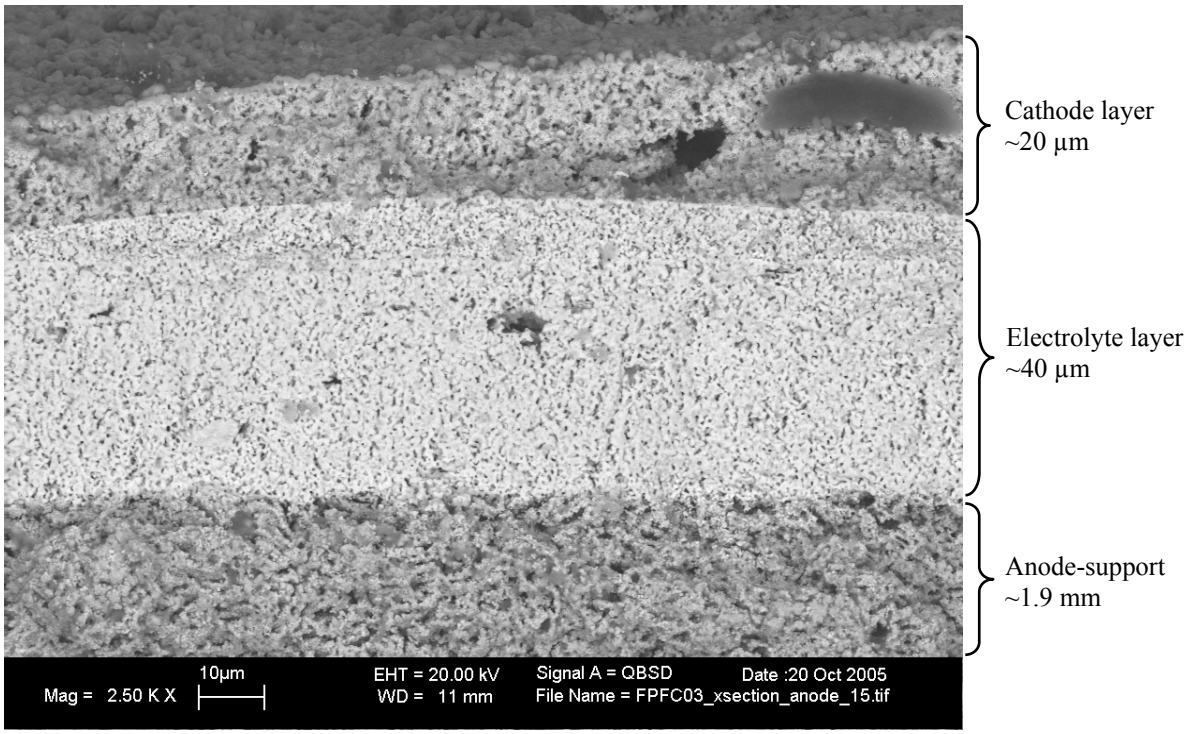

Figure 9.14 Cross sectional view through the electrochemically characterised fully porous SC-SOFC.

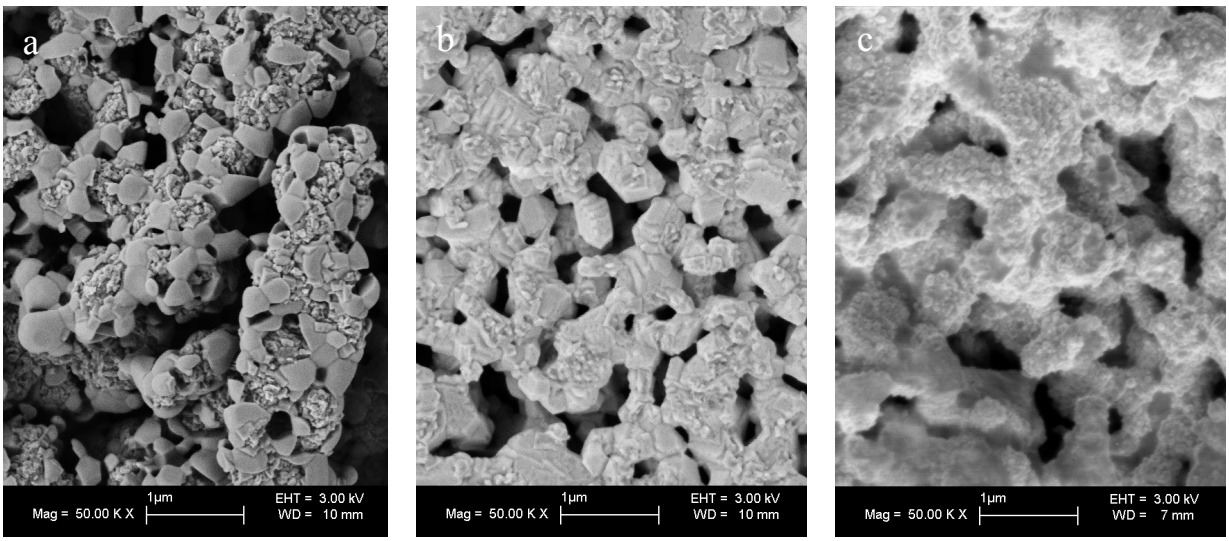

Figure 9.15 Topview of the porous cell components. a) NiO-CGO anode-support, b) CGO electrolyte and c) SSC cathode.

In Figure 9.15, SEM-micrographs are shown for each cell component. The anode showed the highest porosity of 60%. The porosity of the electrolyte and cathode were estimated to be around 20 and 28%, respectively. The grain size of the electrolyte was around 0.5 μm and that of the cathode roughly 1 μm. The sintering of all the cell components seemed to have been satisfactory. The cathode, however, showed a coarse microstructure. It would be reasonable to try to reduce the cathode sintering temperature in future.

9.4 Conclusions

For the first time the concept of fully porous Single Chamber Fuel Cells with a flow-through configuration was proven experimentally and applied for SOFCs. Methane rich gas mixtures with x = 2 (29.5% CH_4, 14.8% O_2) resulted in lower OCVs than oxygen rich mixtures with x = 1 (17.5% CH_4, 17.3% O_2). In conventional SOFCs mixtures with higher CH_4-concentrations have a higher OCV, due to a lower oxygen partial pressure at the anode side [9] but this is not the case here because the cathode is exposed to the gas mixture first and a high oxygen partial pressure is needed at this electrode both for high OCV and high maximum power density. The results indicated that FP-SC-SOFCs require rather high flow rates up to 1000 ml/min in order to keep the reaction products H_2 and CO from the anode away from the cathode. At an anode temperature of 733°C and a methane-air flow rate of 1000 ml/min with an x-value of 1 the cell delivered roughly 10 mW/cm^2. Lower operating temperatures are favourable for obtaining higher OCV. However, thinner electrolyte layers have to be prepared for a reduced operating temperature. Cells with thinner electrolyte layer have the potential for higher power densities. Care must be taken in order to avoid a physical contact of the anode and the cathode, which would cause an internal short circuit in the fully porous cell.

9.5 Outlook

The power output of the prepared and electrochemically characterised fully porous SC-SOFCs can be optimised by using an even thinner electrolyte layer. The preparation of the electrolyte layer must be carefully done in order to avoid pinholes. Screen printing is suited for the preparation of the electrolyte and the cathode layers.

It is reasonable to assume that the open circuit voltage as well as the maximum power density strongly depend on the layer thicknesses. For a too thin electrolyte there is a drastic loss of OCV because of high electronic leakage current, for a too thick electrolyte the resistance for the ionic current is too high. The cathode thickness is another interesting parameter, which can be optimised.

It would be interesting to model fully porous SC-SOFCs. The numerical model would have to include the flow of a reactive gas mixture through the porous cell, the chemical reactions occurring on the anode and cathode, heat generation and transfer and finally the electrochemical reactions at the electrode-electrolyte interfaces. The influence of mixed ionic electronic conductivity of the ceria electrolyte should also be included. From this model the ideal cell parameters such as porosity and layer thicknesses, and suitable operating condition like gas flow through the cell, CH_4/O_2 ratio and operating temperature could be derived.

If a perfect cathode material, totally inert to the fuel could be found and at the same time an anode material that catalyses the direct electrochemical oxidation of CH_4, a fully porous SC-SOFC could be operated in mixtures where the CH_4/O_2 ratio is 0.5. This gas composition would allow the full oxidation of CH_4 to CO_2 and H_2O. The cathode exposed to the incoming gas first, would remove all the oxygen from the mixture and by the ionic conduction through the cell the CH_4 that arrives at the anode could be directly electrochemically oxidised with the oxygen ions coming from the cathode. This SC-SOFC concept would allow high fuel utilisation and very high efficiencies. However, it is uncertain that the perfect anode and cathode materials exist.

9.6 References

[1] I. Riess, P. J. van der Put and J. Schoonman, *Solid State Ionics*, **1995**, 82, 1-4.

[2] T. Suzuki, P. Jasinski, V. Petrovsky, H. U. Anderson and F. Dogan, *Journal of the Electrochemical Society*, **2005**, 152, *3***,** A527-A531.

[3] W. van Gool, *Philips Research Reports*, **1965**, 20, 81-93.

[4] B. E. Buergler, M. Siegrist and L. J. Gauckler, in *Sixth European Solid Oxide Fuel Cell Forum, 2004,* M. Mogensen, 1405-1413.

[5] B. E. Buergler, M. E. Siegrist and L. J. Gauckler, *Solid State Ionics*, **2005**, 176, *19-22***,** 1717-1722.

[6] I. C. Stefan, C. P. Jacobson, S. J. Visco and L. C. De Jonghe, *Electrochemical and Solid State Letters*, **2004**, 7, *7***,** A198-A200.

[7] H. E. Exner, *Rev. Powder Metallurgy Physical Ceramics*, **1979**, 1, 7.

[8] M. Gödickemeier, "Mixed Ionic Electronic Conductors for Solid Oxide Fuel Cells"*,* Ph.D. Thesis, Diss. ETH No. 11348, Swiss Federal Institute of Technology, 1996.

[9] B. E. Buergler, N. A. Grundy and L. J. Gauckler, *Journal of the Electrochemical Society*, **2006**, 153, *7***,** A1378-A1385.

10 Conclusions

This project aimed at obtaining more insight into single chamber solid oxide fuel cells (SC-SOFCs) operating in methane-air mixtures. The thermodynamic equilibrium of the used gas mixtures was calculated for the experimental operating conditions in Chapter 4. The equilibrium constituents of the gas phase are mainly N_2, CH_4, CO, CO_2, H_2, and H_2O. It was shown that the most drastic changes in the equilibrium concentrations of gas constituents occur in the temperature range where SC-SOFCs are operated. Therefore a strong dependency of the cell behaviour on temperature can be expected. Carbon deposition becomes thermodynamically possible at low temperatures for methane-rich mixtures. In addition it was found that temperatures above 800°C are more suitable due to higher concentration of H_2 and CO and smaller amounts of H_2O and CO_2. However, the cathode will oxidise more of the provided methane parasitically if the temperature is too high as could be shown by the measurement of the catalytic activity of SC-SOFCs electrodes (Chapter 5). Thus, there is only a limited temperature range, in which SC-SOFCs can be operated. The addition of catalytic modifiers to the anode can shift the possible temperature range to lower temperatures by keeping the Nickel in the anode in the reduced, metallic state.

The Ni-cermet anode of a SC-SOFC functions both as a catalyst for the partial oxidation and as an electrochemical catalyst for the hydrogen oxidation with oxygen ions. Therefore, the anode thickness has a major impact on the electrochemical performance of SC-SOFCs. In Chapter 7 the influence of the anode thickness was studied. For very thin anode layers (9 μm thickness) an unstable cell behaviour (oscillations of open circuit voltage) was observed especially at high flow rates to the anode. It was found that the open circuit voltage decreased with increasing flow rate to the anode and that thick anodes gave a higher open circuit voltage than thin anodes. The thickest anode led to the highest maximum power density and the most stable behaviour at high gas flows. It could be shown that the maximum power density increased with increasing flow rate to the anode. For obtaining a high performance with SC-SOFCs high flow rates seem to be necessary.

The three basic designs that are possible with the "single chamber approach" were presented in Chapter 3 and all of these designs have been evaluated in this thesis. Cells with the conventional "sandwich"-design were studied in Chapter 6. The prepared cells generated an open circuit voltage of 0.68 V and a maximum power density of 468 mW/cm^2 at 600°C in a flowing mixture of methane and air ($CH_4/O_2 = 1.6$) with a total flow rate of 1500 ml/min.

The high power densities of SC-SOFCs known from literature could be successfully reproduced. A pronounced overheating of the cell to temperatures higher than the furnace temperature was observed. The reason for this temperature rise was the parasitic oxidation reaction of methane that occurred at both electrodes as was shown in Chapter 5.

The proofs of concept for two novel cell designs that are not possible with conventional solid oxide fuel cells were demonstrated in this work. On the one hand micro SC-SOFCs with side by side placement of the electrodes and on the other hand fully porous SC-SOFCs with flow-through configuration were prepared and their electrochemical performance studied.

The prepared micro SC-SOFC (Chapter 8) consisted of an array of 19 individual cells that were connected in parallel. An open circuit voltage of 0.65-0.75 V was measured in flowing gas mixtures of methane and air. The maximum power density was limited by the high ohmic resistance of the long conduction paths along the thin electrode strips. In order to avoid these high ohmic losses, cell arrays should be prepared and characterised, in which the individual cells are connected in series. The experiments showed that it is possible to obtain an OCV even when the electrodes are very closely placed to each other. With this design there is the possibility that the reaction products from the anode (CO and H_2) can diffuse via the gas phase to the cathode side, thereby decreasing or totally suppressing the build-up of an open circuit voltage. It was shown that at suitable conditions this was not the case.

The fully porous design in theory allows for higher fuel utilisations because of the longer contact times of the fuel and oxygen with the catalytic active surfaces. An anode-supported fully porous SC-SOFC was prepared and gave a reasonable open circuit voltage (Chapter 9). The power output was very sensitive to the temperature, the CH_4/O_2-ratio and the total gas flow through the cell. At 733°C an open circuit voltage of 0.52 V and a maximum power density of 10 mW/cm^2 were measured, showing that the fully porous design is feasible. The open circuit voltage of the fully porous cell was lower than for SC-SOFCs with a dense electrolyte and much higher flow rates were required. The reason for this was that the reaction products of the anode could reach the cathode through the porous electrolyte, thereby decreasing the oxygen partial pressure at the cathode and consequently the open circuit voltage. At high flow rates through the cell, the reaction products from the anode were flushed away from the cathode and the measured open circuit voltages were accordingly higher than at low gas flow.

From a theoretical standpoint, an initial CH_4/O_2-ratio (x) of 0.5 would be ideal, because it would allow the full oxidation of methane to CO_2 and H_2O. However, this gas mixture would

have to be passed over both electrodes (first the cathode and then the anode) being perfectly selective for either oxygen or methane adsorption. In practice $x = 0.5$ is not feasible because of the threat of an explosion. However, it might be possible to operate a SC-SOFC at e.g. $x = 1$ and to move the gas equilibrium to $x = 0.5$ by the ionic current through the cell, thereby approaching a reasonable fuel utilisation.

11 Outlook

Single chamber solid oxide fuel cells are receiving increased interest all over the world. Over the last few years there has been a great improvement of the performance that can be reached with single chamber solid oxide fuel cells (SC-SOFCs). A key for improving the cells and gaining a more thorough understanding of SC-SOFCs operating in hydrocarbon-air mixtures is the study of catalytic activities of electrode materials. In order to further improve the performance of SC-SOFCs cathode materials that are tolerant to the used fuels are needed. Furthermore, an anode material that is highly active for the partial oxidation of the hydrocarbon fuel is required. It is likely that Ni-based anodes that will be modified with additions of catalytically active precious metals like Palladium or Ruthenium will be further used for SC-SOFCs.

In this work we have demonstrated the feasibility of micro SC-SOFCs and of fully porous SC-SOFCs. It would be interesting to see if the micro cells connected in series are more flaw-tolerant and if they can give the envisaged voltages. The fully porous design opens a whole new field for electrocatalytic research. It may be possible to alter the reaction products of a fully porous cell by applying a potential between the two electrodes.

Another interesting field is the modelling of fully porous SC-SOFC systems or SC-SOFCs in general. The numerical model would have to include the flow of a reactive gas mixture through the porous cell, the chemical reactions occurring on the anode and cathode, heat generation and transfer and finally the electrochemical reactions at the electrode-electrolyte interfaces. The influence of mixed ionic electronic conductivity of the ceria electrolyte should also be included. From this model the ideal cell parameters such as porosity and layer thicknesses and suitable operating condition like gas flow rate to the cell, CH_4/O_2 ratio and operating temperature could be derived.

The drastically simplified design, the high power output and the possibility of thermally self-sustaining operation of SC-SOFC might lead to a first commercial product in the near future of solid oxide fuel cells.

Curriculum Vitae

Personal	Brandon Edward Bürgler
Date and place of birth:	February 11th, 1975, in Zug, Switzerland
Marital status:	not married
Nationality:	Swiss, Citizen of Illgau (Schwyz)

Education

January 2002-present	Research associate and PhD student, Nonmetallic Inorganic Materials, Swiss Federal Institute of Technology, Department of Materials, ETH-Zürich
2001	4 months work as Engineer at ABB-Research Centre, Dättwil, Switzerland on the project of superconducting fault-current limiters
2001	Diploma in Material Science
1995-2001	Student of Material Science, Swiss Federal Institute of Technology, Department of Materials, ETH Zürich
1995	Matura in Mathematics and Natural Sciences
1989-1995	Mathematisch-naturwissenschaftliches Gymnasium in Basel

Publications

In the course of the dissertation the following publications were accomplished:

1. B. E. Buergler, M. E. Siegrist and L. J. Gauckler, "Single Chamber Solid Oxide Fuel Cells with Integrated Current Collectors", *Solid State Ionics*, **2005**, *176* (19-22), 1717.
2. B. E. Buergler, N. A. Grundy and L. J. Gauckler, "Thermodynamic Equilibrium of Single Chamber Solid Oxide Fuel Cell Relevant Methane-Air mixtures", *Journal of the Electrochemical Society*, **2006**, *153*, (7), A1378.

3. L. J. Gauckler, D. Beckel, B. E. Buergler, E. Jud, U. P. Mücke, M. Prestat, J. L. M Rupp, J. Richter, "Solid Oxide Fuel Cells: Systems and Materials", *CHIMIA International Journal for Chemistry*, **2004**, *58* (12), 837.
4. B. E. Buergler, M. Ochsner, S. Vuillemin and L. J. Gauckler, „Micro Single Chamber Solid Oxide Fuel Cells fabricated by MIMIC", to be submitted to *Journal of Power Sources.*
5. B. E. Buergler, D. Smida and L. J. Gauckler, „Fabrication and Characterisation of a Fully Porous Single Chamber Solid Oxide Fuel Cell with Flow-through Configuration", to be submitted to *Solid State Ionics*.
6. B. E. Buergler and L. J. Gauckler, "The Catalytic Activity of SC-SOFC Electrode Materials in Methane-Air Mixtures", to be submitted to *Journal of the Electrochemical Society.*
7. J. Peña-Martínez, D. Marrero-López, J.C. Ruiz-Morales, B.E. Buergler, P. Núñez and L.J. Gauckler, „Fuel cell studies of perovskite-type materials for IT-SOFC", *Journal Power Sources*, In Press, Corrected Proof.

Proceedings

B. E. Buergler, Y. Santschi, M. Felberbaum and L. J. Gauckler, „Influence of Anode thickness on the Electrochemical Performance of Single Chamber Solid Oxide Fuel Cells", *Ceramic Engineering and Science Proceedings*, 2006, 27, 4, in press.

Presentations

1. B. E. Buergler, "Single Chamber Solid Oxide Fuel Cells", D-MATL Colloquium, ETH, Zürich, Jan. 14th, 2004.
2. B. E. Buergler and L. J. Gauckler, "Single Chamber Solid Oxide Fuel Cells", Fuel Cell Research Symposium: Modelling and Experimental Validation, ETH, Zürich, Jan. 19th, 2004.
3. B. E. Buergler, M. Siegrist and L. J. Gauckler, "Single Chamber Solid Oxide Fuel Cells with Reaction Selective Electrodes", 7th International Symposium on Systems with Fast Ionic Transport (ISSFIT 7), Bled, Slovenia, May 7th, 2004.

4. B. E. Buergler, M. Siegrist and L. J. Gauckler, „Single Chamber Solid Oxide Fuel Cells with Integrated Current Collectors", 6th European SOFC Forum, Lucerne, Switzerland, July 7th, 2004.
5. B. E. Buergler, "Single Chamber Solid Oxide Fuel Cells", invited speaker, Electrochemistry Laboratory (ECL) Seminar, PSI, Villigen, Switzerland, July 7th, 2004.
6. B. E. Buergler, Marco Siegrist and L. J Gauckler, "Single Chamber Solid Oxide Fuel Cells with Mixed Ionic Electronic Conducting Electrolyte", Fifth International Symposium on Ionic and Mixed Conducting Ceramics, Honolulu, Hawaii, USA, Oct. 7th, 2004.
7. B. E. Buergler and L. J. Gauckler, „Solid Electrolyte/Electrocatalyst assemblies for Solid Oxide Fuel Cells a Case Study: SC-SOFCs", International Workshop: Future Concepts in Energy Related Catalysis, Ascona, Switzerland, March 15th, 2005.
8. B. E. Buergler, Y. Santschi, M. Felberbaum and L. J. Gauckler, „Influence of Anode Thickness on the Electrochemical Performance of SC-SOFCs", 30th International Conference on Advanced Ceramics and Composites, Cocoa Beach, Florida, USA, Jan. 23rd, 2005.

Poster Presentations

B. E. Buergler, M. Siegrist, L. J. Gauckler, "Solid Oxide Fuel Cells with Reaction Selective Electrodes", 55th Annual Meeting of the International Society of Electrochemistry, Thessaloniki, Greece, Sept. 23rd, 2004.

Awards

Award for best Diploma Thesis at the Department of Materials, ETHZ, "The formation of Ferromagnetic τ-Mn-Al-C Synthetically Twinned Crystals" donated by the Swiss association for Material Science and Technology (SVMT), 2001.